THE APPLICATION OF THE SEGMENTATION METHOD IN THE DESIGN OF COMPACT SINGLE-FEED CIRCULARLY AND LINEARLY POLARISED MICROSTRIP PATCH ANTENNAS

SIN KENG LEE

A thesis submitted in partial fulfilment of the requirements of the University of Northumbria at Newcastle for the degree of Doctor of Philosophy

School of Computing, Engineering and Information Sciences

Northumbria University at Newcastle, United Kingdom

June 2007

ABSTRACT

This thesis presents the application of coplanar circuit analysis in the design of compact single-feed circularly polarised (CP) and linearly polarised (LP) microstrip patch antennas. A CP nearly square patch antenna and a CP truncated corners square patch antenna are designed. Also a LP U-slot rectangular patch antenna is designed. In order to obtain a faster computational run-time, coplanar circuit analysis and segmentation method are applied for the impedance calculations. The coupling and self impedance formulas for both rectangular and right-angled isosceles triangular segments are given. Explicit formulas for the coupling impedance between a perimeter port and a probe port, and also the probe self impedance on both of these segments are new and are derived in detail.

A CP nearly square patch antenna is designed using both the cavity and equivalent circuit models. New and simple design equations are derived to determine the dimensions of the patch with a feed in any given position. For a microstrip feed offset from a corner of the patch, the area of perturbation segment is increased which reduces the effect of manufacturing errors. A simple matching network consisting of a short length of microstrip line is designed to achieve a more compact form of the matched antenna. The results obtained from both models are good agreement.

A CP truncated corners square patch antenna with a microstrip feed offset from the centre is presented. In previous work the design is a feed along the centre line and the areas of the deleted segments are very small so the performance of the antenna is very sensitive to manufacturing errors. Hence an offset feed is proposed in order to increase the perturbation area and so reduce the effect of the manufacturing errors. The segmentation method is used for which a new explicit matrix input impedance formula is derived. The impedance formula requires a computer run time less than half that required by simulation (full-wave software, Ansoft Ensemble). The change in area of the perturbed segment and input impedance with the microstrip offset feed position is examined. A compromise offset

feed position was chosen so as to maximise the area of the perturbation segment and achieve good impedance matching for a compact antenna structure.

A LP probe feed U-slot rectangular patch is designed and the input impedance is determined. A set of initial design equation is used to produce a first-pass design. In applying segmentation method a new explicit input impedance formula for the antenna is derived. The basic system of eleven coplanar circuit equations is reduced to seven equivalent circuit equations from which the explicit impedance formula is derived. The dimensions of the patch are adjusted to give good impedance matching. In respect of computational efficiency, the run time of the new matrix input impedance formula is at least 10 times faster than is required by simulation. A thicker substrate is also used in order to improve the bandwidth.

The predicted, simulated and measured results of the above three compact patch antennas are in good agreement.

Mathcad programming is used to implement the design calculations of the compact patch antennas.

CONTENTS

ABSTRACT ii
CONTENTS iv
LIST OF FIGURES vii
LIST OF TABLES x
ACKNOWLEDGMENTS xi
DECLARATION xii
GLOSSARY OF ACRONYMS xiii
GLOSSARY OF SYMBOLS xiv
SUBSTRATES AND THEIR PARAMETERS xvi
CHAPTER 1 INTRODUCTION AND OVERVIEW OF THESIS 1
1.1 Introduction 1
1.2 Overview of Thesis 2
1.3 Significant Achievements of the Research Work 4
1.4 Research Work Published 5
CHAPTER 2 REVIEW OF MODELLING, CIRCULAR POLARISATION AND COPLANAR ANALYSIS OF MICROSTRIP PATCH ANTENNAS 6
2.1 Introduction 6
2.2 Introduction to Microstrip Patch Antennas 6
2.2.1 Transmission-line model 9
2.2.2 Cavity model 12
2.2.3 Full-wave modelling analysis 13
2.3 Dual- and Single-Feed CP Patch Antennas 15
2.3.1 Elliptical, linear, and circular polarisation 15
2.3.2 External polarisers for a square patch antenna 17
2.3.3 Single-feed CP patch antennas 18
2.4 Coplanar Multiport Analysis and the Segmentation Method 23
2.4.1 The coupling impedance formula in terms of the Green's function 23
2.4.2 Applications in segmentation method 24
2.4.3 Coplanar matrix circuit equations 26
2.4.3.1 Single segment 26
2.4.3.2 Two segments 27
2.5 Summary 29
CHAPTER 3 DESIGN AND ANALYSIS OF A CP NEARLY SQUARE PATCH ANTENNA 30
3.1 Introduction 30
3.2 Derivation of New Design Equations for a CP Nearly Square Patch Antenna Using the Cavity Model 31
3.3 Design of the CP Antenna Based on the Equivalent Circuit Model of the Patch 35
3.4 The Effect of the Design Parameters on the Area of the Perturbation Segment 39
3.5 Impedance Matching 41
3.6 Comparison between Predicted, Simulated, and Measured Results 44

3.7 Summary 53

CHAPTER 4 EXPLICIT COMPUTATIONALLY EFFICIENT COUPLING IMPEDANCE FORMULAS FOR RECTANGULAR AND TRIANGULAR SEGMENTS 54

4.1 Introduction 54
4.2 The Green's Function for a Rectangular and a Right-Angled Isosceles Triangular Segment 55
4.2.1 The rectangular segment 56
4.2.2 The triangular segment 57
4.3 Coupling Impedances for Perimeter Ports on a Rectangular Segment 58
4.4 New Probe Feed Input Impedance Formula for a Rectangular Segment 63
4.5 Coupling Impedance between Probe Feed and a Perimeter Port on a Rectangular Segment 67
4.6 Coupling Impedances for Perimeter Ports on the Triangular Segment 69
4.7 New Probe Feed Input Impedance Formula for the Triangular Segment 80
4.8 Coupling Impedance between Probe Feed and a Port on a Perpendicular Side on the Triangular Segment 83
4.9 Summary 86

CHAPTER 5 APPLICATION OF SEGMENTATION METHOD TO A CP TRUNCATED CORNERS SQUARE PATCH ANTENNA 87

5.1 Introduction 87
5.2 Derivation of the Explicit Matrix Formula for the Input Impedance Using Segmentation Method 89
5.3 Perturbation Analysis 91
5.4 Investigation of the Feed Position on the Area of the Perturbation Segment 95
5.5 Design of a Matched CP Antenna for a Fixed Offset Feed 104
5.6 Summary 109

CHAPTER 6 SEGMENTATION ANALYSIS AND A DESIGN APPROACH FOR A U-SLOT RECTANGULAR PATCH ANTENNA 111

6.1 Introduction 111
6.2 Design Procedure for the Initial Antenna 112
6.3 The Derivation of an Explicit Matrix Input Impedance Formula Using Segmentation Analysis 116
6.4 Design Procedure for Antenna A 121
6.5 Design of Antenna B 127
6.6 Summary 132

CHAPTER 7 CONCLUSIONS OF THE RESEARCH WORK AND FURTHER WORK 134

7.1 Conclusions 134
7.2 Suggestions for Further Work 136

REFERENCES 141

APPENDIX 3A Q-Factor of a Rectangular Patch 148

APPENDIX 3B Derivation of the Amplitude and Phase Equations 151

APPENDIX 4A Coupling Impedance Formulas for a Rectangle and the Triangle 154

APPENDIX 5A The Mathcad Program Listing for the Impedance of a Truncated Corners Square Patch 174

APPENDIX 6A The Mathcad Program Listing for the Impedance of a U-Slot Rectangular Patch 180

LIST OF FIGURES

Figure 2.1. (a) Microstrip patch antenna. (b) Top view. (c) Side view. 7
Figure 2.2. (a) Rectangular patch. (b) Transmission-line model equivalent circuit. 10
Figure 2.3. Field configurations (modes) for rectangular microstrip patch. (a) TM_{10} mode. (b) TM_{01} mode. 13
Figure 2.4. Wave polarisation (wave approaching). (a) Elliptical polarisation. (b) Horizontal and vertical linear polarisations. (c) Circular polarisation. 16
Figure 2.5. Dual-feed CP patch antennas. (a) A square patch with a 90° hybrid. (b) A square patch with a power divider 17
Figure 2.6. Single-feed CP antennas. (a) Truncated corners square patch with a probe centre line feed, or, with a microstrip centre feed as Type A antenna. (b) Nearly square patch with a probe diagonal feed, or, with a microstrip corner feed as Type B antenna. 19
Figure 2.7. Amplitude and phase of the two modes for Type A and Type B antennas. 19
Figure 2.8. A CP single centre line feed square patch. (a) A notch at corner. (b) A diagonal stub at corner. (c) Two diagonal stubs at corner. (d) Two notches at corners. (e) Two stubs at corner. (f) A diagonal narrow rectangular slot. 20
Figure 2.9. A CP single diagonal feed square patch. (a) A notch at centre-edge. (b) A stub at centre-edge. (c) Two notches at opposite edges. (d) Two stubs at opposite edges. (e) A slit. (f) A centre thin rectangular slot. 21
Figure 2.10. A single-feed CP cross-aperture coupled nearly square patch antenna 22
Figure 2.11. Antenna structure with probe feed – Cavity model. 23
Figure 2.12. Composite structure. 25
Figure 2.13. Segmental structure. 25
Figure 2.14. Single segment with p-port 26
Figure 2.15. Interport structure for two segments. 27
Figure 3.1. CP nearly square patch antenna with effective dimensions $b_e > a_e$. (a) Offset probe feed. (b) Offset microstrip feed. (c) General areas on a patch for a feed. 32
Figure 3.2. Equivalent circuit of a single-feed nearly square patch antenna after perturbation. 35
Figure 3.3. Relationship between the perturbation $\Delta S_e / S_e$ and the offset feed positions and Q-factor. (a) The cavity model. (b) The equivalent circuit model. 39
Figure 3.4. Relationship between the perturbation $\Delta S / S$ and the offset feed positions. 40
Figure 3.5. Calculated and simulated Z_{in} at offset factor x_0 / a. (a) For *FR4 PCB*. (b) For *Duroid*. 42
Figure 3.6. CP nearly square patch antenna with a simple matching network. (a) Matched antenna. (b) A simple transmission-line matching network. 43
Figure 3.7. Region of Z_{in} that can be matched using the matching network. 44
Figure 3.8. The fabricated CP nearly square patch antennas. (a) For *FR4 PCB*. (b) For *Duroid*. 45
Figure 3.9. Simulated and measured input impedance on Smith chart. (a) For *FR4 PCB*. (b) For *Duroid*. 46
Figure 3.10. Simulated and measured return loss. (a) For *FR4 PCB*. (b) For *Duroid* 47
Figure 3.11. Simulated and measured AR versus frequency. (a) For *FR4 PCB*. (b) For *Duroid*. 48

Figure 3.12. Simulated and measured AR versus theta. (a) For *FR4 PCB*. (b) For *Duroid*. 49
Figure 3.13. Simulated and measured gains. (a) For *FR4 PCB*. (b) For *Duroid*. 50
Figure 3.14. Simulated normalised radiation patterns for RHCP and LHCP at $\phi = 0$. (a) For *FR4 PCB*. (b) For *Duroid*. 51
Figure 3.15. Normalised radiation patterns for *FR4 PCB* (a) Simulation at $\phi = 0$. (b) Measurement at $\phi = 0$. (c) Simulation at $\phi = 90^\circ$. (d) Measurement at $\phi = 90^\circ$. 52
Figure 3.16. Normalised radiation patterns for *Duroid* (a) Simulation at $\phi = 0$. (b) Measurement at $\phi = 0$. (c) Simulation at $\phi = 90^\circ$. (d) Measurement at $\phi = 90^\circ$. 53
Figure 4.1. Double series array. 58
Figure 4.2. Perimeter ports on a rectangular segment. (a) For case A: two ports on the same side. (b) For case B: two ports on adjacent sides. (c) For case C: two ports on opposite sides. 59
Figure 4.3. Case A: rectangular segment with two ports on the same side. 59
Figure 4.4. Case B: rectangular segment with two ports on adjacent sides. 61
Figure 4.5. Case C: rectangular segment with two ports on opposite sides. 62
Figure 4.6. Rectangular segment with two probe feeds. 64
Figure 4.7. The comparison between the calculated, simulated, and measured probe feed input impedance for a rectangular segment. 66
Figure 4.8. Rectangular segment with a probe port and a microstrip port. 67
Figure 4.9. Perimeter ports on the triangular segment. (a) For case A: two ports on the same side. (b) For case B: two ports on adjacent sides. (c) For case C: two ports between perpendicular and hypotenuse sides. (d) For case D: two ports on the hypotenuse side. 69
Figure 4.10. Case A: triangular segment with two ports on the same perpendicular side. 70
Figure 4.11. Case B: triangular segment with two ports on adjacent sides. 72
Figure 4.12. Case C: triangular segment with ports between perpendicular and hypotenuse sides. 73
Figure 4.13. Case D: triangular segment with two ports on the hypotenuse side. 75
Figure 4.14. The comparison between the calculated, simulated, and measured perimeter port coupling impedance for a triangular patch. (a) Case A. (b) Case B. (c) Case C. (d) Case D. 79
Figure 4.15. Triangular segment with two probe feeds. 80
Figure 4.16. The comparison between the calculated, simulated, and measured probe feed input impedance for a triangular segment. 83
Figure 4.17. Triangular segment with a probe port and a port on a perpendicular side. 84
Figure 5.1. A truncated corners square patch antenna. (a) The truncated patch. (b) Segmentation of the patch. 89
Figure 5.2. The coordinate system for the square patch antenna. 92
Figure 5.3. A truncated corners square patch with a centre line feed. 92
Figure 5.4. Equivalent circuit of a truncated corners patch antenna after perturbation. 94
Figure 5.5. The patch with an offset feed. 96
Figure 5.6. Segmentation calculated input impedance with the different N for $T_0 = 0$. (a) Real part. (b) Imaginary part. 97
Figure 5.7. Segmentation calculated and simulated input impedance for $T_0 = 0$. (a) Input impedance versus frequencies. (b) Smith chart. 98

Figure 5.8. (a) Relationship between the perturbation $\Delta S / S$ and offset. (b) The input impedance at offset feed locations. 102
Figure 5.9. The calculated, simulated, and measured input impedance of the patch at $T_0 = 0.2a$. (a) Input impedance versus frequencies. (b) Smith chart. 103
Figure 5.10. The patch with a simple matching network. (a) Geometry. (b) Fabricated patch antenna. 104
Figure 5.11. Simulated and measured input impedance in Smith chart. 105
Figure 5.12. Simulated and measured return loss. 106
Figure 5.13. Simulated and measured axial ratio versus frequency. 106
Figure 5.14. Simulated and measured AR versus theta. 107
Figure 5.15. Simulated and measured gain. 107
Figure 5.16. Simulated normalised radiation patterns for RHCP and LHCP at $\phi = 0$ 108
Figure 5.17. Normalised radiation patterns (a) Simulation at $\phi = 0$. (b) Measurement at $\phi = 0$. (c) Simulation at $\phi = 90^\circ$. (d) Measurement at $\phi = 90^\circ$. 109
Figure 6.1. Geometry of a probe feed U-shape slot rectangular microstrip patch antenna. (a) Top view. (b) Side view. 113
Figure 6.2. Segmental structure for the U-slot rectangular patch. 116
Figure 6.3. The fabricated patch antenna. 122
Figure 6.4. Calculated, simulated, and measured input impedance. (a) Input impedance. (b) Smith chart. 123
Figure 6.5. Calculated, simulated, and measured return loss. 124
Figure 6.6. Simulated and measured gain. 125
Figure 6.7. Normalised radiation patterns. (a) Simulated E-plane. (b) Measured E-plane. (c) Simulated H-plane. (d) Measured H-plane. 126
Figure 6.8. The fabricated patch antenna. 128
Figure 6.9. Calculated, simulated, and measured input impedance. (a) Input impedance. (b) Smith chart. 129
Figure 6.10. Calculated, simulated, and measured return loss. 130
Figure 6.11. Simulated and measured gain. 131
Figure 6.12. Normalised radiation patterns. (a) Simulated E-plane. (b) Measured E-plane. (c) Simulated H-plane. (d) Measured H-plane. 132
Figure 7.1. Nearly square ring patch antenna. (a) Microstrip offset feed. (b) Probe offset feed. 136
Figure 7.2. Segmentation structure for a rectangular ring patch antenna with offset feed. 137
Figure 7.3. Overlapping three square-shaped patches antenna. 138
Figure 7.4. Segmental structure. 138
Figure 7.5. A CP perturbed isosceles right-angled triangular patch and its segmental segments. (a) A truncated tip patch. (b) A tip stub patch. (c) An edge stub patch. 139
Figure 7.6. Triangular segment with a probe feed and a port on the hypotenuse. 140

LIST OF TABLES

Table 3.1. For *FR4 PCB*, the calculated and simulated dimensions for CP operation at 2.45 GHz. 38
Table 3.2. For *Duroid*, the calculated and simulated dimensions for CP operation at 2.45 GHz. 38
Table 3.3. The perturbation $\Delta S / S$ with respect to the offset feed positions. 41
Table 3.4. Calculated and simulated design parameters of the matching microstrip line and of the patch antenna. 45
Table 3.5. The impedance bandwidths, the CP bandwidths, and the gains at centre frequency. 50
Table 5.1. The calculated and simulated perturbation areas and dimensions of the patch with a microstrip feed at $T_0 = 0$. 99
Table 5.2. The calculated and simulated dimensions and perturbation for the offset feeds for CP operation at 2.45 GHz. 101
Table 5.3. Calculated and simulated design parameters of the matching microstrip line and of the patch antenna. 105
Table 5.4. The impedance bandwidth, the CP bandwidth, and the gain at centre frequency. 108
Table 6.1. Initial design dimensions in mm. 121
Table 6.2. Tuned the parameters *C*, *D*, *H* (mm) for matching at 2.45 GHz. 122
Table 6.3. The return loss and the impedance bandwidth. 124
Table 6.4. Initial design dimensions in mm. 127
Table 6.5. Tuned the parameters *B*, *C*, *D*, *H* (mm) for matching at 2.45 GHz. 127
Table 6.6. The return loss and the impedance bandwidth. 130

ACKNOWLEDGMENTS

First and foremost I would like to express my sincere thanks to my principal supervisor Professor Alistair Sambell, and supervisors Professor Edward Korolkiewicz, Professor Fary Ghassemlooy for their time, support, guidance, encouragement, patience and understanding to help throughout this project. I also greatly appreciate the knowledge and experience that they shared with me during the project period. With their patience and professional guidance I was able to complete the project with very good results.

I also offer here a very special thanks to Mr. Stan Scott for his assistance in the mathematical aspects of the project.

Thanks to the technicians, especially Peter Elsdon, Ed Holmes and Vincent Hinksman for their help, practical advice and technical assistance. Thanks also to my co-researchers for their support and encouragement.

Finally, I am indebted to my family (Kim Too Lee, Ah Negh Tan, Seng Tiong Lee, Seng Boon Lee, Bee Ean Lee and Bee Chen Lee) for their constant support and encouragement.

DECLARATION

I declare that the work contained in this thesis has not been submitted for any other award and that it is all my own work.

Name: SIN KENG LEE

Signature: Leesinkeng

Date: 06/07/2007

GLOSSARY OF ACRONYMS

AR	.....	Axial ratio
ARBW	.....	Axial ratio bandwidth
CP	.....	Circularly polarised
CPW	.....	Coplanar waveguide
FDTD	.....	Finite difference time domain
GHz	.....	Gigahertz
GIS	.....	Geographic information system
GPS	.....	Global positioning system
LP	.....	Linearly polarised
LHCP	.....	Left-hand circular polarisation
MIC	.....	Microwave integrated circuit
RHCP	.....	Right-hand circular polarisation
TM	.....	Transverse magnetic
VSWR	.....	Voltage standing wave ratio
WLAN	.....	Wireless local area network

GLOSSARY OF SYMBOLS

α	.....	Attenuation constant
γ	.....	propagation constant
ε_0	.....	Permittivity of free space (= 8.854×10^{-12} F/m)
ε_r	.....	Relative permittivity of dielectric or dielectric constant
ε_{reff}	.....	Effective permittivity of dielectric or effective dielectric constant
η_0	.....	Impedance of free space (= 376.7 Ω)
θ	.....	Phase angle of radiated components
θ_m	.....	Electrical length of matching line
λ	.....	Wavelength
λ_0	.....	Free space wavelength
μ	.....	Permeability of dielectric
μ_0	.....	Permeability of free space (= $4\pi \times 10^{-7}$ H/m)
μ_r	.....	Relative permeability of dielectric
σ_c	.....	Conductivity of a conductor
ω	.....	Angular frequency
ΔL	.....	Extended length due to fringing fields
ΔS	.....	Total area of perturbation segment
B_1	.....	Capacitive susceptances due to fringing fields
c_0	.....	Speed of light in free space (= 2.998×10^8 m/s)
G_1	.....	Radiation conductance
G_{12}	.....	Mutual conductance
E_1	.....	Amplitude of electric field in x direction

E_2	.....	Amplitude of electric field in y direction
f_r	.....	Resonant frequency of patch antenna
h	.....	Thickness of a dielectric substrate
i_p	.....	Current at p port
J_0	.....	The order zero Bessel function of the first kind
k_0	.....	Phase constant in free space ($=2\pi/\lambda_0$)
$k_{m,n}$	.....	Wavenumber of TM_{mn} modes in dielectric
P_{rad}	.....	Radiated power
Q_c	.....	Conductor quality factor
Q_d	.....	Dielectric quality factor
Q_r	.....	Radiation quality factor
Q_{sw}	.....	Surface wave quality factor
R_{in}	.....	Real part of input impedance
$\tan\delta$	.....	Dielectric loss tangent
V_p	.....	Voltage at p port
Y_c	.....	Characteristic admittance
Z_{ij}	.....	Coupling impedance between i and j ports
Z_{in}	.....	Antenna input impedance
Z_0	.....	Characteristic impedance
Z_{0m}	.....	Characteristic impedance of matching line
Z_{pp}	.....	Self impedance or input impedance at p port
Z_{pq}	.....	Coupling impedance between p and q ports

SUBSTRATES AND THEIR PARAMETERS

The substrates and their parameters used in this thesis

1) *FR4 PCB*

Substrate's thickness: $h = 1.575$ mm

Loss tangent: $\tan\delta = 0.019$

Dielectric constant: $\varepsilon_r = 4.3$

2) *RT Duroid 5870*

Substrate's thicknesses: $h = 1.575$ mm and $h = 3.175$ mm

Loss tangent: $\tan\delta = 0.0012$

Dielectric constant: $\varepsilon_r = 2.33$

CHAPTER 1 INTRODUCTION AND OVERVIEW OF THESIS

1.1 Introduction

As advances in wireless communication technologies have been made very rapidly in the recent years, there has been considerable work done on compact microstrip antennas with both circular and linear polarisation. The smaller antenna size is required to meet the miniaturisation of mobile units such as mobile phones, laptops, traffic, satellite, airborne, global positioning system (GPS) and wireless local area networks (WLAN) system applications. Hence, in practical applications, the small size antenna is one of importance in design considerations. There have been many significant achievements in the design of CP and LP compact microstrip antennas. Also work on broadband and dual-frequency operations has been reported [1], [2].

In this thesis the design of three different types of matched compact patch antennas operating at 2.45 GHz are presented. These are the CP nearly square patch, the CP truncated corners square patch and the LP U-slot rectangular patch antenna.

The segmentation method is applied to achieve matching for the antennas. In the application it is necessary to calculate port coupling impedances for which new computationally efficient explicit formulas are derived.

The predicted results are compared with both the results from the software simulator (full-wave software, Ansoft Ensemble) and measured values.

An overview of the research works is presented in the following section.

1.2 Overview of Thesis

In Chapter 2 there is a review of the basic principles of microstrip patch antennas, modelling and analysis, polarisations, and general analytic techniques. The transmission-line model, cavity model and full-wave analysis modelling are discussed. For CP operation, dual-feed patch antennas are compared with single-feed antennas.

In Chapter 3 using the cavity and equivalent circuit models, new and simple design equations are derived to determine the dimensions of a nearly square patch antenna with a feed in any given position. For a feed offset from a corner, or on the diagonal of the patch, the area of the perturbation segment is increased and hence reduces the effect of manufacturing errors. The input impedance of the patch is determined to design a simple matching network consisting of a short length of microstrip line for achieving a compact form of the matched antenna. Both *FR4* and *Duroid* substrates with $h = 1.575$ mm are used. The results obtained from both models are compared. The predicted, modelled and practical results are presented.

In Chapter 4 the coupling and self impedance formulas for the rectangular and isosceles right-angled triangular segments are assembled together for general reference. The double infinite series Green's functions of the rectangular and the triangular segments are partitioned and closed forms of infinite series are introduced to obtain explicit and efficient impedance formulas. This greatly improves the computational running time. New formulas involving the probe feed ports on the rectangle and on the triangle are derived in detail. For the triangle computed port coupling impedance values are compared with both simulated and measured results.

In Chapter 5 a CP compact truncated corners square patch antenna with a microstrip feed offset from the centre is presented. For a feed located on a centre line, the areas of the deleted segments are very small and hence the performance of the antenna is very sensitive to manufacturing errors. Hence an offset feed is proposed to increase the perturbation area.

In applying segmentation method an explicit matrix input impedance formula is derived to determining the input impedance. A *Duroid* substrate with 1.575 mm thickness is used. An investigation is carried out to examine how the total area of the perturbed segment and the input impedance varies with the offset position of a microstrip feed. With a compromise offset feed position, a simple matching network is designed to achieve a compact matched antenna. The predicted, simulated and measured results are compared.

In Chapter 6 two compact probe feed U-slot rectangular patch antennas are designed and the input impedance is determined. The initial design equations are used to obtain a first-pass antenna design. An explicit matrix input impedance formula is derived for use in the segmentation method. A new matrix augmentation technique has been employed to solve the matrix circuit equations in the U-slot patch analysis. If the initial design does not achieve good matching the antenna dimensions are adjusted using the segmentation method. A *Duroid* substrate was used for each antenna one antenna substrate having a thickness of 1.575 mm and the other a thickness of 3.175 mm. The thicker substrate is used to improve the bandwidth. Predicted, simulated and measured results are presented and compared.

In Chapter 7 the conclusions of the thesis are discussed and a few suggestions for further work to other compact patch antennas are proposed for which the formulas and techniques presented in this thesis will be needed.

1.3 Significant Achievements of the Research Work

The significant research work have been achieved as

- Three compact patch antennas have been investigated and, the dimensions and the input impedances also were determined.
- Using the cavity model and the equivalent circuit model, new and simple design equations have been derived for a CP nearly square patch antenna.
- An offset feed on a CP patch was used to increase the perturbation area thereby reducing the effect of the manufacturing errors.
- A simple matching network consisting of a short length of microstrip line was designed to achieve a compact matched antenna.
- New formulas involving the internal feed port on a rectangle and on an isosceles right-angled triangle were derived in detail.
- For the application of the segmentation method, new explicit matrix input impedance formulas were derived to determining the input impedance of a CP offset microstrip feed truncated corners square patch antenna, and a LP probe feed U-slot rectangular patch antenna.
- A new matrix augmentation technique has been employed to solve the matrix circuit equations in the U-slot patch analysis.
- The design procedures of the antenna have been implemented using Mathcad programs.
- Using the new impedance formulas the computational run time is considerably less than that required by simulation for obtaining the input impedances.
- All the predicted, simulated and measured results were in a good agreement.

1.4 Research Work Published

The research papers have been published or accepted.

1. S. K. Lee, Y. Qin, and E. Korolkiewicz, "Reduction of the second and third harmonics for a rectangular microstrip patch antenna," *Microw. Opt. Technol. Lett.,* vol. 40, no. 6, pp. 455-460, Mar. 2004.
2. S. K. Lee, A. Sambell, E. Korolkiewicz, S. F. Ooi, and Y. Qin, "Design of a circular polarized nearly square microstrip patch antenna with offset feed," in *9th IEEE High Frequency Postgraduate Student Colloquium*, Sep. 2004, pp. 61-66.
3. S. K. Lee, A. Sambell, E. Korolkiewicz, S. F. Loh, S. F. Ooi, and Y. Qin, "A design procedure for a circular polarized, nearly square patch antenna," *Microw. Journal*, vol. 48, no. 1, pp. 116-128, Jan. 2005.
4. S. K. Lee, A. Sambell, E. Korolkiewicz, and S. F. Ooi, "Analysis and design of a circular-polarized nearly-square-patch antenna using a cavity model," *Microw. Opt. Technol. Lett.,* vol. 46, no. 4, pp. 406-410, Aug. 2005.
5. S. K. Lee, S. F. Ooi, E. G. Lim, E. Korolkiewicz, and A. Sambell, "Efficient coupling impedance formulas for the right-angled isosceles triangular patch for use in segmentation analysis," in *Proc. 36th Eur. Microw. Conf.*, Manchester, UK, Sep. 2006, pp. 241-244.
6. S. F. Ooi, S. K. Lee, A. Sambell, E. Korolkiewicz, and P. Butterworth, "Design of a high efficiency power amplifier with input and output harmonic terminations," *Microw. Opt. Technol. Lett.,* vol. 49, no. 2, pp. 391-395, Feb. 2007.
7. S. F. Ooi, S. K. Lee, A. Sambell, E. Korolkiewicz, and S. Scott, "The design of H-shaped microstrip patch antennas," *Microw. Opt. Technol. Lett.,* vol. 49, no. 4, pp. 791-795, Apr. 2007.
8. S. F. Ooi, S. K. Lee, A. Sambell, E. Korolkiewicz, and S. Scott, "A new and explicit matrix input impedance formula for the H-shaped microstrip patch antenna," *Microw. Opt. Technol. Lett.,* vol. 49, no. 7, pp. 1756-1759, Jul. 2007.
9. S. F. Ooi, S. K. Lee, A. Sambell, E. Korolkiewicz, S. Gao, and P. Butterworth, "Harmonic-suppressed slot-coupled microstrip patch antenna with enhanced bandwidth," *Microw. Opt. Technol. Lett.,* vol. 49, no. 8, pp. 1827-1829, Aug. 2007.
10. S. K. Lee, S. F. Ooi, E. G. Lim, E. Korolkiewicz, and A. Sambell, "Explicit efficient coupling impedance formulas for the right-angled isosceles triangle and application to a circularly polarised truncated corners square patch antenna," *IET Microw. Antenna Propag.*, 2007 (Accepted for publication).

CHAPTER 2 REVIEW OF MODELLING, CIRCULAR POLARISATION AND COPLANAR ANALYSIS OF MICROSTRIP PATCH ANTENNAS

2.1 Introduction

Microstrip patch antennas are normally analysed and designed using the transmission-line, cavity, and full-wave models which are discussed in Section 2.2. In this thesis, both the transmission-line and cavity models are used in the design of single-feed CP and LP patch antennas.

The polarisations of an antenna are discussed in Section 2.3.1. Dual-feed CP antennas are discussed in Section 2.3.2 and the single-feed case in Section 2.3.3.

An introduction to coplanar multiport circuit analysis and its application in the segmentation method is given in Section 2.4. Applications of this analysis to obtain input impedances are used throughout this thesis for composite antenna geometric shapes.

2.2 Introduction to Microstrip Patch Antennas

Microstrip antennas because of their many advantages are widely used in satellite systems, telemetry, mobile radios, control systems, remote sensing, medical equipment, GPS, geographic information system (GIS), WLAN, and tolling systems.

Their main advantages are that they have a low profile, are lightweight and inexpensive to fabricate, and, are conformable with planar and non-planar surfaces. In addition as the antenna is compact it is compatible with microwave integrated circuits (MIC). The main disadvantages are that the antenna has a narrow bandwidth, low gain, and is sensitive to fabrication errors [2]-[5].

Patch antennas usually have regular geometrical shapes such as rectangular, circular, triangular, dipole (thin strip), elliptical, circular sector, annular ring, and ring sector. Feed arrangements include microstrip line, probe, aperture-coupled, electromagnetic-coupled feed, and coplanar waveguide (CPW) excitations.

The rectangular patch shown in Figure 2.1 is possibly the most commonly used configuration as it is simple to design and model. It consists of a very thin metallic patch placed on a dielectric substrate of thickness 'h' on a ground plane. The physical length L controls the resonant frequency while the width W determines the input impedance of the antenna.

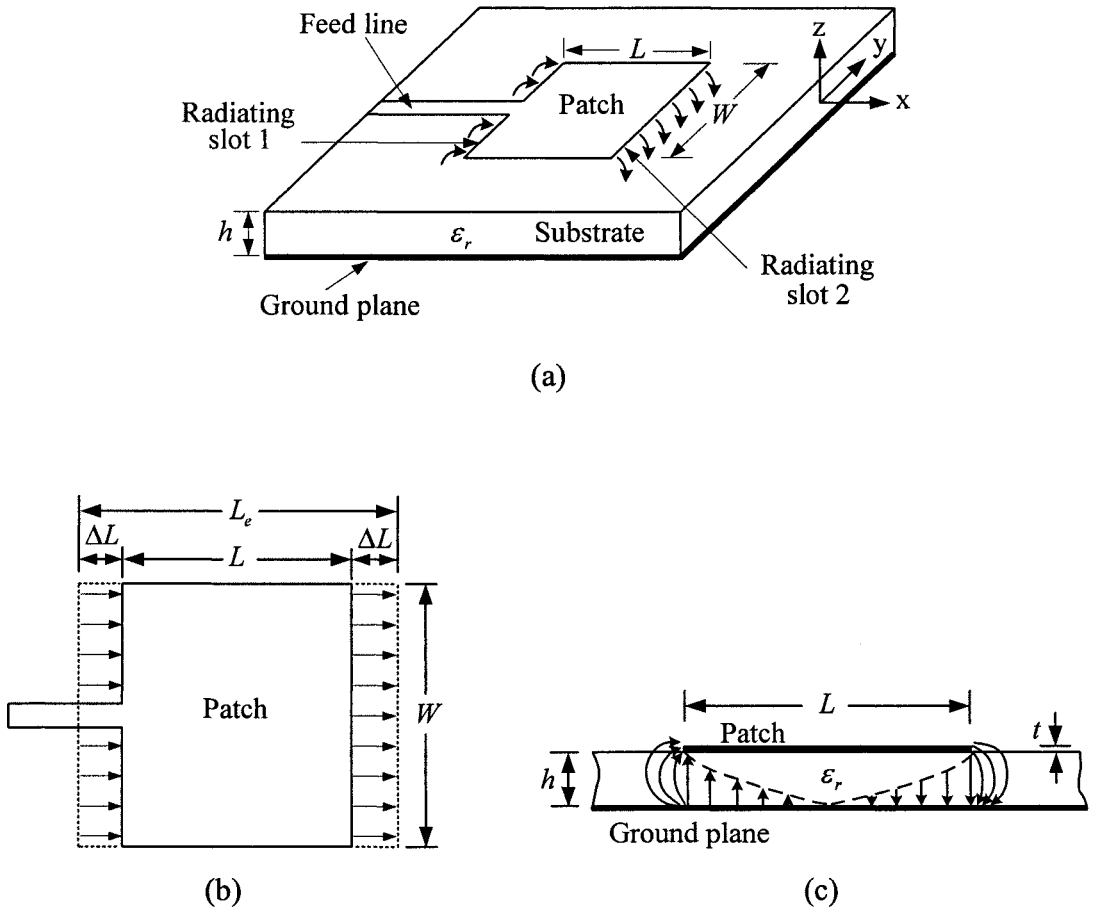

Figure 2.1. (a) Microstrip patch antenna. (b) Top view. (c) Side view.

The horizontal components of the fringing electric fields present at the feed edge and at the opposite edge of the antenna patch generate far field radiation while the vertical field components cancel in the far field.

The fringing electric fields along the length L are partly in the substrate and partly in air. Hence an effective dielectric constant ε_{reff} is introduced which is a function of width and the height of the substrate and is given by equation (2.1) [6]

$$\varepsilon_{reff} = \frac{\varepsilon_r + 1}{2} + \frac{\varepsilon_r - 1}{2\sqrt{1 + 12h/W}}. \tag{2.1}$$

The length of the fringing field ΔL is given by an approximate equation (2.2) given in [6].

$$\Delta L = 0.412h \frac{(\varepsilon_{reff} + 0.3)\left(\frac{W}{h} + 0.262\right)}{(\varepsilon_{reff} - 0.258)\left(\frac{W}{h} + 0.813\right)}. \tag{2.2}$$

A more accurate formula for ΔL is given by the following equation [7].

$$\Delta L = (\xi_1 \xi_3 \xi_5 / \xi_4)h \tag{2.3}$$

where

$$\xi_1 = 0.434907 \frac{\varepsilon_{reff}^{0.81} + 0.26}{\varepsilon_{reff}^{0.81} - 0.189} \frac{(W/h)^{0.8544} + 0.236}{(W/h)^{0.8544} + 0.87} \tag{2.4a}$$

$$\xi_2 = 1 + \frac{(W/h)^{0.371}}{2.358\varepsilon_r + 1} \tag{2.4b}$$

$$\xi_3 = 1 + \frac{0.5274 \arctan\left[0.084(W/h)^{1.9413/\xi_2}\right]}{\varepsilon_{reff}^{0.9236}} \tag{2.4c}$$

$$\xi_4 = 1 + 0.0377 \arctan\left[0.067(W/h)^{1.456}\right]\left[6 - 5e^{0.036(1-\varepsilon_r)}\right] \tag{2.4d}$$

$$\xi_5 = 1 - 0.218e^{-7.5W/h}. \tag{2.4e}$$

As reported in [7] the formula (2.3) is more accurate than formula (2.2) hence formula (2.3) is adopted in this thesis.

A simple design equation for the physical dimension W of the rectangular patch [5] is

$$W = \frac{c_0}{2f}\sqrt{\frac{2}{\varepsilon_r + 1}}. \tag{2.5}$$

The effective length L_e of the magnetic wall is a half-wavelength long so the physical L length of the patch is given by

$$L = \frac{c_0}{2f\sqrt{\varepsilon_{reff}}} - 2\Delta L \tag{2.6}$$

where f is the resonant frequency of the TM_{10} mode.

The most popular models used in antenna design include the transmission-line [8]-[10], cavity [11], [12], and full-wave models [13]-[15]. The transmission-line model is by far the most commonly used method as it gives a good physical and engineering insight into the operation of the antenna. Compared to the transmission-line model, the cavity model is more complex but is more accurate and it can be used for other antenna geometrics [5]. The advantages of both models are in terms of computational simplicity but their basic limitation is that in application, accuracy decreases as the substrate thickness and/or the dielectric constant increases.

Full-wave models are more complex and require extensive computer time, but they are very accurate, very versatile, and can model single elements, arbitrary geometrical shaped elements, arrays, stacked elements, and coupling.

The three modelling approaches are described briefly in the following sections.

2.2.1 Transmission-line model

The basic transmission-line model for a rectangular patch antenna with a centred microstrip line feed (see Figure 2.2(a)) was proposed by Munson [9]. In Figure 2.2(b), the radiating slots 1 and 2 produced by the electric fringing fields are modelled as two parallel

admittances Y connected by a transmission line of physical length L and characteristic admittance Y_c. The radiated power at each edge is modelled by the conductance G_1 and the power lost due to the coupling between the two slots by (G_{12}) [16]. The electrical length extensions due to the two slots are modelled as two capacitive susceptances B_1.

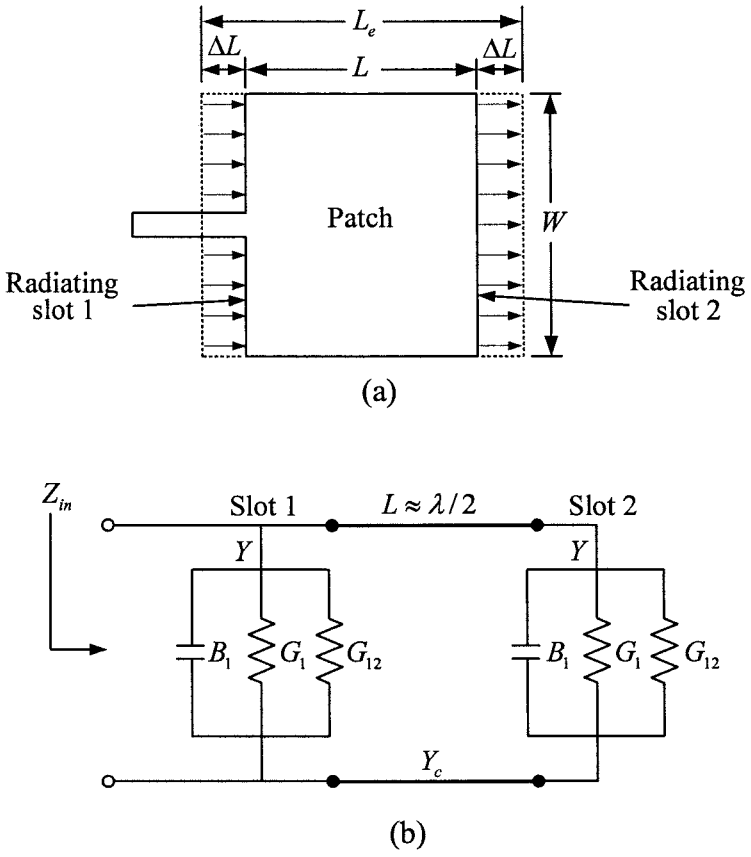

Figure 2.2. (a) Rectangular patch. (b) Transmission-line model equivalent circuit.

As the physical length L is slightly less than $\lambda/2$ the resonant input impedance for the TM_{10} mode is given by equation (2.7)

$$Z_{in} = R_{in} = \frac{1}{2(G_1 \pm G_{12})} \tag{2.7}$$

where the (+) sign corresponds to the odd modes and the (−) sign to the even modes. The conductances G_1 and G_{12} can be obtained from the following equations given in [5].

The conductance G_1 is given by

$$G_1 = \frac{2P_{rad}}{|V_0|^2} \tag{2.8}$$

The radiated power is given by

$$P_{rad} = \frac{|V_0|^2}{2\pi\eta_0} \int_0^{\pi} \left[\frac{\sin\left(\frac{k_0 W}{2}\cos\theta\right)}{\cos\theta} \right]^2 \sin^3\theta \, d\theta \tag{2.9}$$

where $\eta_0 = 120\pi$ ohms, $k_0 = 2\pi/\lambda_0$ is the phase constant in free space, and V_0 is the voltage across the slot.

The mutual conductance G_{12} is given by [16], [17],

$$G_{12} = \frac{1}{120\pi^2} \int_0^{\pi} \left[\frac{\sin\left(\frac{k_0 W}{2}\cos\theta\right)}{\cos\theta} \right]^2 J_0(k_0 L \sin\theta) \sin^3\theta \, d\theta \tag{2.10}$$

where J_0 is the order zero Bessel function of the first kind.

This basic model [9] was improved in [10] where the effect of the complex coupling impedance is taken into account by voltage dependent current generators. Also included is the effect of the side slots on the radiation conductance.

The transmission-line model was originally developed for rectangular patches but has been extended to more general patch shapes [2], [18]. A transmission-line model has also been used in the modelling of a wide bandwidth slot-coupled rectangular patch antenna [19] where different substrates are used for the feed network and the patch.

2.2.2 Cavity model

In the cavity model, the region between the patch and the ground plane is considered as a cavity bounded by four vertical magnetic walls and, electric walls on the patch and ground plane [11]. If the thickness of the substrate is much less than a wavelength the electric field inside the cavity is uniform in the z direction along the thickness of the substrate (see Figure 2.3).

Applying the magnetic wall boundary conditions the wavenumber components are given by [5]

$$k_x = m\pi / L_e, \quad k_y = n\pi / W_e, \tag{2.11}$$

where L_e and W_e are the effective dimensions of the patch and

$$k_x^2 + k_y^2 = \left(\frac{m\pi}{L_e}\right)^2 + \left(\frac{n\pi}{W_e}\right)^2 = k_{m,n}^2 = \omega^2 \mu\varepsilon = \omega^2 \mu_0 \varepsilon_0 \varepsilon_{reff} \tag{2.12}$$

where $m = 0,1,2,\ldots$, $n = 0,1,2,\ldots$, and $m = n \neq 0$.

The resonant frequencies for the TM_{mn} modes are given by

$$f_{mn} = \frac{c_0}{2\pi\sqrt{\varepsilon_{reff}}}\sqrt{\left(\frac{m\pi}{L_e}\right)^2 + \left(\frac{n\pi}{W_e}\right)^2}\,. \tag{2.13}$$

The electric fields for the TM_{10} and TM_{01} modes are shown in Figure 2.3, their resonant frequencies f_{10}, f_{01} are given by

$$f_{10} = \frac{c_0}{2L_e\sqrt{\varepsilon_{reff}}}, \tag{2.14}$$

and,

$$f_{01} = \frac{c_0}{2W_e\sqrt{\varepsilon_{reff}}}. \tag{2.15}$$

These two modes are important as they are used to generate circular polarisation.

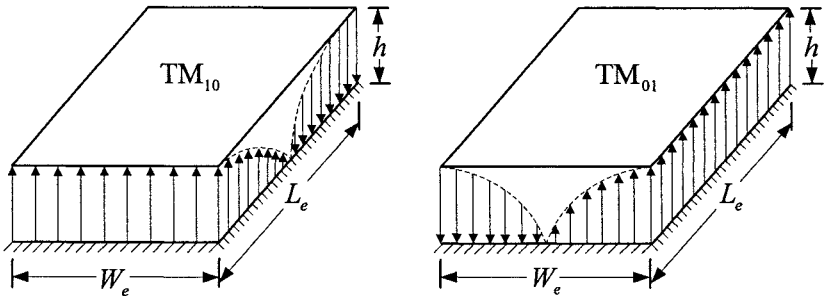

(a) (b)

Figure 2.3. Field configurations (modes) for rectangular microstrip patch. (a) TM_{10} mode. (b) TM_{01} mode.

The design for a CP rectangular patch antenna and the input impedance, using the cavity model are discussed in [20], [21]. In [22], using the reaction theorem the input impedance is derived in terms of the dimensions of a coax-fed stacked dual frequency electromagnetic-coupled antenna. A modified Wolf model was proposed in [23] to compute a more accurate value of the resonant frequency for a rectangular patch antenna with a thick substrate. Zhang and Wang [24] suggested an improved cavity model to obtain the input impedance of a differentially driven rectangular antenna which is used in efficient active power amplifiers. For a circular patch antenna with a variable air gap below the substrate an improved design formula for the input impedance is derived in [25].

2.2.3 Full-wave modelling analysis

In full-wave modelling analysis the electric current density distribution on the patch conductor is used to determine the mode frequencies. This model maintains rigor and accuracy at the expense of computational simplicity. The principle assumption in the full-wave model is that the substrate and ground plane are infinite in lateral dimensions, thus no

fringing field is considered. The formulation of the solution is based on rigorously enforcing the boundary conditions at the air-dielectric interface. This is done by using the exact Green's function for the composite dielectric [2]-[4].

The boundary condition at the patch produces an integral equation of the form

$$E(x,y) = \int_{S(x,y)} G\, J(x,y)\, dx\, dy \tag{2.16}$$

where, $J(x,y)$ is the current density on the patch.

This equation is solved by the moment method, by taking $J(x,y)$ in the expanded form

$$J(x,y) = \sum_{n=1}^{\infty} c_n\, J_n(x,y) \tag{2.17}$$

where, $J_n(x,y)$ are a chosen set of basis functions, and, c_n are the expansion coefficients obtained by solving the above integral equation.

In a purely numerical approach the finite difference time domain (FDTD) method given in [26] replaces Maxwell's equations by their finite difference equivalence. The infinite space is replaced by an enclosed absorbing boundary domain on which conditions are imposed emulating the condition at infinity so that there are no reflected waves [26], [27]. An initial field is injected into the antenna structure and the difference equations solved for the fields throughout the space domain for each time step until a steady state is obtained. The electric current distributions at all points on the difference grid on the conducting element can then be obtained from which all the other parameters of interest can be derived.

2.3 Dual- and Single-Feed CP Patch Antennas

In this section a review is presented of different patch geometries and feeds used to produce circular polarisation. For a single-feed the geometries discussed in this section are based on a perturbed square patch.

2.3.1 Elliptical, linear, and circular polarisation

Linear, circular, and elliptical polarisations are shown in Figure 2.4 where the plane wave is assumed to be travelling in the positive z direction.

If the electric field has unequal field components E_1, E_2 with an arbitrary phase difference, then the resultant vector **E** produces an ellipse as shown in Figure 2.4(a).

Two linear polarisations are shown in Figure 2.4(b) where the electric field has only one component either E_1 (horizontal) or E_2 (vertical).

Circular polarisation is produced when E_1 and E_2 are equal in magnitude and $\pm 90^\circ$ out of phase. As shown in Figure 2.4(c), if $\theta = +90^\circ$, the electric field vector is rotating clockwise (LHCP), and, for $\theta = -90^\circ$, the electric field vector rotates counter-clockwise (RHCP) [28].

For practical antennas it is not possible to achieve ideal circular polarisation and the deviation from the ideal condition is measured by the axial ratio (AR) [2]. The axial ratio is defined as [5], [28],

$$\mathrm{AR} = \frac{\text{major axis}}{\text{minor axis}} = \frac{OA}{OB}, \qquad (1 \le AR \le \infty) \tag{2.18}$$

where,

$$OA = \left[\frac{1}{2}\left\{E_1^2 + E_2^2 + \left[E_1^4 + E_2^4 + 2E_1^2E_2^2\cos(2\theta)\right]^{1/2}\right\}\right]^{1/2}, \tag{2.19}$$

$$OB = \left[\frac{1}{2}\left\{E_1^2 + E_2^2 - \left[E_1^4 + E_2^4 + 2E_1^2E_2^2\cos(2\theta)\right]^{1/2}\right\}\right]^{1/2}. \tag{2.20}$$

For practical antennas the 3-dB bandwidth for the axial ratio is normally used.

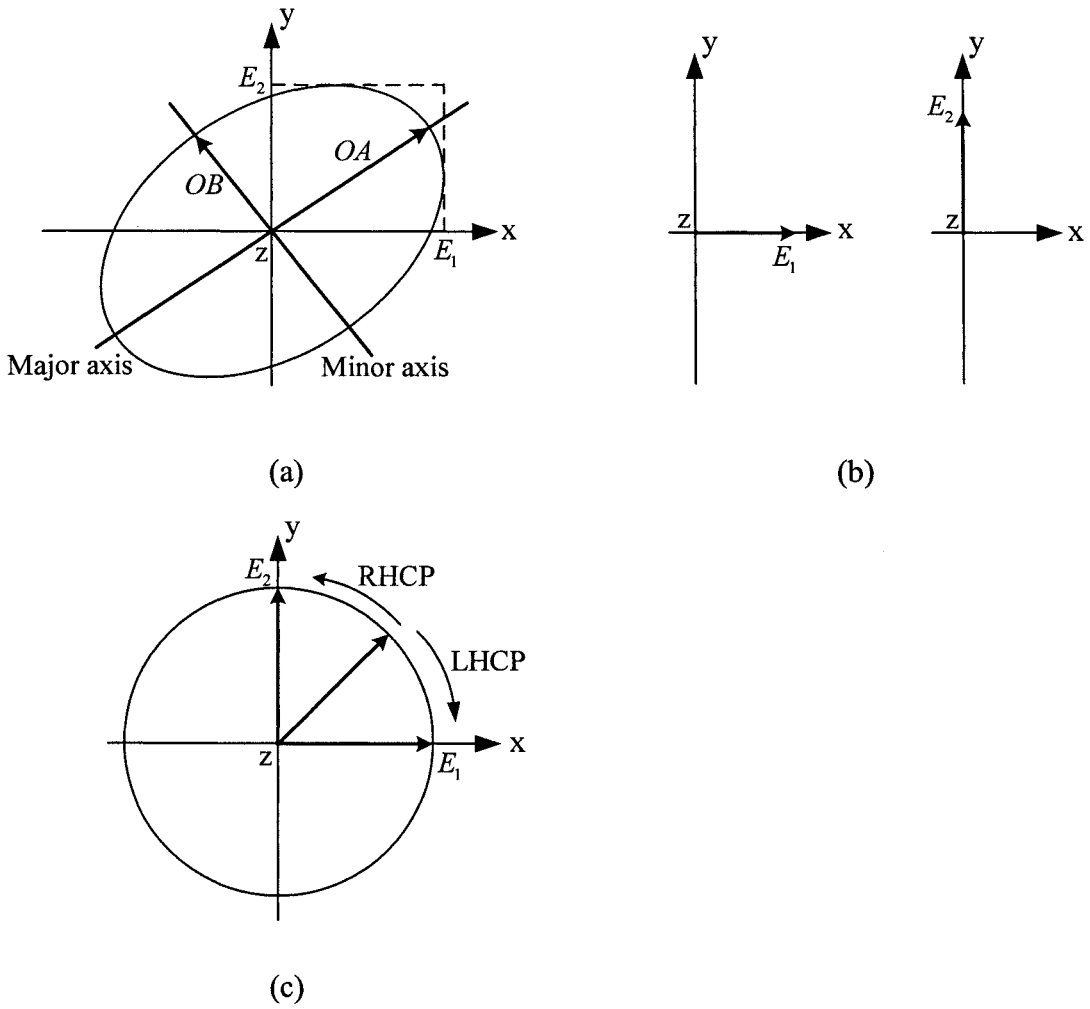

Figure 2.4. Wave polarisation (wave approaching). (a) Elliptical polarisation. (b) Horizontal and vertical linear polarisations. (c) Circular polarisation.

Circular polarised patch antennas can be realised using either a dual-feed, or, a single-feed. For the dual-feed patch antenna an external polariser is required. A single-feed does not require an external polariser, the patch being perturbed in such a way that the conditions for circular polarisation are met.

2.3.2 External polarisers for a square patch antenna

The two common external polarisers (see Figure 2.5) used to excite a square patch are, the 90° hybrid coupler [8], [29], [30], and, the power divider [8], [31].

RHCP or LHCP can be obtained by using a coupler with a feed either at port 1 or port 4 as shown in Figure 2.5(a) while in Figure 2.5(b), the square patch is excited by a power divider with one length a quarter-wavelength longer than the other so as to obtain circular polarisation.

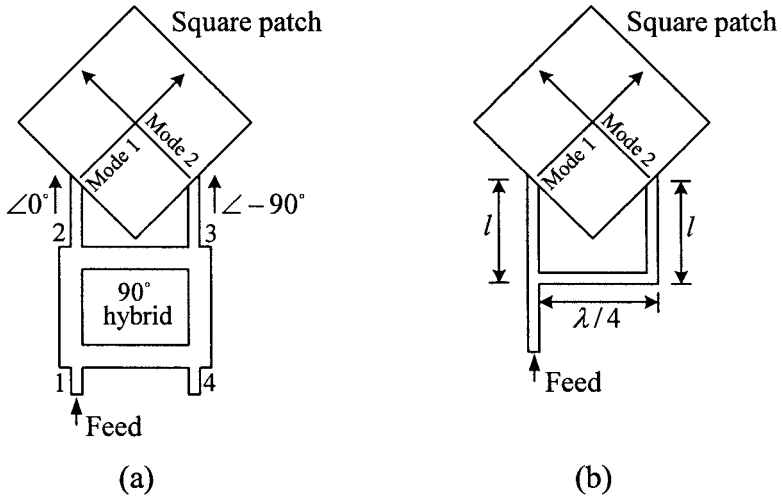

Figure 2.5. Dual-feed CP patch antennas. (a) A square patch with a 90° hybrid. (b) A square patch with a power divider.

The bandwidth for both matching and axial ratio is broader [32] for the 90° hybrid than for the power splitter. A CP antenna can also be obtained using an electromagnetically-coupled dual-feed square patch antenna [33]. This antenna structure is used in phased array applications for mobile satellite communications.

The bandwidth was further increased by feeding an aperture-coupled square patch antenna with a three-branch hybrid coupler [34]. For an array, the bandwidth of the matching and the axial ratio can be increased for a 2x2 or 4x4 configuration by using a corporate feed to produce sequential rotation as discussed in [35].

2.3.3 Single-feed CP patch antennas

A single-feed CP patch antenna has the advantages that it does not require an external polariser, is compact, and, the feed impedance can be controlled by the feed location. Further, the complexity of the dual-feed arrangement is avoided.

The main disadvantage of the single-feed antenna is that it has a narrow axial ratio bandwidth when compared with the dual-feed CP patch antennas using a 90° hybrid. This narrow bandwidth is due to the fact that the perturbation segment causes the designed operating frequency to lie between the frequencies of the two orthogonal generated modes [36] which are very close to each other.

Single-feed circular polarisation is produced by perturbing a square patch [12], [32] to generate two orthogonal modes of equal amplitude and 90° out of phase. Two such perturbations of a square patch are shown in Figure 2.6 [12], [32], [37]. The area of the perturbation must satisfy the circular polarisation condition as shown in Figure 2.7. Both types of antennas are designed using perturbation theory [32], together with the equivalent circuit model, or, the cavity model [12], [38].

For the feeds shown in Figure 2.6 formulas for the area of perturbation have been obtained in [32].

For the corner deleted patch (Figure 2.6(a)) the ratio of the area of the perturbation segment (ΔS), and, the area of the unperturbed square patch S, is given by,

$$\frac{\Delta S}{S} = \frac{1}{2Q} \tag{2.21}$$

and for the nearly square patch

$$\frac{\Delta S}{S} = \frac{1}{Q} \tag{2.22}$$

where, Q is total quality factor.

It is interesting to note that from equations (2.21) and (2.22) the area of the perturbing element for the nearly square patch antenna is larger than that for the truncated corners square patch.

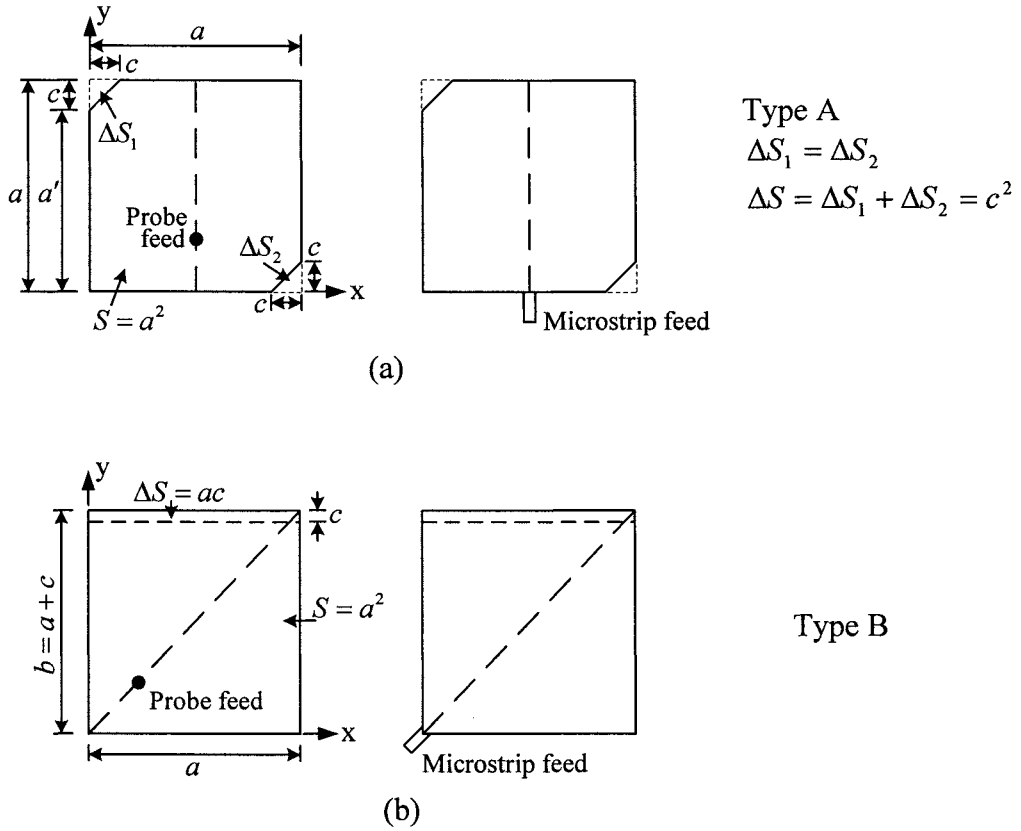

Figure 2.6. Single-feed CP antennas. (a) Truncated corners square patch with a probe centre line feed, or, with a microstrip centre feed as Type A antenna. (b) Nearly square patch with a probe diagonal feed, or, with a microstrip corner feed as Type B antenna.

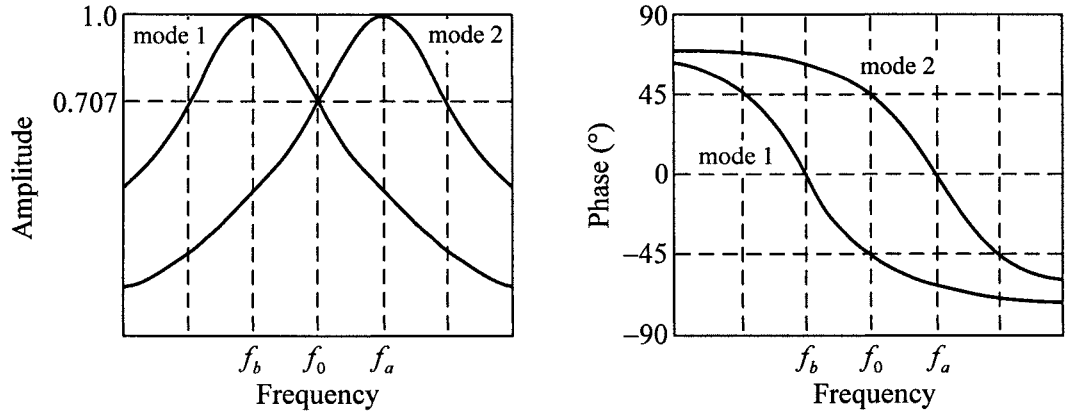

Figure 2.7. Amplitude and phase of the two modes for Type A and Type B antennas.

Richards *et al* [12], [39] has obtained equations for the modulus and phase conditions in terms of the patch dimensions. For a given feed position these equations are plotted, and circular polarisation is realised if they intersect and the dimensions of the perturbed patch can then be obtained.

An alternative approach [20] is to use the following equation in which 'a' and 'b' are the dimension of the nearly square patch.

$$A=\frac{b-a}{b}Q\pm\left[\left(\frac{b-a}{b}Q\right)^2-\frac{a}{b}\right]^{1/2}. \tag{2.23}$$

where, $A=\left[\cos(\pi y_0/b)\right]/\left[\cos(\pi x_0/a)\right]$ and, (x_0,y_0) is the feed position. For a given Q-factor, and feed location, the patch dimensions for circular polarisation are realised only if the roots A_1, A_2 of equation (2.23) are real.

Other shapes for perturbed CP patch antennas for a single centre line feed shown in Figure 2.8(a)-(f) have been reported in [4], [40]. In these antennas the mode resonant frequency of one diagonal is higher than the mode of the other diagonal.

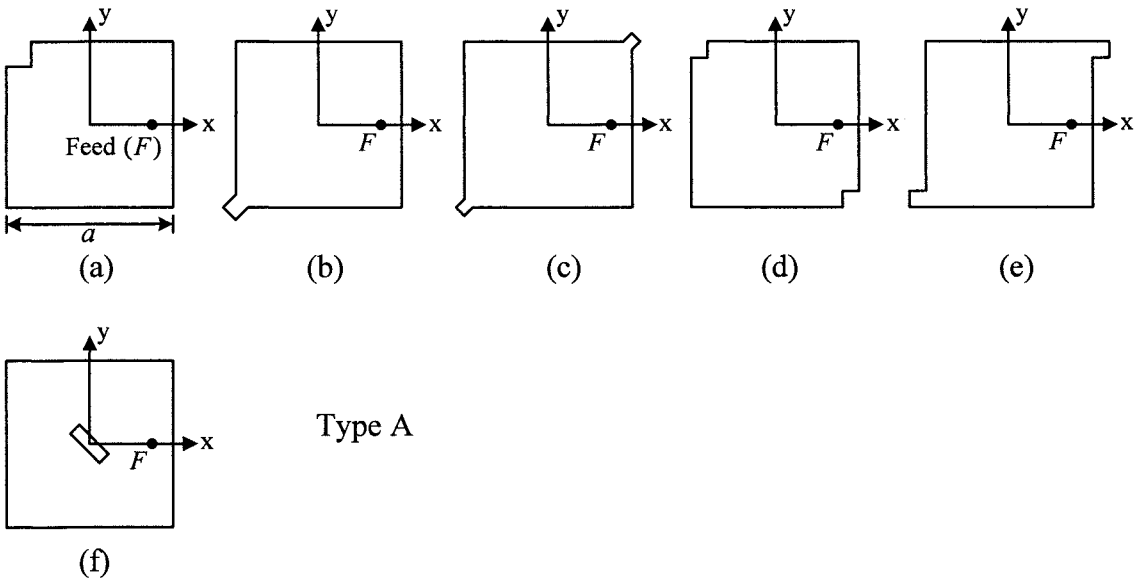

Figure 2.8. A CP single centre line feed square patch. (a) A notch at corner. (b) A diagonal stub at corner. (c) Two diagonal stubs at corner. (d) Two notches at corners. (e) Two stubs at corner. (f) A diagonal narrow rectangular slot.

Other topologies that can be used to produce circular polarisation are shown in Figure 2.9 where the feed is along the diagonal [40]-[42]. The advantage of these configurations is that they lend themselves to fine-tuning by adjusting the size of the perturbation segment.

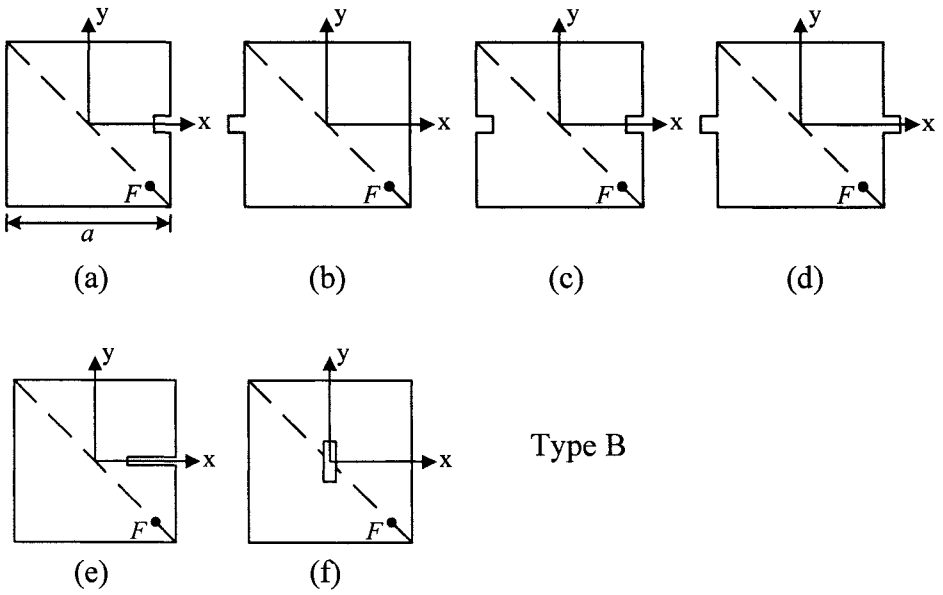

Figure 2.9. A CP single diagonal feed square patch. (a) A notch at centre-edge. (b) A stub at centre-edge. (c) Two notches at opposite edges. (d) Two stubs at opposite edges. (e) A slit. (f) A centre thin rectangular slot.

In order to improve the axial ratio bandwidth, a cross-aperture coupled-patch antenna shown in Figure 2.10 is used. The two orthogonal slots of the cross-aperture excite the independently two separate TM_{10} mode and the TM_{01} modes to produce circular polarisation.

This antenna was analysed using a transmission-line model [43], and, using a cavity model [44]. In the transmission-line model, the two modes are modelled by two transmission lines in the x and y directions. The dimensions of the patch, lengths of slots and that of the open stub, are determined to satisfy the conditions for circular polarisation.

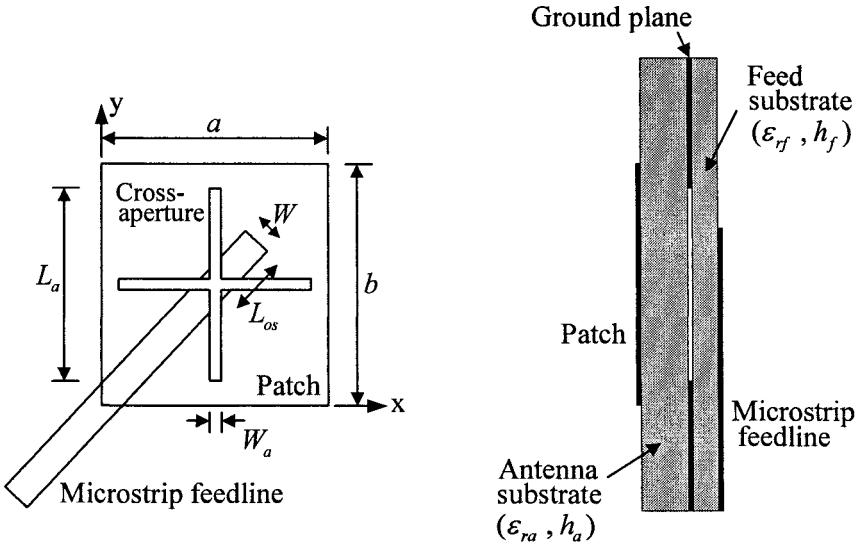

Figure 2.10. A single-feed CP cross-aperture coupled nearly square patch antenna.

In the cavity model equivalent magnetic current sources are used to determine the electric and magnetic fields under the patch. Expressions for the patch admittances at the aperture are then derived. These admittances are used in the equivalent circuit [44] to determine the input impedance and the axial ratio.

To increase the bandwidth of the axial ratio stacked microstrip patch antennas are used with an air gap between the driven patch and the parasitic patch [45]-[48]. A single-feed array structure is reported [49].

To obtain a more compact form of single-feed CP antenna, a square-shaped slot can be used at the centre of the patch in order to lengthen the fundamental mode current path thereby lowering the operating frequency [50], [51]. A compact antenna can also be achieved using cutting slits [52], or, slits and L-shaped slots [53] or, by using a high permittivity substrate [54].

2.4 Coplanar Multiport Analysis and the Segmentation Method

In this thesis the segmentation method is used to obtain the matrix input impedance formula for thin substrate antennas with composite antenna geometries made up of regular shapes for which the Green's function is known. For a thin substrate antenna structure it is possible to apply coplanar circuit analysis to derive the elements in the coupling impedance matrices which are used in the segmentation method.

2.4.1 The coupling impedance formula in terms of the Green's function

A general patch antenna structure with the magnetic wall is shown in Figure 2.11 below.

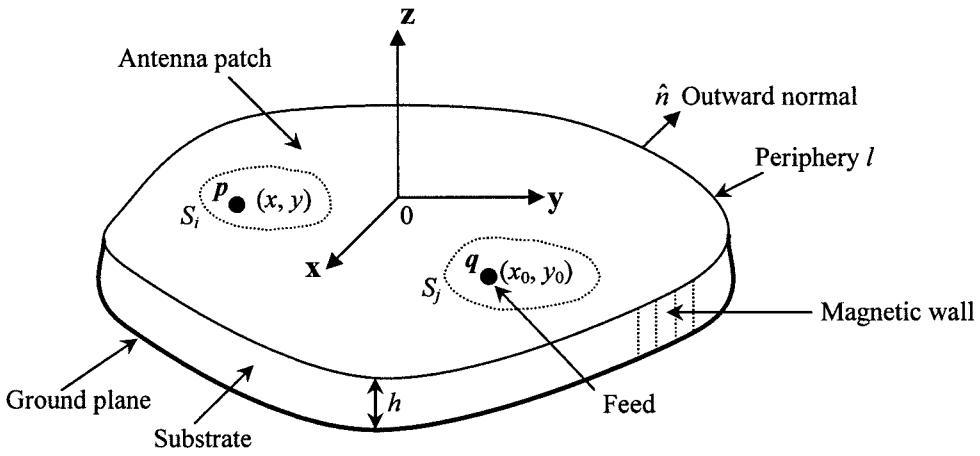

Figure 2.11. Antenna structure with probe feed – Cavity model.

From Maxwell's equations applied to the above structure it can be shown that the patch voltage $V(x,y)$ on the port (S_i) due to a current source density, $J(x_0,y_0)$ on the port (S_j) is given by [55]

$$V(x,y) = \int_{S_j} G(x,y|\,x_0,y_0)\,J(x_0,y_0)\,dx_0\,dy_0 \tag{2.24}$$

where, $G(x,y|x_0,y_0)$ is the Green's function for the patch geometry.

A terminal voltage V_i on the segment S_i is defined as the average voltage over the port area S_i, so that

$$V_i = \frac{1}{S_i}\int_{S_i} V(x,y)\,dx\,dy. \tag{2.25}$$

On substituting $V(x,y)$ from equation (2.24) into equation (2.25) then gives

$$V_i = \frac{1}{S_i}\int_{S_i}\int_{S_j} G(x,y|x_0,y_0)J(x_0,y_0)\,dx\,dy\,dx_0dy_0\,. \tag{2.26}$$

In applications the areas S_i, S_j of current sources are very small so that the current density $J(x_0,y_0)$ may be replaced by the average density I_j/S_j, where I_j is the total current through S_j. Substituting for $J(x_0,y_0)$ in equation (2.26) gives

$$V_i = \frac{1}{S_i}\int_{S_i}\int_{S_j} G(x,y|x_0,y_0)\frac{I_j}{S_j}\,dx\,dy\,dx_0dy_0$$

$$= \frac{I_j}{S_iS_j}\int_{S_i}\int_{S_j} G(x,y|x_0,y_0)\,dx\,dy\,dx_0dy_0. \tag{2.27}$$

The ratio V_i/I_j is defined [55] as the coupling impedance Z_{ij} between the two ports so that

$$Z_{ij} = \frac{1}{S_iS_j}\int_{S_i}\int_{S_j} G(x,y|x_0,y_0)\,dx\,dy\,dx_0dy_0\,. \tag{2.28}$$

2.4.2 Applications in segmentation method

The segmentation method was first proposed by Okoshi *et al* [56] [57] and was formulated in terms of *S*-matrices. For more efficient computation the *S*-matrices were replaced by *Z*-matrices [58].

This method has been used to determine the input impedance of a compact microstrip probe feed rectangular ring patch antenna [59], [60], and, a bow-tie shaped patch antenna

consisting of a rectangular with four connected triangular segments [61]. The input impedance for arrays of dual-corner-fed square patch antennas is obtained in [62], [63].

The basis of the segmentation method is that the current density distribution on the patch is preserved on each component segment of the segmented structure. Figures 2.12, 2.13 show a simple composite structure of two segments, (α, β) which are connected electrically by interconnecting ports [64].

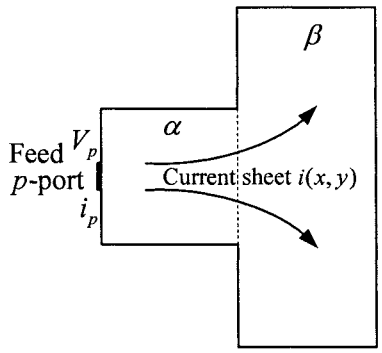

Figure 2.12. Composite structure.

The segmented structure with connecting ports is shown in Figure 2.13, below.

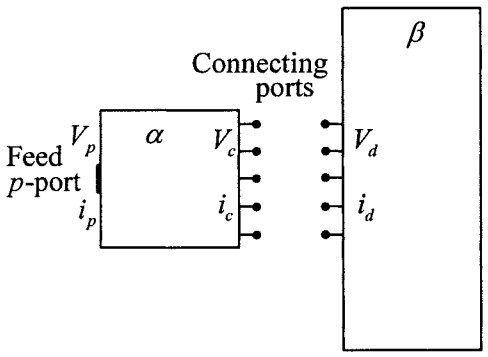

Figure 2.13. Segmental structure.

In the analysis the ports are assigned electric currents and voltages which emulate approximately the original currents and voltages in the composite structure and so preserve, approximately, the original current sheet density distribution on the segments. The system of electric circuit equations connecting the voltages and currents at the connecting ports is used to determine the matrix input impedance formula.

2.4.3 Coplanar matrix circuit equations

The governing current/voltage matrix circuit equations are based upon the coupling impedances. Matrix circuit equations for a single patch and for a two segmented structure are given in examples below.

2.4.3.1 Single segment

A single segment is shown in Figure 2.14.

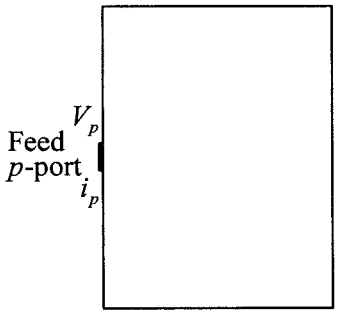

Figure 2.14. Single segment with p-port.

For this elementary case,

$$V_p = Z_{pp} i_p \tag{2.29}$$

where, Z_{pp} is the self-coupling impedance given by formula (2.28), with $i = j = p$.

Hence, the input impedance is given by

$$Z_{in} = \frac{V_p}{i_p} = Z_{pp}. \tag{2.30}$$

2.4.3.2 Two segments

For a two segments structure (see Figure 2.15) there are three matrix circuit equations.

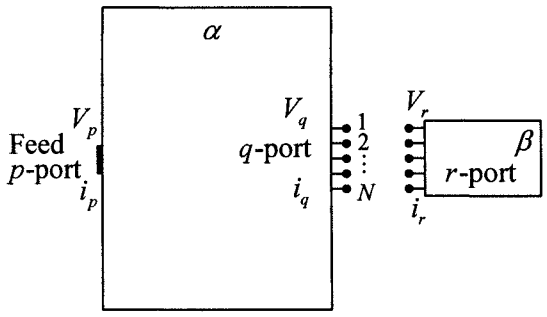

Figure 2.15. Interport structure for two segments.

For the α-segment

$$V_p = Z_{pp} i_p + Z_{pq} i_q \tag{2.31}$$

and

$$V_q = Z_{qp} i_p + Z_{qq} i_q. \tag{2.32}$$

where, the coupling impedance matrices Z_{pq}, Z_{qp}, Z_{qq} are given by

$$Z_{pq} = [Z_{pq_1} \quad Z_{pq_2} \quad \cdots \quad Z_{pq_N}]$$

with, $Z_{qp} = Z_{pq}^{T}$,

and, $$Z_{qq} = \begin{bmatrix} Z_{q_1q_1} & Z_{q_1q_2} & \cdots & Z_{q_1q_N} \\ Z_{q_2q_1} & Z_{q_2q_2} & \cdots & Z_{q_2q_N} \\ \vdots & \vdots & \vdots & \vdots \\ Z_{q_Nq_1} & Z_{q_Nq_2} & \cdots & Z_{q_Nq_N} \end{bmatrix}.$$

The i_q matrix (vector) is

$$i_q = \begin{bmatrix} i_{q_1} \\ i_{q_2} \\ \vdots \\ i_{q_N} \end{bmatrix}.$$

For the β-segment,

$$V_r = Z_{rr} i_r . \tag{2.33}$$

Since $V_q = V_r$, and, $i_q = -i_r$, therefore from equations (2.32) and (2.33),

$$Z_{qp} i_p + Z_{qq} i_q = -Z_{rr} i_q$$

so that,

$$(Z_{qq} + Z_{rr}) i_q = -Z_{qp} i_p$$

hence,

$$i_q = -(Z_{qq} + Z_{rr})^{-1} Z_{qp} i_p . \tag{2.34}$$

The input impedance can now be found by substituting i_q from equation (2.34) into equation (2.31) to give

$$V_p = Z_{pp} i_p + Z_{pq}(-1)(Z_{qq} + Z_{rr})^{-1} Z_{qp} i_p$$

whence,

$$Z_{in} = \frac{V_p}{i_p} = Z_{pp} - Z_{pq}(Z_{qq} + Z_{rr})^{-1} Z_{qp} . \tag{2.35}$$

2.5 Summary

The basic theory, modelling and analysis of microstrip patch antennas have been discussed. The CP dual-feed and single-feed patch antennas have been reviewed and compared.

In respect of the segmentation method the coupling impedances and, matrix circuit equations have been discussed. The elements of the coupling impedance matrices are obtained from coplanar circuit analysis which is based on the cavity model. Also for a simple two-segment patch the determination of the input impedance is demonstrated. The input impedances of the patch antennas discussed in the following chapters have been obtained using the basic methodology described in this chapter.

Based on this study, single-feed CP compact patch antennas are designed in Chapters 3 and 5.

CHAPTER 3 DESIGN AND ANALYSIS OF A CP NEARLY SQUARE PATCH ANTENNA

3.1 Introduction

A CP single-feed microstrip patch antenna can be realised using a perturbed square patch as discussed in Chapter 2. The perturbation element(s) may be in the form of deleted corner segments, slots or, the addition of a rectangle to produce a nearly square patch. For the nearly square patch antenna the feed is normally along the diagonal [12], [32] for which, however, the area of perturbation segment is very small and hence the antenna is very sensitive to manufacturing errors.

Using the cavity model, new design equations to determine the dimensions of the nearly square patch, with a feed in any position, are derived in Section 3.2. Also, new design equations using an equivalent circuit for the antenna are derived in Section 3.3. In this section, for a microstrip feed offset from one corner of the patch, the dimensions of the patch obtained from the two models are compared.

In Section 3.4 the predicted results for two antennas with different substrates, show that the perturbation area increases with offset which reduces the effect of manufacturing errors.

For an offset microstrip feed the input impedance of the antenna is determined, and, the design of a simple matching network is given in Section 3.5. By increasing the offset position the area of the perturbation segment is increased but as the input impedance reduces it becomes difficult to use the proposed simple matching network. It is shown that there is a trade-off between the offset position required to increase the area of the perturbation segment and the realisation of the above matching network.

In Section 3.6 the predicted, modelled and practical results for an antenna design to operate at 2.45 GHz are presented.

Based on the work presented in this chapter three papers have been published [65]-[67].

3.2 Derivation of New Design Equations for a CP Nearly Square Patch Antenna Using the Cavity Model

A design approach using the cavity model for a nearly square patch antenna was proposed by Aksun *et al* [20]. In this approach the effective patch dimensions a_e and b_e were first selected and then tested in a derived equation to determine if they were compatible with the conditions of circular polarisation.

If not compatible the dimensions of the patch were iterated by trial and error to obtain suitable values. To circumvent this cumbersome methodology a new approach is presented in this section.

For a nearly square patch two feed loci which produce RHCP and LHCP are shown in Figure 3.1(a). A microstrip feed $(0 \le x_{0e} < 0.5a_e$ and, $y_{0e} = 0)$ for RHCP is shown Figure 3.1(b). In Figure 3.1(c), A_1 and A_2 indicate the areas on the patch where the feed positions give RHCP and LHCP.

The general objectives of the design are to determine the dimensions of the patch and the loci of the feed.

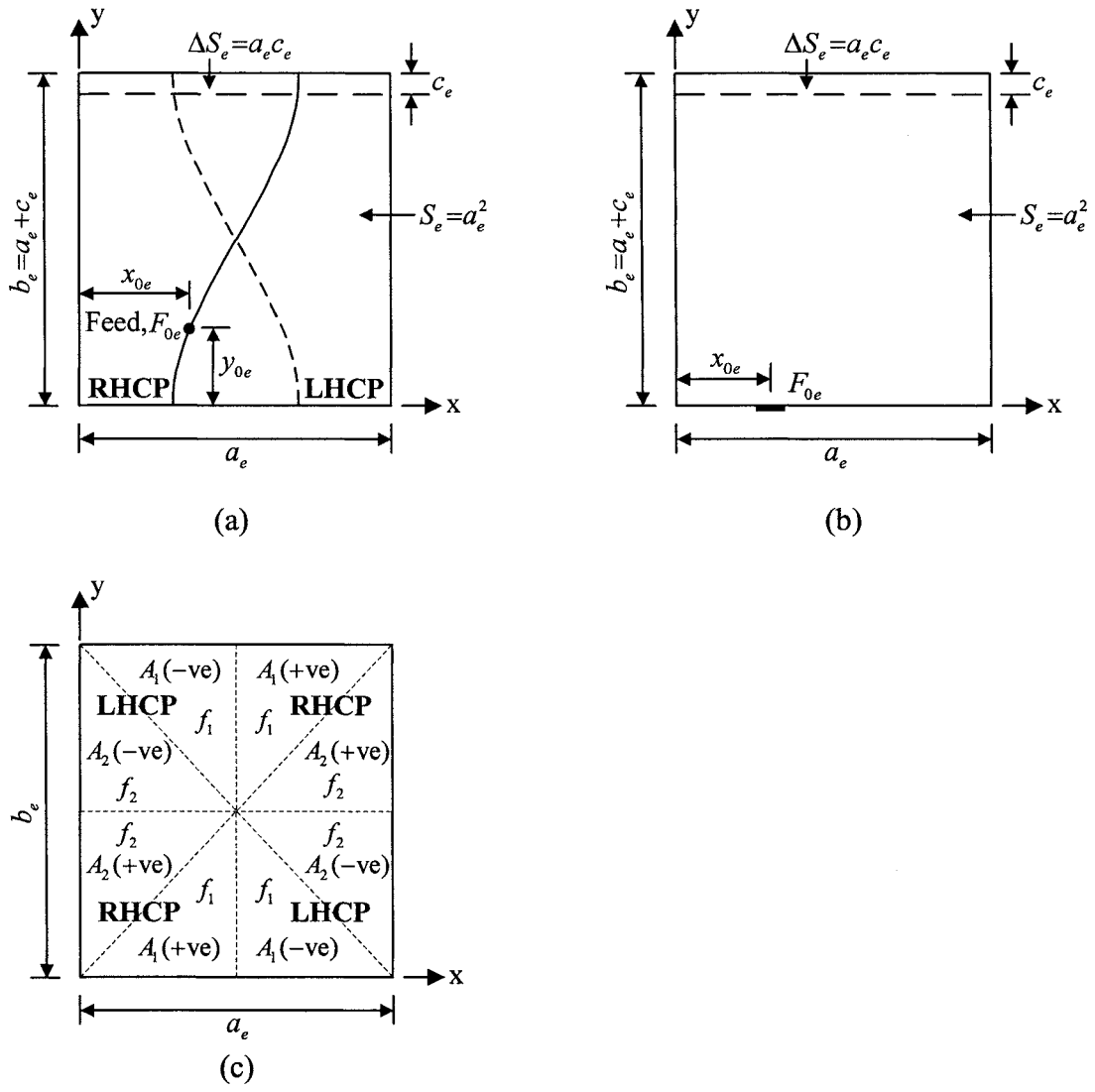

Figure 3.1. CP nearly square patch antenna with effective dimensions $b_e > a_e$. (a) Offset probe feed. (b) Offset microstrip feed. (c) General areas on a patch for a feed.

For the cavity model the electric fields for the TM_{10} and TM_{01} modes are given by [20], [39],

$$E_x \propto \frac{\cos(\pi x_{0e} / a_e)}{k_e - k_{10}}, \tag{3.1a}$$

and,

$$E_y \propto \frac{\cos(\pi y_{0e} / b_e)}{k_e - k_{01}}. \tag{3.1b}$$

For circular polarisation the ratio E_y / E_x must satisfy the following two conditions

$$\frac{E_y}{E_x} \cong A\frac{k_e - k_{10}}{k_e - k_{01}} = 1\angle \pm 90^\circ = \pm j \tag{3.2}$$

where,

$$A = \frac{\cos(\pi y_{0e} / b_e)}{\cos(\pi x_{0e} / a_e)}. \tag{3.3}$$

The effective wavenumber, k_e, which takes into account the losses on the patch, is

$$k_e = k_0\sqrt{\varepsilon_{reff}(1 - j/Q)} \cong k_0\sqrt{\varepsilon_{reff}}(1 - j/2Q) = k_r - jk_i \tag{3.4}$$

where, $k_0 = 2\pi f / c_0, k_r = k_0\sqrt{\varepsilon_{reff}}$, $k_i = k_r / 2Q$.

The two resonant wavenumbers k_{10} and k_{01} are

$$k_{10} = f_{10}(2\pi\sqrt{\varepsilon_{reff}} / c_0) = \pi / a_e, \tag{3.5}$$

$$k_{01} = f_{01}(2\pi\sqrt{\varepsilon_{reff}} / c_0) = \pi / b_e \tag{3.6}$$

where, f_{10} and f_{01} are the frequencies of the two modes.

Applying the phase and modulus conditions to equation (3.2) the following two design equations are derived

$$k_i = \frac{k_r}{2Q} = \frac{A^2 k_{10} + k_{01}}{2Q(A^2 + 1)} \tag{3.7}$$

for the magnitude condition, while for the phase condition

$$\left(k_r - \frac{k_{10} + k_{01}}{2}\right)^2 + k_i^2 = \left(\frac{k_{10} - k_{01}}{2}\right)^2. \tag{3.8}$$

Equations (3.7) and (3.8) are then used to obtain the following quadratic equation,

$$A^2 - 2QA\left(\frac{b_e - a_e}{b_e}\right) + \frac{a_e}{b_e} = 0. \tag{3.9}$$

The roots A_1 and A_2 of the above quadratic equation give the two possible feed positions and hence are required to be real. For the quadratic equation the product $A_1 A_2$ of the roots has the value a_e / b_e.

In the design method proposed in [20], [39] the effective dimensions of the patch were chosen and then equation (3.9) was checked to confirm if the roots are real. If the roots are not real the dimensions of the patch were changed until real roots were obtained. A new and different design approach is presented below.

Equation (3.2) is expressed in the following form

$$\frac{E_y}{E_x} \cong A\frac{\left(k_r - \frac{\pi}{a_e} - \frac{jk_r}{2Q}\right)}{\left(k_r - \frac{\pi}{b_e} - \frac{jk_r}{2Q}\right)} = \pm j \tag{3.10}$$

where, $+j$ produces LHCP and $-j$ results in RHCP.

Comparing the real and imaginary parts of equation (3.10) results in the following two independent equations for a_e and b_e in terms of the feed position A and the Q-factor of the patch. For RHCP, equation (3.10) produces the following two simple design formulas [67],

$$a_e = \frac{2QA\pi}{k_r(2QA+1)}$$

$$= \frac{QAc_0}{(2QA+1)f\sqrt{\varepsilon_{reff}}} \tag{3.11}$$

and,

$$b_e = \frac{2Q\pi}{k_r(2Q-A)}$$

$$= \frac{Qc_0}{(2Q-A)f\sqrt{\varepsilon_{reff}}}. \tag{3.12}$$

In the design the dimension a_e for a square patch is first determined so that the antenna operates at the design frequency. This value of a_e is given by $a_e = c_0 / 2f\sqrt{\varepsilon_{reff}}$.

The Q-factor of the square patch is then obtained either by simulation or by using equations given in *Appendix 3A*. Then for a given feed position (x_{0e}, y_{0e}) the dimensions of the nearly square patch are given directly from the above design equations.

3.3 Design of the CP Antenna Based on the Equivalent Circuit Model of the Patch

The cavity model approach leads to simple design equations but does not provide a good engineering understanding of the properties of the nearly square patch antenna. Consequently, in this section a design is presented based on the equivalent circuit of the patch where new design equations are presented.

Haneishi *et al.* [32], [40] used an equivalent circuit model to obtain the design equations for a diagonal feed on a nearly square patch antenna. This model is modified as shown in Figure 3.2 by taking the two turns ratios (N_a and N_b) to be different when an offset feed is used. The two transformers T_a and T_b transform the edge impedances of the patch to the feed position. The admittance Y_a is obtained from the parallel circuit with inductance (L_a), capacitance (C) and conductance (G_a). For the TM_{10} mode the voltage V_{Fa} at the feed is proportional to edge voltage $V_a \cos(\pi x_{0e} / a_e)$, and similarly V_{Fb} is proportional to $V_b \cos(\pi y_{0e} / b_e)$.

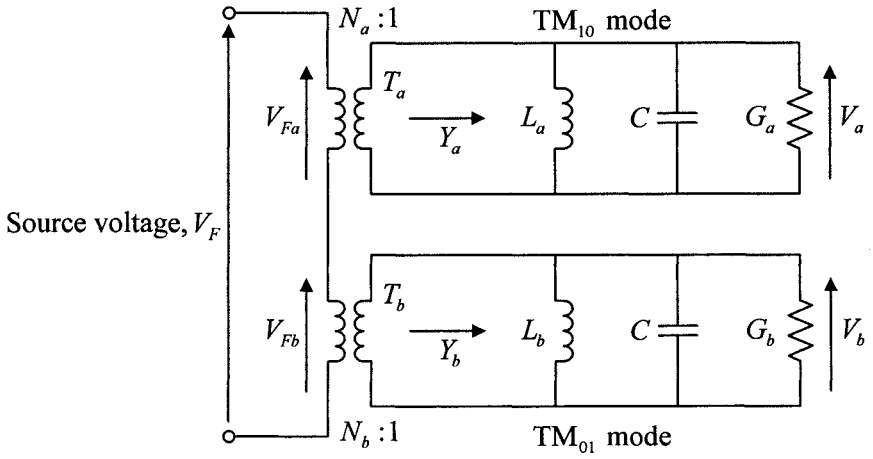

Figure 3.2. Equivalent circuit of a single-feed nearly square patch antenna after perturbation.

Consequently,

$$\frac{N_b}{N_a} = \frac{\cos(\pi y_{0e}/b_e)}{\cos(\pi x_{0e}/a_e)} \,. \tag{3.13}$$

From the equivalent circuit shown in Figure 3.2 the ratio V_b / V_a is given by

$$\frac{V_b}{V_a} = A \cdot \frac{\left[\frac{f_a}{Q} + j\left(f - \frac{f_a^2}{f}\right)\right]}{\left[\frac{f_b}{Q} + j\left(f - \frac{f_b^2}{f}\right)\right]} = 1\angle \pm 90^\circ = \pm j \tag{3.14}$$

where, $A = N_b / N_a$, and, f_a, f_b are the two mode frequencies.

The frequencies for the two modes are given by $f_b = c_0 / 2b_e\sqrt{\varepsilon_{reff}}$, and $f_a = c_0 / 2a_e\sqrt{\varepsilon_{reff}}$, therefore

$$\frac{f_a}{f_b} = \frac{b_e}{a_e} = \frac{a_e + c_e}{a_e} = 1 + \frac{\Delta S_e}{S_e} \,. \tag{3.15}$$

The two design equations may be obtained from equation (3.14) by either using the modulus/argument form of analysis or, by simply comparing real and imaginary in the complex form.

Using the former approach [65], [66], results in the following two simultaneous fourth order non-linear algebraic equations. The modulus condition, gives,

$$\alpha^4(r-1) + \alpha^2\left(rM^2 - 1\right)\left(\frac{1}{Q^2} - 2\right) + rM^4 - 1 = 0 \tag{3.16}$$

and the phase condition gives,

$$\alpha^4 + \alpha^2\left(\frac{M}{Q^2} - M^2 - 1\right) + M^2 = 0 \tag{3.17}$$

where, $r = (N_b / N_a)^2$, and, $\alpha = f / f_b$, $M = f_a / f_b$. The derivation of equations (3.16) and (3.17) is given in *Appendix 3B*.

Equations (3.16) and (3.17) can be solved numerically to determine the values of the effective patch dimensions a_e and b_e for a given feed location. The above design equations do not however distinguish between RHCP and LHCP.

In the alternative approach taking the minus sign gives two relatively simple second order algebraic equations, for RHCP$(-j)$, as shown below. Equating the real part of equation (3.14), gives

$$\frac{Af_a}{Q} - \left(f - \frac{f_b^2}{f} \right) = 0 \tag{3.18}$$

and, equating the imaginary part gives

$$A\left(f - \frac{f_a^2}{f} \right) + \frac{f_b}{Q} = 0. \tag{3.19}$$

For the cavity model and equivalent circuit model the predicted and simulated results for the patch dimensions and the axial ratio, are summarised in Table 3.1 and Table 3.2.

For a microstrip edge-feed on the a-edge $(0 \le x_0 < 0.5a$ and, $y_0 = 0)$ the value of a should remain constant. However, for the above Table 3.1 and Table 3.2, there is a smaller variation in this parameter as compared with dimension b. The percentage difference of the simulated and calculated dimensions is much smaller for the *Duroid* substrate as compared with the *FR4 PCB* substrate. Nevertheless the percentage difference of the dimensions for the both models is quite close. The calculated dimensions of a and b were used in simulation and then fine-tuned to obtain good AR.

FR4 PCB with h = 1.575 mm																
Offset edge-feed, x_{0e}	Simulation			The cavity model (calculation)						The equivalent circuit model (calculation)						
	a (mm)	b (mm)	Tuned AR (dB)	a_e (mm)	b_e (mm)	a (mm)	Compared with simulated a, Error (%)	b (mm)	Compared with simulated b, Error (%)	a_e (mm)	b_e (mm)	a (mm)	Compared with simulated a, Error (%)	b (mm)	Compared with simulated b, Error (%)
0	28.29	29.3	0.04	30.325	31.268	28.626	1.17	29.571	0.92	30.336	31.279	28.637	1.21	29.582	0.95
$0.1a_e$	28.36	29.43	0.16	30.348	31.293	28.649	1.01	29.596	0.56	30.358	31.305	28.659	1.04	29.608	0.6
$0.2a_e$	28.42	29.53	0.11	30.413	31.383	28.714	1.02	29.686	0.53	30.422	31.397	28.723	1.05	29.7	0.57
$0.3a_e$	28.525	29.805	0.19	30.515	31.613	28.815	1.01	29.915	0.37	30.523	31.632	28.824	1.04	29.934	0.43
$0.35a_e$	28.56	30.06	0.19	30.577	31.864	28.877	1.1	30.166	0.35	30.585	31.891	28.885	1.13	30.193	0.44
$0.4a_e$	28.59	30.75	0.19	30.645	32.394	28.943	1.22	30.696	0.18	30.652	32.446	28.951	1.25	30.748	0.01
$0.45a_e$	28.608	32.57	0.18	30.716	34.128	29.011	1.39	32.431	0.43	30.724	34.34	29.018	1.41	32.642	0.22

Table 3.1. For *FR4 PCB*, the calculated and simulated dimensions for CP operation at 2.45 GHz.

Duroid with h = 1.575 mm																
Offset edge-feed, x_{0e}	Simulation			The cavity model (calculation)						The equivalent circuit model (calculation)						
	a (mm)	b (mm)	Tuned AR (dB)	a_e (mm)	b_e (mm)	a (mm)	Compared with simulated a, Error (%)	b (mm)	Compared with simulated b, Error (%)	a_e (mm)	b_e (mm)	a (mm)	Compared with simulated a, Error (%)	b (mm)	Compared with simulated b, Error (%)
0	38.365	39.18	0.27	40.735	41.485	38.625	0.67	39.378	0.5	40.74	41.49	38.631	0.69	39.383	0.52
$0.1a_e$	38.427	39.26	0.19	40.753	41.505	38.643	0.56	39.397	0.35	40.758	41.51	38.648	0.57	39.403	0.36
$0.2a_e$	38.451	39.33	0.19	40.805	41.575	38.696	0.63	39.468	0.35	40.81	41.582	38.7	0.64	39.474	0.36
$0.3a_e$	38.584	39.58	0.19	40.887	41.755	38.777	0.5	39.647	0.17	40.891	41.764	38.781	0.51	39.656	0.19
$0.35a_e$	38.59	39.74	0.05	40.937	41.95	38.827	0.61	39.842	0.26	40.941	41.962	38.83	0.62	39.854	0.29
$0.4a_e$	38.62	40.3	0.24	40.991	42.358	38.88	0.67	40.25	0.12	40.994	42.381	38.883	0.68	40.273	0.07
$0.45a_e$	38.644	41.64	0.27	41.048	43.653	38.934	0.74	41.545	0.23	41.051	43.741	38.937	0.75	41.633	0.02

Table 3.2. For *Duroid*, the calculated and simulated dimensions for CP operation at 2.45 GHz.

3.4 The Effect of the Design Parameters on the Area of the Perturbation Segment

One of the main problems in the realisation of a single microstrip feed CP patch antenna is that the area of the perturbation segment is small and hence the performance of the antenna is very sensitive to manufacturing errors. In this section the effect on the area of the perturbation segment with respect to both the microstrip feed position, and, the Q-factor is investigated. Based on the results obtained from the new equations for each of the two models of the antenna, the predicted results (see Figure 3.3) show that the area of the perturbation segment increases with the amount of feed offset, and, decreases with increasing values of the Q-factor of the antenna.

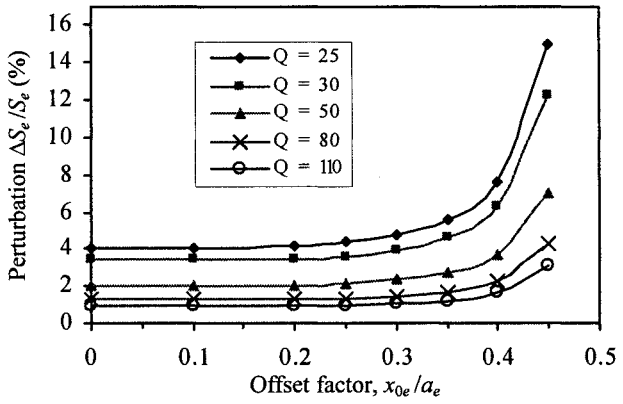

(a)

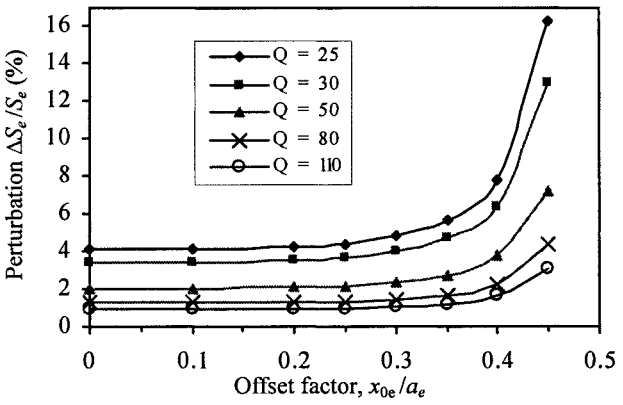

(b)

Figure 3.3. Relationship between the perturbation $\Delta S_e / S_e$ and the offset feed positions and Q-factor. (a) The cavity model. (b) The equivalent circuit model.

To compare the results obtained for the two models with simulation results, two nearly square patch antennas were designed using *FR4 PCB* ($Q = 32.6$), and, *Duroid* ($Q = 54.8$) substrates.

As can be seen in Figure 3.4 there is a good agreement between the predicted results and the results obtained from simulation for both antenna models.

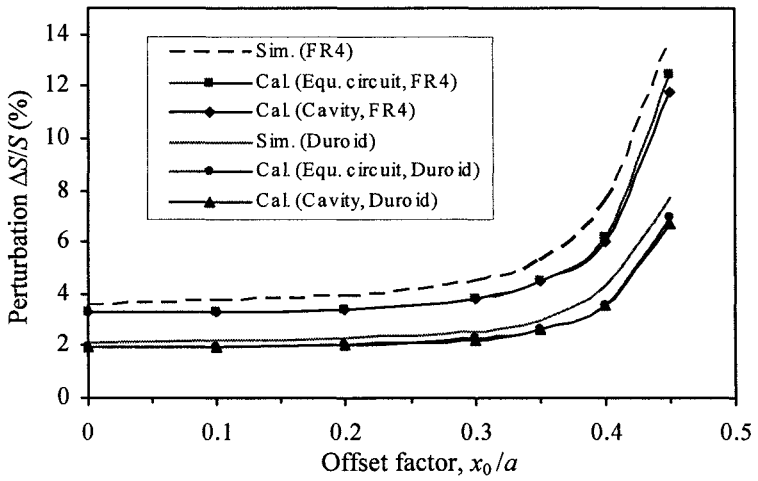

Figure 3.4. Relationship between the perturbation $\Delta S / S$ and the offset feed positions.

Table 3.3 shows the increase in $\Delta S / S$ as a function of the offset feed for each of the two substrates obtained by calculation and simulation.

The above results show that to increase the area of perturbation a thick substrate can be used.

Offset edge-feed, x_0	*FR4 PCB*			*Duroid*		
	Simulation	The cavity model	The equivalent circuit model	Simulation	The cavity model	The equivalent circuit model
	$\Delta S/S$ (%)	$\Delta S/S$ (%)	$\Delta S/S$ (%)	$\Delta S/S$ (%)	$\Delta S/S$ (%)	$\Delta S/S$ (%)
0	3.57	3.301	3.302	2.12	1.948	1.948
$0.1a$	3.77	3.307	3.311	2.17	1.951	1.952
$0.2a$	3.91	3.387	3.399	2.29	1.996	2
$0.3a$	4.49	3.818	3.853	2.58	2.243	2.255
$0.35a$	5.25	4.466	4.531	2.98	2.615	2.637
$0.4a$	7.56	6.057	6.209	4.35	3.524	3.574
$0.45a$	13.85	11.79	12.488	7.75	6.708	6.925

Table 3.3. The perturbation $\Delta S/S$ with respect to the offset feed positions.

3.5 Impedance Matching

The input impedance of the antenna for the offset position $(x_0,0)$ is given by the following equation [64],

$$Z_{in} = j\omega\mu h\left[-\frac{\cot(b_e k_e)}{a_e k_e}\right.$$

$$\left.+\frac{2a_e^2}{w^2\pi^3}\sum_{m=1}^{\infty}\frac{(\sin m\theta_1-\sin m\theta_2)^2}{m^2\sqrt{m^2-A_a^2}}\coth\left(\frac{b_e\pi}{a_e}\sqrt{m^2-A_a^2}\right)\right] \tag{3.20}$$

where $\theta_1=(x_{0e}+w/2)\pi/a_e$, $\theta_2=(x_{0e}-w/2)\pi/a_e$, $A_a=a_e k_e/\pi$, and w is the width of the feed line. First five terms of the above series are used to determine Z_{in} for the *FR4 PCB*, and, the first ten terms are used for the *Duroid*.

Figure 3.5 shows that the input impedance reduces with an offset feed and that there is a good agreement between the predicted results based on equation (3.20) and simulation. In order to design a compact matched CP antenna it is convenient to use a short length of

microstrip line as a matching network as shown in Figure 3.6. However, this network cannot produce matching for all ranges of the input impedance of the antenna. Consequently, there is a trade off between the requirement of increasing the perturbation area by increasing the feed offset, and, the realisation of the above matching network.

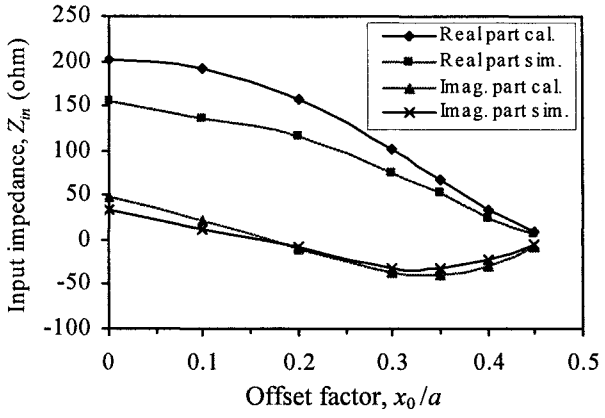

(a)

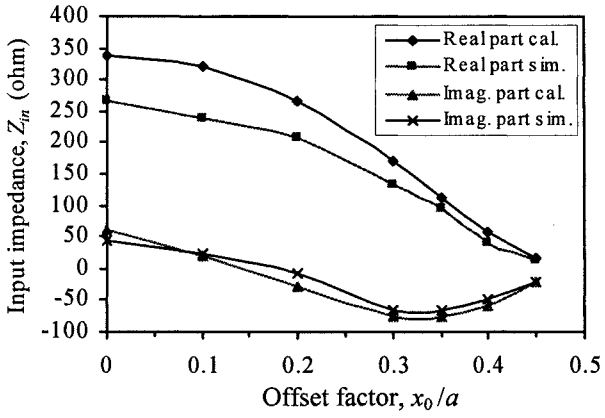

(b)

Figure 3.5. Calculated and simulated Z_{in} at offset factor x_0 / a. (a) For *FR4 PCB*. (b) For *Duroid*.

In the design of the matching network there are two variables, the length and characteristic impedance (width of the microstrip line) in order to match the complex impedance of the antenna to Z_0 (= 50 ohms).

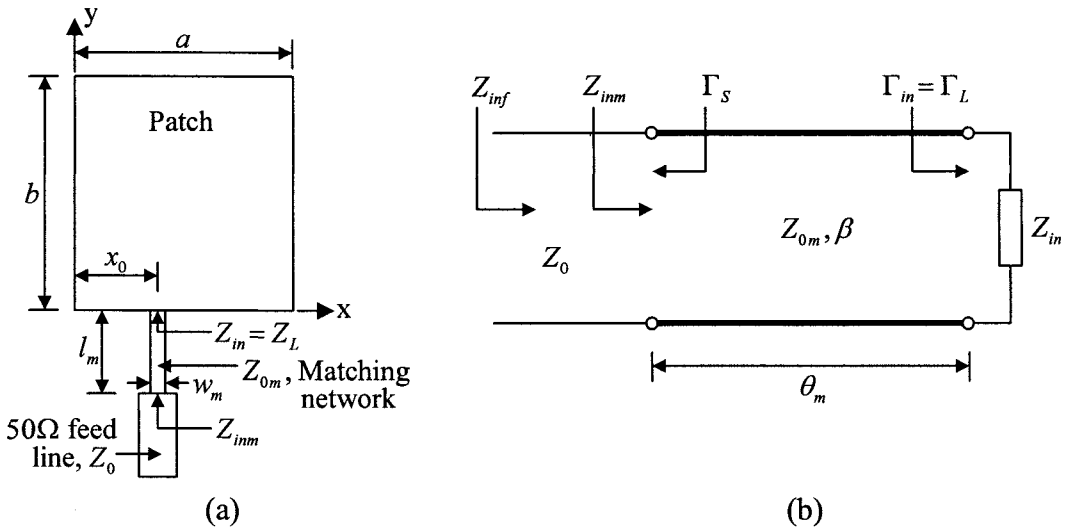

Figure 3.6. CP nearly square patch antenna with a simple matching network. (a) Matched antenna. (b) A simple transmission-line matching network.

The required characteristic impedance Z_{0m} of the microstrip line is given by [68],

$$Z_{0m} = \sqrt{Z_0 \frac{\left(Z_0 R - R^2 - X^2\right)}{Z_0 - R}} \tag{3.21}$$

where, $Z_{in} = R + jX$ is the input impedance of the patch.

For $R > Z_0$ with X(-ve), or, $R < Z_0$ with X(+ve) for Z_{in}, the electrical length of the matching microstrip line is given by

$$\theta_m = \tan^{-1}\left(jZ_{0m} \frac{Z_{in} - Z_0}{Z_{0m}^2 - Z_{in} Z_0} \right). \tag{3.22a}$$

For $R > Z_0$ with X(+ve), or, $R < Z_0$ with X(-ve)

$$\theta_m = \pi + \tan^{-1}\left(jZ_{0m} \frac{Z_{in} - Z_0}{Z_{0m}^2 - Z_{in} Z_0} \right). \tag{3.22b}$$

The regions of the input impedance of the patch which can be matched are shown on the Smith chart in Figure 3.7.

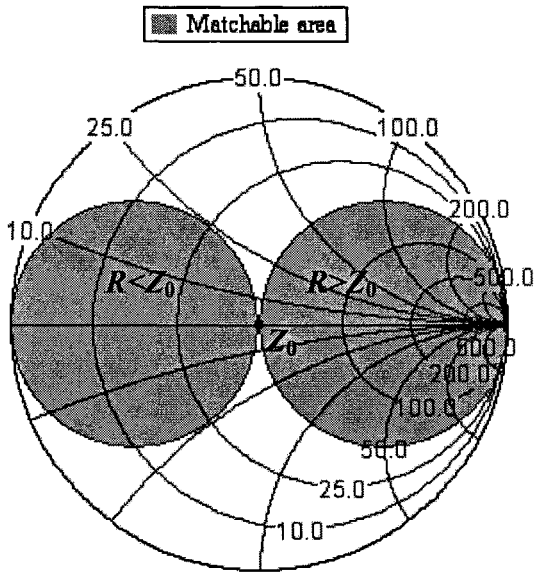

Figure 3.7. Region of Z_{in} that can be matched using the matching network.

It was found that for matching to be realised the maximum offset feed locations were $0.3a$ for *FR4 PCB* and $0.35a$ for *Duroid* respectively.

3.6 Comparison between Predicted, Simulated, and Measured Results

Two nearly square patch antennas for RHCP were designed using different substrates, and offset microstrip feed locations. From simulation, it was found that $Z_{in} = 75.5 - j32.2\ \Omega$ for the *FR4* substrate, and, $Z_{in} = 93.8 - j64.3\ \Omega$ for the *Duroid* substrate. These values were then used to design the corresponding matching networks. The design parameters of the antenna, operating at 2.45 GHz, are summarised in Table 3.4.

Parameters	*FR4 PCB*		*Duroid*	
	Calculated	Simulated	Calculated	Simulated
Z_{0m} (ohm)	76.2	--	97	--
θ_m (rad)	0.879	--	0.923	--
w_m (mm)	1.33	1.266	1.375	1.36
l_m (mm)	8.614	8.32	12.08	12.4
a (mm)	28.824	28.52	38.83	38.6
b (mm)	29.934	29.75	39.854	39.71
Q (square patch)	32.6	30.5	54.8	53.1

Table 3.4. Calculated and simulated design parameters of the matching microstrip line and of the patch antenna.

The fabricated CP nearly square patch antennas with simple matching networks are shown in Figure 3.8.

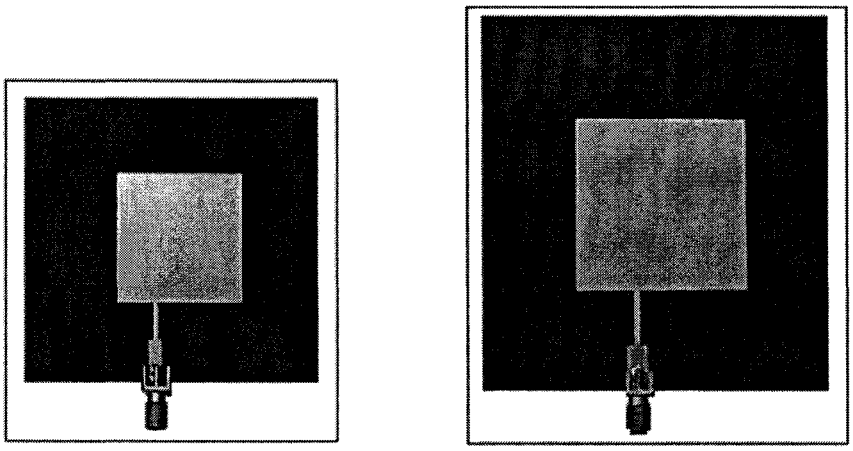

(a) (b)

Figure 3.8. The fabricated CP nearly square patch antennas. (a) For *FR4 PCB*. (b) For *Duroid*.

The simulated and measured input impedance are in very good agreement and are plotted on a Smith chart as shown in Figure 3.9. A dip or a kink in the impedance plot indicates that two resonant modes are excited at very close frequencies, which gives the

best AR at the cusp frequency. If there is a small dip or no dip in the impedance plot, the design will yield a poor AR.

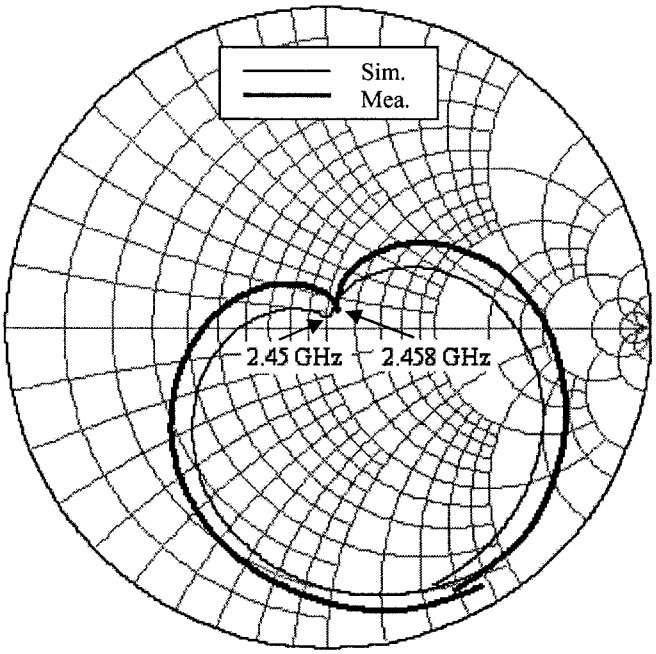

(a)

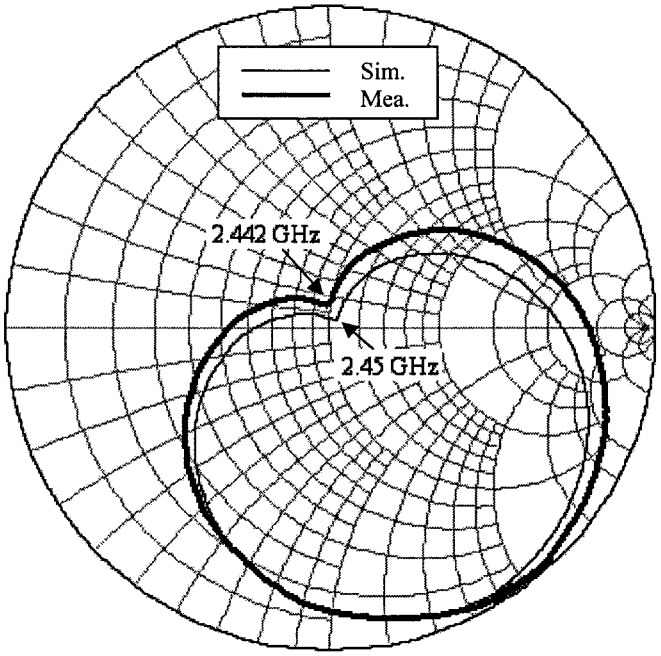

(b)

Figure 3.9. Simulated and measured input impedance on Smith chart. (a) For *FR4 PCB*. (b) For *Duroid*.

The cusp in the impedance plot in Figure 3.9 is very close to a 50-ohm match point for the designed frequency showing that a very good impedance matching has been obtained.

Figure 3.10 shows a good return loss (S_{11}) and a good agreement of the simulated and measured S_{11}, for the two patch antennas.

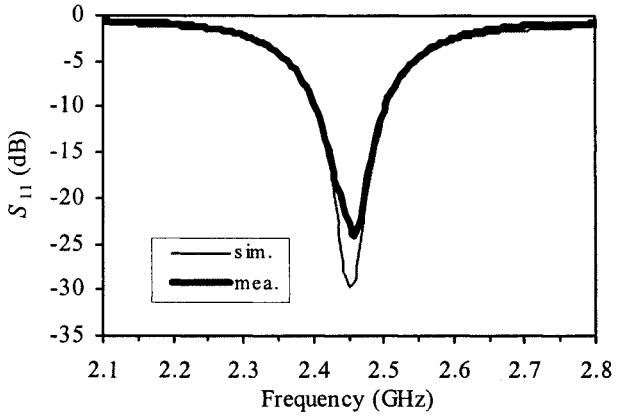

(a)

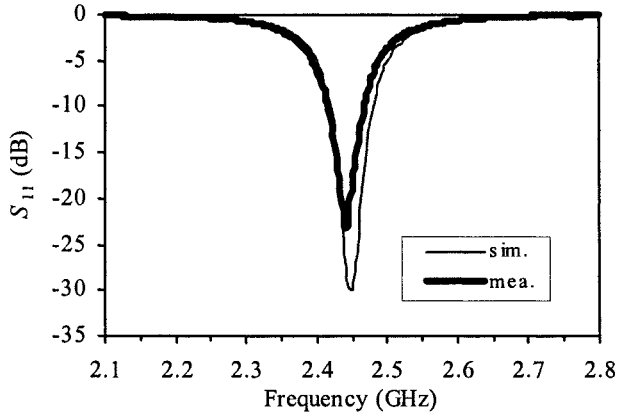

(b)

Figure 3.10. Simulated and measured return loss. (a) For *FR4 PCB*. (b) For *Duroid*.

Figure 3.11 shows a comparison of the simulated and measured results for the AR at ($\theta = 0, \phi = 0$) as a function of frequency. For the *FR4 PCB* substrate, the measured minimum AR was 0.45 dB at 2.458 GHz which is less than a 0.5% shift from the design frequency. For the *Duroid* substrate, the measured minimum AR was 0.35 dB at 2.442 GHz which is also less than a 0.5% shift from the design frequency.

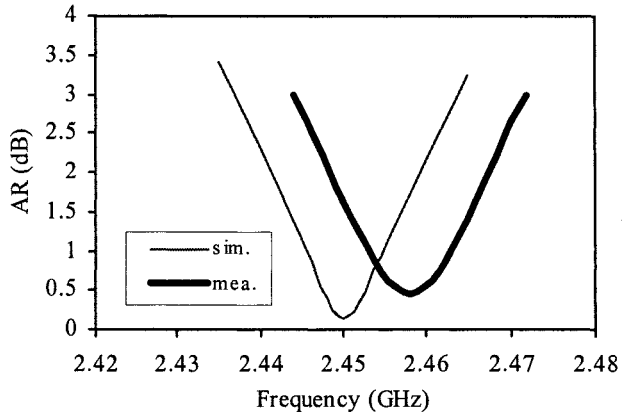

(a)

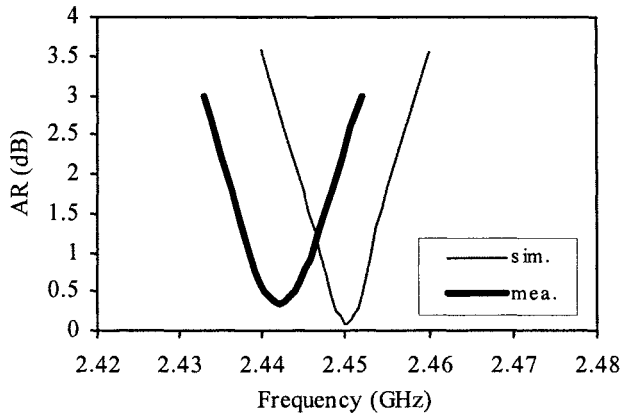

(b)

Figure 3.11. Simulated and measured AR versus frequency. (a) For *FR4 PCB*. (b) For *Duroid*.

The simulated and measured AR versus theta (θ) at centre frequency is shown in Figure 3.12. The simulated and measured 3-dB AR beamwidths are between −51° and 51°, and between −54° and 43° respectively, for the *FR4 PCB* substrate. The simulated and measured 3-dB AR beamwidths are between −58° and 59°, and between −69° and 54° respectively, for the *Duroid* substrate.

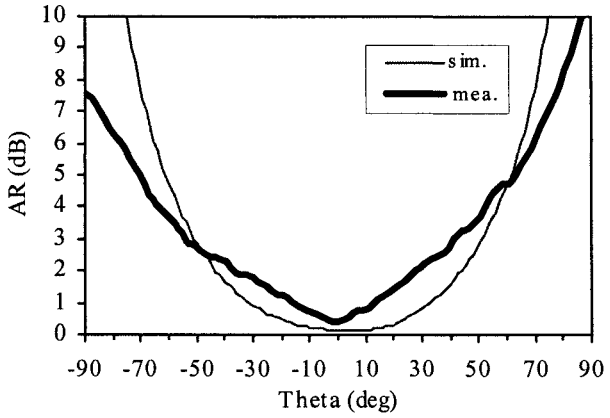

(a)

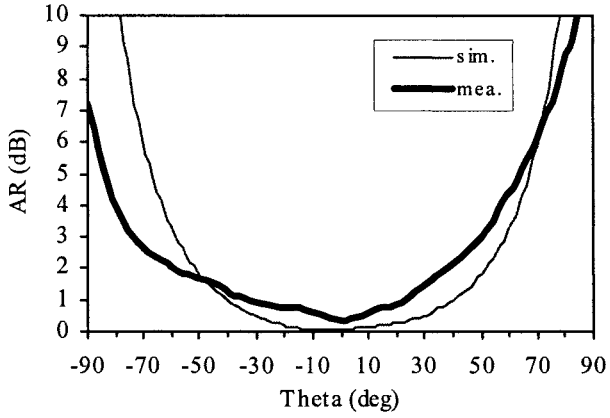

(b)

Figure 3.12. Simulated and measured AR versus theta. (a) For *FR4 PCB*. (b) For *Duroid*.

A comparison between the simulated and measured results for the gain of the antenna is shown in Figure 3.13. It shows that the gain of the *Duroid* antenna is much higher than the gain from using the *FR4 PCB* substrate.

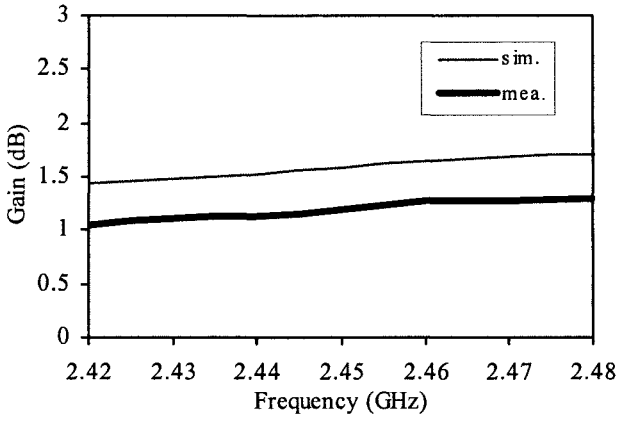

(a)

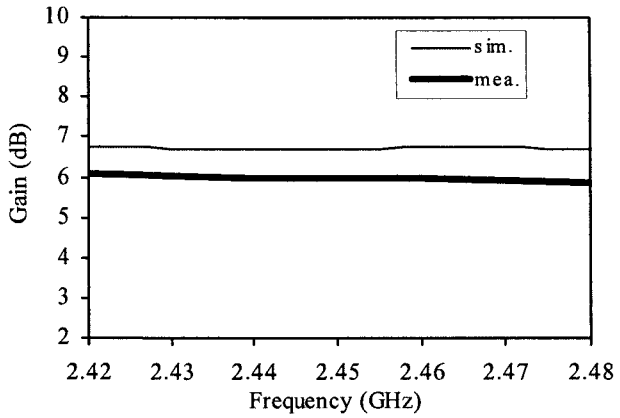

(b)

Figure 3.13. Simulated and measured gains. (a) For *FR4 PCB*. (b) For *Duroid*.

The simulated and measured impedance bandwidths, the CP bandwidths, and the gains at the centre frequency are listed in Table 3.5.

	FR4 PCB		*Duroid*	
	Simulation	Measurement	Simulation	Measurement
Centre frequency f (GHz)	2.45	2.458	2.45	2.442
-10-dB S_{11} for impedance bandwidth (MHz, %)	104, 4.24	99, 4.04	60, 2.45	52, 2.13
3-dB AR for CP bandwidth (MHz, %)	27, 1.1	28, 1.14	17, 0.7	19, 0.78
Gain (dB)	1.59	1.25	6.71	6

Table 3.5. The impedance bandwidths, the CP bandwidths, and the gains at centre frequency.

Figure 3.14 shows the simulated normalised RHCP and LHCP radiation patterns at $\phi = 0$ for both antennas. It can be seen that good RHCP is obtained, and the isolation with respect to LHCP is good.

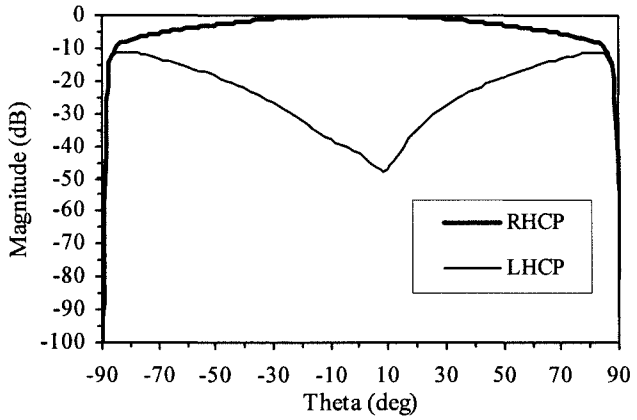

(a)

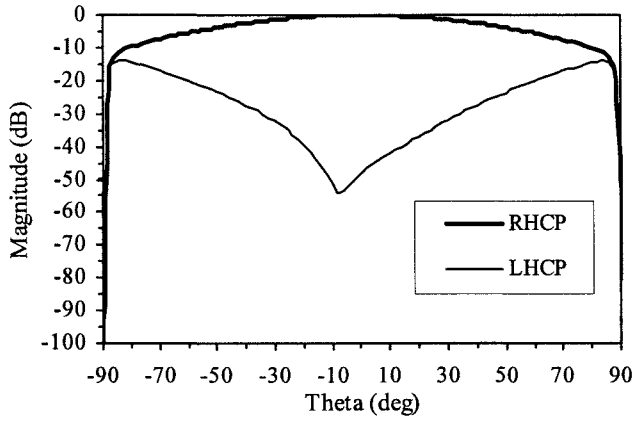

(b)

Figure 3.14. Simulated normalised radiation patterns for RHCP and LHCP at $\phi = 0$. (a) For *FR4 PCB*. (b) For *Duroid*.

Simulated and measured normalised radiation patterns at $\phi = 0$ and $\phi = 90^{\circ}$ are shown in Figure 3.15 for *FR4 PCB*, and in Figure 3.16 for *Duroid*.

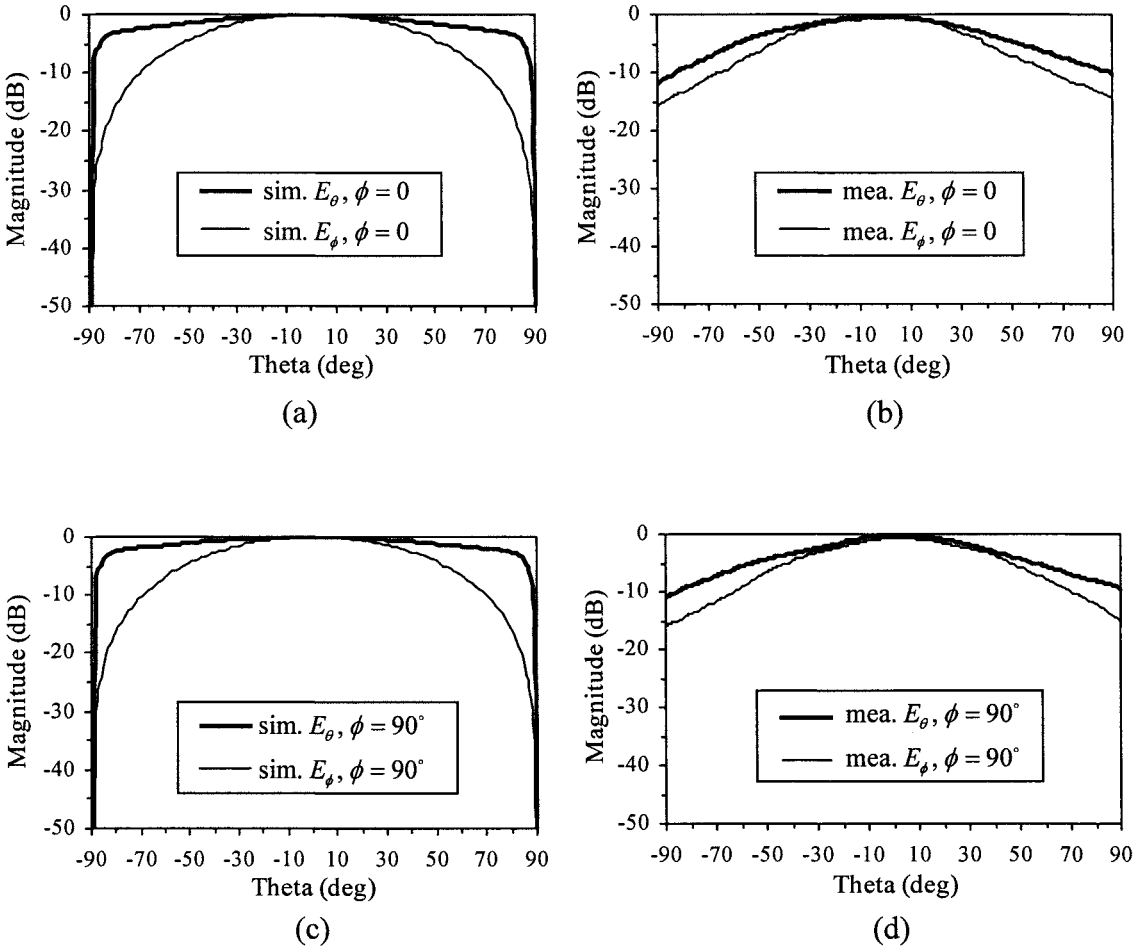

Figure 3.15. Normalised radiation patterns for *FR4 PCB* (a) Simulation at $\phi = 0$. (b) Measurement at $\phi = 0$. (c) Simulation at $\phi = 90^\circ$. (d) Measurement at $\phi = 90^\circ$.

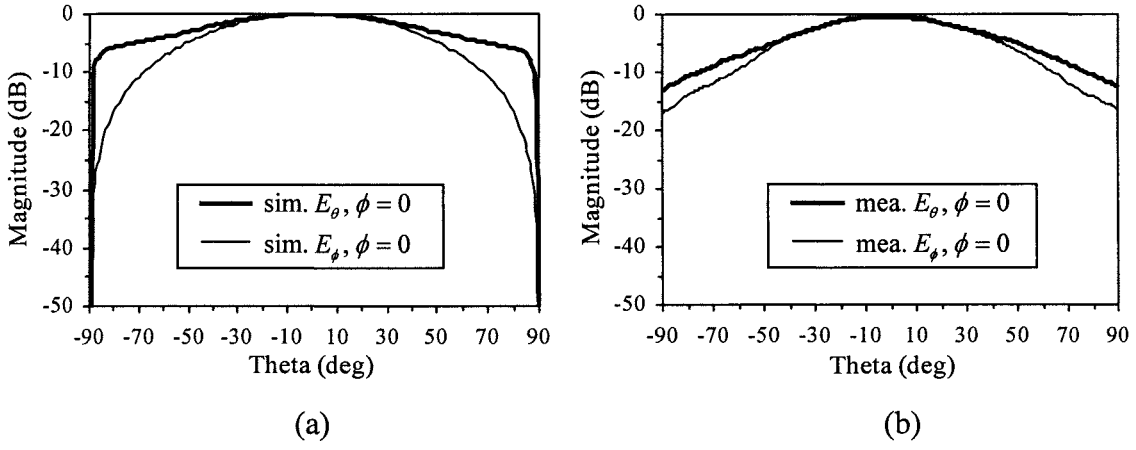

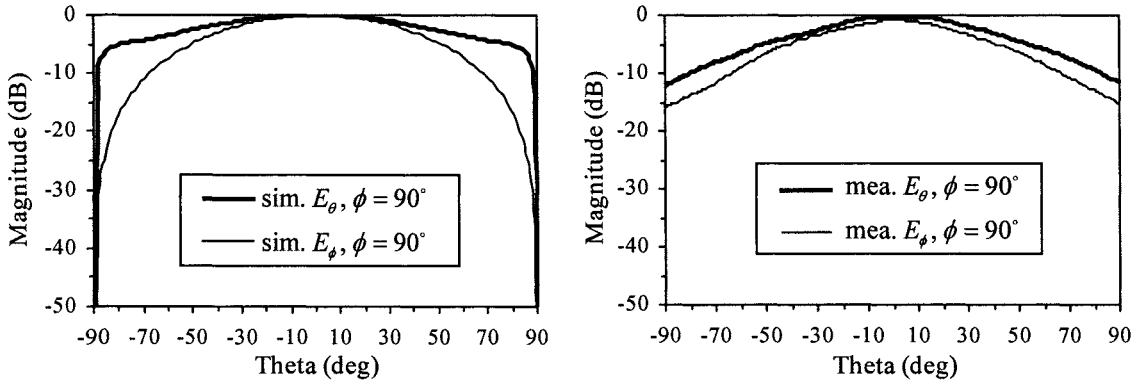

(c) (d)

Figure 3.16. Normalised radiation patterns for *Duroid* (a) Simulation at $\phi = 0$. (b) Measurement at $\phi = 0$. (c) Simulation at $\phi = 90^\circ$. (d) Measurement at $\phi = 90^\circ$.

3.7 Summary

Based on both the cavity model and the equivalent circuit model analysis of the nearly square patch antenna the circular polarisation conditions and the patch dimensions were determined. For a given offset feed, new equations for both models were derived. Simple formulas, using the cavity model, have been derived and used to design a CP patch antenna. It has been shown that the use of an offset microstrip feed line and/or a thicker substrate increases the size of the perturbing segment of the patch thereby reducing the effect of manufacturing errors. The input impedances of the patch with the offset line feed locations were calculated. To complete the antenna design and obtain a compact form of the matched antenna, a simple matching network consisting of a short length of microstrip line was designed. The measured and simulated results show a good axial ratio and good return loss, and are in good agreement with predicted values.

CHAPTER 4 EXPLICIT COMPUTATIONALLY EFFICIENT COUPLING IMPEDANCE FORMULAS FOR RECTANGULAR AND TRIANGULAR SEGMENTS

4.1 Introduction

In this thesis the patch antennas studied involve the rectangular and right-angled isosceles triangular segments.

The double infinite series Green's function for the rectangle is given in [55]. Green's functions for the $30°–60°–90°$ triangle, the equilateral triangle, and the right-angled isosceles triangle are derived by the method of images using line current sources [70].

A computationally efficient general coupling impedance formula for ports on a rectangle is derived in [71]. This was derived by first reducing the double series Green's function to a single series, using a closed form of Fourier series, prior to the integration step. In application it is necessary to follow several complicated selection rules. However, as reported, for large values of the complex arguments in the trigonometric functions numerical convergence problems arise and at this point in the series these functions had to be replaced by their large argument approximations.

S. H. Lee *et al* [72] have derived general coupling impedance formulas for the $30°–60°–90°$ triangle and the equilateral triangle.

New efficient explicit coupling impedance formulas for the rectangle and isosceles triangle are proposed in this thesis. In each case the Green's functions are first partitioned (see Section 4.2) the integration is performed prior to the introduction of closed forms of infinite series [64], [73]-[76]. This procedure identifies both the single terms and the infinite series terms which cancel each other out and this is primarily due to the initial partitioning. No problems arise with large values of arguments in the trigonometric functions.

In Chapters 5, and 6, the segmentation method is applied to determine the input impedance of the patch antennas which involve rectangular segments, and, the right-angled isosceles triangular segments.

Because of the common analytic techniques employed in the derivation of the port coupling impedances all the segment coupling impedance formulas are assembled in this chapter. Outlines of the derivation of these formulas are given for the perimeter port coupling impedances. Formulas involving the probe feed port on a rectangle (in Sections 4.4 and 4.5) [75], and, on the triangle (in Sections 4.7 and 4.8), are new, and are derived in detail. The latter result is included because of its potential application in further work. For the probe feeds the calculated, simulated and measured input impedances are compared.

In Section 4.6, a comparison between the calculated, simulated, and measured perimeter port coupling impedance for the triangular patch are presented. All measured impedance results were obtained using a *Duroid* substrate of thickness 1.575 mm.

4.2 The Green's Function for a Rectangular and a Right-Angled Isosceles Triangular Segment

For any microstrip segment the formula for coupling impedance between two ports p and q is given by Okoshi [55],

$$Z_{pq} = \frac{1}{W_p W_q} \int_{W_p} \int_{W_q} G(x_p, y_p \mid x_q, y_q)\, dr_q\, dr_p \tag{4.1}$$

where dr_p and dr_q are incremental distances over the port widths W_p, W_q. The condition $W_p,\ W_q << \lambda$ is required to ensure that the current density does not vary appreciably across the port width [2].

The coupling impedance formulas used in this thesis are based upon the integration of the associated Green's functions prior to introducing the closed forms given in the Gradshteyn [77] collection. An additional eight closed forms used in the present analysis were derived from the Gradshteyn results by suitable integrations which increased the convergence rate of formulas. In the application of these results no problems with numerical convergence arise.

A great advantage in this approach is that in the analysis certain infinite series are eliminated by cancellation. This is primarily due to the initial stage of partitioning the Green's functions into elementary ranges in the summation indices m, and, n, which brings into view the infinite series and single terms which cancel.

4.2.1 The rectangular segment

The Green's function for a rectangular segment of sides a, b, is given by Okoshi [55],

$$G(x_p, y_p \mid x_q, y_q) = \frac{j\omega\mu h}{ab} \sum_{m=0}^{\infty} \sum_{n=0}^{\infty} \varepsilon_m^2 \varepsilon_n^2 \frac{\cos\frac{m\pi}{a} x_p \cos\frac{n\pi}{b} y_p \cos\frac{m\pi}{a} x_q \cos\frac{n\pi}{b} y_q}{\left(\frac{m\pi}{a}\right)^2 + \left(\frac{n\pi}{b}\right)^2 - k^2}, \tag{4.2}$$

where,

$$\varepsilon_m = \begin{cases} 1 & (\text{for } m = 0) \\ \sqrt{2} & (\text{for } m \neq 0) \end{cases}, \quad \varepsilon_n = \begin{cases} 1 & (\text{for } n = 0) \\ \sqrt{2} & (\text{for } n \neq 0) \end{cases}. \tag{4.3}$$

Partitioning the above expression into the ranges, $(m = 0, n = 0)$, $(m \geq 1, n = 0)$, $(m = 0, n \geq 1)$, and, $(m \geq 1, n \geq 1)$ gives the following arrangement

$$G(x_p, y_p \mid x_q, y_q) = \frac{j\omega\mu h}{ab}\left[-\frac{1}{k^2} + \frac{2a^2}{\pi^2}\sum_{m=1}^{\infty} \frac{\cos\frac{m\pi}{a}x_p \cos\frac{m\pi}{a}x_q}{m^2 - A^2} \right.$$

$$+ \frac{2b^2}{\pi^2}\sum_{n=1}^{\infty} \frac{\cos\frac{n\pi}{b}y_p \cos\frac{n\pi}{b}y_q}{n^2 - B^2}$$

$$\left. + \frac{4}{\pi^2}\sum_{m=1}^{\infty}\sum_{n=1}^{\infty} \frac{\cos\frac{m\pi}{a}x_p \cos\frac{m\pi}{a}x_q \cos\frac{n\pi}{b}y_p \cos\frac{n\pi}{b}y_q}{\frac{m^2}{a^2} + \frac{n^2}{b^2} - \frac{k^2}{\pi^2}} \right] \tag{4.4}$$

where, $\omega = 2\pi f$, $A = ak/\pi$, $B = bk/\pi$, h is the thickness of the dielectric substrate, $k^2 = \omega^2\mu\varepsilon_0\varepsilon_{reff}(1 - j/Q)$, and, Q is the total quality factor.

4.2.2 The triangular segment

The Green's function for the right-angled isosceles triangular segment, of perpendicular sides, length a, is given by [70],

$$G(x_p, y_p \mid x_q, y_q) = \frac{j\omega\mu h}{2}\sum_{m=-\infty}^{\infty}\sum_{n=-\infty}^{\infty} \frac{T_{mn}(x_p, y_p)T_{mn}(x_q, y_q)}{(m^2 + n^2)\pi^2 - a^2k^2} \tag{4.5}$$

where $T_{mn}(x, y)$ is given by

$$T_{mn}(x, y) = \cos\frac{m\pi x}{a}\cos\frac{n\pi y}{a} + (-1)^{m+n}\cos\frac{n\pi x}{a}\cos\frac{m\pi y}{a}. \tag{4.6}$$

The Green's function is partitioned into the following (m, n) index ranges: $(0, 0)$, $(-\infty < m \le -1, 0)$, $(1 \le m < \infty, 0)$, $(0, -\infty < n \le -1)$, $(0, 1 \le n < \infty)$, $(-\infty < m \le -1, 1 \le n < \infty)$, $(1 \le m < \infty, 1 \le n < \infty)$, $(-\infty < m \le -1, -\infty < n \le -1)$, $(1 \le m < \infty, -\infty \le n < -1)$.

The above partitions of the double infinite series indices (m,n) are illustrated in the following diagram, Figure 4.1.

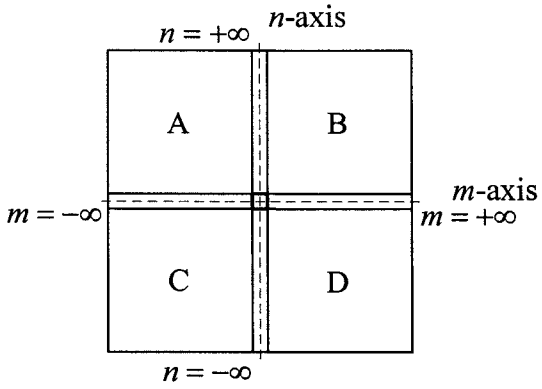

Figure 4.1. Double series array.

From the symmetries of the function $T_{mn}(x,y)$ it is clear that the elements in the sections A, B, C, and, D are the same, as are, the four sets of elements along the m and, n axes. Therefore the Green's function can be presented in the form

$$G(x_p,y_p\,|\,x_q,y_q)=\frac{j2\omega\mu h}{\pi^2}\left\{-\frac{\pi^2}{a^2k^2}+\sum_{m=1}^{\infty}\frac{T_{m0}(x_p,y_p)T_{m0}(x_q,y_q)}{m^2-A^2}\right.$$

$$\left.+\sum_{m=1}^{\infty}\sum_{n=1}^{\infty}\frac{T_{mn}(x_p,y_p)T_{mn}(x_q,y_q)}{m^2+n^2-A^2}\right\} \tag{4.7}$$

where $A=ak/\pi$.

4.3 Coupling Impedances for Perimeter Ports on a Rectangular Segment

The coupling impedances locations of the two perimeter ports on a rectangular segment are shown in Figure 4.2.

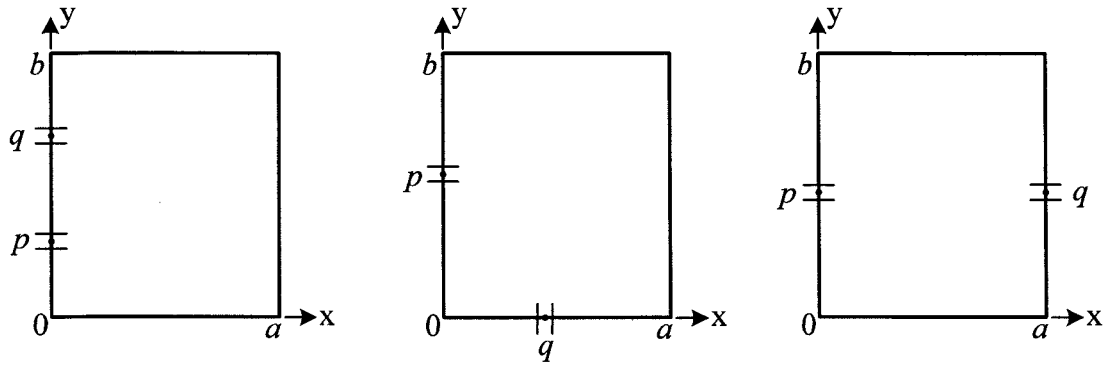

Figure 4.2. Perimeter ports on a rectangular segment. (a) For case A: two ports on the same side. (b) For case B: two ports on adjacent sides. (c) For case C: two ports on opposite sides.

In the following sections the coupling impedance formulas are given for the above cases.

Case A: Two ports on the same side

The two ports p and q, have widths W_p, W_q respectively, and are on the same side is shown in Figure 4.3.

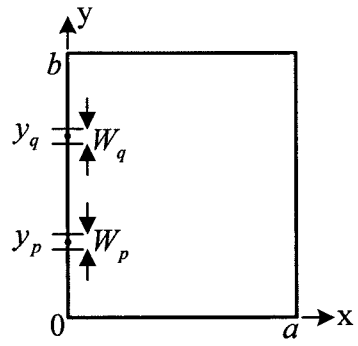

Figure 4.3. Case A: rectangular segment with two ports on the same side.

The two ports p, q are located at $(0, y_p)$, $(0, y_q)$, hence the Green's function in equation (4.4) becomes

$$G(0,y_p\,|\,0,y_q)=\frac{j\omega\mu h}{ab}\left[-\frac{1}{k^2}+\frac{2a^2}{\pi^2}\sum_{m=1}^{\infty}\frac{1}{m^2-A^2}+\frac{2b^2}{\pi^2}\sum_{n=1}^{\infty}\frac{\cos\frac{n\pi}{b}y_p\cos\frac{n\pi}{b}y_q}{n^2-B^2}\right.$$

$$\left.+\frac{4}{\pi^2}\sum_{m=1}^{\infty}\sum_{n=1}^{\infty}\frac{\cos\frac{n\pi}{b}y_p\cos\frac{n\pi}{b}y_q}{\frac{m^2}{a^2}+\frac{n^2}{b^2}-\frac{k^2}{\pi^2}}\right] \tag{4.8}$$

and the coupling impedance is given by

$$Z_{pq}=\frac{1}{W_pW_q}\int_{W_p}\int_{W_q}G(0,y_p\,|\,0,y_q)\,dy_q\,dy_p\,. \tag{4.9}$$

By integration, and using the closed form summations [77] (see *Appendix 4A.1*) the economised coupling impedance formula is then given by

$$Z_{pq}=j\omega\mu h\left[-\frac{\cot ak}{bk}\right.$$

$$\left.+\frac{2b^2}{W_pW_q\pi^3}\sum_{n=1}^{\infty}\frac{(\sin n\theta_1-\sin n\theta_2)(\sin n\theta_3-\sin n\theta_4)}{n^2\sqrt{n^2-B^2}}\coth\frac{a\pi}{b}\sqrt{n^2-B^2}\right] \tag{4.10}$$

where, $\theta_1=\frac{\pi}{b}\left(y_p+\frac{W_p}{2}\right)$; $\theta_2=\frac{\pi}{b}\left(y_p-\frac{W_p}{2}\right)$; $\theta_3=\frac{\pi}{b}\left(y_q+\frac{W_q}{2}\right)$; $\theta_4=\frac{\pi}{b}\left(y_q-\frac{W_q}{2}\right)$.

The coupling impedance Z_{pq} is obtained in terms of a closed form and a single infinite series.

For a rectangular patch antenna the input, or, self impedance for a microstrip feed is obtained from the formula (4.10) by taking $q=p, \theta_3=\theta_1$, and, $\theta_4=\theta_2$. Therefore, an economised microstrip feed input impedance formula is given by

$$Z_{pp}=Z_{in}=j\omega\mu h\left[-\frac{\cot ak}{bk}+\frac{2b^2}{W_p{}^2\pi^3}\sum_{n=1}^{\infty}\frac{(\sin n\theta_1-\sin n\theta_2)^2}{n^2\sqrt{n^2-B^2}}\coth\frac{a\pi}{b}\sqrt{n^2-B^2}\right]. \tag{4.11}$$

The perimeter port input impedance Z_{pp} is obtained in terms of a closed form and a single infinite series.

Case B: Two ports on adjacent sides

The two ports p, q are on adjacent sides, as shown in Figure 4.4.

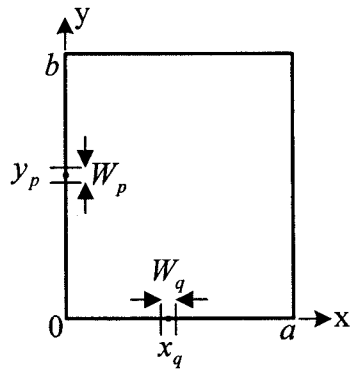

Figure 4.4. Case B: rectangular segment with two ports on adjacent sides.

The two ports p, q are located at $(0, y_p)$, $(x_q, 0)$, hence the Green's function becomes

$$G(0,y_p \mid x_q,0) = \frac{j\omega\mu h}{ab}\left[-\frac{1}{k^2}+\frac{2a^2}{\pi^2}\sum_{m=1}^{\infty}\frac{\cos\frac{m\pi}{a}x_q}{m^2-A^2}+\frac{2b^2}{\pi^2}\sum_{n=1}^{\infty}\frac{\cos\frac{n\pi}{b}y_p}{n^2-B^2}\right.$$

$$\left.+\frac{4}{\pi^2}\sum_{m=1}^{\infty}\sum_{n=1}^{\infty}\frac{\cos\frac{m\pi}{a}x_q\cos\frac{n\pi}{b}y_p}{\frac{m^2}{a^2}+\frac{n^2}{b^2}-\frac{k^2}{\pi^2}}\right]. \qquad (4.12)$$

and, the coupling impedance is given by

$$Z_{pq} = \frac{1}{W_p W_q}\int_{W_p}\int_{W_q} G(0,y_p \mid x_q,0)\, dx_q\, dy_p\,. \qquad (4.13)$$

Applying the methodology used in case A, the economised coupling impedance formula is given by

$$Z_{pq} = j\omega\mu h\left[\frac{\sin A(\pi-\theta_4)-\sin A(\pi-\theta_3)}{bk^2W_q\sin ak}+\frac{2b^2}{W_pW_q\pi^3}\right.$$

$$\left.\cdot\sum_{n=1}^{\infty}\frac{(\sin n\theta_1-\sin n\theta_2)\left[\sinh\frac{a(\pi-\theta_3)}{b}\sqrt{n^2-B^2}-\sinh\frac{a(\pi-\theta_4)}{b}\sqrt{n^2-B^2}\right]}{n(n^2-B^2)\sinh\frac{a\pi}{b}\sqrt{n^2-B^2}}\right] \tag{4.14}$$

where, $\theta_1=\frac{\pi}{b}\left(y_p+\frac{W_p}{2}\right);\theta_2=\frac{\pi}{b}\left(y_p-\frac{W_p}{2}\right);\theta_3=\frac{\pi}{a}\left(x_q+\frac{W_q}{2}\right);\ \theta_4=\frac{\pi}{a}\left(x_q-\frac{W_q}{2}\right)$.

The coupling impedance Z_{pq} is obtained in terms of two closed forms, and, a single infinite series.

Case C: Two ports on opposite sides

The two ports p, q are on opposite sides as shown in Figure 4.5.

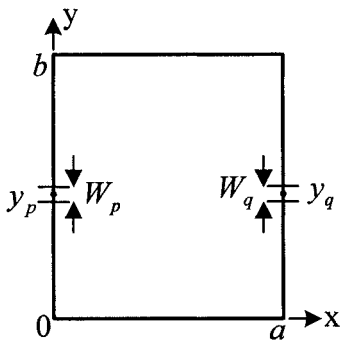

Figure 4.5. Case C: rectangular segment with two ports on opposite sides.

The two ports p, q are located at $(0,y_p)$, (a,y_q), hence the Green's function becomes

$$G(0,y_p\mid a,y_q)=\frac{j\omega\mu h}{ab}\left[-\frac{1}{k^2}+\frac{2a^2}{\pi^2}\sum_{m=1}^{\infty}\frac{(-1)^m}{m^2-A^2}+\frac{2b^2}{\pi^2}\sum_{n=1}^{\infty}\frac{\cos\frac{n\pi}{b}y_p\cos\frac{n\pi}{b}y_q}{n^2-B^2}\right.$$

$$\left.+\frac{4}{\pi^2}\sum_{m=1}^{\infty}\sum_{n=1}^{\infty}\frac{(-1)^m\cos\frac{n\pi}{b}y_p\cos\frac{n\pi}{b}y_q}{\frac{m^2}{a^2}+\frac{n^2}{b^2}-\frac{k^2}{\pi^2}}\right] \tag{4.15}$$

and the coupling impedance is given by

$$Z_{pq} = \frac{1}{W_p W_q} \int_{W_p} \int_{W_q} G(0, y_p \mid a, y_q)\, dy_q\, dy_p \tag{4.16}$$

The economised coupling impedance formula is then given by

$$Z_{pq} = j\omega\mu h \left[\frac{1}{bk \sin ak} - \frac{2b^2}{W_p W_q \pi^3} \sum_{n=1}^{\infty} \frac{(\sin n\theta_1 - \sin n\theta_2)(\sin n\theta_3 - \sin n\theta_4)}{n^2 \sqrt{n^2 - B^2} \sinh \frac{a\pi}{b} \sqrt{n^2 - B^2}} \right] \tag{4.17}$$

where, $\theta_1 = \frac{\pi}{b}\left(y_p + \frac{W_p}{2}\right)$; $\theta_2 = \frac{\pi}{b}\left(y_p - \frac{W_p}{2}\right)$; $\theta_3 = \frac{\pi}{b}\left(y_q + \frac{W_q}{2}\right)$; $\theta_4 = \frac{\pi}{b}\left(y_q - \frac{W_q}{2}\right)$.

The coupling impedance Z_{pq} is obtained in terms of a closed form and a single infinite series.

In this section, the results for the perimeter port coupling impedance formulas have been given. For case A the formula for a perimeter port input impedance has been given.

Economised formulas for a probe port input impedance, and, the coupling impedance between the probe and a perimeter port, are derived in the following sections.

4.4 New Probe Feed Input Impedance Formula for a Rectangular Segment

The input, or, self impedance at the probe is obtained by, initially, constructing a non economised formula for a coupling impedance Z_{pq}, between two separate probe feeds, as shown in Figure 4.6.

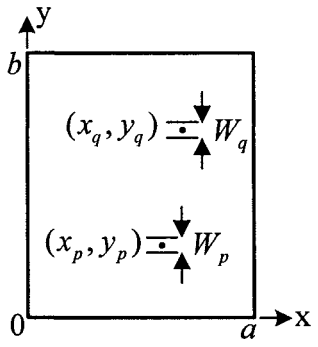

Figure 4.6. Rectangular segment with two probe feeds.

The general coupling impedance formula

$$Z_{pq} = \frac{1}{W_p W_q} \int_{W_p} \int_{W_q} G(x_p, y_p \mid x_q, y_q)\, dy_q\, dy_p \tag{4.18}$$

is applied using the partitioned Green's function given in equation (4.4).

On integration, (see *Appendix 4A.2*) the initial non economised coupling impedance formula obtained is given by

$$Z_{pq} = \frac{j\omega\mu h}{ab W_p W_q}\left\{ -\frac{W_p W_q}{k^2} + \frac{2a^2 W_p W_q}{\pi^2} \sum_{m=1}^{\infty} \frac{\cos\frac{m\pi}{a} x_p \cos\frac{m\pi}{a} x_q}{m^2 - A^2} \right.$$

$$+ \frac{2b^4}{\pi^4} \sum_{n=1}^{\infty} \frac{(\sin n\theta_1 - \sin n\theta_2)(\sin n\theta_3 - \sin n\theta_4)}{n^2(n^2 - B^2)}$$

$$\left. + \frac{4b^2}{\pi^4} \sum_{m=1}^{\infty} \sum_{n=1}^{\infty} \frac{\cos\frac{m\pi}{a} x_p \cos\frac{m\pi}{a} x_q (\sin n\theta_1 - \sin n\theta_2)(\sin n\theta_3 - \sin n\theta_4)}{n^2\left(\frac{m^2}{a^2} + \frac{n^2}{b^2} - \frac{k^2}{\pi^2}\right)} \right\} \tag{4.19}$$

and, $\theta_1 = \frac{\pi}{b}\left(y_p + \frac{W_p}{2}\right)$; $\theta_2 = \frac{\pi}{b}\left(y_p - \frac{W_p}{2}\right)$; $\theta_3 = \frac{\pi}{b}\left(y_q + \frac{W_q}{2}\right)$; $\theta_4 = \frac{\pi}{b}\left(y_q - \frac{W_q}{2}\right)$.

The probe input impedance is then obtained by taking, $q = p$, and, then, to apply the economisation procedure as described below.

With, $q = p$

$$Z_{pp}=\frac{j\omega\mu h}{abW_p^2}\left\{-\frac{W_p^2}{k^2}+\frac{2a^2W_p^2}{\pi^2}\sum_{m=1}^{\infty}\frac{\cos^2\frac{m\pi}{a}x_p}{m^2-A^2}+\frac{2b^4}{\pi^4}\sum_{n=1}^{\infty}\frac{(\sin n\theta_1-\sin n\theta_2)^2}{n^2(n^2-B^2)}\right.$$

$$\left.+\frac{4a^2b^2}{\pi^4}\sum_{m=1}^{\infty}\sum_{n=1}^{\infty}\frac{\cos^2\frac{m\pi}{a}x_p(\sin n\theta_1-\sin n\theta_2)^2}{n^2(m^2+D^2)}\right\}, \tag{4.20}$$

or,

$$Z_{pp}=\frac{j\omega\mu h}{abW_p^2}\left\{-\frac{W_p^2}{k^2}+\frac{2a^2W_p^2}{\pi^2}S_1(m)+\frac{2b^4}{\pi^4}S_2(n)+\frac{4a^2b^2}{\pi^4}S_3(m,n)\right\} \tag{4.21}$$

where, $D^2=\frac{a^2}{b^2}\left(n^2-\frac{b^2k^2}{\pi^2}\right)=\frac{a^2}{b^2}(n^2-B^2)$.

The closed forms have been applied to the each of above infinite series as follows:

$$S_1(m)=\sum_{m=1}^{\infty}\frac{\cos^2\frac{m\pi}{a}x_p}{m^2-A^2}=\frac{\pi^2}{2a^2k^2}-\frac{\pi^2[\cos ak+\cos k(a-2x_p)]}{4ak\sin ak}, \tag{4.22}$$

$$S_2(n)=\sum_{n=1}^{\infty}\frac{(\sin n\theta_1-\sin n\theta_2)^2}{n^2(n^2-B^2)}, \tag{4.23}$$

$$S_3(m,n)=\sum_{m=1}^{\infty}\sum_{n=1}^{\infty}\frac{\cos^2\frac{m\pi}{a}x_p(\sin n\theta_1-\sin n\theta_2)^2}{n^2(m^2+D^2)}$$

$$=\frac{b\pi}{4a}\sum_{n=1}^{\infty}\frac{(\sin n\theta_1-\sin n\theta_2)^2\left[\cosh\frac{a\pi}{b}\sqrt{n^2-B^2}+\cosh\frac{(a-2x_p)\pi}{b}\sqrt{n^2-B^2}\right]}{n^2\sqrt{n^2-B^2}\sinh\frac{a\pi}{b}\sqrt{n^2-B^2}}-\frac{b^2}{2a^2}S_2(n). \tag{4.24}$$

The series for $S_1(m)$ is summed to closed form. Substituting $S_1(m)$, and $S_3(m,n)$ from equations (4.22), and (4.24) respectively into equation (4.21) eliminates the terms $-W_p^2/k^2$, and the infinite series $S_2(n)$. Also the double infinite series $S_3(m,n)$ has been reduced to single series form.

The new resulting economised formula for Z_{pp} is then given by [75]

$$Z_{pp} = Z_{in} = j\omega\mu h\left\{-\frac{\cos ak + \cos k(a-2x_p)}{2bk\sin ak}\right.$$

$$\left. + \frac{b^2}{W_p^2\pi^3}\sum_{n=1}^{\infty}\frac{(\sin n\theta_1 - \sin n\theta_2)^2\left[\cosh\frac{a\pi}{b}\sqrt{n^2-B^2} + \cosh\frac{(a-2x_p)\pi}{b}\sqrt{n^2-B^2}\right]}{n^2\sqrt{n^2-B^2}\sinh\frac{a\pi}{b}\sqrt{n^2-B^2}}\right\}. \quad (4.25)$$

The probe input impedance Z_{pp} is obtained in terms of a closed form and a single infinite series.

For a rectangular segment with the dimensions $a = 38.75\,\text{mm}$, $b = 47.42\,\text{mm}$, $W_p = 1.26\,\text{mm}$, a Q-factor of 40, and probe feed located at $x_p = 12.7\,\text{mm}$ $(0.3277a)$, $y_p = 23.71\,\text{mm}$ $(0.5b)$ the calculated, simulated and measured input impedance are compared as shown in Figure 4.7. The results show good agreement. For the calculation an upper limit of 10 was used in evaluating the infinite series.

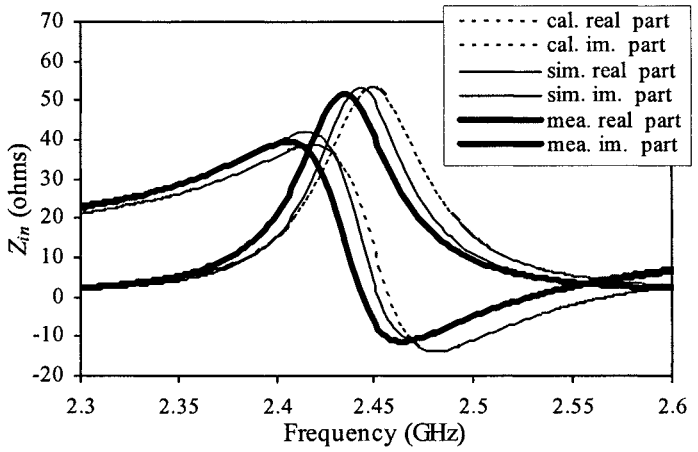

Figure 4.7. The comparison between the calculated, simulated, and measured probe feed input impedance for a rectangular segment.

4.5 Coupling Impedance between Probe Feed and a Perimeter Port on a Rectangular Segment

The port locations (x_p, y_p), $(0, y_q)$ are shown in Figure 4.8.

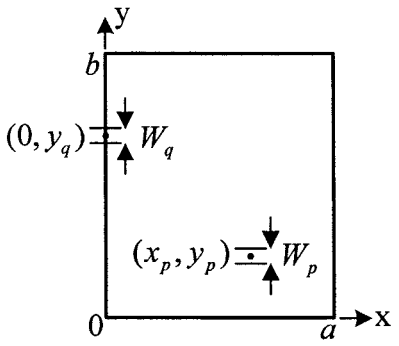

Figure 4.8. Rectangular segment with a probe port and a microstrip port.

The coupling impedance is given by

$$Z_{pq} = \frac{1}{W_p W_q} \int_{W_p} \int_{W_q} G(x_p, y_p \mid 0, y_q)\, dy_q\, dy_p \tag{4.26}$$

being a special case of the two probe cases in Section 4.4. In particular letting, $x_q = 0$, in the equation (4.19) gives the non economised formula for the impedance (see *Appendix 4A.3*),

$$Z_{pq} = \frac{j\omega\mu h}{abW_pW_q}\left\{-\frac{W_pW_q}{k^2} + \frac{2a^2W_pW_q}{\pi^2}S_1(m) + \frac{2b^4}{\pi^4}S_2(n) + \frac{4a^2b^2}{\pi^4}S_3(m,n)\right\} \tag{4.27}$$

where, $S_1(m), S_2(n)$, and, $S_3(m,n)$, together with their closed form treatment are given below,

$$S_1(m) = \sum_{m=1}^{\infty} \frac{\cos\frac{m\pi}{a}x_p}{m^2 - A^2} = \frac{\pi^2}{2a^2k^2} - \frac{\pi^2 \cos k(a - x_p)}{2ak \sin ak}, \tag{4.28}$$

$$S_2(n) = \sum_{n=1}^{\infty} \frac{(\sin n\theta_1 - \sin n\theta_2)(\sin n\theta_3 - \sin n\theta_4)}{n^2(n^2 - B^2)}, \tag{4.29}$$

$$S_3(m,n)=\sum_{m=1}^{\infty}\sum_{n=1}^{\infty}\frac{\cos\frac{m\pi}{a}x_p(\sin n\theta_1-\sin n\theta_2)(\sin n\theta_3-\sin n\theta_4)}{n^2(m^2+D^2)}$$

$$=\frac{b\pi}{2a}\sum_{n=1}^{\infty}\frac{(\sin n\theta_1-\sin n\theta_2)(\sin n\theta_3-\sin n\theta_4)\cosh\frac{(a-x_p)\pi}{b}\sqrt{n^2-B^2}}{n^2\sqrt{n^2-B^2}\sinh\frac{a\pi}{b}\sqrt{n^2-B^2}}-\frac{b^2}{2a^2}S_2(n), \qquad (4.30)$$

where, $\theta_1=\frac{\pi}{b}\left(y_p+\frac{W_p}{2}\right)$; $\theta_2=\frac{\pi}{b}\left(y_p-\frac{W_p}{2}\right)$; $\theta_3=\frac{\pi}{b}\left(y_q+\frac{W_q}{2}\right)$; $\theta_4=\frac{\pi}{b}\left(y_q-\frac{W_q}{2}\right)$,

$D^2=\frac{a^2}{b^2}(n^2-B^2)$.

The series for $S_1(m)$ is summed to closed form. Substituting $S_1(m)$, and $S_3(m,n)$ from equations (4.28), and (4.30) respectively into equation (4.27) eliminates the terms $-W_pW_q/k^2$, and the infinite series $S_2(n)$. Also the double infinite series $S_3(m,n)$ has been reduced to a single series.

The new economised formula for Z_{pq} is then given by [75]

$$Z_{pq}=j\omega\mu h\left\{-\frac{\cos k(a-x_p)}{bk\sin ak}\right.$$

$$\left.+\frac{2b^2}{W_pW_q\pi^3}\sum_{n=1}^{\infty}\frac{(\sin n\theta_1-\sin n\theta_2)(\sin n\theta_3-\sin n\theta_4)\cosh\frac{(a-x_p)\pi}{b}\sqrt{n^2-B^2}}{n^2\sqrt{n^2-B^2}\sinh\frac{a\pi}{b}\sqrt{n^2-B^2}}\right\}. \qquad (4.31)$$

The coupling impedance Z_{pq} is obtained in terms of a closed form and a single infinite series.

In the above sections economised coupling impedance formulas for three cases between two perimeter ports on a rectangular segment have been obtained. By coalescing two ports on the same side an expression for the input impedance of a microstrip feed has been obtained. Further new formulas for the input impedance of a probe feed on a

rectangular patch, and, the coupling impedance between the probe and a perimeter port has been obtained.

4.6 Coupling Impedances for Perimeter Ports on the Triangular Segment

The coupling impedances between two perimeter ports on a right-angled isosceles triangular segment for the four cases shown in Figure 4.9 are derived in this section.

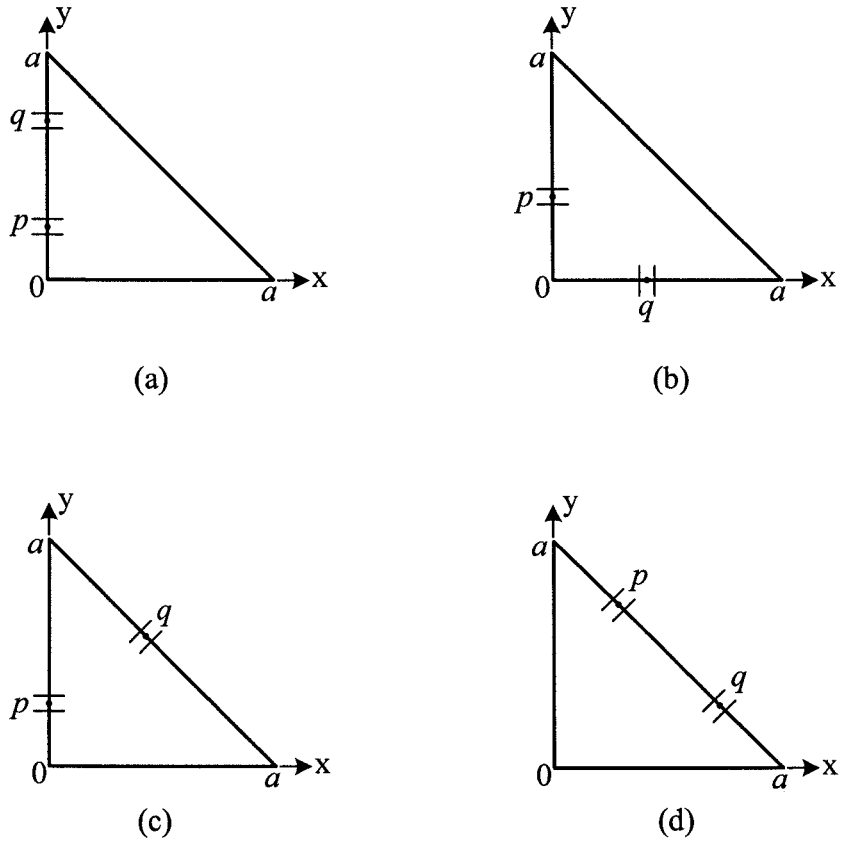

Figure 4.9. Perimeter ports on the triangular segment. (a) For case A: two ports on the same side. (b) For case B: two ports on adjacent sides. (c) For case C: two ports between perpendicular and hypotenuse sides. (d) For case D: two ports on the hypotenuse side.

Case A: two ports on the same perpendicular side

A triangular segment with two ports p and q, on the same side, with widths W_p, W_q is shown in Figure 4.10.

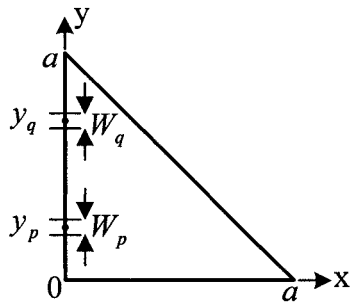

Figure 4.10. Case A: triangular segment with two ports on the same perpendicular side.

The two ports p, q are located at $(0, y_p)$, $(0, y_q)$, and the Green's function in equation (4.7) becomes

$$G(0,y_p \mid 0,y_q) = \frac{j2\omega\mu h}{\pi^2}\left\{ -\frac{\pi^2}{a^2k^2} + \sum_{m=1}^{\infty} \frac{\left[1+(-1)^m \cos(m\pi y_p/a)\right]\left[1+(-1)^m \cos(m\pi y_q/a)\right]}{m^2 - A^2} \right.$$

$$\left. + \sum_{m=1}^{\infty}\sum_{n=1}^{\infty} \frac{\left[\cos(n\pi y_p/a)+(-1)^{m+n}\cos(m\pi y_p/a)\right]\left[\cos(n\pi y_q/a)+(-1)^{m+n}\cos(m\pi y_q/a)\right]}{m^2+n^2-A^2} \right\} \tag{4.32}$$

and the coupling impedance is given by

$$Z_{pq} = \frac{1}{W_p W_q} \int_{W_p}\int_{W_q} G(0,y_p \mid 0,y_q)\, dy_q\, dy_p\,. \tag{4.33}$$

By integration, and using the closed form summations [77] (see *Appendix 4A.1*) the economised coupling impedance formula is then given by

$$Z_{pq} = j\omega\mu h\Bigg\{-\frac{\cot ak}{ak}+\frac{\sin A\theta_4-\sin A\theta_3}{ak^2W_q\sin ak}$$

$$+\frac{2a^2}{W_pW_q\pi^3}\sum_{m=1}^{\infty}\frac{(\sin m\theta_1-\sin m\theta_2)(\sin m\theta_3-\sin m\theta_4)\coth\pi\sqrt{m^2-A^2}}{m^2\sqrt{m^2-A^2}}$$

$$+\frac{2a^2}{W_pW_q\pi^3}\sum_{m=1}^{\infty}\frac{(-1)^m(\sin m\theta_1-\sin m\theta_2)\left(\sinh\theta_3\sqrt{m^2-A^2}-\sinh\theta_4\sqrt{m^2-A^2}\right)}{m(m^2-A^2)\sinh\pi\sqrt{m^2-A^2}}\Bigg\} \quad (4.34)$$

where, $\theta_1=\frac{\pi}{a}\left(y_p+\frac{W_p}{2}\right)$; $\theta_2=\frac{\pi}{a}\left(y_p-\frac{W_p}{2}\right)$; $\theta_3=\frac{\pi}{a}\left(y_q+\frac{W_q}{2}\right)$; $\theta_4=\frac{\pi}{a}\left(y_q-\frac{W_q}{2}\right)$.

The coupling impedance formula is obtained in terms of closed forms and single infinite series.

For a single microstrip feed on the perpendicular side of the triangular segment, the self impedance formula can be obtained by taking $q=p$, $\theta_3=\theta_1$,and, $\theta_4=\theta_2$. Therefore, an economised microstrip feed self impedance formula is given by

$$Z_{pp}=Z_{in}=j\omega\mu h\Bigg\{-\frac{\cot ak}{ak}+\frac{\sin A\theta_2-\sin A\theta_1}{ak^2W_p\sin ak}$$

$$+\frac{2a^2}{W_p^2\pi^3}\sum_{m=1}^{\infty}\frac{(\sin m\theta_1-\sin m\theta_2)^2\coth\pi\sqrt{m^2-A^2}}{m^2\sqrt{m^2-A^2}}$$

$$+\frac{2a^2}{W_p^2\pi^3}\sum_{m=1}^{\infty}\frac{(-1)^m(\sin m\theta_1-\sin m\theta_2)\left(\sinh\theta_1\sqrt{m^2-A^2}-\sinh\theta_2\sqrt{m^2-A^2}\right)}{m(m^2-A^2)\sinh\pi\sqrt{m^2-A^2}}\Bigg\}. \quad (4.35)$$

A perpendicular side perimeter port input impedance formula is obtained in terms of closed forms and single infinite series.

Case B: two ports on adjacent side

The two ports p, q are shown in Figure 4.11.

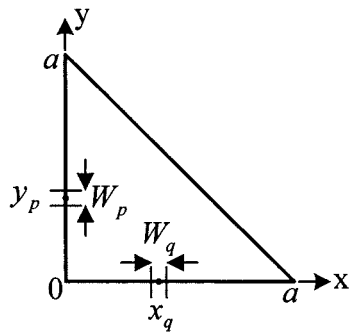

Figure 4.11. Case B: triangular segment with two ports on adjacent sides.

The two ports p, q are located at $(0, y_p)$, $(x_q, 0)$, and the Green's function becomes

$$G(0,y_p \mid x_q,0)=\frac{j2\omega\mu h}{\pi^2}\left\{-\frac{\pi^2}{a^2k^2}+\sum_{m=1}^{\infty}\frac{\left[1+(-1)^m\cos(m\pi y_p/a)\right]\left[(-1)^m+\cos(m\pi x_q/a)\right]}{m^2-A^2}\right.$$

$$\left.+\sum_{m=1}^{\infty}\sum_{n=1}^{\infty}\frac{\left[\cos(n\pi y_p/a)+(-1)^{m+n}\cos(m\pi y_p/a)\right]\left[\cos(m\pi x_q/a)+(-1)^{m+n}\cos(n\pi x_q/a)\right]}{m^2+n^2-A^2}\right\} \tag{4.36}$$

and, the coupling impedance is given by

$$Z_{pq}=\frac{1}{W_pW_q}\int_{W_p}\int_{W_q}G(0,y_p \mid x_q,0)\,dx_q\,dy_p\,. \tag{4.37}$$

Applying the methodology used in case A, the economised coupling impedance formula is given by

$$Z_{pq}=j\omega\mu h\left\{\frac{1}{ak\sin ak}-\frac{\sin A(\pi-\theta_3)-\sin A(\pi-\theta_4)}{ak^2W_q\sin ak}\right.$$

$$+\frac{2a^2}{W_pW_q\pi^3}\sum_{m=1}^{\infty}\frac{(\sin m\theta_1-\sin m\theta_2)\left[\sinh(\pi-\theta_3)\sqrt{m^2-A^2}-\sinh(\pi-\theta_4)\sqrt{m^2-A^2}\right]}{m(m^2-A^2)\sinh\pi\sqrt{m^2-A^2}}$$

$$\left.-\frac{2a^2}{W_pW_q\pi^3}\sum_{m=1}^{\infty}\frac{(-1)^m(\sin m\theta_1-\sin m\theta_2)(\sin m\theta_3-\sin m\theta_4)}{m^2\sqrt{m^2-A^2}\sinh\pi\sqrt{m^2-A^2}}\right\} \tag{4.38}$$

where, $\theta_1 = \frac{\pi}{a}\left(y_p + \frac{W_p}{2}\right)$; $\theta_2 = \frac{\pi}{a}\left(y_p - \frac{W_p}{2}\right)$; $\theta_3 = \frac{\pi}{a}\left(x_q + \frac{W_q}{2}\right)$; $\theta_4 = \frac{\pi}{a}\left(x_q - \frac{W_q}{2}\right)$.

The coupling impedance formula is obtained in terms of closed forms and single infinite series.

Case C: two ports between perpendicular and hypotenuse sides

The two ports p, q are shown in Figure 4.12.

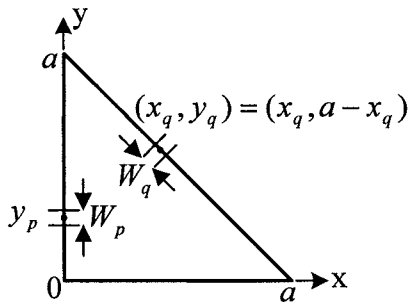

Figure 4.12. Case C: triangular segment with ports between perpendicular and hypotenuse sides.

The two ports p, q are located at $(0, y_p)$, $(x_q, a - x_q)$, and the Green's function becomes

$$G(0, y_p \mid x_q, a - x_q) = \frac{j2\omega\mu h}{\pi^2}\left\{-\frac{\pi^2}{a^2 k^2}\right.$$

$$+\sum_{m=1}^{\infty}\frac{\left[1+(-1)^m\cos\frac{m\pi y_p}{a}\right]\left[\cos\frac{m\pi x_q}{a}+(-1)^m\cos\frac{m\pi(a-x_q)}{a}\right]}{m^2 - A^2}$$

$$+\sum_{m=1}^{\infty}\sum_{n=1}^{\infty}\frac{\left[\cos\frac{n\pi y_p}{a}+(-1)^{m+n}\cos\frac{m\pi y_p}{a}\right]}{m^2+n^2-A^2}$$

$$\left.\cdot\left[\cos\frac{m\pi x_q}{a}\cos\frac{n\pi(a-x_q)}{a}+(-1)^{m+n}\cos\frac{n\pi x_q}{a}\cos\frac{m\pi(a-x_q)}{a}\right]\right\} \quad (4.39)$$

and, the coupling impedance is given by

$$Z_{pq} = \frac{\sqrt{2}}{W_p W_q} \int_{W_p} \int_{W_q} G(0, y_p \mid x_q, a - x_q)\, dx_q\, dy_p \,. \tag{4.40}$$

The economised coupling impedance formula is then given by

$$\begin{aligned} Z_{pq} = j\omega\mu h \Bigg\{ & \frac{2}{a^2 k^2} + \frac{2\sqrt{2}\left[\sin A(\pi - \theta_3) - \sin A(\pi - \theta_4)\right]}{ak^2 W_q \sin ak} \\ & - \frac{2\left[\sin\left(A\theta_1/\sqrt{2}\right) - \sin\left(A\theta_2/\sqrt{2}\right)\right]}{ak^2 W_p \sin\left(ak/\sqrt{2}\right)} \\ & + \frac{4\sqrt{2}a^2}{W_p W_q \pi^4} \sum_{m=1}^{\infty} \frac{(-1)^m (\sin m\theta_1 - \sin m\theta_2)(\sin m\theta_3 - \sin m\theta_4)}{m^2 (m^2 - A^2)} \\ & + \frac{\sqrt{2}a^2}{W_p W_q \pi^4} \sum_{m=1}^{\infty} \frac{(-1)^m (\sin m\theta_1 - \sin m\theta_2)(\sin m2\theta_3 - \sin m2\theta_4)}{m^2 (m^2 - A^2/2)} \\ & + \frac{4\sqrt{2}a^2}{W_p W_q \pi^4} \sum_{n=1}^{\infty} \sum_{m=n+1}^{\infty} \left[\frac{(-1)^n (\sin n\theta_1 - \sin n\theta_2)}{n(m^2 + n^2 - A^2)} + \frac{(-1)^m (\sin m\theta_1 - \sin m\theta_2)}{m(m^2 + n^2 - A^2)} \right] \\ & \cdot \left[\frac{\sin(m+n)\theta_3 - \sin(m+n)\theta_4}{m+n} + \frac{\sin(m-n)\theta_3 - \sin(m-n)\theta_4}{m-n} \right] \Bigg\} \end{aligned} \tag{4.41}$$

where, $\theta_1 = \frac{\pi}{a}\left(y_p + \frac{W_p}{2}\right)$; $\theta_2 = \frac{\pi}{a}\left(y_p - \frac{W_p}{2}\right)$; $\theta_3 = \frac{\pi}{a}\left(x_q + \frac{W_q}{2\sqrt{2}}\right)$; $\theta_4 = \frac{\pi}{a}\left(x_q - \frac{W_q}{2\sqrt{2}}\right)$.

The coupling impedance formula involves closed forms, single series, and, a semi-infinite double series.

Case D: two ports on the hypotenuse side

The two ports p, q are shown in Figure 4.13.

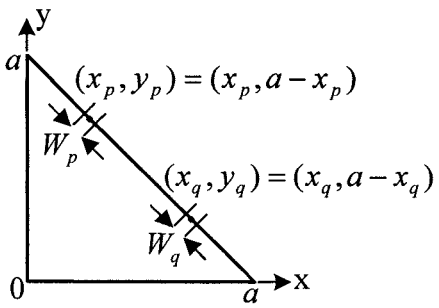

Figure 4.13. Case D: triangular segment with two ports on the hypotenuse side.

The two ports p, q are located at $(x_p, a-x_p), (x_q, a-x_q)$, and the Green's function becomes

$$G(x_p, a-x_p \mid x_q, a-x_q) = \frac{j2\omega\mu h}{\pi^2}\left\{-\frac{\pi^2}{a^2k^2}\right.$$

$$+\sum_{m=1}^{\infty}\frac{\left[\cos\frac{m\pi x_p}{a}+(-1)^m\cos\frac{m\pi(a-x_p)}{a}\right]\left[\cos\frac{m\pi x_q}{a}+(-1)^m\cos\frac{m\pi(a-x_q)}{a}\right]}{m^2-A^2}$$

$$+\sum_{m=1}^{\infty}\sum_{n=1}^{\infty}\frac{\left[\cos\frac{m\pi x_p}{a}\cos\frac{n\pi(a-x_p)}{a}+(-1)^{m+n}\cos\frac{n\pi x_p}{a}\cos\frac{m\pi(a-x_p)}{a}\right]}{m^2+n^2-A^2}$$

$$\left.\cdot\left[\cos\frac{m\pi x_q}{a}\cos\frac{n\pi(a-x_q)}{a}+(-1)^{m+n}\cos\frac{n\pi x_q}{a}\cos\frac{m\pi(a-x_q)}{a}\right]\right\} \qquad (4.42)$$

and, the coupling impedance is given by

$$Z_{pq} = \frac{2}{W_p W_q}\int_{W_p}\int_{W_q} G(x_p, a-x_p \mid x_q, a-x_q)\, dx_q\, dx_p\,. \qquad (4.43)$$

The economised coupling impedance formula is then given by

$$Z_{pq} = j\omega\mu h\left\{\frac{1}{a^2k^2}-\frac{\cot\left(ak/\sqrt{2}\right)}{\sqrt{2}\,ak}+\frac{\sin\left[A(\pi-2\theta_1)/\sqrt{2}\right]-\sin\left[A(\pi-2\theta_2)/\sqrt{2}\right]}{\sqrt{2}\,ak^2W_p\sin\left(ak/\sqrt{2}\right)}\right.$$

$$\left.+\frac{\sin\left[A(\pi-2\theta_3)/\sqrt{2}\right]-\sin\left[A(\pi-2\theta_4)/\sqrt{2}\right]}{\sqrt{2}\,ak^2W_q\sin\left(ak/\sqrt{2}\right)}\right.$$

$$+\frac{16a^2}{W_pW_q\pi^4}\sum_{m=1}^{\infty}\frac{(\sin m\theta_1-\sin m\theta_2)(\sin m\theta_3-\sin m\theta_4)}{m^2(m^2-A^2)}$$

$$+\frac{a^2}{2W_pW_q\pi^4}\sum_{m=1}^{\infty}\frac{(\sin m2\theta_1-\sin m2\theta_2)(\sin m2\theta_3-\sin m2\theta_4)}{m^2(m^2-A^2/2)}$$

$$+\frac{8a^2}{W_pW_q\pi^4}\sum_{n=1}^{\infty}\sum_{m=n+1}^{\infty}\left[\frac{\sin(m+n)\theta_1-\sin(m+n)\theta_2}{(m+n)(m^2+n^2-A^2)}+\frac{\sin(m-n)\theta_1-\sin(m-n)\theta_2}{(m-n)(m^2+n^2-A^2)}\right]$$

$$\cdot\left[\frac{\sin(m+n)\theta_3-\sin(m+n)\theta_4}{m+n}+\frac{\sin(m-n)\theta_3-\sin(m-n)\theta_4}{m-n}\right]\Bigg\} \quad (4.44)$$

where, $\theta_1=\frac{\pi}{a}\left(x_p+\frac{W_p}{2\sqrt{2}}\right)$; $\theta_2=\frac{\pi}{a}\left(x_p-\frac{W_p}{2\sqrt{2}}\right)$; $\theta_3=\frac{\pi}{a}\left(x_q+\frac{W_q}{2\sqrt{2}}\right)$; $\theta_4=\frac{\pi}{a}\left(x_q-\frac{W_q}{2\sqrt{2}}\right)$.

The coupling impedance formula involves closed forms, single series, and, a semi-infinite double series.

For a single microstrip feed on the hypotenuse, the self impedance formula can be obtained by taking port $q=p$, $\theta_3=\theta_1$, and, $\theta_4=\theta_2$, in equation (4.44). An economised microstrip feed self impedance formula is then given by

$$Z_{pp}=j\omega\mu h\Bigg\{\frac{1}{a^2k^2}-\frac{\cot\left(ak/\sqrt{2}\right)}{\sqrt{2}\,ak}$$

$$+\frac{\sqrt{2}\left\{\sin\left[A(\pi-2\theta_1)/\sqrt{2}\right]-\sin\left[A(\pi-2\theta_2)/\sqrt{2}\right]\right\}}{ak^2W_p\sin\left(ak/\sqrt{2}\right)}$$

$$+\frac{16a^2}{W_p^2\pi^4}\sum_{m=1}^{\infty}\frac{(\sin m\theta_1-\sin m\theta_2)^2}{m^2(m^2-A^2)}+\frac{a^2}{2W_p^2\pi^4}\sum_{m=1}^{\infty}\frac{(\sin m2\theta_1-\sin m2\theta_2)^2}{m^2(m^2-A^2/2)}$$

$$+\frac{8a^2}{W_p^2\pi^4}\sum_{n=1}^{\infty}\sum_{m=n+1}^{\infty}\frac{1}{m^2+n^2-A^2}\left[\frac{\sin(m+n)\theta_1-\sin(m+n)\theta_2}{m+n}+\frac{\sin(m-n)\theta_1-\sin(m-n)\theta_2}{m-n}\right]^2\Bigg\}. \quad (4.45)$$

In this special case $(q=p)$ the term $\sum_{m=1}^{\infty}\frac{(\sin m\theta_1-\sin m\theta_2)^2}{m^2(m^2-A^2)}$ can be summed to the three closed form terms, as shown below,

$$\sum_{m=1}^{\infty}\frac{(\sin m\theta_1-\sin m\theta_2)^2}{m^2(m^2-A^2)}=\sum_{m=1}^{\infty}\frac{1}{m^2(m^2-A^2)}-\frac{1}{2}\sum_{m=1}^{\infty}\frac{\cos m2\theta_1}{m^2(m^2-A^2)}-\frac{1}{2}\sum_{m=1}^{\infty}\frac{\cos m2\theta_2}{m^2(m^2-A^2)}$$

$$-\sum_{m=1}^{\infty}\frac{\cos m(\theta_1-\theta_2)}{m^2(m^2-A^2)}+\sum_{m=1}^{\infty}\frac{\cos m(\theta_1+\theta_2)}{m^2(m^2-A^2)}$$

$$=\frac{W_p^2\pi^4}{4a^4k^2}-\frac{W_p\pi^4}{2\sqrt{2}a^3k^2}+\frac{\pi^4}{4a^3k^3\sin ak}[-2\cos A\pi+\cos A(\pi-2\theta_1)+\cos A(\pi-2\theta_2)$$

$$+2\cos A(\pi-\theta_1+\theta_2)-2\cos A(\pi-\theta_1-\theta_2)]. \quad (4.46)$$

The economised self impedance can also be presented as

$$Z_{pp}=Z_{in}=j\omega\mu h\left\{\frac{5}{a^2k^2}-\frac{\cot\left(ak/\sqrt{2}\right)}{\sqrt{2}\,ak}-\frac{4\sqrt{2}}{ak^2W_p}\right.$$

$$+\frac{\sqrt{2}\left\{\sin\left[A(\pi-2\theta_1)/\sqrt{2}\right]-\sin\left[A(\pi-2\theta_2)/\sqrt{2}\right]\right\}}{ak^2W_p\sin\left(ak/\sqrt{2}\right)}+\frac{4}{ak^3W_p^2\sin ak}[-2\cos A\pi$$

$$+\cos A(\pi-2\theta_1)+\cos A(\pi-2\theta_2)+2\cos A(\pi-\theta_1+\theta_2)-2\cos A(\pi-\theta_1-\theta_2)]$$

$$+\frac{a^2}{2W_p^2\pi^4}\sum_{m=1}^{\infty}\frac{(\sin m2\theta_1-\sin m2\theta_2)^2}{m^2(m^2-A^2/2)}+\frac{8a^2}{W_p^2\pi^4}\sum_{n=1}^{\infty}\sum_{m=n+1}^{\infty}\frac{1}{m^2+n^2-A^2}$$

$$\left.\cdot\left[\frac{\sin(m+n)\theta_1-\sin(m+n)\theta_2}{m+n}+\frac{\sin(m-n)\theta_1-\sin(m-n)\theta_2}{m-n}\right]^2\right\}. \quad (4.47)$$

A hypotenuse side perimeter port input impedance formula is obtained in terms of closed forms, single series, and, a semi-infinite double series.

To verify the coupling impedance formulas, a triangular patch with, the length of the perpendicular side $a=39.02\,\text{mm}$, $W_p=W_q=1\,\text{mm}$, and a Q-factor of 81, was modelled, and fabricated [76]. For the calculations, an upper limit of 30 was used in evaluating the infinite series.

For Case A (see Figure 4.10), the two ports are located at $y_p=13.657\,\text{mm}$ $(0.35a)$, and $y_q=25.363\,\text{mm}$ $(0.65a)$. For Case B (see Figure 4.11), the two ports are located at

$y_p = 13.657\,\text{mm}$ $(0.35a)$, and $x_q = 11.706\,\text{mm}$ $(0.3a)$. For Case C (see Figure 4.12), the two ports are located at $y_p = 13.657\,\text{mm}$ $(0.35a)$, and $x_q = 11.706\,\text{mm}$ $(0.3a)$. For Case D (see Figure 4.13), the two ports are located at $x_p = 17.559\,\text{mm}$ $(0.45a)$, and $x_q = 27.314\,\text{mm}$ $(0.7a)$.

Good agreement between the calculated, simulated (Ansoft Ensemble) and measured results for Z_{pq} are shown in Figure 4.14.

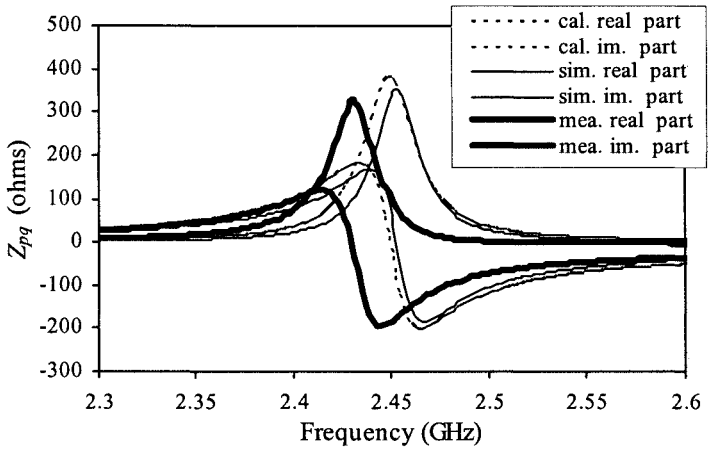

(a)

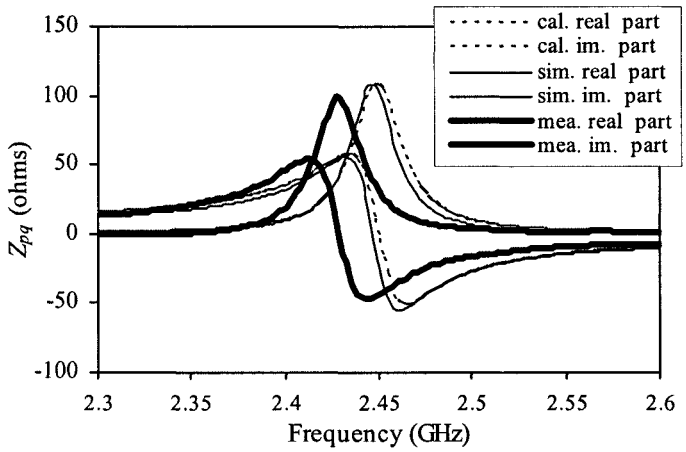

(b)

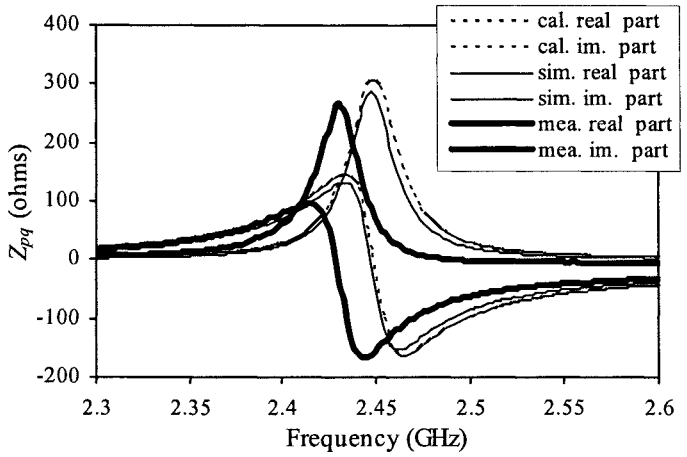

(c)

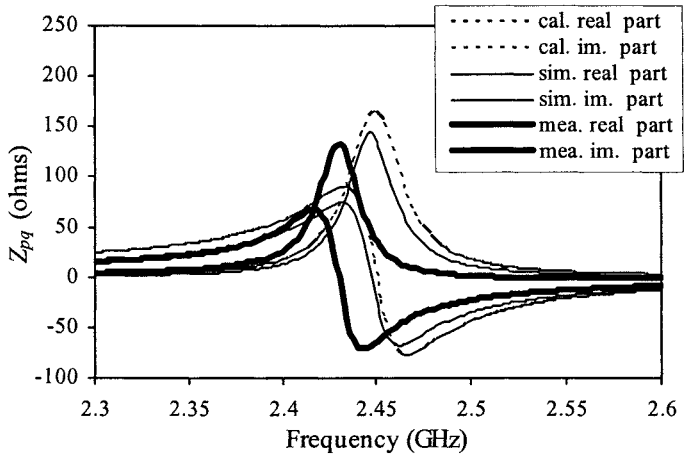

(d)

Figure 4.14. The comparison between the calculated, simulated, and measured perimeter port coupling impedance for a triangular patch. (a) Case A. (b) Case B. (c) Case C. (d) Case D.

4.7 New Probe Feed Input Impedance Formula for the Triangular Segment

The self impedance is obtained by, initially, constructing a non economised formula for the coupling impedance Z_{pq}, between two separate probe feeds, as shown in Figure 4.15.

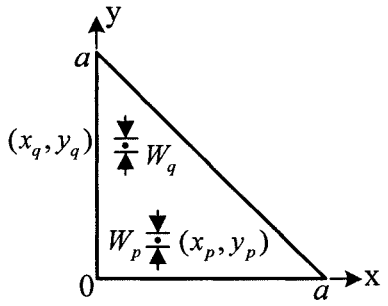

Figure 4.15. Triangular segment with two probe feeds.

The general coupling impedance formula

$$Z_{pq} = \frac{1}{W_p W_q} \int_{W_p} \int_{W_q} G(x_p, y_p \mid x_q, y_q)\, dy_q\, dy_p \tag{4.48}$$

is applied using the partitioned Green's function given in equation (4.7).

By integration (see *Appendix 4A.4*) the initial non economised coupling impedance formula is given by

$$Z_{pq} = \frac{j2\omega\mu h}{W_p W_q \pi^2} \left\{ -\frac{W_p W_q \pi^2}{a^2 k^2} + \sum_{m=1}^{\infty} \left[W_p W_q \cos\frac{m\pi}{a} x_p \cos\frac{m\pi}{a} x_q \right.\right.$$

$$+(-1)^m \frac{aW_p}{m\pi}(\sin m\theta_3 - \sin m\theta_4)\cos\frac{m\pi}{a} x_p + (-1)^m \frac{aW_q}{m\pi}(\sin m\theta_1 - \sin m\theta_2)\cos\frac{m\pi}{a} x_q$$

$$\left.\left. + \frac{a^2}{m^2\pi^2}(\sin m\theta_1 - \sin m\theta_2)(\sin m\theta_3 - \sin m\theta_4) \right] / (m^2 - A^2) \right.$$

$$+ \frac{2a^2}{\pi^2} \sum_{m=1}^{\infty} \sum_{n=1}^{\infty} \left[\frac{(\sin m\theta_1 - \sin m\theta_2)(\sin m\theta_3 - \sin m\theta_4)}{m^2} \cos\frac{n\pi}{a} x_p \cos\frac{n\pi}{a} x_q \right.$$

$$+\frac{(-1)^{m+n}(\sin n\theta_1-\sin n\theta_2)(\sin m\theta_3-\sin m\theta_4)}{mn}\cos\frac{m\pi}{a}x_p\cos\frac{n\pi}{a}x_q\Bigg]/(m^2+n^2-A^2)\Bigg\}$$

(4.49)

and, $\theta_1=\frac{\pi}{a}\left(y_p+\frac{W_p}{2}\right)$; $\theta_2=\frac{\pi}{a}\left(y_p-\frac{W_p}{2}\right)$; $\theta_3=\frac{\pi}{a}\left(y_q+\frac{W_q}{2}\right)$; $\theta_4=\frac{\pi}{a}\left(y_q-\frac{W_q}{2}\right)$.

The self impedance is then obtained by taking, $q=p$, and, then, to apply the economisation procedure as described below.

When $q=p$ for a single probe port,

$$Z_{pp}=\frac{j2\omega\mu h}{W_p^2\pi^2}\Bigg\{-\frac{W_p^2\pi^2}{a^2k^2}+W_p^2\sum_{m=1}^{\infty}\frac{\cos^2(m\pi x_p/a)}{m^2-A^2}$$

$$+\frac{2aW_p}{\pi}\sum_{m=1}^{\infty}\frac{(-1)^m(\sin m\theta_1-\sin m\theta_2)\cos(m\pi x_p/a)}{m(m^2-A^2)}+\frac{a^2}{\pi^2}\sum_{m=1}^{\infty}\frac{(\sin m\theta_1-\sin m\theta_2)^2}{m^2(m^2-A^2)}$$

$$+\frac{2a^2}{\pi^2}\sum_{m=1}^{\infty}\sum_{n=1}^{\infty}\frac{(\sin m\theta_1-\sin m\theta_2)^2\cos^2(n\pi x_p/a)}{m^2(m^2+n^2-A^2)}$$

$$+\frac{2a^2}{\pi^2}\sum_{m=1}^{\infty}\sum_{n=1}^{\infty}\frac{(-1)^{m+n}(\sin m\theta_1-\sin m\theta_2)(\sin n\theta_1-\sin n\theta_2)\cos(m\pi x_p/a)\cos(n\pi x_p/a)}{mn(m^2+n^2-A^2)}\Bigg\}$$

(4.50)

$$=\frac{j2\omega\mu h}{W_p^2\pi^2}\Bigg\{-\frac{W_p^2\pi^2}{a^2k^2}+W_p^2S_1(m)+\frac{2aW_p}{\pi}S_2(m)+\frac{a^2}{\pi^2}S_3(m)$$

$$+\frac{2a^2}{\pi^2}S_4(m,n)+\frac{2a^2}{\pi^2}S_5(m,n)\Bigg\} \tag{4.51}$$

where, the series, $S_1(m)$, $S_2(m)$, $S_3(m)$, $S_4(m,n)$, and, $S_5(m,n)$, together with their associated forms, are given below,

$$S_1(m)=\sum_{m=1}^{\infty}\frac{\cos^2(m\pi x_p/a)}{m^2-A^2}=\frac{\pi^2}{2a^2k^2}-\frac{\pi^2\left[\cos ak+\cos k(a-2x_p)\right]}{4ak\sin ak}, \tag{4.52}$$

$$S_2(m)=\sum_{m=1}^{\infty}\frac{(-1)^m(\sin m\theta_1-\sin m\theta_2)\cos(m\pi x_p/a)}{m(m^2-A^2)}$$

$$= \frac{W_p \pi^3}{2a^3 k^2} - \frac{\pi^3 (\sin A\theta_1 - \sin A\theta_2)\cos kx_p}{2a^2 k^2 \sin ak}, \tag{4.53}$$

$$S_3(m) = \sum_{m=1}^{\infty} \frac{(\sin m\theta_1 - \sin m\theta_2)^2}{m^2(m^2 - A^2)}, \tag{4.54}$$

$$S_4(m,n) = \sum_{m=1}^{\infty}\sum_{n=1}^{\infty} \frac{(\sin m\theta_1 - \sin m\theta_2)^2 \cos^2(n\pi x_p / a)}{m^2(m^2 + n^2 - A^2)}$$

$$= \frac{\pi}{4}\sum_{m=1}^{\infty} \frac{(\sin m\theta_1 - \sin m\theta_2)^2 \left[\cosh \pi\sqrt{m^2 - A^2} + \cosh \pi(1 - 2x_p / a)\sqrt{m^2 - A^2}\right]}{m^2\sqrt{m^2 - A^2}\sinh \pi\sqrt{m^2 - A^2}} - \frac{1}{2} S_3(m), \tag{4.55}$$

$$S_5(m,n) = \sum_{m=1}^{\infty}\sum_{n=1}^{\infty} \frac{(-1)^{m+n}(\sin m\theta_1 - \sin m\theta_2)(\sin n\theta_1 - \sin n\theta_2)\cos(m\pi x_p / a)\cos(n\pi x_p / a)}{mn(m^2 + n^2 - A^2)}$$

$$= -\frac{W_p \pi}{2a} S_2(m) + \frac{\pi}{2}\sum_{m=1}^{\infty} \frac{(-1)^m (\sin m\theta_1 - \sin m\theta_2)(\sinh \theta_1\sqrt{m^2 - A^2} - \sinh \theta_2\sqrt{m^2 - A^2})}{m(m^2 - A^2)\sinh \pi\sqrt{m^2 - A^2}}$$

$$\cdot \cos(m\pi x_p / a)\cosh(\pi x_p\sqrt{m^2 - A^2} / a). \tag{4.56}$$

The series for $S_1(m)$,and $S_2(m)$ are summed to closed form. Substituting $S_1(m)$, $S_2(m)$, $S_4(m,n)$ and $S_5(m,n)$ from equations (4.52), (4.53), (4.55), and (4.56) respectively into equation (4.51) eliminates the terms $-W_p^2\pi^2 / a^2k^2$, and the infinite series $S_3(m)$. Also the double infinite series $S_4(m,n)$, and $S_5(m,n)$ have been reduced to single series form.

The economised formula for Z_{pp} is then given by

$$Z_{pp} = Z_{in} = j\omega\mu h\left\{-\frac{\cos ak + \cos k(a - 2x_p)}{2ak \sin ak} - \frac{(\sin A\theta_1 - \sin A\theta_2)\cos kx_p}{ak^2 W_p \sin ak}\right.$$

$$+ \frac{a^2}{W_p^2\pi^3}\sum_{m=1}^{\infty} \frac{(\sin m\theta_1 - \sin m\theta_2)^2 \left[\cosh \pi\sqrt{m^2 - A^2} + \cosh \pi(1 - 2x_p / a)\sqrt{m^2 - A^2}\right]}{m^2\sqrt{m^2 - A^2}\sinh \pi\sqrt{m^2 - A^2}}$$

$$+ \frac{2a^2}{W_p^2\pi^3}\sum_{m=1}^{\infty} \frac{(-1)^m (\sin m\theta_1 - \sin m\theta_2)(\sinh \theta_1\sqrt{m^2 - A^2} - \sinh \theta_2\sqrt{m^2 - A^2})}{m(m^2 - A^2)\sinh \pi\sqrt{m^2 - A^2}}$$

$$\left.\cdot \cos(m\pi x_p / a)\cosh(\pi x_p\sqrt{m^2 - A^2} / a)\right\}. \tag{4.57}$$

The single probe port Z_{pp} is obtained in terms of closed forms and single infinite series.

A triangular segment with the dimension $a = 39.02\,\text{mm}$, $W_p = 1.26\,\text{mm}$, a Q-factor of 81, for a probe feed located at $x_p = 11.706\,\text{mm}$ $(0.3a)$, $y_p = 4.682\,\text{mm}$ $(0.12a)$ the calculated, simulated and measured input impedance are compared as shown in Figure 4.16. The results show good agreement. For the calculation an upper limit of 30 was used in evaluating the infinite series.

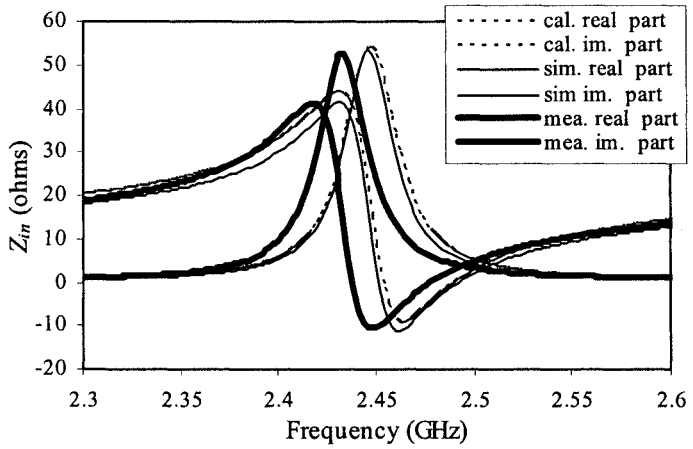

Figure 4.16. The comparison between the calculated, simulated, and measured probe feed input impedance for a triangular segment.

4.8 Coupling Impedance between Probe Feed and a Port on a Perpendicular Side on the Triangular Segment

The port locations (x_p, y_p), $(0, y_q)$ are shown in Figure 4.17.

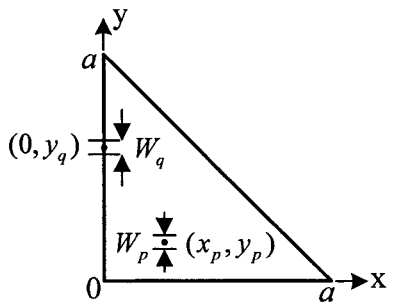

Figure 4.17. Triangular segment with a probe port and a port on a perpendicular side.

The coupling impedance is given by

$$Z_{pq} = \frac{1}{W_p W_q} \int_{W_p} \int_{W_q} G(x_p, y_p \mid 0, y_q)\, dy_q\, dy_p \tag{4.58}$$

being a special case of the two probe cases in Section 4.7. In particular letting, $x_q = 0$, in the equation (4.49) gives the non economised formula for the impedance (see *Appendix 4A.5*),

$$Z_{pq} = \frac{j2\omega\mu h}{W_p W_q \pi^2}\left\{ -\frac{W_p W_q \pi^2}{a^2 k^2} + W_p W_q S_1(m) + \frac{aW_q}{\pi} S_2(m) + \frac{aW_p}{\pi} S_3(m) + \frac{a^2}{\pi^2} S_4(m) \right.$$

$$\left. + \frac{2a^2}{\pi^2} S_5(m,n) + \frac{2a^2}{\pi^2} S_6(m,n) \right\}, \tag{4.59}$$

where, the series, $S_1(m), S_2(m), S_3(m), S_4(m), S_5(m,n), S_6(m,n)$ together with their closed forms are given below:

$$S_1(m) = \sum_{m=1}^{\infty} \frac{\cos(m\pi x_p / a)}{m^2 - A^2} = \frac{\pi^2}{2a^2 k^2} - \frac{\pi^2 \cos k(a - x_p)}{2ak \sin ak} \tag{4.60}$$

$$S_2(m) = \sum_{m=1}^{\infty} \frac{(-1)^m (\sin m\theta_1 - \sin m\theta_2)}{m(m^2 - A^2)} = \frac{W_p \pi^3}{2a^3 k^2} - \frac{\pi^3 (\sin A\theta_1 - \sin A\theta_2)}{2a^2 k^2 \sin ak}, \tag{4.61}$$

$$S_3(m) = \sum_{m=1}^{\infty} \frac{(-1)^m (\sin m\theta_3 - \sin m\theta_4) \cos(m\pi x_p / a)}{m(m^2 - A^2)}, \tag{4.62}$$

$$S_4(m) = \sum_{m=1}^{\infty} \frac{(\sin m\theta_1 - \sin m\theta_2)(\sin m\theta_3 - \sin m\theta_4)}{m^2 (m^2 - A^2)}, \tag{4.63}$$

$$S_5(m,n)=\sum_{m=1}^{\infty}\sum_{n=1}^{\infty}\frac{(\sin m\theta_1-\sin m\theta_2)(\sin m\theta_3-\sin m\theta_4)\cos(n\pi x_p/a)}{m^2(m^2+n^2-A^2)}$$

$$=\frac{\pi}{2}\sum_{m=1}^{\infty}\frac{(\sin m\theta_1-\sin m\theta_2)(\sin m\theta_3-\sin m\theta_4)\cosh E\pi(1-x_p/a)}{m^2E\sinh E\pi}-\frac{1}{2}S_4(m), \quad (4.64)$$

$$S_6(m,n)=\sum_{m=1}^{\infty}\sum_{n=1}^{\infty}\frac{(-1)^{m+n}(\sin n\theta_1-\sin n\theta_2)(\sin m\theta_3-\sin m\theta_4)\cos(m\pi x_p/a)}{mn(m^2+n^2-A^2)}$$

$$=\frac{\pi}{2}\sum_{m=1}^{\infty}\frac{(-1)^m(\sin m\theta_3-\sin m\theta_4)(\sinh E\theta_1-\sinh E\theta_2)\cos(m\pi x_p/a)}{m(m^2-A^2)\sinh E\pi}-\frac{W_p\pi}{2a}S_3(m).$$

(4.65)

where, $\theta_1=\frac{\pi}{a}\left(y_p+\frac{W_p}{2}\right)$; $\theta_2=\frac{\pi}{a}\left(y_p-\frac{W_p}{2}\right)$; $\theta_3=\frac{\pi}{a}\left(y_q+\frac{W_q}{2}\right)$; $\theta_4=\frac{\pi}{a}\left(y_q-\frac{W_q}{2}\right)$,

$E^2=m^2-A^2$.

The series for $S_1(m)$ and $S_2(m)$ are summed to closed form. Substituting $S_1(m)$, $S_2(m)$, $S_5(m,n)$ and $S_6(m,n)$ from equations (4.60), (4.61), (4.64), and (4.65) respectively into equation (4.59) eliminates the terms $-W_pW_q\pi^2/a^2k^2$, and the infinite series $S_3(m)$, $S_4(m)$. Also the double infinite series $S_5(m,n)$, and $S_6(m,n)$ have been reduced to single series form.

The economised formula for Z_{pq} is then given by

$$Z_{pq}=j\omega\mu h\left\{-\frac{\cos k(a-x_p)}{ak\sin ak}-\frac{\sin A\theta_1-\sin A\theta_2}{ak^2W_p\sin ak}\right.$$

$$+\frac{2a^2}{W_pW_q\pi^3}\sum_{m=1}^{\infty}\frac{(\sin m\theta_1-\sin m\theta_2)(\sin m\theta_3-\sin m\theta_4)\cosh\pi(1-x_p/a)\sqrt{m^2-A^2}}{m^2\sqrt{m^2-A^2}\sinh\pi\sqrt{m^2-A^2}}$$

$$\left.+\frac{2a^2}{W_pW_q\pi^3}\sum_{m=1}^{\infty}\frac{(-1)^m(\sin m\theta_3-\sin m\theta_4)(\sinh\theta_1\sqrt{m^2-A^2}-\sinh\theta_2\sqrt{m^2-A^2})\cos(m\pi x_p/a)}{m(m^2-A^2)\sinh\pi\sqrt{m^2-A^2}}\right\}.$$

(4.66)

The single probe port Z_{pq} is obtained in terms of closed forms and single infinite series.

4.9 Summary

Single port input, or, self impedance and the two ports coupling impedances for both a rectangular segment and a right-angled isosceles triangular segment were discussed. The Green's function has been reformulated and used to obtain explicit efficient coupling impedance formulas. New formulas for a probe feed self impedance, and, a probe to microstrip feed coupling impedance, on a rectangular segment, have been derived. These have been applied to calculate the impedance matrix elements in Chapter 6 for determining the input impedance of a U-slot rectangular patch using segmentation analysis.

A new formula for a probe feed self impedance, and a coupling impedance between a probe feed and port on the perpendicular side of the triangular segment have also been derived.

For a probe feed on each segment, the calculated, simulated, and measured input impedances were in good agreement.

Good agreement between the calculated, simulated, and measured perimeter port coupling impedance for the triangular patch were presented.

The explicit efficient impedances formulas for rectangular and triangular segments, in segmentation analysis, have been applied in Chapters 5, and 6.

CHAPTER 5 APPLICATION OF SEGMENTATION METHOD TO A CP TRUNCATED CORNERS SQUARE PATCH ANTENNA

5.1 Introduction

A single-feed CP antenna can also be realised by deleting two opposite corners of a square patch [12], [40]. Simple design equations are given in [32] for a centre line feed as discussed in Chapter 2, Section 2.3.3. The antenna was analysed using the method of moment in [78].

The size of the antenna can be reduced by using a high permittivity substrate which however increases the cost of the antenna [54]. An alternative approach is to reduce the size by using slits and L-shaped slots as discussed in [53]. A dual-band CP antenna has been obtained for global positioning system applications [79] by using two overlapped corner-truncated square patches with a probe feed. To produce multi-band operation a deleted corners square patch antenna was used to excite a stacked square patch having a U-slot [80]. The truncated corner antenna has also been used as a basic radiating element in the design of an array using a sequentially rotated feed structure to improve the bandwidth and radiating patterns [49]. However, for all the above designs, as the feed is located on a centre line, the areas of the deleted segments are very small and hence the performance of the antenna is very sensitive to manufacturing errors. In this chapter it is shown that the perturbation area can be increased by using a microstrip feed offset from the centre and so reduce the effect of the manufacturing errors.

The segmentation method has been used for a number of different antennas to determine the optimum matched feed location for a probe feed. In [81] it was used to determine the position of the probe along the centre line of truncated corners patch antenna.

This method [61] has also been used to determine the input impedance of a compact microstrip antenna consisting of a rectangular and four connected right-angled isosceles triangular segments. A dual-corner-fed square patch was replaced by a dual-corner-deleted geometry, and the input impedance of the corner-fed patch array is determined using segmentation technique [62].

In this chapter the explicit computationally efficient coupling impedance formulas (given in Chapter 4) are used to determine the input impedance of a CP truncated corners patch antenna for an offset microstrip feed. In Section 5.2, the truncated patch is segmented into two triangular segments and a rectangular segment, and, a new explicit matrix input impedance formula is derived.

In Section 5.3 the perturbation analysis and the derivation of the general equivalent circuit a deleted corner patch antenna as proposed by Haneishi [32] is reviewed. Based on this equivalent circuit and for a probe feed along the centre line of the patch, a simple design equation for the ratio of the total perturbed area and the unperturbed area is obtained.

An investigation is carried out in Section 5.4 to examine how the total area of the perturbed segment and the input impedance varies with the offset position of a microstrip feed. The results obtained from the equivalent circuit, segmentation and a commercial software package are compared. In the segmentation method the locus of the input impedance is plotted on the Smith chart and the perturbation areas are tuned to obtain good circular polarisation. The condition for good circular polarisation is determined when a sharp cusp in the impedance locus is obtained at the design frequency.

Also for the segmentation method the number of ports required to produce accurate results is investigated.

A compromise offset feed position was chosen so as to maximise the area of the perturbation segment and to obtain good impedance matching and a compact antenna

structure. In Section 5.5, a RHCP truncated patch antenna for was designed for a fixed offset microstrip feed location, and a matching network consisting of a short length of a microstrip line was designed. A good agreement between the predicted, simulated and practical results was obtained.

5.2 Derivation of the Explicit Matrix Formula for the Input Impedance Using Segmentation Method

In order to determine the input impedance for an offset microstrip feed from the center of the patch (see Figure 5.1(a)) the patch is segmented into three segments, as shown in Figure 5.1(b), where 'T_0' is the amount of offset. There are two right-angled isosceles triangular segments of the same size (α- and γ-segments) and one rectangular segment (β-segments).

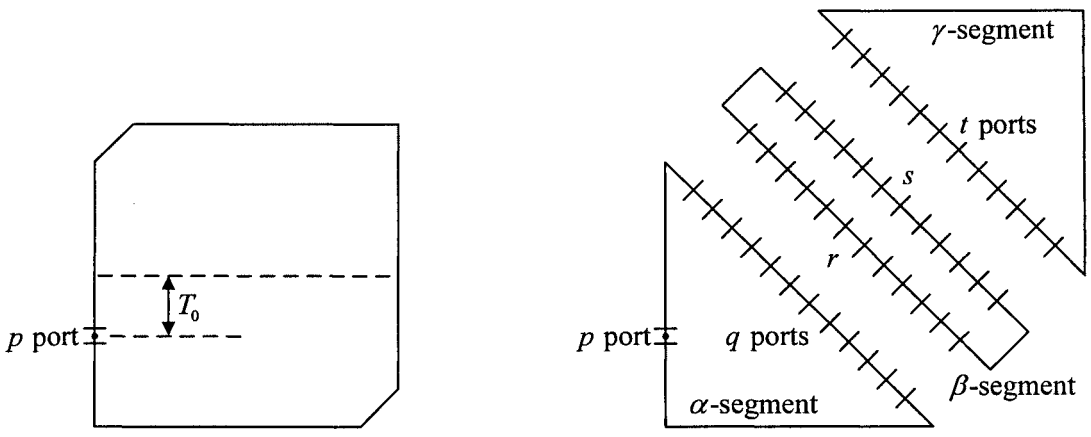

Figure 5.1. A truncated corners square patch antenna. (a) The truncated patch. (b) Segmentation of the patch.

For the connecting ports on the segments shown in Figure 5.1(b) the five matrix circuit equations for the port voltages are given below.

$$V_p = Z_{pp} i_p + Z_{pq} i_q , \tag{5.1}$$

$$V_q = Z_{qq} i_q + Z_{qp} i_p , \tag{5.2}$$

$$V_r = Z_{rr} i_r + Z_{rs} i_s , \tag{5.3}$$

$$V_s = Z_{ss} i_s + Z_{sr} i_r , \tag{5.4}$$

$$V_t = Z_{tt} i_t . \tag{5.5}$$

Applying the conditions, $V_r = V_q , V_t = V_s$, and, $i_r = -i_q$, $i_t = -i_s$, results in the following two equations

$$(Z_{qq} + Z_{rr}) i_q + Z_{qp} i_p = Z_{rs} i_s \tag{5.6}$$

and,

$$i_s = (Z_{ss} + Z_{tt})^{-1} Z_{sr} i_q . \tag{5.7}$$

As the two triangular segments are identical and symmetrical about the centre segment then $Z_{tt} = Z_{qq}$ and $Z_{ss} = Z_{rr}$ and from the reciprocity condition on each of the matrix elements, $Z_{sr} = Z_{rs}$. Using these relationships in equations (5.6) and (5.7), i_s can be eliminated and the following relationship between i_q and i_p is obtained:

$$(Z_{qq} + Z_{rr}) i_q + Z_{qp} i_p = Z_{rs} (Z_{rr} + Z_{qq})^{-1} Z_{rs} i_q$$

hence,

$$i_q = -\left[Z_{qq} + Z_{rr} - Z_{rs} (Z_{qq} + Z_{rr})^{-1} Z_{rs} \right]^{-1} Z_{qp} i_p . \tag{5.8}$$

Finally substituting for i_q from equation (5.8) into (5.1) gives

$$V_p = Z_{pp} i_p - Z_{pq} \left[Z_{qq} + Z_{rr} - Z_{rs} (Z_{qq} + Z_{rr})^{-1} Z_{rs} \right]^{-1} Z_{qp} i_p \tag{5.9}$$

whence an explicit matrix input impedance formula for Z_{in}, is then given by

$$Z_{in} = \frac{V_p}{i_p} = Z_{pp} - Z_{pq}\left[Z_{qq} + Z_{rr} - Z_{rs}(Z_{qq} + Z_{rr})^{-1} Z_{rs}\right]^{-1} Z_{pq}^{T} \tag{5.10}$$

where $Z_{qp} = Z_{pq}^{T}$.

The elements in the coupling impedance matrices Z_{pp}, Z_{pq}, Z_{qq} for the triangular segments were derived in Section 4.6 and the coupling impedance matrices Z_{rr}, Z_{rs}, for the rectangular segment, are given in Section 4.3.

Equation (5.10) was used in Section 5.4 to investigate how the input impedance varies with offset and in the design of the matching network. The detail of the Mathcad program used is given in *Appendix 5A*.

5.3 Perturbation Analysis

In general for a single-feed to produce circular polarisation, perturbation analysis can be applied to a square patch for both the deleted corner case, and, the added segment case, to determine amount of perturbation required for circular polarisation [32], [40].

A variational expression for the eigenvalues and eigenfunctions of the perturbed patch were obtained by Haneishi [32] for both cases. Then an equivalent circuit model was used to derive simple and useful design expression for the required total area of the perturbation segments to produce circular polarisation, for a feed along the centre line ($T_0 = 0$).

Figure 5.2 shows the co-ordinate system for a single-feed square patch antenna with dimensions '*a*', and the dielectric thickness *h*. The thickness *h* in the z-direction is much smaller than the wavelength of the fields in the dielectric, therefore, the field variations in the z-direction can be neglected and the wave equation in the dielectric the x-y plane is given by,

$$\nabla^2\phi + \lambda^2\phi = 0\ , \quad 0 \le z \le h\ . \tag{5.11}$$

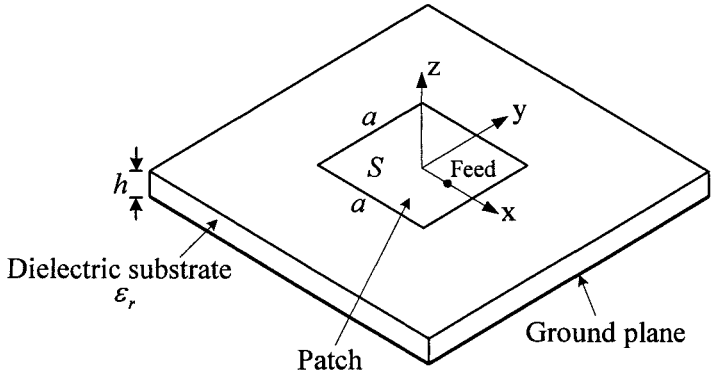

Figure 5.2. The coordinate system for the square patch antenna.

The principal eigenvalue k of the unperturbed square patch antenna is given by the following variational expression [32], [64]

$$k^2 = \frac{\iint_S (\nabla\phi)\cdot(\nabla\phi)\,dS}{\iint_S \phi^2\,dS}\ . \tag{5.12}$$

Circular polarisation can be obtained by a perturbed square patch with deleted corners as shown in Figure 5.3.

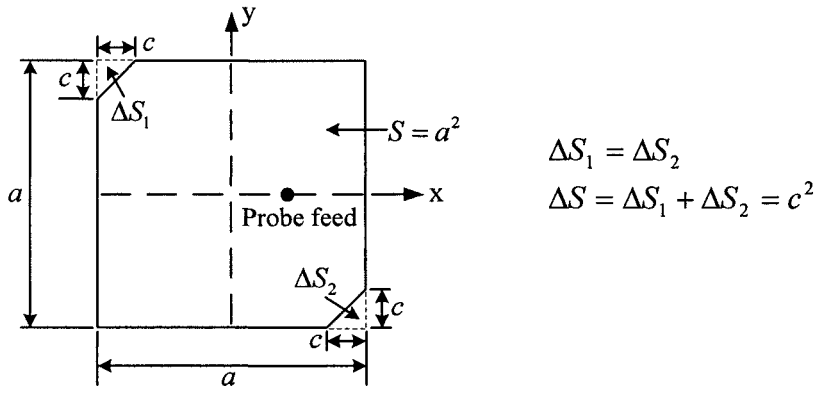

Figure 5.3. A truncated corners square patch with a centre line feed.

The new eigenfunction ϕ' and the eigenvalue k' of the perturbed patch are given by the following two equations.

$$\phi' = P\phi_a + Q\phi_b \tag{5.13}$$

and,

$$k'^2 = \frac{\iint_{S+\Delta S}\left(P\nabla\phi_a + Q\nabla\phi_b\right)^2 dS}{\iint_{S+\Delta S}\left(P\phi_a + Q\phi_b\right)^2 dS} \tag{5.14}$$

where P and Q are unknown expansion coefficients of the ϕ'.

Assuming a perfect magnetic wall boundary condition at $x = \pm a/2$, $y = \pm b/2$ the eigenfunctions ϕ_a and ϕ_b of the unperturbed patch for the TM_{10} and TM_{01} modes, are given by

$$\phi_a = V_0 \sin kx \text{ , and } \phi_b = V_0 \sin ky \tag{5.15}$$

where, $V_0 = \sqrt{2}/a$, and $k = \pi/a$.

The parameter k'^2 of equation (5.14) can be derived by the following matrix,

$$\det\begin{vmatrix} k^2 + q_1 - k'^2(1+p_1) & q_{12} - k'^2 p_{12} \\ q_{12} - k'^2 p_{12} & k^2 + q_2 - k'^2(1+p_2) \end{vmatrix} = 0. \tag{5.16}$$

where the parameters in equation (5.16) are given by [32]

$$q_1 = q_2 = q_{12} = 0 \tag{5.17a}$$

$$p_1 = p_2 = 2(\Delta S/S) \tag{5.17b}$$

$$p_{12} = -2(\Delta S/S). \tag{5.17c}$$

The perturbed resonant frequency is related to the area of perturbation by the following equation

$$f_a = f_0 + \Delta f_a' = f_b(1 - 2\Delta S/S) \tag{5.18}$$

and f_b is the unperturbed resonant frequency.

An equivalent circuit of the perturbed antenna is shown in Figure 5.4 where the two parallel tuned circuits represent the two modes which transform the potential to the edges of the patch. The turn ratios are given by

$$N_a = K(\sin kx - \sin ky), \tag{5.19a}$$

$$N_b = K(\sin kx + \sin ky) \tag{5.19b}$$

where K is a constant of proportionality.

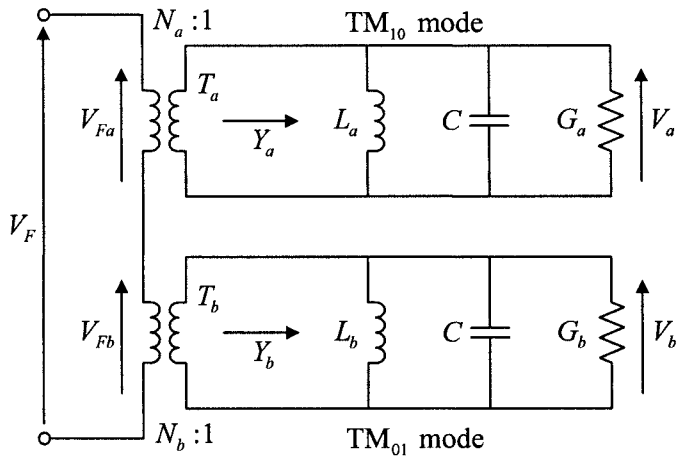

Figure 5.4. Equivalent circuit of a truncated corners patch antenna after perturbation.

The ratio of the edge voltages V_b / V_a is given by

$$\frac{V_b}{V_a} = \frac{N_b}{N_a} \cdot \frac{Y_a}{Y_b}$$

$$= \frac{N_b}{N_a} \cdot \frac{\left[\frac{f_a}{Q} + j\left(f - \frac{f_a^2}{f}\right)\right]}{\left[\frac{f_b}{Q} + j\left(f - \frac{f_b^2}{f}\right)\right]}. \tag{5.20}$$

For an antenna with a centre line feed the turns ratios $N_b / N_a = 1$ and for this case, applying the circular polarisation condition to equation (5.20), produces the following simple design expressions for the ratio of the effective perturbed and unperturbed areas,

$$\frac{\Delta S_e}{S_e} = \frac{c_e^2}{a_e^2} = \frac{1}{2Q}. \tag{5.21}$$

In the above equation the effect of field fringing is taken into account.

In order to increase the area of the perturbation segment ΔS_e a thick substrate should be used as this decreases the unloaded Q-factor. Alternately as shown in the following section this area can be increased by using an offset feed.

The design equation (5.21) is a good first-pass design equation that can be used to obtain the design dimensions for a CP truncated patch. The dimensions of the patch can then be fine tuned by using the segmentation method program and observing the sharp notch in the impedance locus displayed on the Smith chart. Also it possible to use a commercial simulation tool (e.g. Ensemble) and fine tune the dimensions in order to obtain a good axial ratio. Both methods are used in Section 5.4 to obtain the dimensions of the patch for design frequency of 2.45 GHz.

5.4 Investigation of the Feed Position on the Area of the Perturbation Segment

In this section the effect of the feed position on the area of perturbation segment is investigated by the following methods:

a) The equivalent circuit model.

b) Plotting the input impedance locus obtained from segmentation analysis on the Smith chart.

c) Using commercial software (Ensemble).

The substrate used in this investigation is *Duroid* with h =1.575 mm and the Q-factor of the antenna is 54.8 at the design frequency of 2.45 GHz.

A microstrip offset feed position (T_0) from the centre line of the patch is shown in Figure 5.5.

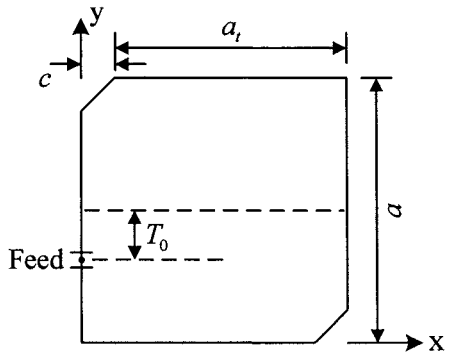

Figure 5.5. The patch with an offset feed.

Two feed positions are considered and discussed below.

(a) Feed Position $T_0 = 0$

For the feed position $T_0 = 0$ equation (5.21) based on the equivalent circuit with $N_b / N_a = 1$, the area of the perturbation segment obtained shown in Table 5.1.

The segmentation program based on equation (5.10) was then used to plot the locus of the input impedance on the Smith chart.

The obtained dimensions were fine tuned to obtain good circular polarisation as indicated by a sharp cusp in the locus at the design frequency. Initially however, it was necessary to investigate the number of ports which should be used in the segmentation analysis.

To determine the number of the ports (N), required for the q, r, s ports, in matrix input impedance equation (5.10) was examined by taking $N = 4$ to 9. For different values of N the real and imaginary parts of the input impedance as a function of frequency are plotted.

It was found that as shown in Figure 5.6 that seven ports were required to give accurate results. The width of each port is between $\lambda/10$ to $\lambda/20$, or less [2].

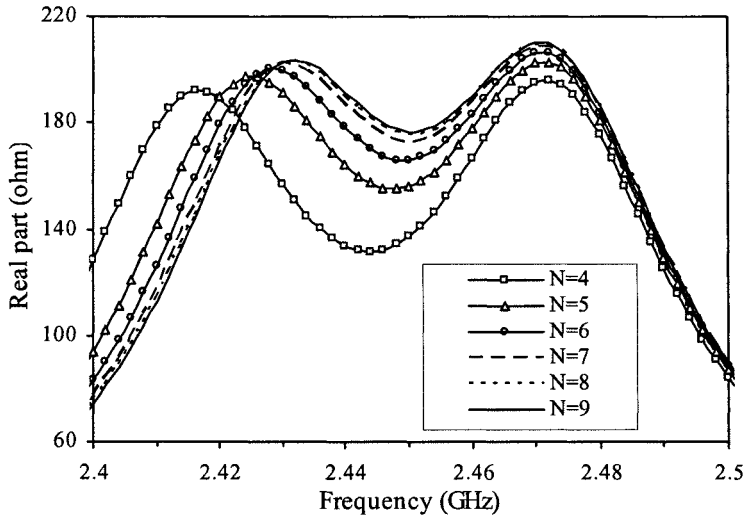

(a)

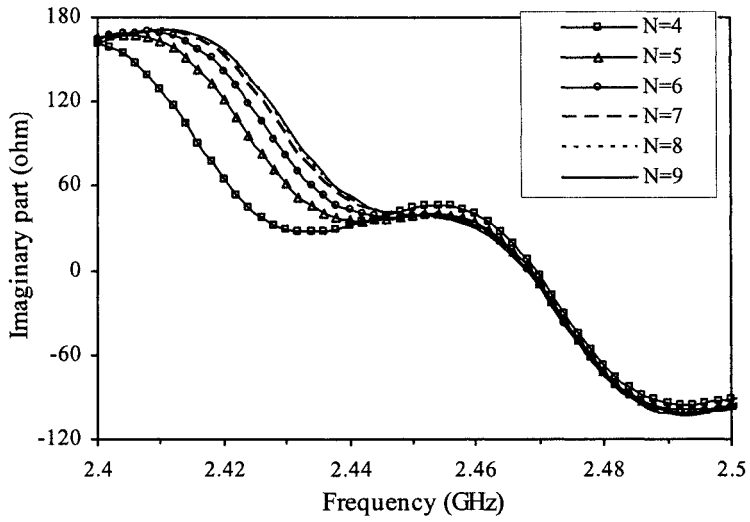

(b)

Figure 5.6. Segmentation calculated input impedance with the different N for $T_0 = 0$.
(a) Real part. (b) Imaginary part.

For the feed position, $T_0 = 0$, the segmentation results and simulated results for the input impedance are plotted on Smith chart as shown in Figure 5.7. As can be seen the cusp in the impedance plot is at 2.45 GHz showing a good circular polarisation has been obtained and that there is a good agreement between the predicted and simulated results.

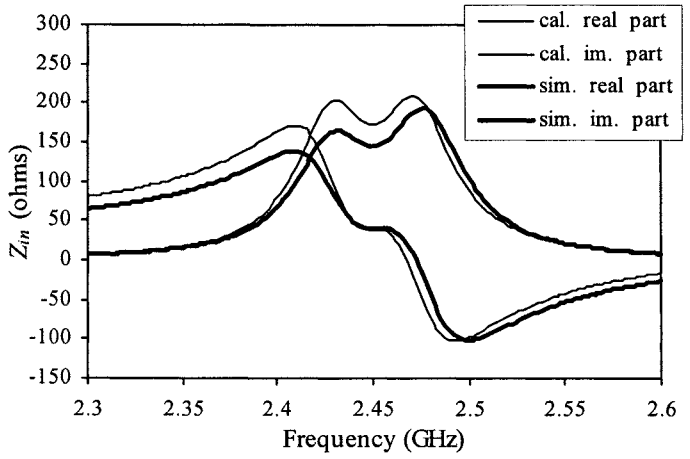

(a)

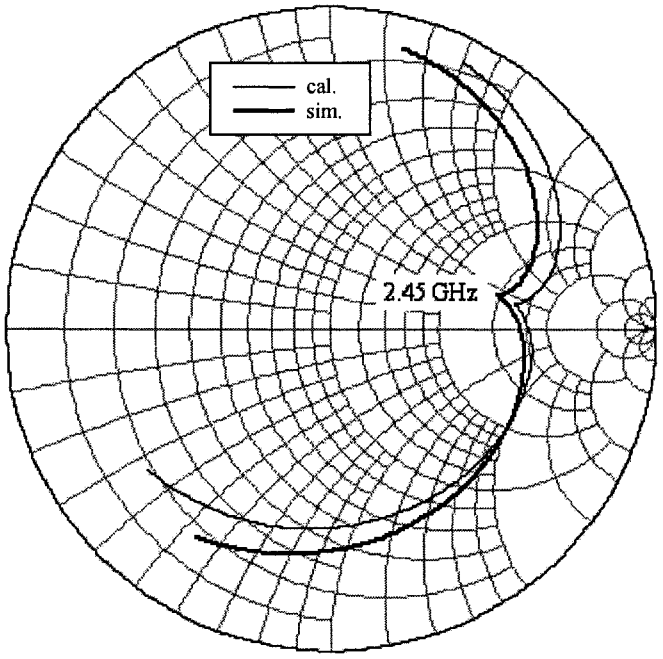

(b)

Figure 5.7. Segmentation calculated and simulated input impedance for $T_0 = 0$. (a) Input impedance versus frequencies. (b) Smith chart.

The dimensions obtained for the antenna using the equivalent circuit, impedance plot obtained by the segmentation method, and, by using Ensemble software, are shown in Table 5.1.

Parameters	Calculation (equation (5.21))	Calculation (equation (5.10) for segmentation method)	Simulation (Ensemble)
Q (square patch)	54.8	54.8	53.1
$\Delta S_e / S_e$ (%)	0.91	0.93	---
a_e (mm)	41.11	41.46	---
a (mm)	39	39.35	39.18
$c \cong c_e$ (mm)	3.93	4	3.88
$\Delta S / S$ (%)	1.01	1.03	0.98

Table 5.1. The calculated and simulated perturbation areas and dimensions of the patch with a microstrip feed at $T_0 = 0$.

(b) Feed Position $T_0 \neq 0$

As seen in Chapter 3, in the case of the nearly square patch antenna, the area of the perturbation segment can be increased by using an offset feed. This increase in the area for the truncated corners patch is examined using each of the above three methods. The equivalent circuit equations (5.19a) and (5.19b) were used to obtain the two resonant frequencies f_a and f_b. Then the area of the perturbation segment was obtained using the equation (5.18).

The results obtained using the three methods are summarised in Table 5.2. Comparing the calculated and simulated results, the percentage difference in the dimension a is less than 1% for either the centre, or, the offset feed. For the dimensions c the maximum difference is 5.5% which represents only a 0.24 mm discrepancy for between the predicted and simulation results at $T_0 = 0.1a$. However, with increase in offset, the percentage difference for the dimension c is reduced. The dimension c increases faster than dimension

a as T_0 increases. Nevertheless there is a good agreement for $\Delta S / S$ between the predicted and simulation results.

Offset edge-feed, T_0	Simulation (Ensemble software)					Calculation (equation (5.10))								
	a (mm)	c (mm)	a_t (mm)	$\Delta S/S$ (%)	Optimised AR (dB)	a_e (mm)	a (mm)	$c \cong c_e$ (mm)	a_t (mm)	$\Delta S_e/S_e$ (%)	$\Delta S/S$ (%)	Compared with simulated a, Error (%)	Compared with simulated c, Error (%)	Compared with simulated a_t, Error (%)
0	39.18	3.88	35.3	0.98	0.1	41.458	39.35	4	35.35	0.93	1.03	0.43	3	0.14
0.1a	39.4	4.11	35.29	1.08	0.2	41.748	39.64	4.35	35.29	1.09	1.2	0.61	5.5	0
0.2a	39.96	5.2	34.76	1.69	0.15	42.288	40.18	5.4	34.78	1.63	1.8	0.55	3.7	0.06
0.25a	40.53	6.3	34.23	2.42	0.1	42.848	40.74	6.5	34.24	2.3	2.55	0.52	3.08	0.03
0.3a	41.23	7.56	33.67	3.36	0.18	43.608	41.5	7.85	33.65	3.24	3.58	0.65	3.69	0.06
0.35a	42.6	9.8	32.8	5.29	0.13	44.808	42.7	9.9	32.8	4.88	5.38	0.23	1.01	0
0.4a	45.32	13.74	31.58	9.19	0.15	47.368	45.26	13.5	31.76	8.12	8.9	0.13	1.78	0.57
0.45a	48.46	17.7	30.76	13.34	0.14	50.858	48.75	18	30.75	12.53	13.7	0.59	1.67	0.03

Table 5.2. The calculated and simulated dimensions and perturbation for the offset feeds for CP operation at 2.45 GHz.

The prediction and simulation increase in the area of the perturbation segment as a function of offset are compared in Figure 5.8(a) and Figure 5.8(b) shows that the input impedance decreases as a function of offset feed. For a simple matching network, consisting of a length of a microstrip line [67] and discussed in Chapter 3, only a certain range of Z_{in} can be matched. Hence, there is trade-off between increasing the area and the realisation of this matching network.

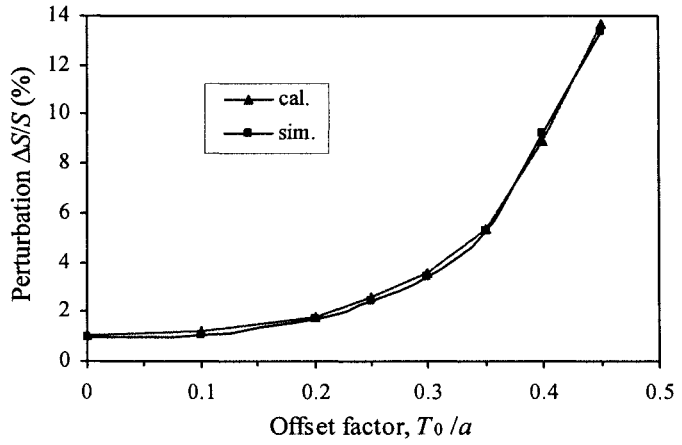

(a)

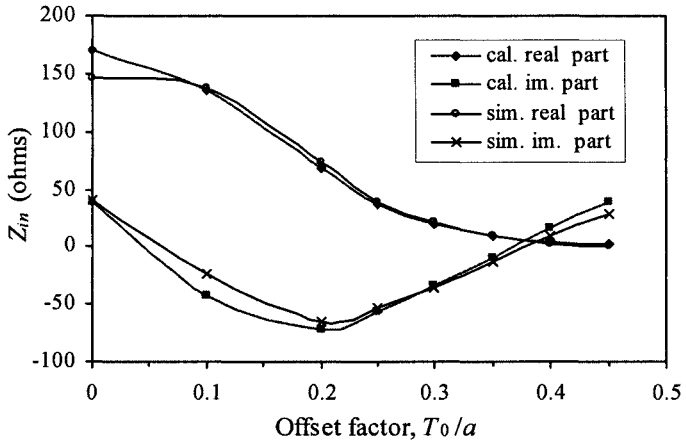

(b)

Figure 5.8. (a) Relationship between the perturbation $\Delta S / S$ and offset. (b) The input impedance at offset feed locations.

A compromise feed position, $T_0 = 0.2a$ was chosen and Figure 5.9 shows that there is a good agreement between the predicted, simulated and practical results. The calculated and simulated input impedances are $68 - j73\ \Omega$, and $74 - j65\ \Omega$ respectively, at a frequency of 2.45 GHz, whereas, the measured input impedance is $63 - j65\ \Omega$ at 2.438 GHz. The cusp shows good circular polarisation at is 2.438 GHz has been obtained and that there is less than 0.5% error from the pre-assigned frequency of 2.45 GHz.

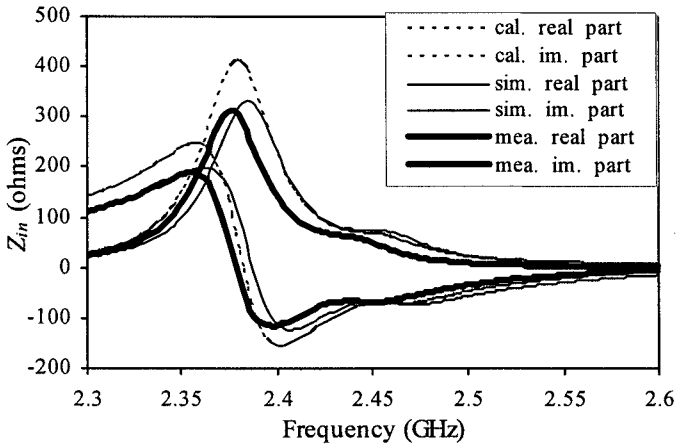

(a)

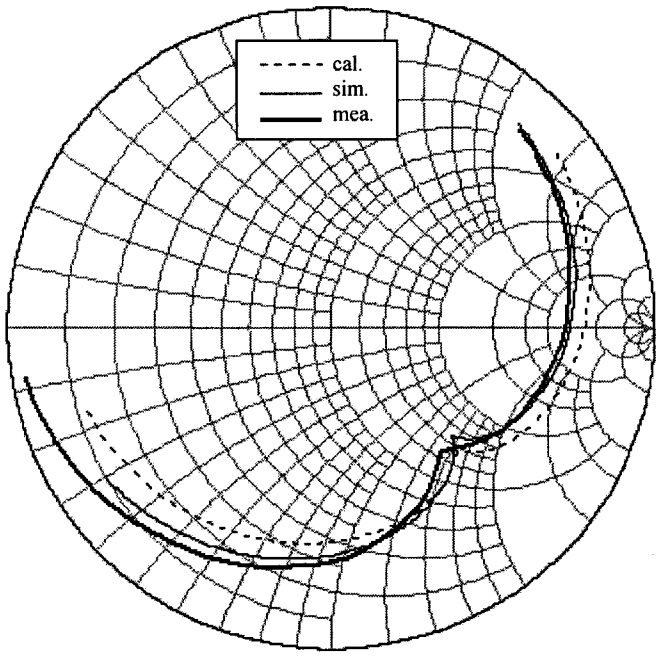

(b)

Figure 5.9. The calculated, simulated, and measured input impedance of the patch at $T_0 = 0.2a$. (a) Input impedance versus frequencies. (b) Smith chart.

5.5 Design of a Matched CP Antenna for a Fixed Offset Feed

A RHCP antenna (see Figure 5.10(a)) was designed with an offset microstrip feed location $T_0 = 0.2a$ and from simulation it was found that $Z_{in} = 74 - j65\,\Omega$. For this impedance a matching network consisting of a short length of a microstrip line was designed using equations (3.21) and (3.22).

A photograph of the fabricated matched patch is shown in Figure 5.10(b).

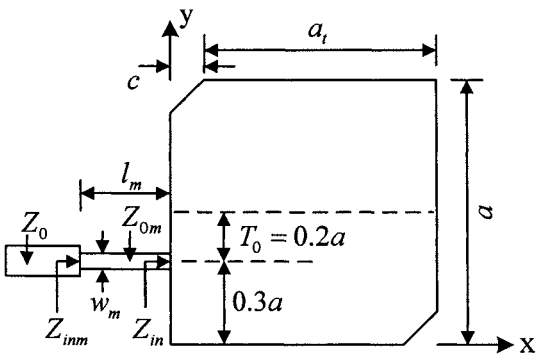

(a)

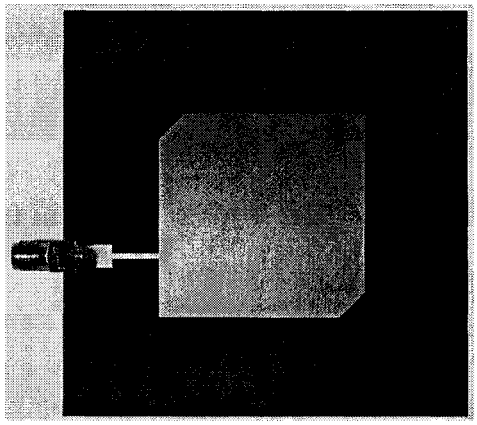

(b)

Figure 5.10. The patch with a simple matching network. (a) Geometry. (b) Fabricated patch antenna.

The parameters of the designed matched antenna operating at 2.45 GHz are summarised in Table 5.3.

Parameters	Calculated	Simulated
Z_{0m} (ohm)	111.8	--
θ_m (rad)	0.69	--
w_m (mm)	0.97	1.05
l_m (mm)	9.03	9
a (mm)	40.18	39.9
c (mm)	5.4	5.03
a_t (mm)	34.78	34.87
Q (square patch)	54.8	53.1

Table 5.3. Calculated and simulated design parameters of the matching microstrip line and of the patch antenna.

The simulated and measured input impedance of the matched patch antenna are plotted in Smith chart are shown in Figure 5.11. The cusp frequencies of the simulation and measurement are 2.45 GHz and 2.44 GHz respectively. The cusps in the impedance plot are very close to a 50-ohm match point showing that good matching has been achieved.

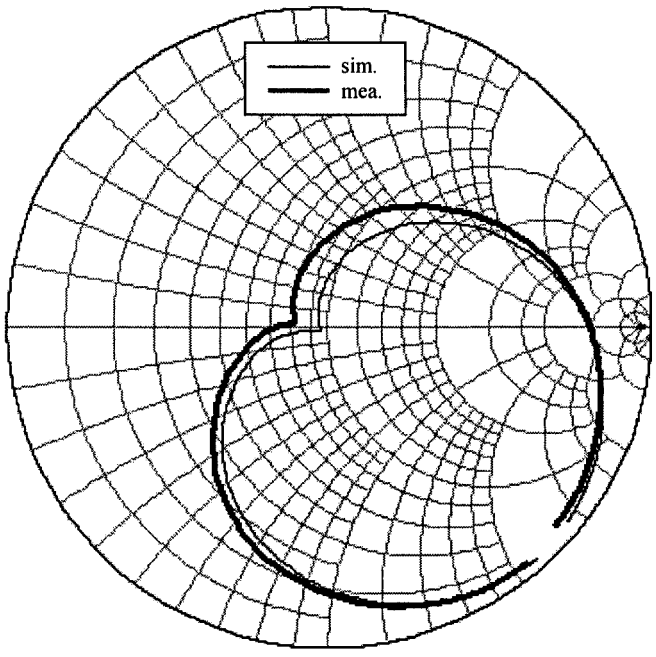

Figure 5.11. Simulated and measured input impedance in Smith chart.

Figure 5.12 shows a good return loss (S_{11}) and a good agreement between the simulated and measured return loss, for the patch antenna.

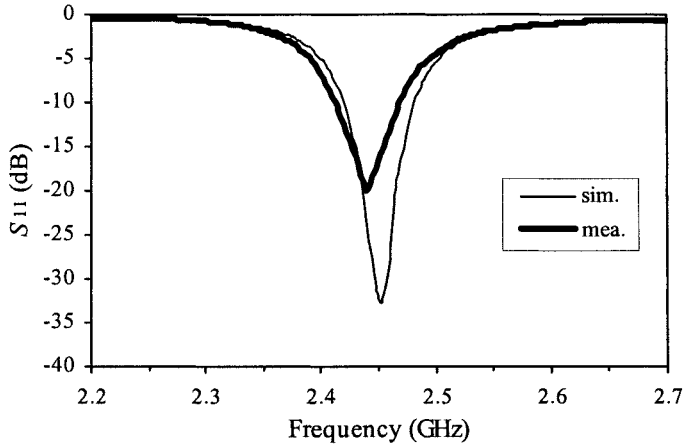

Figure 5.12. Simulated and measured return loss.

Figure 5.13 shows a comparison of the simulated and measured results for the axial ratio (AR) at ($\theta = 0, \phi = 0$) as a function of frequency. The measured minimum AR was 0.3 dB at 2.44 GHz which is less than a 0.5% frequency shift from the designed frequency.

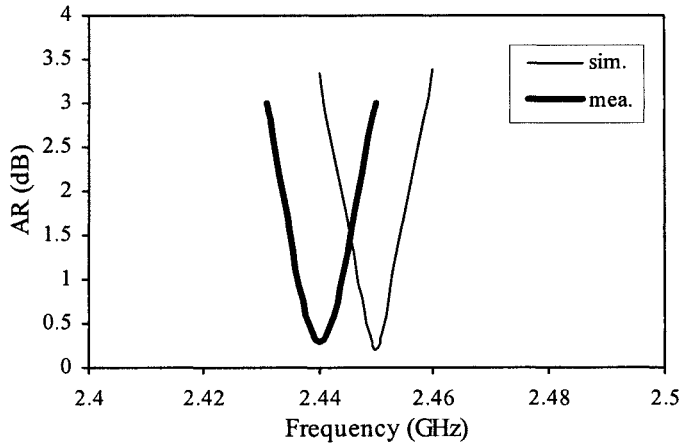

Figure 5.13. Simulated and measured axial ratio versus frequency.

The simulated and measured AR as a function of theta at centre frequency is shown in Figure 5.14. The 3-dB AR beamwidth is between −60° and 54° for simulation, and between −68° and 61° for measurement.

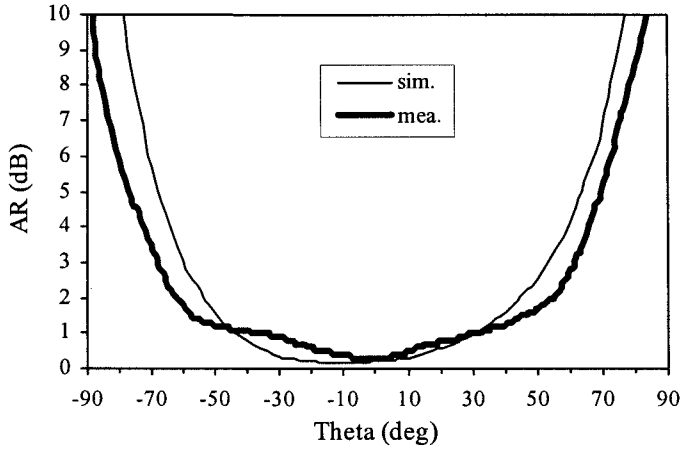

Figure 5.14. Simulated and measured AR versus theta.

A comparison between the simulated and measured results for the gain of the antenna is shown in Figure 5.15.

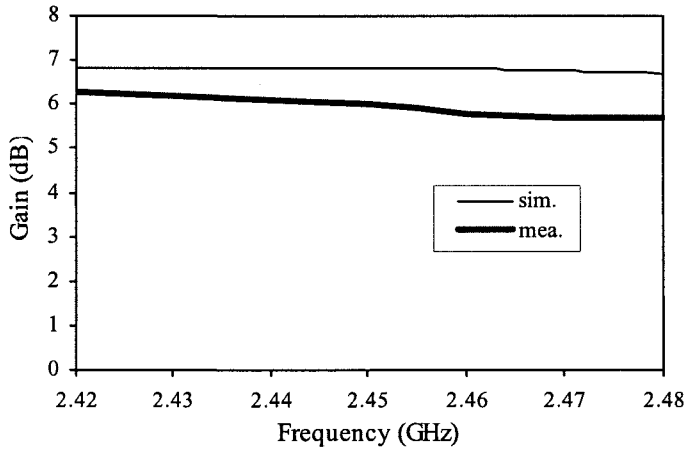

Figure 5.15. Simulated and measured gain.

The simulated and measured impedance bandwidth, the CP bandwidth and the gain at the centre frequency are listed in Table 5.4.

	Simulation	Measurement
Centre frequency f_0 (GHz)	2.45	2.44
−10-dB S_{11} for impedance bandwidth (MHz, %)	62, 2.53	58, 2.38
3-dB AR for CP bandwidth (MHz, %)	18, 0.73	19, 0.78
Gain (dB)	6.84	6.1

Table 5.4. The impedance bandwidth, the CP bandwidth, and the gain at centre frequency.

Figure 5.16 shows the simulated normalised RHCP and LHCP radiation patterns at $\phi = 0$ for the antenna. It can be seen that there is nearly 40 dB isolation between the two polarisations.

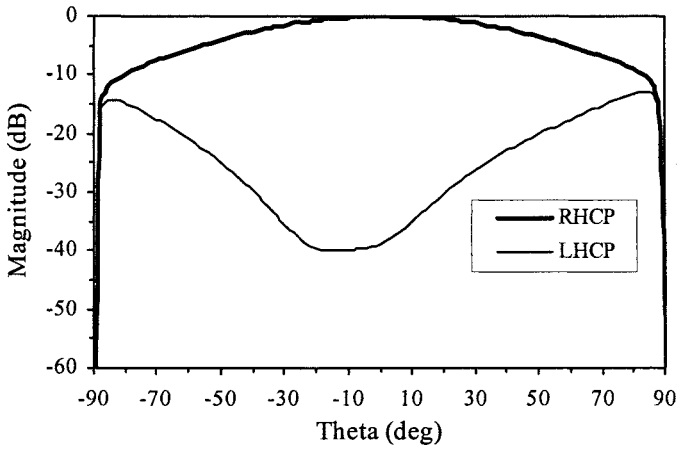

Figure 5.16. Simulated normalised radiation patterns for RHCP and LHCP at $\phi = 0$.

Figure 5.17 shows the simulated and measured normalised radiation patterns at $\phi = 0$ and $\phi = 90^{\circ}$ for the antenna.

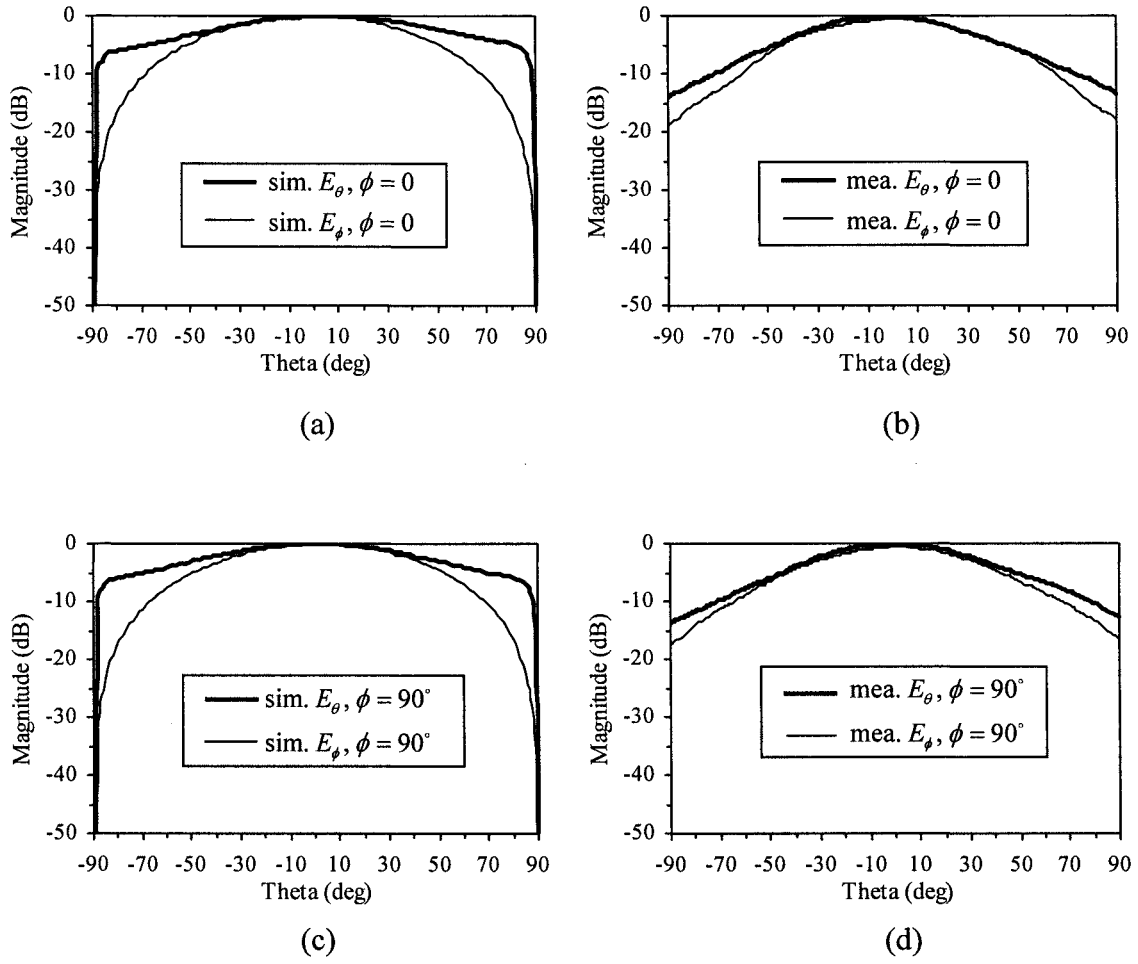

Figure 5.17. Normalised radiation patterns (a) Simulation at $\phi = 0$. (b) Measurement at $\phi = 0$. (c) Simulation at $\phi = 90^{\circ}$. (d) Measurement at $\phi = 90^{\circ}$.

5.6 Summary

A new explicit matrix input impedance formula, for use in the segmentation method, has been derived. Using the efficient coupling impedance formulas from Chapter 4 in the new matrix input impedance formula requires a computer run time less than half that

required by simulation. This advantage has been used in the trial-and-error optimum design calculations.

It has been found that with an offset feed the area of the perturbation element is increased thereby reducing the effect of manufacturing errors. A simple matching network consisting of a short length of microstrip line was used for matching. A compact matched CP antenna has been achieved. The results obtained for the predicted, simulated, and measured values are in good agreement.

CHAPTER 6 SEGMENTATION ANALYSIS AND A DESIGN APPROACH FOR A U-SLOT RECTANGULAR PATCH ANTENNA

6.1 Introduction

The design of a compact single-layer probe feed U-slot rectangular patch antenna with an air or foam substrate and with wideband characteristic has been presented [82]. Using a foam substrate and changing the patch width and feed position of this antenna the wideband characteristic was converted into a dual-frequency characteristic [83]. A broadband U-slot rectangular patch antenna on a microwave (non-air) substrate has been studied [84]. A design procedure with design equations, based on parametric studies, for the antenna on a microwave substrate has been studied [85].

The U-slot configuration has many design parameters therefore has good flexibility for matching.

Since the antenna geometry can be formed from a combination of rectangular segments the segmentation method presents a computationally efficient method to determine the input impedance. For the application of the method a new explicit matrix input impedance formula is derived in Section 6.3. The new probe feed self impedance and coupling impedance formulas derived in Chapter 4, [75], are used in the calculation of elements in the matrix impedance formula.

In this chapter, the design of two U-slot rectangular patch antennas operating at 2.45 GHz with a common substrate material *Duroid* is presented. Antenna A has substrate thickness, $h = 1.575$ mm, and, antenna B has a substrate thickness, $h = 3.175$ mm. Antenna B is used to improve the bandwidth.

By applying the design procedure and equations given in [85], an initial set of antenna dimensions are calculated. If the initial design does not achieve a good match, the dimensions are adjusted to give good match.

The segmentation structure consists of five segments with ten sets of connecting ports and a probe feed port. Application of coplanar matrix circuit analysis gives eleven voltage-impedance-current matrix equations. It is shown that four pairs of these equations may, each, be combined into a single equivalent matrix equation, thereby considerably reducing the analytic complexity of the equations. This reduces the original eleven circuit equations to seven equivalent circuit equations from which the explicit matrix input impedance formula is derived. The above technique has general wider potential applications.

The design procedure for a broadband probe feed U-slot microwave substrate rectangular patch antenna given in [85] is presented in Section 6.2, and the effect of the design parameters is discussed.

In Sections 6.4 and 6.5, the design equations are applied to calculate initial design dimensions for each of the antennas A, B. The matrix input impedance formula is applied to calculate the input impedances and the dimensions of the patch fine-tuned to achieve a good matching at the design frequency. Predicted, simulated and measured results are presented and compared.

6.2 Design Procedure for the Initial Antenna

The geometry of a single-layer U-slot rectangular microstrip patch antenna with a centre probe feed is shown in Figure 6.1.

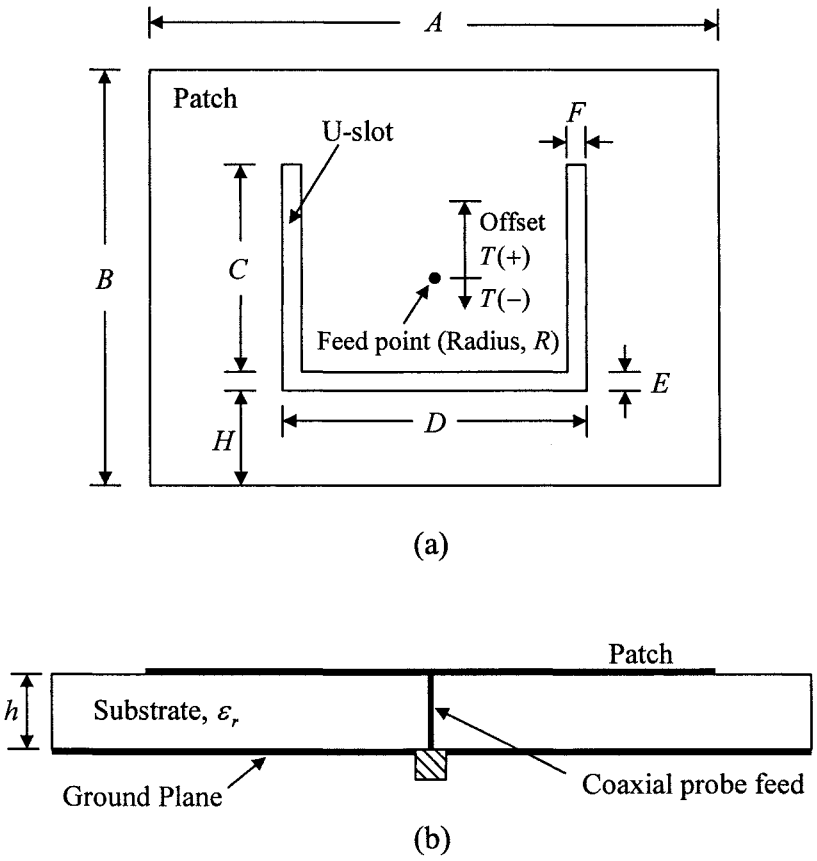

Figure 6.1. Geometry of a probe feed U-shape slot rectangular microstrip patch antenna. (a) Top view. (b) Side view.

The procedure [85] provides approximate design rules that result in an initial design with prescribed characteristics and requires only minimal tuning to obtain good matching. In the design the width of the U-slot is assumed to be uniform.

The design procedure considers only the second resonance (f_{r2}), the third resonance (f_{r3}), and, the fourth resonance (f_{r4}) for broadband operation, and ignores the first resonance (f_{r1}) that has a very high input impedance.

Approximate design equations are shown below.

1) Specify the centre frequency f_{r3}, the lower frequency f_{r2}, and, the upper frequency f_{r4}, of the bandwidth.

2) Given a substrate permittivity ε_r, calculate a substrate thickness h for broadband operation, from

$$h \geq 0.06 \frac{c_0}{f_{r3}\sqrt{\varepsilon_r}}. \tag{6.1}$$

3) Estimate the length $B + 2\Delta B$, from

$$B + 2\Delta B \approx \frac{c_0}{2 f_{r3}\sqrt{\varepsilon_r}} \tag{6.2}$$

where, ΔB is the effective extended length.

4) Calculate the width A from

$$A = 1.5(B + 2\Delta B). \tag{6.3}$$

5) Calculate the effective permittivity ε_{reff}, and, the $2\Delta B$, from the formulas

$$\varepsilon_{reff} = \frac{\varepsilon_r + 1}{2} + \frac{\varepsilon_r - 1}{2}\left(1 + \frac{12h}{A}\right)^{-1/2} \tag{6.4}$$

and,

$$2\Delta B = 0.824h \frac{(\varepsilon_{reff} + 0.3)(0.262 + A/h)}{(\varepsilon_{reff} - 0.258)(0.813 + A/h)}. \tag{6.5}$$

6) Calculate the length B, from

$$B = \frac{c_0}{2 f_{r3}\sqrt{\varepsilon_{reff}}} - 2\Delta B. \tag{6.6}$$

7) Select a starting value of the slot width, from

$$E = F = \frac{c_0}{60 f_{r3}}. \tag{6.7}$$

8) Calculate D, from

$$D = \frac{c_0}{f_{r2}\sqrt{\varepsilon_{reff}}} - 2(B + 2\Delta B - E). \tag{6.8}$$

9) Select C from the conditions,

$$\frac{C}{A} \geq 0.3, \quad \text{and} \quad \frac{C}{D} \geq 0.75. \tag{6.9}$$

10) Calculate the effective permittivity, and, the effective extended length for the fourth resonance from the formulas

$$\varepsilon_{reff(pp)} = \frac{\varepsilon_r + 1}{2} + \frac{\varepsilon_r - 1}{2}\left(1 + \frac{12h}{D-2F}\right)^{-1/2} \tag{6.10}$$

and,

$$2\Delta_{B-E-H} = 0.824h\frac{(\varepsilon_{reff(pp)} + 0.3)[0.262 + (D-2F)/h]}{(\varepsilon_{reff(pp)} - 0.258)[0.813 + (D-2F)/h]}. \tag{6.11}$$

11) Calculate H, from

$$H \approx B - E + 2\Delta_{B-E-H} - \frac{1}{\sqrt{\varepsilon_{reff(pp)}}}\left(\frac{c_0}{f_{r4}} - (2C + D)\right). \tag{6.12}$$

12) Ensure that $C + E + H > B$, and if not, adjust C and H.

Changes in the above parameters can significantly alter the resonant frequency and the input impedance. In this chapter, the radius (R) of the probe feed and the substrate's dielectric constant (ε_r) are fixed but the other parameters of the patch are available for impedance matching.

The resonant frequency f_{r3} is mainly determined by the patch length B, while the length C and width D of the slot will have an important affect on the resonant frequency. By increasing the length B, or by increasing the total length of the slot, the resonant frequency is lowered since the current path is lengthened [83], [86].

The input impedance of the patch can be adjusted by altering the length C, width D, [87], and the position H of the slot, and the position T of the feed. As C and T are increased, or, D and H are decreased the real part of the resonant input impedance is reduced.

With fixed dimensions A, E, F, and a fixed centre feed ($T = 0$), and the dimensions B, C, D, H are used as the design parameters to achieve the operational frequency, and, impedance matching.

An increase in the bandwidth can be achieved by increasing C and/or D as shown by a smaller impedance loop on the Smith chart.

With an increase in substrate thickness, a lower Q is obtained, so the bandwidth can be further improved.

6.3 The Derivation of an Explicit Matrix Input Impedance Formula Using Segmentation Analysis

The segmental structure of the probe feed U-slot rectangular patch antenna is shown in Figure 6.2 below.

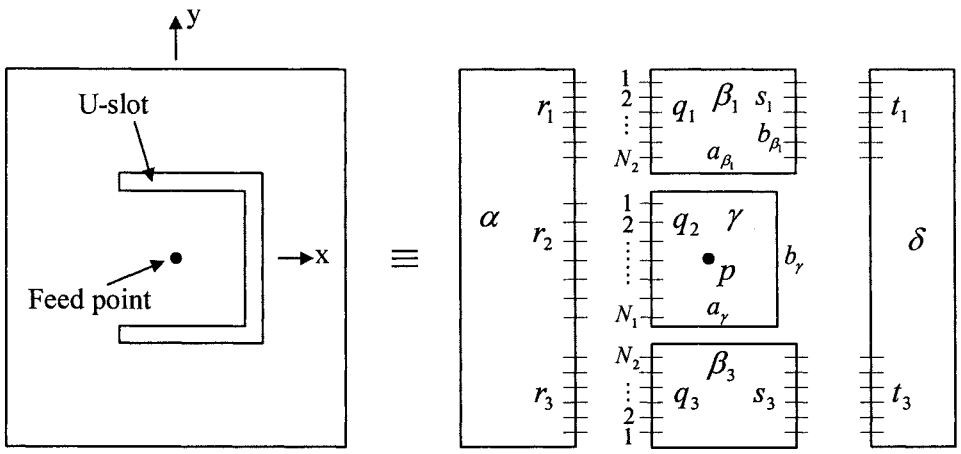

Figure 6.2. Segmental structure for the U-slot rectangular patch.

There are eleven basic matrix circuit-equations for the voltages V_{r_1}, V_{r_2}, V_{r_3}, V_{q_1}, V_{q_2}, V_{q_3}, V_{s_1}, V_{s_3}, V_{t_1}, V_{t_3}, and, V_p. The following constructions show how by combining the four pairs of equations, (V_{r_1}, V_{r_3}), (V_{q_1}, V_{q_3}), (V_{s_1}, V_{s_3}), and, (V_{t_1}, V_{t_3}) into single equivalent equations in partitioned form, the total system is reduced to an equivalent set of seven matrix equations.

The matrix circuit equations for the r ports on the α-segment are:

$$V_{r_1} = Z_{r_1r_1} i_{r_1} + Z_{r_1r_2} i_{r_2} + Z_{r_1r_3} i_{r_3} \tag{6.13}$$

$$V_{r_2} = Z_{r_2r_1} i_{r_1} + Z_{r_2r_2} i_{r_2} + Z_{r_2r_3} i_{r_3} \tag{6.14}$$

$$V_{r_3} = Z_{r_3r_1} i_{r_1} + Z_{r_3r_2} i_{r_2} + Z_{r_3r_3} i_{r_3} . \tag{6.15}$$

The equations for V_{r_1} and V_{r_3} are combined in the partitioned form

$$\begin{bmatrix} V_{r_1} \\ V_{r_3} \end{bmatrix} = \begin{bmatrix} Z_{r_1r_1} & Z_{r_1r_3} \\ Z_{r_3r_1} & Z_{r_3r_3} \end{bmatrix} \begin{bmatrix} i_{r_1} \\ i_{r_3} \end{bmatrix} + \begin{bmatrix} Z_{r_1r_2} \\ Z_{r_3r_2} \end{bmatrix} i_{r_2} \tag{6.16}$$

or,

$$V_{r_1,r_3} = A i_{r_1,r_3} + B i_{r_2} \tag{6.17}$$

where, $V_{r_1,r_3} = \begin{bmatrix} V_{r_1} \\ V_{r_3} \end{bmatrix}$, $A = \begin{bmatrix} Z_{r_1r_1} & Z_{r_1r_3} \\ Z_{r_3r_1} & Z_{r_3r_3} \end{bmatrix}$, $B = \begin{bmatrix} Z_{r_1r_2} \\ Z_{r_3r_2} \end{bmatrix}$, $i_{r_1,r_3} = \begin{bmatrix} i_{r_1} \\ i_{r_3} \end{bmatrix}$.

Also, the equation for V_{r_2} can be put in the form

$$V_{r_2} = C i_{r_1,r_3} + Z_{r_2r_2} i_{r_2} \tag{6.18}$$

where, $C = \begin{bmatrix} Z_{r_2r_1} & Z_{r_2r_3} \end{bmatrix}$.

Similarly the circuit equations for the two segments β_1, β_3 can be put in the combined form

$$V_{q_1,q_3} = D i_{q_1,q_3} + E i_{s_1,s_3} \tag{6.19}$$

where, $D = \begin{bmatrix} Z_{q_1q_1} & 0 \\ 0 & Z_{q_3q_3} \end{bmatrix}$, $E = \begin{bmatrix} Z_{q_1s_1} & 0 \\ 0 & Z_{q_3s_3} \end{bmatrix}$, $i_{q_1,q_3} = \begin{bmatrix} i_{q_1} \\ i_{q_3} \end{bmatrix}$, $i_{s_1,s_3} = \begin{bmatrix} i_{s_1} \\ i_{s_3} \end{bmatrix}$.

For V_{q_2} in the γ-segment, the circuit equation is

$$V_{q_2} = Z_{q_2q_2} i_{q_2} + Z_{q_2p} i_p . \tag{6.20}$$

For the s ports, the combined circuit equations are given by

$$V_{s_1,s_3} = F i_{s_1,s_3} + G i_{q_1,q_3} \tag{6.21}$$

where, $F = \begin{bmatrix} Z_{s_1 s_1} & 0 \\ 0 & Z_{s_3 s_3} \end{bmatrix}$, $G = \begin{bmatrix} Z_{s_1 q_1} & 0 \\ 0 & Z_{s_3 q_3} \end{bmatrix}$.

For the δ-segment, the circuit equations are given by

$$V_{t_1,t_3} = H i_{t_1,t_3} \tag{6.22}$$

where, $H = \begin{bmatrix} Z_{t_1 t_1} & Z_{t_1 t_3} \\ Z_{t_3 t_1} & Z_{t_3 t_3} \end{bmatrix}, i_{t_1,t_3} = \begin{bmatrix} i_{t_1} \\ i_{t_3} \end{bmatrix}$.

The feed p port equation of the γ-segment is given by

$$V_p = Z_{pp} i_p + Z_{pq_2} i_{q_2}. \tag{6.23}$$

The eleven original circuit equations have thus been reduced to the seven circuit equations (6.17)-(6.23), which greatly simplify the determination of the input impedance formula for Z_{in}, as shown below.

Since, $V_r = V_q, i_r = -i_q$, equating equation (6.17) and (6.19), gives

$$(A+D) i_{q_1,q_3} + B i_{q_2} + E i_{s_1,s_3} = 0$$

or,

$$P i_{q_1,q_3} + B i_{q_2} + E i_{s_1,s_3} = 0 \tag{6.24}$$

where, $P = A + D$.

Since, $V_{r_2} = V_{q_2}, i_r = -i_q$, equating equation (6.18) and (6.20), gives

$$(Z_{r_2 r_2} + Z_{q_2 q_2}) i_{q_2} + C i_{q_1,q_3} + Z_{q_2 p} i_p = 0$$

or,

$$R i_{q_2} + C i_{q_1,q_3} + Z_{q_2 p} i_p = 0 \tag{6.25}$$

where, $R = (Z_{r_2 r_2} + Z_{q_2 q_2})$.

Since $V_s = V_t$, $i_t = -i_s$, equating equation (6.21) and (6.22), gives

$$G i_{q_1,q_3} + (F+H) i_{s_1,s_3} = 0$$

$$G i_{q_1,q_3} + Q i_{s_1,s_3} = 0 \tag{6.26}$$

where, $Q = F + H$.

Multiply equation (6.24) by E^{-1}, and, multiplying equation (6.26) by Q^{-1}, and, subtracting, gives

$$(E^{-1}P - Q^{-1}G)i_{q_1,q_3} + E^{-1}Bi_{q_2} = 0$$

hence,

$$i_{q_1,q_3} = (Q^{-1}G - E^{-1}P)^{-1}E^{-1}Bi_{q_2}. \tag{6.27}$$

Substitutes the i_{q_1,q_3} from the equation (6.27) into (6.25), gives

$$[R + C(Q^{-1}G - E^{-1}P)^{-1}E^{-1}B]\,i_{q_2} + Z_{q_2p}i_p = 0$$

which from the inverse product rule can be put in the form,

$$\{R + C[E(Q^{-1}G - E^{-1}P)]^{-1}B\}i_{q_2} + Z_{q_2p}i_p = 0$$

and, hence,

$$[R + C(EQ^{-1}G - P)^{-1}B]\,i_{q_2} + Z_{q_2p}i_p = 0$$

or,

$$Z_M i_{q_2} + Z_{q_2p}i_p = 0 \tag{6.28}$$

where,

$$Z_M = R + C(EQ^{-1}G - P)^{-1}B$$

$$= Z_{q_2q_2} + Z_{r_2r_2} + \begin{bmatrix} Z_{r_2r_1} & Z_{r_2r_3} \end{bmatrix}$$

$$\cdot\left(\begin{bmatrix} Z_{q_1s_1} & 0 \\ 0 & Z_{q_3s_3} \end{bmatrix}\begin{bmatrix} Z_{s_1s_1} + Z_{t_1t_1} & Z_{t_1t_3} \\ Z_{t_3t_1} & Z_{s_3s_3} + Z_{t_3t_3} \end{bmatrix}^{-1}\begin{bmatrix} Z_{s_1q_1} & 0 \\ 0 & Z_{s_3q_3} \end{bmatrix} - \begin{bmatrix} Z_{r_1r_1} + Z_{q_1q_1} & Z_{r_1r_3} \\ Z_{r_3r_1} & Z_{r_3r_3} + Z_{q_3q_3} \end{bmatrix}\right)^{-1}$$

$$\cdot\begin{bmatrix} Z_{r_1r_2} \\ Z_{r_3r_2} \end{bmatrix}.$$

From (6.28),

$$i_{q_2} = -Z_M^{-1}Z_{q_2p}i_p. \tag{6.29}$$

Substitute i_{q_2} from the equation (6.29) into (6.23) to obtain, the new, explicit matrix input impedance formula

$$Z_{in} = \frac{V_p}{i_p} = Z_{pp} - Z_{pq_2} Z_M^{-1} Z_{pq_2}^T . \tag{6.30}$$

Usually the U-slot rectangular patch antenna is symmetric, so that, with a suitable ordering of the ports within each port set, the following simplifications are present:

$Z_{q_2 p} = Z_{pq_2}^T$, $Z_{s_3 s_3} = Z_{q_3 q_3} = Z_{s_1 s_1} = Z_{q_1 q_1}$, $Z_{s_3 q_3} = Z_{q_3 s_3} = Z_{s_1 q_1} = Z_{q_1 s_1}$, $Z_{r_3 r_3} = Z_{r_1 r_1}$, $Z_{r_2 r_1} = Z_{r_1 r_2}^T$,

$Z_{r_3 r_1} = Z_{r_1 r_3}$, $Z_{r_3 r_2} = Z_{r_2 r_3}^T$, $Z_{t_3 t_3} = Z_{t_1 t_1}$, and, $Z_{t_3 t_1} = Z_{t_1 t_3}$.

Also, the row elements in $Z_{r_2 r_3}$ and $Z_{r_2 r_1}$ are the same but in reverse order, while, the column elements in $Z_{r_1 r_2}$, $Z_{r_3 r_2}$ are likewise in reverse order.

The above expression for the matrix Z_M then takes the simpler form

$$Z_M = Z_{q_2 q_2} + Z_{r_2 r_2} + \begin{bmatrix} Z_{r_2 r_1} & Z_{r_2 r_3} \end{bmatrix}$$

$$\cdot \left(\begin{bmatrix} Z_{q_1 s_1} & 0 \\ 0 & Z_{q_1 s_1} \end{bmatrix} \begin{bmatrix} Z_{q_1 q_1} + Z_{t_1 t_1} & Z_{t_1 t_3} \\ Z_{t_1 t_3} & Z_{q_1 q_1} + Z_{t_1 t_1} \end{bmatrix}^{-1} \begin{bmatrix} Z_{q_1 s_1} & 0 \\ 0 & Z_{q_1 s_1} \end{bmatrix} - \begin{bmatrix} Z_{r_1 r_1} + Z_{q_1 q_1} & Z_{r_1 r_3} \\ Z_{r_1 r_3} & Z_{r_1 r_1} + Z_{q_1 q_1} \end{bmatrix} \right)^{-1}$$

$$\cdot \begin{bmatrix} Z_{r_2 r_1} & Z_{r_2 r_3} \end{bmatrix}^T . \tag{6.31}$$

The coupling impedance elements in the impedance matrices are evaluated using the formulas given in Chapter 4, [73], [75].

The width of the feed port W_p is given by the diameter of the probe feed.

A Mathcad program listing for the above impedance evaluation is given in *Appendix 6A*.

6.4 Design Procedure for Antenna A

Applying the design equations (6.1)-(6.12) in Section 6.2, the initial dimensions of the patch antenna A, are given in Table 6.1.

Antenna A: $h = 1.575$ mm								
A	*B*	*C*	*D*	*E*	*F*	*H*	*R*	*T*
60	38.4	20	22	2	2	4.2	0.63	0

Table 6.1. Initial design dimensions in mm.

In order to test the above initial parameter estimates for impedance matching the input impedance was calculated using equation (6.30). In the calculation it was found that for each of the port sets q, r, s, t only six interconnecting ports were required. The probe feed of diameter, 1.26 mm, was replaced by a 'port feed', $W_p = 1.26$ mm [88]. In evaluating the infinite series an upper limit of summation, 10, was used, and the calculated Q-factor is 38.

The calculated input impedance of antenna was $62 - j0.5\ \Omega$ at 2.452 GHz.

By a little trial and error, the dimensions C, D and H were adjusted to achieve a good match and slight improvement in the bandwidth was obtained.

In order to reduce the above value of $62\ \Omega$, the parameters C, D, and H were adjusted to obtain a better match to $50\ \Omega$. The adjusted parameter set is given in Table 6.2 below.

Antenna A: $h = 1.575$ mm								
A	*B*	*C*	*D*	*E*	*F*	*H*	*R*	*T*
60	38.4	23	17	2	2	4	0.63	0

Table 6.2. Tuned the parameters *C*, *D*, *H* (mm) for matching at 2.45 GHz.

Both simulated and measured results for the antenna were obtained and compared with the design results. The fabricated patch antenna is shown in Figure 6.3.

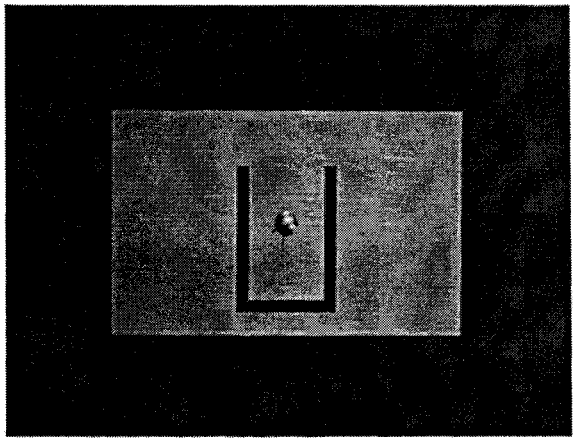

Figure 6.3. The fabricated patch antenna.

The predicted, simulated, and measured input impedance curves are shown in Figure 6.4(a), and, plotted on the Smith chart in Figure 6.4(b). There is good agreement between the predicted, simulated and practical results. The calculated and simulated input impedance are $55 + j4\,\Omega$, and $52 - j1\,\Omega$ respectively, at 2.45 GHz, while, the measured input impedance is $52.5 - j1.5\,\Omega$ at 2.44 GHz. The measured resonant frequency is 2.44 GHz which is less than a 0.5% shift from the design frequency 2.45 GHz.

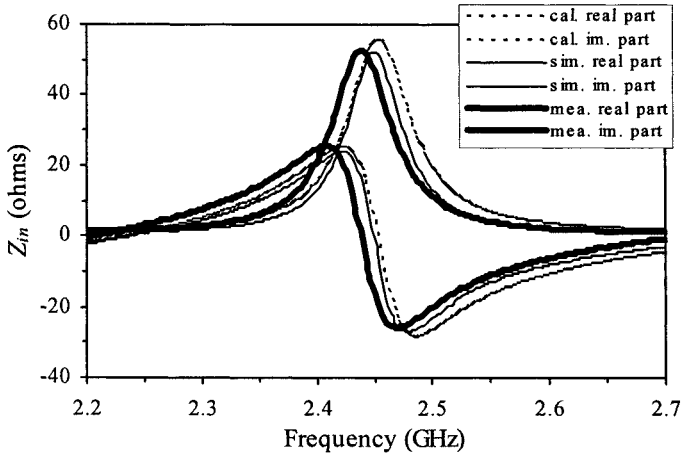

(a)

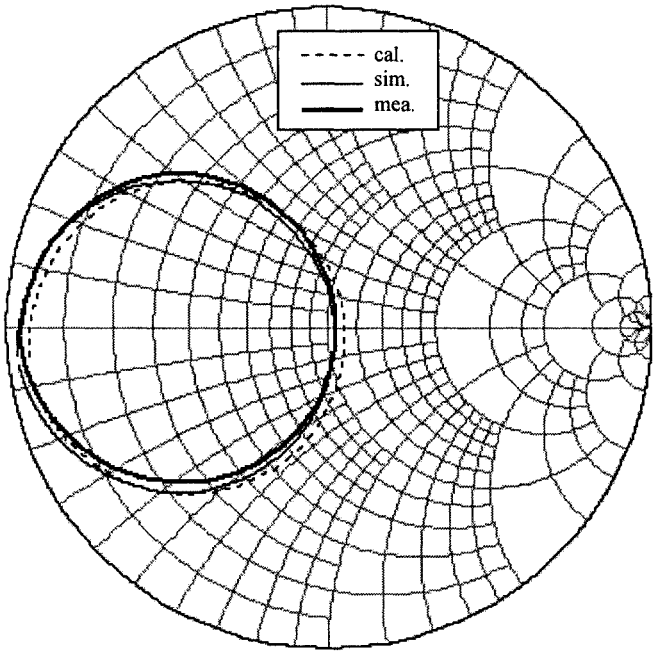

(b)

Figure 6.4. Calculated, simulated, and measured input impedance. (a) Input impedance. (b) Smith chart.

Figure 6.5 shows good return loss (S_{11}) and a good agreement between the predicted, simulated and measured values. The return loss and the -10-dB return loss bandwidth at the centre frequency are listed in Table 6.3.

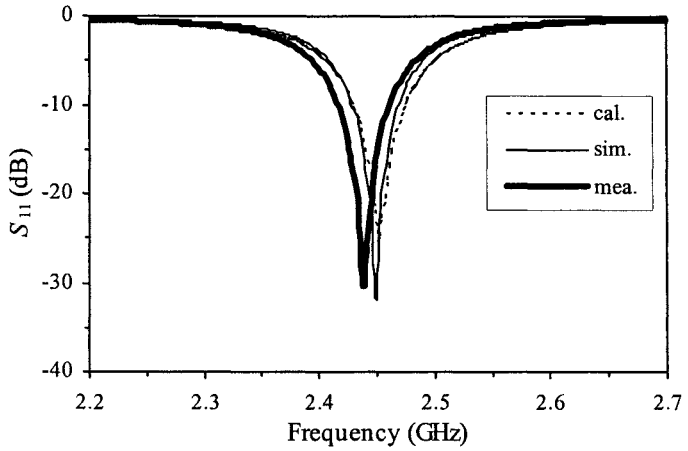

Figure 6.5. Calculated, simulated, and measured return loss.

	Calculation	Simulation	Measurement
Centre frequency f_0 (GHz)	2.45	2.45	2.44
S_{11} (dB)	-24.2	-32	-30.5
−10-dB S_{11} for impedance bandwidth (MHz, %)	45, 1.84	41, 1.67	44, 1.8

Table 6.3. The return loss and the impedance bandwidth.

A comparison between the simulated and measured results for the gain is shown in Figure 6.6. The simulated and measured values of gain of the resonant frequency are 7.1 dB and 6.6 dB respectively.

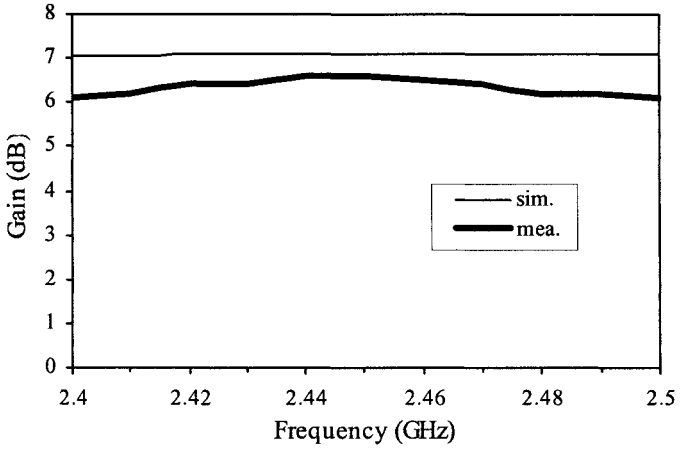

Figure 6.6. Simulated and measured gain.

Figure 6.7 shows the simulated and measured normalised radiation patterns at the E-plane ($\phi = 0$) and H-plane ($\phi = 90^\circ$). The simulated and measured far field characteristics are at 2.45 GHz and 2.44 GHz respectively.

The simulated and measured values of 3-dB beamwidth (half-power beamwidth) in the E-plane are 96° (between −46° and 50°), and, 76° (between −33° and 43°) respectively. The corresponding 3-dB beamwidth in H-plane are 70° (between −35° and 35°), and, 63° (between −31° and 32°) respectively.

The measured cross-polarisation levels are 36 dB and 43 dB below the co-polarisation component at boresight in the E- and H-planes respectively. The maximum measured cross-polarisation levels are −33 dB and −25 dB in the E- and H- planes respectively.

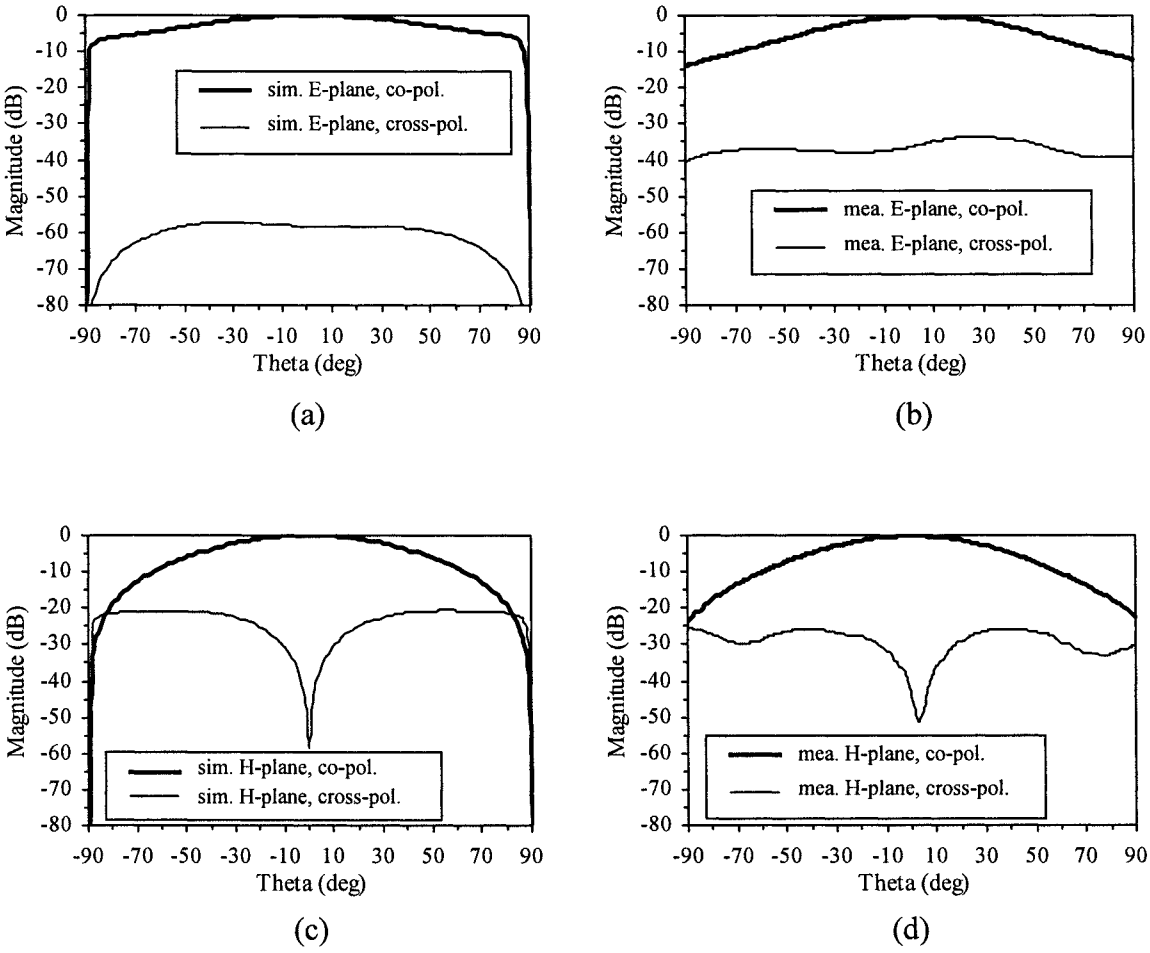

Figure 6.7. Normalised radiation patterns. (a) Simulated E-plane. (b) Measured E-plane. (c) Simulated H-plane. (d) Measured H-plane.

6.5 Design of Antenna B

The design procedure follows that used for the antenna A, with the initial parameters given below in Table 6.4.

Antenna B: $h = 3.175$ mm								
A	*B*	*C*	*D*	*E*	*F*	*H*	*R*	*T*
60	36.8	20	22	2	2	3.4	0.63	0

Table 6.4. Initial design dimensions in mm.

The calculated input impedance was $47.5 - j1\,\Omega$ at 2.47 GHz resonant frequency. A calculated Q of 19 was used. For matching, and, resonance, the parameters B, C, D, and H of the antenna were adjusted and an impedance of $56 - j0.4\,\Omega$ at 2.45 GHz was obtained.

The modified parameters are given in Table 6.5 below.

Antenna B: $h = 3.175$ mm								
A	*B*	*C*	*D*	*E*	*F*	*H*	*R*	*T*
60	36.55	23	18	2	2	4.5	0.63	0

Table 6.5. Tuned the parameters B, C, D, H (mm) for matching at 2.45 GHz.

A simulated input impedance of $55 + j0.6\,\Omega$ at 2.47 GHz was obtained showing a 0.8% shift from the design frequency 2.45 GHz.

It was found that adjusting the length B by simulation, from 36.55 mm to 36.9 mm (a difference of 0.95%) a simulated resonant frequency of 2.45 GHz was obtained.

The antenna was fabricated (Figure 6.8) using the dimensions given in Table 6.5, with the value $B = 36.55$ mm replaced by the new value of 36.9 mm.

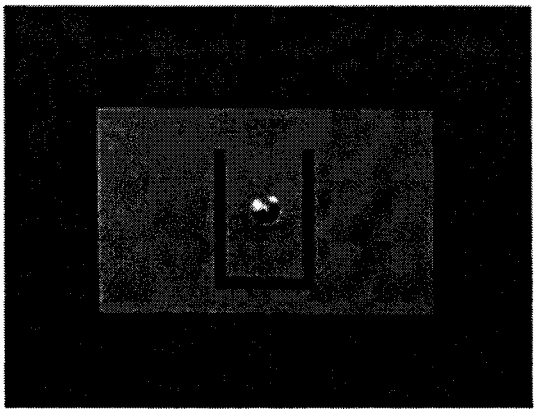

Figure 6.8. The fabricated patch antenna.

Predicted, simulated, and measured input impedance curves are shown in Figure 6.9(a), and, plotted on the Smith chart in Figure 6.9(b). There is good agreement between the predicted, simulated and practical results. The calculated, simulated and measured input impedances are $56.8 - j0.4\ \Omega$ at 2.434 GHz (0.65% shift from 2.45 GHz), and, $54.8 + j1.5\ \Omega$ at 2.45 GHz, and, $53.5 - j0.5\ \Omega$ at 2.438 GHz (0.49% shift from 2.45 GHz), respectively.

By adjusting the impedance loop on the Smith chart into the area of $\text{VSWR} \leq 2$, a general improvement in bandwidth was obtained together with a resonant input impedance of $55\ \Omega$. This improvement is significantly more than was achieved in the design of antenna A, which is shown by the smaller loop on the Smith chart.

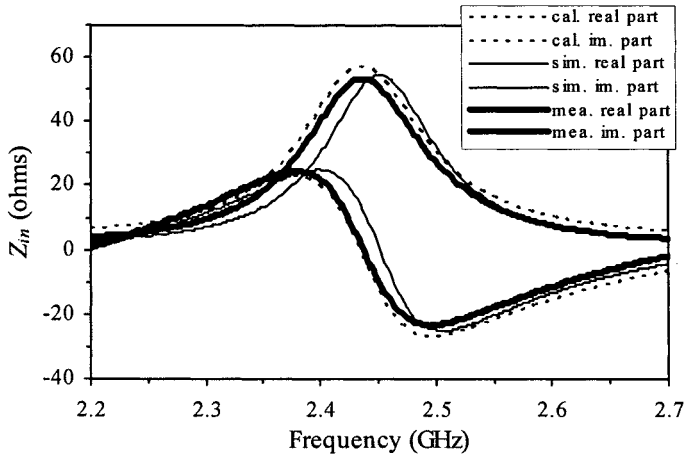

(a)

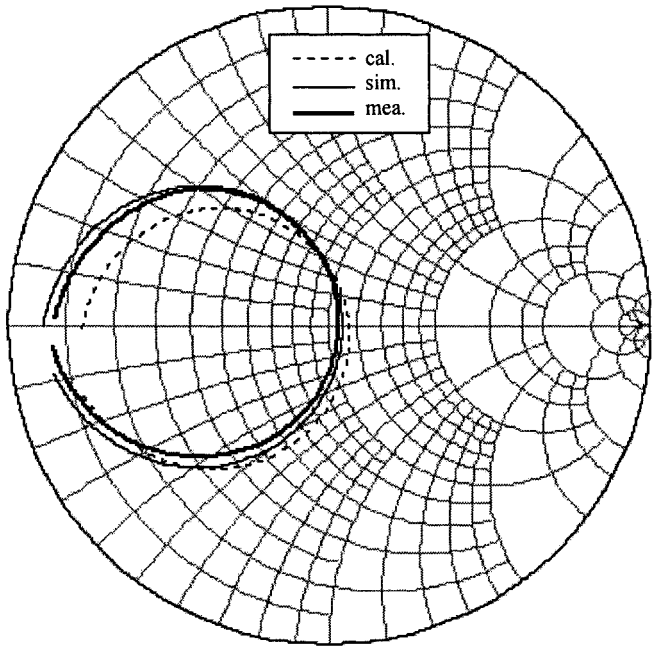

(b)

Figure 6.9. Calculated, simulated, and measured input impedance. (a) Input impedance. (b) Smith chart.

Figure 6.10 shows good return loss and good agreement between the predicted, simulated and measured values of return loss. The return loss and the −10-dB return loss bandwidth at the centre frequency are listed in Table 6.6.

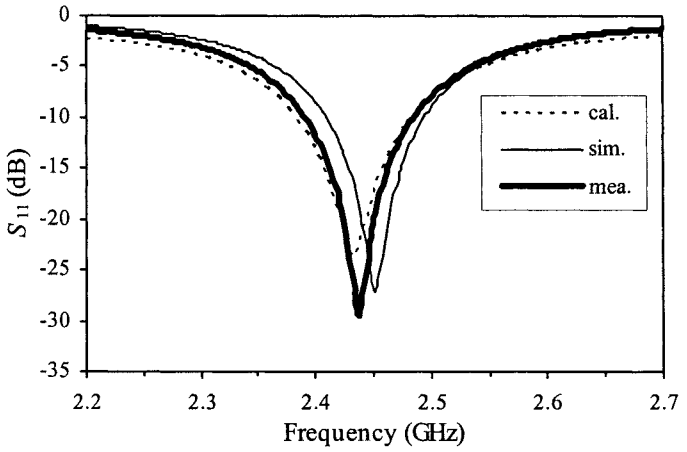

Figure 6.10. Calculated, simulated, and measured return loss.

	Calculation	Simulation	Measurement
Centre frequency f_0 (GHz)	2.434	2.45	2.438
S_{11} (dB)	-24	-26.5	-29.5
−10-dB S_{11} for impedance bandwidth (MHz, %)	99, 4.04	85, 3.47	94, 3.84

Table 6.6. The return loss and the impedance bandwidth.

A comparison between the simulated and measured results for the gain is shown in Figure 6.11. The simulated and measured values of gain of the resonant frequency are 7.15 dB and 6.8 dB respectively.

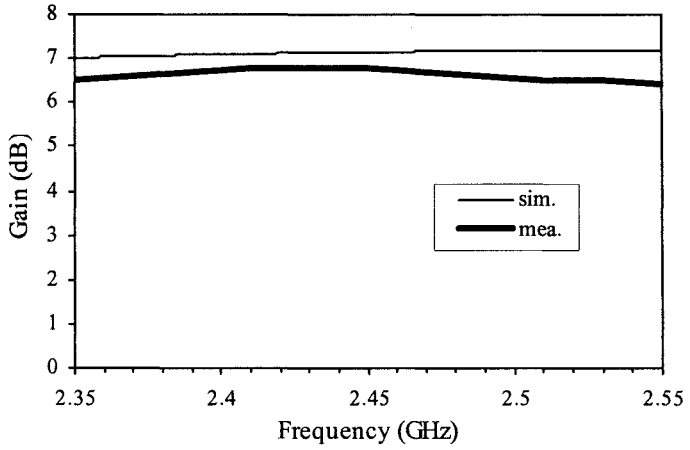

Figure 6.11. Simulated and measured gain.

Figure 6.12 shows the simulated and measured normalised radiation patterns at the E- and H-planes. The simulated and measured far field characteristics are at 2.45 GHz and 2.438 GHz respectively.

The simulated and measured values of 3-dB beamwidth in the E-plane are 96° (between −43° and 53°), and 74° (between −32° and 42°) respectively. The corresponding 3-dB beamwidth in H-plane are 68° (between −34° and 34°), and 64° (between −32° and 32°) respectively.

The measured cross-polarisation levels are 41 dB and 42 dB below the co-polarisation component at boresight in the E- and H-planes respectively. The maximum measured cross-polarisation levels are −36 dB and −30 dB in the E- and H- planes respectively.

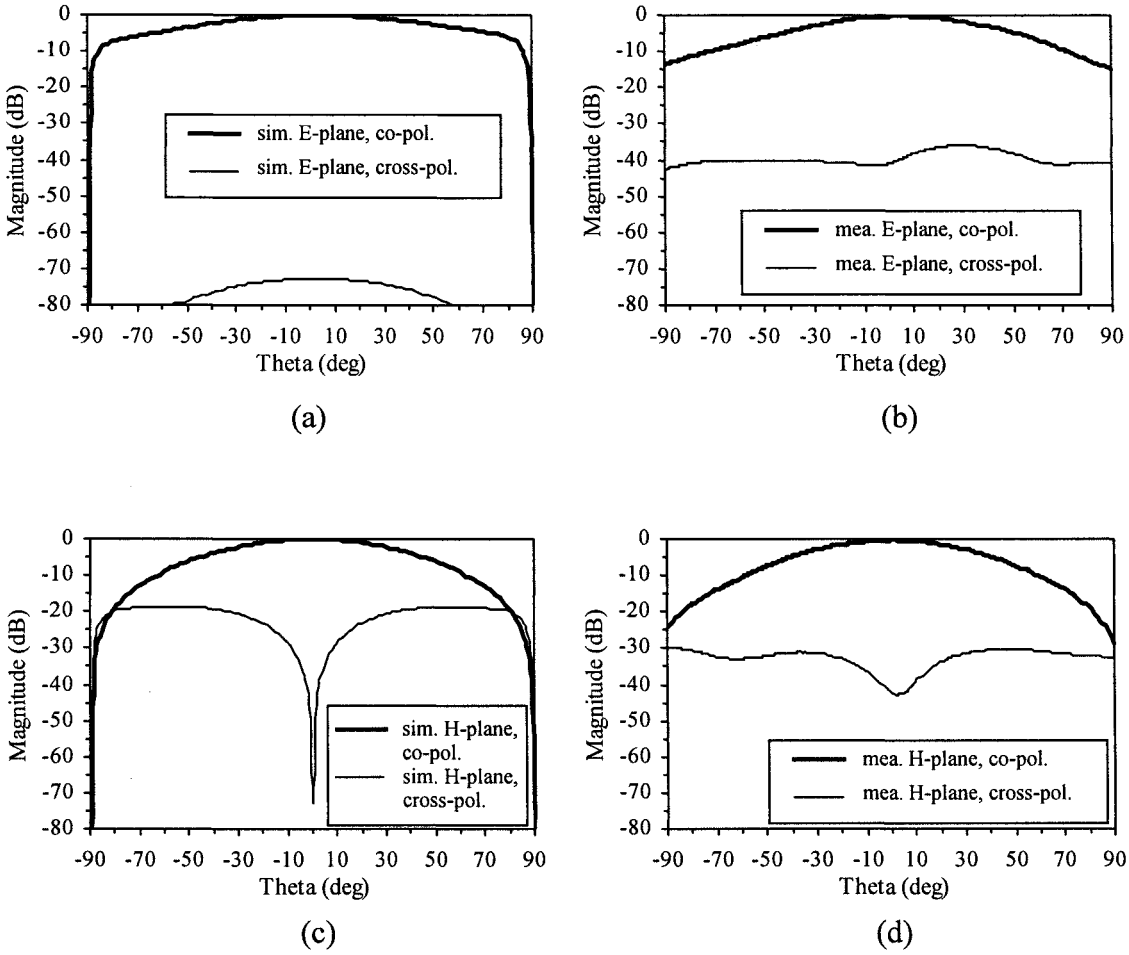

Figure 6.12. Normalised radiation patterns. (a) Simulated E-plane. (b) Measured E-plane. (c) Simulated H-plane. (d) Measured H-plane.

6.6 Summary

The analytic complexity of the system of coplanar circuit equations is reduced, and, a new explicit efficient matrix input impedance formula for a probe feed U-slot rectangular patch has been derived. The new probe self impedance formula and coupling impedance formula between the feed and a perimeter port, derived in Chapter 4, are applied in the segmentation method.

Using the above results the parameters of the patch antenna can be tuned to achieve a good match at the design frequency 2.45 GHz, and, also to obtain an improved bandwidth,

especially with the thicker substrate. In respect of computational efficiency, the run time of the matrix input impedance formula is at least 10 times faster than required by simulation for the input impedances.

The input impedance and the return loss for two U-slot rectangular patch antennas have been determined by the segmentation method. There are good agreements between the predicted, simulated, and measured results.

With the thicker substrate (3.175 mm) antenna the bandwidth is much wider than that for the substrate (1.575 mm) antenna, which is due to the thicker substrate having a lower Q. The gains and radiation patterns are not significantly different between the two antennas.

CHAPTER 7 CONCLUSIONS OF THE RESEARCH WORK AND FURTHER WORK

7.1 Conclusions

This thesis presents the results of the research that has been carried out in order to design compact single-feed CP, and LP microstrip patch antennas. By applying coplanar circuit analysis based on a cavity model, explicit computationally efficient coupling impedance and self impedance formulas for the rectangular and isosceles right-angled triangular patches were obtained. For a nearly square patch a new design formula was derived, and the input impedance was determined by using the above impedance formula. For the truncated corners square patch and U-slot rectangular patch which have composite geometries the input impedances were determined using the segmentation method with the new explicit matrix input impedance formulas. The predicted, simulated and measured results were compared.

In Chapter 2 the basic principles, modelling and analysis, polarisations, and general analytic techniques of microstrip patch antenna were reviewed. The basic design for CP single-feed compact patch antennas and CP dual-feed patch antennas was reviewed. Coplanar circuit analysis and its application in the derivation of coupling impedance formulas have been studied.

In Chapter 3 for a given feed position new equations for cavity and equivalent circuit models were derived in order to obtain the design dimensions of a CP nearly square patch antenna. It has been shown that increasing the offset feed and/or the substrate thickness increases the size of the perturbing segment so reducing the effect of manufacturing errors. The input impedance of the patch with varying offset microstrip line feed locations were calculated. Using a short length of microstrip line a compact form of a matched antenna was achieved. The measured and simulated results show a good axial ratio and good return loss, and are also in good agreement with predicted values.

In Chapter 4 the Green's functions have been partitioned and used to obtain explicit efficient coupling impedance formulas for rectangular and isosceles right triangular segments. New formulas for a probe feed self impedance and coupling impedance between a probe and a microstrip feed on the vertical side of each of these segments have been derived. Good agreement between the calculated, simulated and measured self impedance and perimeter port coupling impedance was obtained. The explicit efficient impedances formulas for both segments have been used in Chapters 5 and 6.

In Chapter 5 a new explicit matrix input impedance formula, for use in the segmentation method, has been derived to determine the input impedance of a CP offset microstrip feed truncated corners square patch antenna. A compact matched offset microstrip feed patch antenna has been designed to achieve an optimum increase in the area of the perturbation segments which reduces the effect of manufacturing errors. The results obtained for the predicted, simulated and measured values were compared.

In Chapter 6 for a probe feed U-slot rectangular patch the analytic complexity of the system of coplanar circuit equations is reduced by use of a new matrix augmentation technique that reduces the eleven matrix circuit equations to seven equations from which a new explicit efficient matrix input impedance formula was derived. The new probe self impedance formula and coupling impedance formula between the feed and a perimeter port were used for the matrix impedance formula. Applying the matrix impedance formula the parameters of the patch antenna were fine-tuned to achieve a good match and also to obtain an improved bandwidth, especially for the thicker substrate. The run time for the matrix input impedance formula is at least 10 times faster than required by simulation. There are good agreements between the predicted, simulated, and measured input impedance and the return loss. Due to lower Q, the bandwidth of the 3.175 mm thicker substrate antenna is much wider than the 1.575 mm substrate antenna.

7.2 Suggestions for Further Work

A number of areas of further research work and investigation are identified below.

1. The CP compact offset feed nearly square patch antenna, presented in Chapter 3, can be loaded with a centre square-shaped slot to obtain a compact antenna in the form of a nearly square ring patch antenna [51], [60]. The square-shaped loaded slot at the centre of the patch increases the length of the fundamental mode current path thereby lowering the operating frequency. This characteristic makes the size of the patch antenna smaller than that of the conventional perturbed square patch antenna. The patch antenna with microstrip feed and probe feed is shown in Figure 7.1.

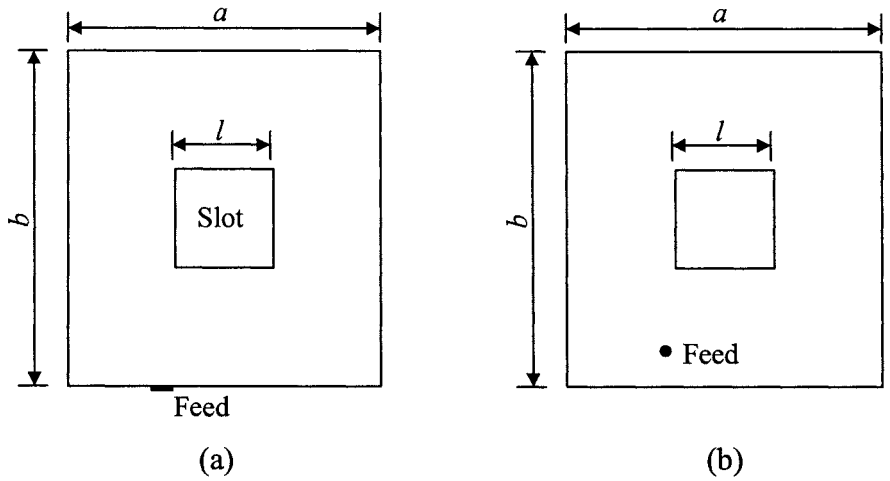

Figure 7.1. Nearly square ring patch antenna. (a) Microstrip offset feed. (b) Probe offset feed.

The segmentation structure is shown in Figure 7.2 and the nine matrix impedance-current equations can be reduced to five using the new matrix augmentation technique. A matrix input impedance formula can more easily be derived as shown below.

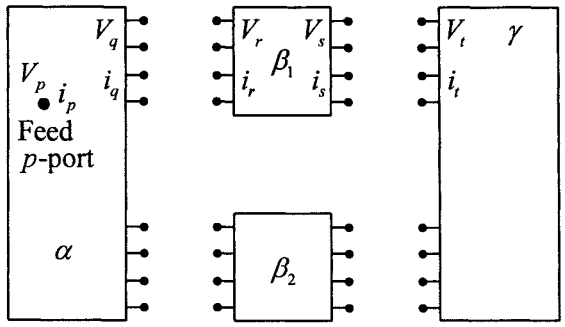

Figure 7.2. Segmentation structure for a rectangular ring patch antenna with offset feed.

The five matrix circuit equations are given as,

$$V_p = Z_{pp} i_p + Z_{pq} i_q \tag{7.1}$$

$$V_q = Z_{qp} i_p + Z_{qq} i_q \tag{7.2}$$

$$V_r = Z_{rr} i_r + Z_{rs} i_s \tag{7.3}$$

$$V_s = Z_{ss} i_s + Z_{sr} i_r \tag{7.4}$$

$$V_t = Z_{tt} i_t . \tag{7.5}$$

Solving the above equations (7.1)-(7.5), the explicit matrix equation is given by

$$Z_{in} = Z_{pp} - Z_{pq}[(Z_{qq} + Z_{rr}) - Z_{rs}(Z_{qq} + Z_{rr})^{-1} Z_{rs}]^{-1} Z_{pq}^{T} . \tag{7.6}$$

2. By overlapping three square-shaped patches along the diagonals a compact wideband dual-polarised patch antenna was obtained in [89], as shown in Figure 7.3.

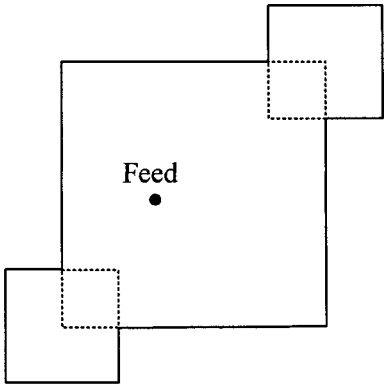

Figure 7.3. Overlapping three square-shaped patches antenna.

The input impedance of this composite geometry patch antenna can be determined by the segmentation method and its segmental structure is shown in Figure 7.4.

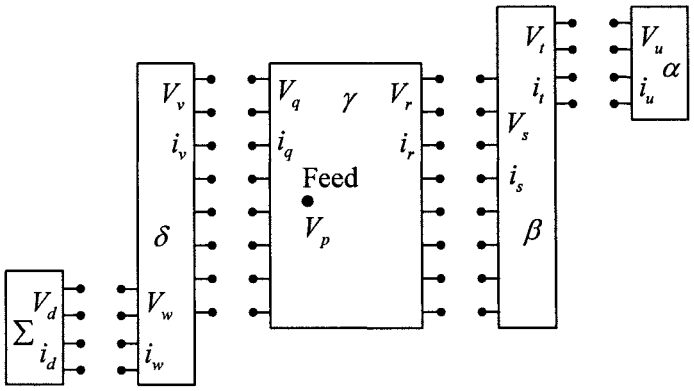

Figure 7.4. Segmental structure.

The matrix input impedance is given by

$$Z_{in} = Z_{pp} + Z_{pq} Z_{rq}^{-1} (AC^{-1}D - Z_{rp}) - Z_{pr} C^{-1} D \tag{7.7}$$

where, $A = Z_{qq} + Z_{ss} - Z_{st}(Z_{tt} + Z_{uu})^{-1} Z_{ts}$, $C = A - Z_{rq} A^{-1} Z_{qr}$ and $D = Z_{rp} - Z_{rq} A^{-1} Z_{qp}$.

3. A compact single-feed equilateral triangular patch antenna with the perturbation segment as a truncated tip segment [90] and a tip stub segment [91] are used to produce circular polarisation. The above geometries with the equilateral triangle replaced by an isosceles right-angled triangle can be investigated. Also an edge stub patch (Figure 7.5(c)) which can produce circular polarisation can be studied. The area of the triangular patch antenna is about half that of the perturbed square patch antenna operating at same frequency. The patch antennas and associated segmental structures are shown in Figure 7.5.

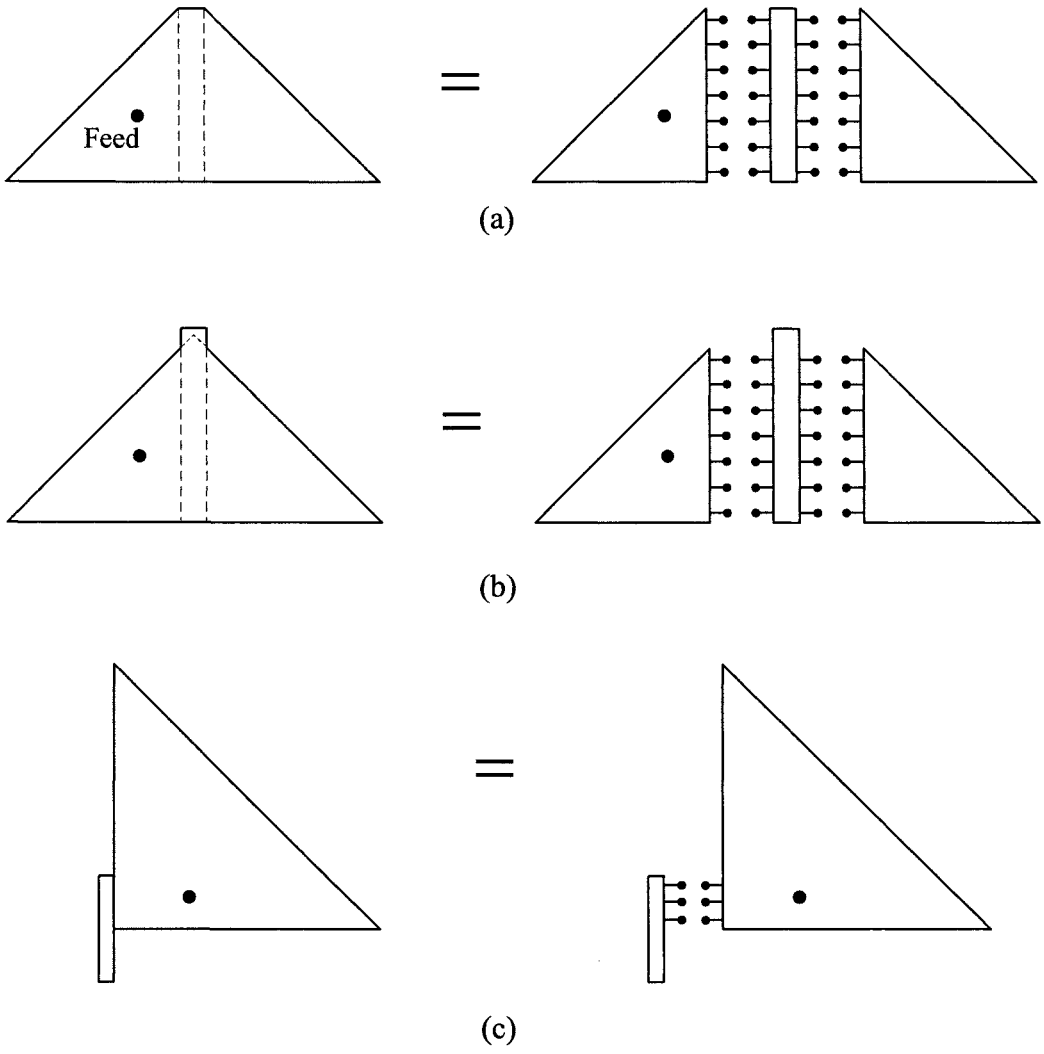

Figure 7.5. A CP perturbed isosceles right-angled triangular patch and its segmental segments. (a) A truncated tip patch. (b) A tip stub patch. (c) An edge stub patch.

Segmentation method can be applied to calculate the input impedance for each of the above structures.

4. In Chapter 4 the efficient probe self impedance formula and a coupling impedance formula between a probe feed and a port on the perpendicular side were derived for an isosceles right-angled triangle. For further study, using the same methodology, a coupling impedance formula between a probe feed and a port on the hypotenuse (see Figure 7.6) can be derived. This would present a difficult piece of analysis. The result would greatly assist the derivation of the input impedance of the truncated corners square patch (Chapter 5) with a probe feed located in a triangular segment.

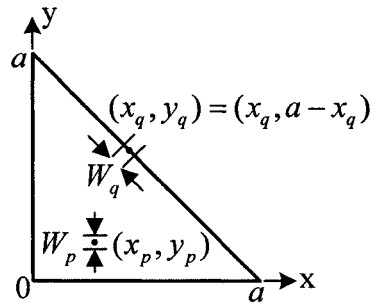

Figure 7.6. Triangular segment with a probe feed and a port on the hypotenuse.

REFERENCES

[1] K. L. Wong, *Compact and Broadband Microstrip Antennas*. New York: John Wiley & Sons, Inc., 2002.

[2] R. Garg, P. Bhartia, I. Bahl, and A. Ittipiboon, *Microstrip Antenna Design Handbook*. Boston, London: Artech House, 2001.

[3] J. R. James and P. S. Hall, *Handbook of Microstrip Antennas*. London, UK: Peter Peregrinus Ltd., 1989.

[4] G. Kumar and K. P. Ray, *Broadband Microstrip Antennas*. London: Artech House, 2003.

[5] C. A. Balanis, *Antenna Theory: Analysis and Design*. New York: John Wiley & Sons, Inc., 1997.

[6] E. O. Hammerstad, "Equations for microstrip circuit design," in *Proc. 5th Eur. Microw. Conf.*, Hamburg, Germany, 1975, pp. 268-272.

[7] M. Kirschning, R. H. Jansen, and N. H. L. Koster, "Accurate model for open end effect of microstrip lines," *Electron. Lett.*, vol. 17, no. 3, pp.123-125, Feb. 1981.

[8] K. R. Carver and J. W. Mink, "Microstrip antenna technology," *IEEE Trans. Antennas Propagat.*, vol. AP-29, no. 1, pp. 2-24, Jan. 1981.

[9] R. E. Munson, "Conformal microstrip antennas and microstrip phased arrays," *IEEE Trans. Antennas Propagat.*, vol. 22, no. 1, pp. 74-78, Jan. 1974.

[10] A. Van de Capelle, "Transmission-line model for rectangular microstrip antennas," in *Handbook of Microstrip Antennas*, Chap. 10, J. R. James and P. S. Hall (Eds.). London, UK: Peter Peregrinus Ltd., 1989.

[11] Y. T. Lo, D. Solomon, and W. F. Richards, "Theory and experiment on microstrip antennas," *IEEE Trans. Antennas Propagat.*, vol. AP-27, no. 2, pp. 137-145, Mar. 1979.

[12] W. F. Richards, Y. T. Lo, and D. D. Harrison, "An improved theory for microstrip antennas and applications," *IEEE Trans. Antennas Propagat.*, vol. AP-29, no. 1, pp. 38-46, Jan. 1981.

[13] J. R. Mosig and F. E. Gardiol, "General integral equation formulation for microstrip antenna and scatterers," *IEE Proc., Microw. Antennas Propag.*, vol. 132, no. 7, pp. 424-432, Dec. 1985.

[14] D. M. Pozar, "A reciprocity method of analysis for printed slot and slot-coupled microstrip antennas," *IEEE Trans. Antennas Propagat.*, vol. Ap-34, no. 12, pp. 1439-1446, Dec. 1986.

[15] Z. G. Qian, T. J. Cui, W. B. Lu, X. X. Yin, W. Hong, and W. C. Chew, "An improved MoM model for line-fed patch antennas and printed circuits," *IEEE Trans. Antennas Propagat.*, vol. 53, no. 9, pp. 2969-2976, Sep. 2005.

[16] A. G. Derneryd, "A theoretical investigation of the rectangular microstrip antenna element," *IEEE Trans. Antennas Propagat.*, vol. AP-26, no. 4, pp. 532-535, Jul. 1978.

[17] W. F. Richards, "Microstrip antennas," in *Antenna Handbook: Theory, Applications, and Design*, Chap. 10, Y. T. Lo and S. W. Lee (Eds.). New York: Van Nostrand Reinhold Co., 1988.

[18] K. Moussakhani and A. Ghorbani, "A novel transmission line model for analyzing bowtie patch antennas," in *Progress in Electromagnetics Research Symp.*, Cambridge, USA, Mar. 2006, pp. 168-171.

[19] D. Jaisson, "Transmission line model for the input impedance of a slot-coupled rectangular patch antenna," *IEE Proc., Microw. Antennas Propag.*, vol. 153, no. 5, pp. 461-468, Oct. 2006.

[20] M. I. Aksun, S. L. Chuang, and Y. T. Lo, "On slot-coupled microstrip antennas and their applications to CP operation — theory and experiment," *IEEE Trans. Antennas Propagat.*, vol. 38, no. 8, pp. 1224-1230, Aug. 1990.

[21] T. Fujimoto, K. Tanaka, and M. Taguchi, "Analytical method for a circularly polarised rectangular microstrip antenna," *IEE Proc., Microw. Antennas Propag.*, vol. 148, no. 2, pp. 85-90, Apr. 2001.

[22] M. Edimo, K. Mahdjoubi, A. Sharaiha, and C. Terret, "Simple circuit model for coax-fed stacked rectangular microstrip patch antenna," *IEE Proc., Microw. Antennas Propag.*, vol. 145, no. 3, pp. 268-272, Jun. 1998.

[23] A. K. Verma and Nasimuddin, "Resonance frequency and bandwidth of rectangular microstrip antenna on thick substrate," *IEEE Microw. Wireless Comp. Lett.*, vol. 12, no. 2, pp. 60-62, Feb. 2002.

[24] Y. P. Zhang and J. J. Wang, "Theory and analysis of differentially-driven microstrip antennas," *IEEE Trans. Antennas Propagat.*, vol. 54, no. 4, pp. 1092-1099, Apr. 2006.

[25] D. Guha, Y. M. M. Antar, J. Y. Siddiqui, and M. Biswas, "Resonant resistance of probe- and microstrip-line-fed circular microstrip patches," *IEE Proc., Microw. Antennas Propag.*, vol. 152, no. 6, pp. 481-484, Dec. 2005.

[26] K. S. Yee, "Numerical solution of initial boundary value problems involving Maxwell's equations in isotropic media," *IEEE Trans. Antennas Propagat.*, vol. AP-14, no. 3, pp. 302-307, May 1966.

[27] I. R. Capoglu and G. S. Smith, "A direct time-domain FDTD near-field-to-far-field transform in the presence of an infinite grounded dielectric slab," *IEEE Trans. Antennas Propagat.*, vol. 54, no. 12, pp. 3805-3814, Dec. 2006.

[28] J. D. Kraus and D. A. Fleisch, *Electromagnetics with Applications*, 5th ed. London: McGraw-Hill, Inc., 1999.

[29] J. Q. Howell, "Microstrip antennas," *IEEE Trans. Antennas Propagat.*, vol. 23, pp. 90-93, Jan. 1975.

[30] Tak Kwong Chan, "Development of a two-way microwave communication system for traffic applications," Ph.D. thesis, University of Northumbria at Newcastle, UK, 1994.

[31] G. G. Sanford, "Conformal microstrip phased array for aircraft tests with ATS-6," *IEEE Trans. Antennas Propagat.*, vol. AP-26, no. 5, pp. 642-646, Sep. 1978.

[32] M. Haneishi and Y. Suzuki, "Circular polarisation and bandwidth," in *Handbook of Microstrip Antennas*, Chap. 4, J. R. James and P. S. Hall (Eds.). London: Peter Peregrinus Ltd., UK, 1989.

[33] Q. Y. Wang, "Electromagnetically-coupled patch antenna for phased array applications for mobile satellite communications," *Microw. Opt. Technol. Lett.*, vol. 48, no. 7, pp. 1279-1282, Jul. 2006.

[34] X. M. Qing, "Broadband aperture-coupled circularly polarized microstrip antenna fed by a three-stub hybrid coupler," *Microw. Opt. Technol. Lett.*, vol. 40, no. 1, pp. 38-41, Jan. 2004.

[35] M. Mathian, E. Korolkiewicz, P. Gale, and E. G. Lim, "Design of a circularly polarized 2x2 patch array operating in the 2.45 GHz ISM band," *Microw. Journal*, pp. 280-286, May 2002.

[36] J. F. Zurcher and F. Gardiol, *Broadband Patch Antennas*, London: Artech House, 1995.

[37] B. W. Lim, E. Korolkiewicz, and S. Scott, "Optimised design of corner microstrip fed nearly square patch antenna for circular polarisation," *Electron. Lett.*, vol. 32, no. 7, pp. 610-612, Mar. 1996.

[38] F. Lumini, L. Cividances, and J. C. da. S. Lacava, "Computer aided design algorithm for singly fed circularly polarized rectangular microstrip patch antennas," *Int. J. RF Microw. CAE*, vol. 9, no. 1, pp. 32-41, Jan. 1999.

[39] Y. T. Lo, B. Engst, and R. Q. Lee, "Simple design formulas for circularly polarised microstrip antennas," *IEE Proc., Microw. Antennas Propag.*, vol. 135, no. 3, pp. 213-215, Jun. 1988.

[40] M. Haneishi and S. Yoshida, "A design method of circularly polarized rectangular microstrip antenna by one-point feed," *Electronics and Communications in Japan*, vol. 64-B, no. 4, pp. 46-54, 1981.

[41] J. L. Kerr, "Microstrip polarization techniques," in *Proceedings of the 1978 Antenna Applications Symposium*, University of Illinois, Urbana, Allerton Park, USA, Sep. 1978.

[42] Beng Wee Lim, "Design and modelling of a corner fed circularly polarised patch antenna," Ph.D. thesis, University of Northumbria at Newcastle, UK, 1996.

[43] B. Al-Jibouri, T. Vlasits, E. Korolkiewicz, S. Scott, and A. Sambell, "Transmission-line modelling of the cross-aperture-coupled circular polarised microstrip antenna," *IEE Proc., Microw. Antennas Propag.*, vol. 147, no. 2, pp. 82-86, Apr. 2000.

[44] B. Al-Jibouri, H. Evans, E. Korolkiewicz, E. G. Lim, A. Sambell, and T. Vlasits, "Cavity model of circularly polarised cross-aperture-coupled microstrip antenna," *IEE Proc., Microw. Antennas Propag.*, vol. 148, no. 3, pp. 147-152, Jun. 2001.

[45] N. Herscovici, Z. Sipus, and D. Bonefacic, "Circularly polarized single-fed wide-band microstrip patch," *IEEE Trans. Antennas Propagat.*, vol. 51, no. 6, pp. 1277-1280, Jun. 2003.

[46] K. L. Chung and A. S. Mohan, "A systematic design method to obtain broadband characteristics for singly-fed electromagnetically coupled patch antennas for circular polarization," *IEEE Trans. Antennas Propagat.*, vol. 51, no. 12, pp. 3239-3248, Jun. 2003.

[47] T. Sudha, T. S. Vedavathy, and N. Bhat, "Wideband single-fed circularly polarised patch antenna," *Electron. Lett.*, vol. 40, no. 11, pp. 648-649, May 2004.

[48] Nasimuddin, K. P. Esselle, and A. K. Verma, "Wideband circularly polarized stacked microstrip antennas," *IEEE Antennas Wireless Propag. Lett.*, vol. 6, pp. 21-24, 2007.

[49] M. N. Jazi and M. N. Azarmanesh, "Design and implementation of circularly polarised microstrip antenna array using a new serial feed sequentially rotated technique," *IEE Proc., Microw. Antennas Propag.*, vol. 153, no. 2, pp. 133-140, Apr. 2006.

[50] W. S. Chen, C. K. Wu, and K. L. Wong, "Single-feed square-ring microstrip antenna with truncated corners for compact circular polarisation operation," *Electron. Lett.*, vol. 34, no. 11, pp. 1045-1047, May 1998.

[51] M. Elsdon, A. Sambell, S. C. Gao, and Y. Qin, "Compact circular polarised patch antenna with relaxed manufacturing tolerance and improved axial ratio bandwidth," *Electron. Lett.*, vol. 39, no. 18, pp. 1296-1298, Sep. 2003.

[52] W. S. Chen, C. K. Wu, and K. L. Wong, "Novel compact circularly polarized square microstrip antenna," *IEEE Trans. Antennas Propagat.*, vol. 49, no. 3, pp. 340-342, Mar. 2001.

[53] H. T. Chou and Y. L. Chiu, "A compact-sized microstrip antenna for GPS applications," *Microw. Opt. Technol. Lett.*, vol. 48, no. 4, pp. 810-814, Apr. 2006.

[54] C. F. Tseng, C. L. Huang, and A. Hsu, "A compact-size circularly polarized antenna using low-loss alumina substrates," *Microw. Opt. Technol. Lett.*, vol. 48, no. 11, pp. 2317-2320, Nov. 2006.

[55] T. Okoshi, *Planar Circuits for Microwaves and Lightwaves*. New York: Springer-Verlag, 1985.

[56] T. Okoshi, Y. Uehara, and T. Takeuchi, "The segmentation method – an approach to the analysis of microwave planar circuits," *IEEE Trans. Microw. Theory Tech.*, vol. MTT-24, pp. 662-668, Oct. 1976.

[57] T. Okoshi and T. Takeuchi, "Analysis of planar circuits by segmentation method," *Electronics and Communications in Japan*, vol. 58-B, no. 8, pp. 71-79, 1975.

[58] R. Chadha and K. C. Gupta, "Segmentation method using impedance matrices for analysis of planar microwave circuits," *IEEE Trans. Microw. Theory Tech.*, vol. MTT-29, no. 1, pp. 71-74, Jan. 1981.

[59] V. Palanisamy and R. Garg, "Analysis of arbitrarily shape microstrip patch antennas using segmentation technique and cavity model," *IEEE Trans. Antennas Propagat.*, vol. AP-34, no. 10, pp. 1208-1213, Oct. 1986.

[60] V. Palanisamy and R. Garg, "Analysis of circular polarized square ring and crossed-strip microstrip antennas," *IEEE Trans. Antennas Propagat.*, vol. AP-34, pp. 1340-1346, Nov. 1986.

[61] J. George, C. K. Aanandan, P. Mohanan, and K. G. Nair, "Analysis of a new compact microstrip antenna," *IEEE Trans. Antennas Propagat.*, vol. 46, no. 11, pp. 1712-1717, Nov. 1998.

[62] S. S. Zhong, X. X. Yang, S. C. Gao, and J. H. Cui, "Corner-fed microstrip antenna element and arrays for dual-polarization operation," *IEEE Trans. Antennas Propagat.*, vol. 50, no. 10, pp. 1473-1480, Oct. 2002.

[63] S. S. Zhong, X. X. Yang, and S. C. Gao, "Polarization-agile microstrip antenna array using a single phase-shift circuit," *IEEE Trans. Antennas Propagat.*, vol. 52, no. 1, pp. 84-87, Jan. 2004.

[64] Eng Gee Lim, "Circular polarised microstrip antenna design using segmental methods," Ph.D. thesis, University of Northumbria at Newcastle, UK, 2002.

[65] S. K. Lee, A. Sambell, E. Korolkiewicz, S. F. Ooi, and Y. Qin, "Design of a circular polarized nearly square microstrip patch antenna with offset feed," in *9th IEEE High Frequency Postgraduate Student Colloquium*, Sep. 2004, pp. 61-66.

[66] S. K. Lee, A. Sambell, E. Korolkiewicz, S. F. Loh, S. F. Ooi, and Y. Qin, "A design procedure for a circular polarized, nearly square patch antenna," *Microw. Journal*, vol. 48, no. 1, Jan. 2005.

[67] S. K. Lee, A. Sambell, E. Korolkiewicz, and S. F. Ooi, "Analysis and design of a circular-polarized nearly-square-patch antenna using a cavity model," *Microw. Opt. Technol. Lett.*, vol. 46, no. 4, pp. 406-410, Aug. 2005.

[68] H. A. Atwater, "Reflection coefficient transformations for phase-shift circuits," *IEEE Trans. Microw. Theory Tech.*, vol. MTT-28, no. 6, pp. 563-568, Jun. 1980.

[69] D. M. Pozar, *Microwave Engineering*, 2nd edition. New York: John Wiley & Sons, Inc., 1998.

[70] R. Chadha and K. C. Gupta, "Green's functions for triangular segments in planar microwave circuits," *IEEE Trans. Microw. Theory Tech.*, vol. MTT-28, no. 10, pp. 1139-1143, Oct. 1980.

[71] A. Benalla and K. C. Gupta, "Faster computation of Z-matrices for rectangular segments in planar microstrip circuits," *IEEE Trans. Microw. Theory Tech.*, vol. MTT-34, no. 6, pp. 733-736, Jun. 1986.

[72] S. H. Lee, A. Benalla, and K. C. Gupta, "Faster computation of Z-matrices for triangular segments in planar circuits," *Int. J. Microw. Millimeter-Wave CAE*, vol. 2, no. 2, pp. 98-107, Apr. 1992.

[73] E. G. Lim, E. Korolkiewicz, S. Scott, B. Aljibouri, and S. C. Gao, "Efficient impedance coupling formulas for rectangular segment in planar microstrip circuits," *IEEE Trans. Antennas Propag.*, vol. 51, no. 8, pp. 2137-2140, Aug. 2003.

[74] E. G. Lim, E. Korolkiewicz, S. Scott, A. Sambell, and B. Aljibouri, "An efficient formula for the input impedance of a microstrip right-angled isosceles triangular patch antenna," *IEEE Antennas Wireless Propag. Lett.*, vol. 1, no. 1, pp. 18-21, 2002.

[75] S. F. Ooi, S. K. Lee, A. Sambell, E. Korolkiewicz, and S. Scott, "A new and explicit matrix input impedance formula for the H-shaped microstrip patch antenna," *Microw. Opt. Technol. Lett.*, vol. 49, no. 7, pp. 1756-1759, Jul. 2007.

[76] S. K. Lee, S. F. Ooi, E. G. Lim, E. Korolkiewicz, and A. Sambell, "Efficient coupling impedance formulas for the right-angled isosceles triangular patch for use in segmentation analysis," in *Proc. 36th Eur. Microw. Conf.*, Manchester, UK, Sep. 2006, pp. 241-244.

[77] I. S. Gradshteyn and I. M. Ryzhik, *Table of Integrals, Series, and Products*. New York: Academic Press, 1994.

[78] F. Bilotti and C. Vegni, "Basis functions for an MoM solution of a corner-truncated patch antenna," *Int. J. RF Microw. CAE*, vol. 15, no. 3, pp. 272-277, March 2005.

[79] X. F. Peng, S. S. Zhong, S. Q. Xu, and Q. Wu, "Compact dual-band GPS microstrip antenna," *Microw. Opt. Technol. Lett.*, vol. 44, no. 1, pp. 58-61, Jan. 2005.

[80] J. S. Row, "A triple-band microstrip patch antenna," *Microw. Opt. Technol. Lett.*, vol. 38, no. 2, pp. 120-123, Jul. 2003.

[81] P. C. Sharma and K. C. Gupta, "Analysis and optimized design of single feed circularly polarized microstrip antennas," *IEEE Trans. Antennas Propag.*, vol. AP-31, no. 6, pp. 949-955, Nov. 1983.

[82] T. Huynh and K. F. Lee, "Single-layer single-patch wideband microstrip antenna," *Electron. Lett.*, vol. 31, no. 16, pp. 1310-1312, Aug. 1995.

[83] K. F. Lee, K. M. Luk, K. F. Tong, S. M. Shum, T. Huynh, and R. Q. Lee, "Experimental and simulation studies of coaxially-fed U-slot rectangular patch antenna," *IEE Proc., Microw. Antennas Propag.*, vol. 144, no. 5, pp. 354-358, Oct. 1997.

[84] K. F. Tong, K. M. Luk, K. F. Lee, and R. Q. Lee, "A broad-band U-slot rectangular patch antenna on a microwave substrate," *IEEE Trans. Antennas Propag.*, vol. 48, no. 6, pp. 954-960, Jun. 2000.

[85] S. Weigand, G. H. Huff, K. H. Pan, and J. T. Bernhard, "Analysis and design of broad-band single-layer rectangular U-slot microstrip patch antennas," *IEEE Trans. Antennas Propagat.*, vol. 51, no. 3, pp. 457-468, Mar. 2003.

[86] Y. L. Chow, Z. N. Chen, K. F. Lee, and K. M. Luk, "A design theory on broadband patch antennas with slot," in *Antennas Prop. Soc. Int. Symp. Digest*, vol. 2, Jun. 1998, pp. 1124-1127.

[87] K. F. Tong, K. M. Luk, K. F. Lee, and S. M. Shum, "Analysis of broadband U-slot microstrip antenna," in 10th *International Conf. Antennas Prop.*, vol. 1, Apr. 1997, pp. 110-113.

[88] K. C. Gupta, "Multiport network approach for modelling and analysis of microstrip patch antennas and arrays," in *Handbook of Microstrip Antennas*, Chap. 9, J. R. James and P. S. Hall (Eds.). London: Peter Peregrinus Ltd., UK, 1989.

[89] K. Rambabu, M. Z. Alam, and J. Bornemann, "Design of compact dual-polarized printed-circuit antenna for ultra-wideband applications," in *Proc. 36th Eur. Microw. Conf.*, Manchester, UK, Sep. 2006, pp. 626-629.

[90] C. L. Tang, J. H. Lu, and K. L. Wong, "Circularly polarised equilateral-triangular microstrip antenna with truncated tip," *Electron. Lett.*, vol. 34, no. 13, pp. 1277-1278, Jun. 1998.

[91] J. H. Lu and K. L. Wong, "Single-feed circularly polarized equilateral-triangular microstrip antenna with a tuning stub," *IEEE Trans. Antennas Propagat.*, vol. 48, no. 12, pp. 1869-1872, Dec. 2000.

APPENDIX 3A Q-Factor of a Rectangular Patch

The formula for the Q-factor which includes radiation(Q_r), dielectric(Q_d), conductor(Q_c), and surface wave (Q_{sw}) quality factors, is given in [2], [23].

$$\frac{1}{Q}=\frac{1}{Q_r}+\frac{1}{Q_d}+\frac{1}{Q_c}+\frac{1}{Q_{sw}}. \tag{3A.1}$$

The surface wave losses are very small, so Q_{sw} can be neglected for a thin substrate. The quality factors of the various losses can be expressed as

$$Q_d=\frac{1}{\tan\delta}, \tag{3A.2}$$

$$Q_c=h\sqrt{\pi f\mu\sigma_c} \tag{3A.3}$$

where, $\tan\delta$ is the loss tangent of the dielectric substrate, σ_c is the conductivity of the conductors associated with a patch and ground plane.

The radiation quality factor is given by,

$$Q_r=\frac{\omega W_T}{P_r} \tag{3A.4}$$

where, W_T is the time-averaged total energy stored under the patch geometry, and P_r is the power radiated by the patch antenna in the form of space wave.

The radiation quality factor obtained using the transmission-line model, is used in this thesis and is given in [23], [64].

$$Q_r=\frac{\pi}{2G_{in}Z_0}, \tag{3A.5}$$

where, $G_{in}=2(G_1+G_{12})$ is the total input conductance of a rectangular patch, G_1 is the radiation conductance and G_{12} is the mutual conductance, and, Z_0 is the characteristic impedance of a patch [5]. The derivation of the Q_r (3A.5) is given in the following section.

3A.1 Review and derivation of the radiation quality factor

From [69], the input impedance Z_{in} at a distance l from a load is

$$Z_{in} = Z_0 \frac{Z_L + Z_0 \tanh \gamma l}{Z_0 + Z_L \tanh \gamma l} \tag{3A.6}$$

where Z_0 is the characteristic line impedance, Z_L is the load impedance, γ is the propagation constant, $\gamma = \alpha + j\beta$, and, α is the attenuation constant and β is the phase constant (wavenumber).

A microstrip circuit consists of an open-circuited line length, $l = \lambda/2$, of lossy transmission line (Figure 3A.1) which has a very high load impedance Z_L. In the lossless case, $Z_L = \infty$ for an open-circuited line.

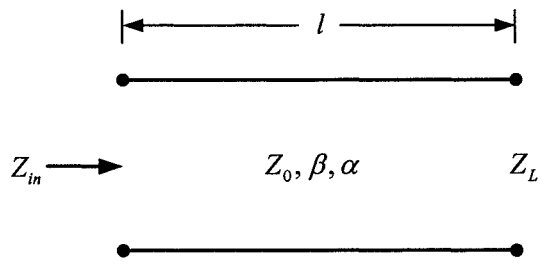

Figure 3A.1. An open-circuited length ($l = \lambda/2$) of lossy transmission line.

Therefore, the input impedance of an open-circuited line given equation (3A.6) becomes

$$\begin{aligned} Z_{in} &= Z_0 \frac{Z_L}{Z_L \tanh \gamma l} = Z_0 \coth \gamma l \\ &= Z_0 \coth(\alpha l + j\beta l) = Z_0 \frac{1}{\tanh(\alpha l + j\beta l)} \\ &= Z_0 \frac{1 + \tanh \alpha l \cdot \tanh j\beta l}{\tanh \alpha l + \tanh j\beta l} \\ &= Z_0 \frac{1 + j \tan \beta l \cdot \tanh \alpha l}{\tanh \alpha l + j \tan \beta l}. \end{aligned} \tag{3A.7}$$

For $l = \lambda/2$ and $\omega = \omega_0 + \Delta\omega$,

$$\beta l = \frac{\omega}{v_p} l = \frac{\omega_0 l}{v_p} + \frac{\Delta\omega\, l}{v_p} = \frac{\omega_0}{v_p}\frac{\pi v_p}{\omega_0} + \frac{\Delta\omega}{v_p}\frac{\pi v_p}{\omega_0} = \pi + \frac{\pi\Delta\omega}{\omega_0},$$

$$\tan\beta l = \tan\left(\pi + \frac{\pi\Delta\omega}{\omega_0}\right) = \tan\left(\frac{\pi\Delta\omega}{\omega_0}\right) \simeq \frac{\pi\Delta\omega}{\omega_0} \tag{3A.8}$$

for, $\dfrac{\pi\Delta\omega}{\omega_0} \ll 1$, and,

$$\tanh\alpha l \simeq \alpha l \tag{3A.9}$$

for, $\alpha l \ll 1$.

Substituting equations (3A.8) and (3A.9) into (3A.7) gives

$$Z_{in} = Z_0 \frac{1}{\alpha l + j\left(\dfrac{\pi\Delta\omega}{\omega_0}\right)}$$

$$= \frac{Z_0/\alpha l}{1 + j\left(\dfrac{\pi}{\alpha l}\dfrac{\Delta\omega}{\omega_0}\right)}. \tag{3A.10}$$

The input impedance of a parallel resonant *RLC* circuit is

$$Z_{in} = \frac{R_{in}}{1 + j\left(2Q_r\dfrac{\Delta\omega}{\omega_0}\right)}. \tag{3A.11}$$

Comparing equation (3A.10) with (3A.11), the total input resistance is given by

$$R_{in} = \frac{Z_0}{\alpha l}, \tag{3A.12}$$

and, the radiation quality factor is given by [23], [64]

$$Q_r = \frac{\pi}{2\alpha l} = \frac{\pi R_{in}}{2Z_0}$$

$$= \frac{\pi}{2G_{in}Z_0} \tag{3A.13}$$

where the total input conductance, $G_{in} = 1/R_{in}$.

APPENDIX 3B Derivation of the Amplitude and Phase Equations

The ratio V_b / V_a is given by

$$\frac{V_b}{V_a} = A \cdot \frac{\left[\frac{f_a}{Q} + j\left(f - \frac{f_a^2}{f}\right)\right]}{\left[\frac{f_b}{Q} + j\left(f - \frac{f_b^2}{f}\right)\right]} = 1\angle \pm 90^\circ = \pm j . \tag{3B.1}$$

(i) *Magnitude condition:*

For the two modes is equal amplitude $(|V_b| = |V_a|)$, the equation (3B.1) becomes

$$\left|\frac{V_b}{V_a}\right| = \left|\frac{N_b}{N_a} \cdot \frac{\left[\frac{f_b M}{Q} + j\left(f_0 - \frac{f_b^2 M^2}{f_0}\right)\right]}{\left[\frac{f_b}{Q} + j\left(f_0 - \frac{f_b^2}{f_0}\right)\right]}\right| = 1 \tag{3B.2}$$

$$\left|\frac{N_b}{N_a}\right| \cdot \left\|\left[\frac{f_b M}{Q} + j\left(f_0 - \frac{f_b^2 M^2}{f_0}\right)\right]\right\| = \left\|\left[\frac{f_b}{Q} + j\left(f_0 - \frac{f_b^2}{f_0}\right)\right]\right\| .$$

Let $\sqrt{r} = \frac{N_b}{N_a}$, and, $r = \left(\frac{N_b}{N_a}\right)^2 = \left|\left(\frac{N_b}{N_a}\right)\right|^2$, where, $\frac{N_b}{N_a} = \left|\frac{N_b}{N_a}\right|$,

$$r \cdot \left[\left(\frac{f_b M}{Q}\right)^2 + \left(f_0 - \frac{f_b^2 M^2}{f_0}\right)^2\right] = \left[\left(\frac{f_b}{Q}\right)^2 + \left(f_0 - \frac{f_b^2}{f_0}\right)^2\right]$$

$$r \cdot \left[\frac{f_b^2 M^2}{Q^2} + f_0^2 - 2 f_b^2 M^2 + \frac{f_b^4 M^4}{f_0^2}\right] = \left[\frac{f_b^2}{Q^2} + f_0^2 - 2 f_b^2 + \frac{f_b^4}{f_0^2}\right]$$

$$\frac{r f_b^2 M^2}{Q^2} - \frac{f_b^2}{Q^2} + r f_0^2 - f_0^2 - 2 r f_b^2 M^2 + 2 f_b^2 + \frac{r f_b^4 M^4}{f_0^2} - \frac{f_b^4}{f_0^2} = 0$$

$$\frac{f_b^2}{Q^2}\left(rM^2 - 1\right) + f_0^2 (r-1) - 2 f_b^2 \left(rM^2 - 1\right) + \frac{f_b^4}{f_0^2}\left(rM^4 - 1\right) = 0 .$$

Both sides divided by f_b^2, and let $\alpha = f_0 / f_b$,

$$\frac{1}{Q^2}(rM^2 - 1) + \alpha^2 (r-1) - 2(rM^2 - 1) + \frac{1}{\alpha^2}(rM^4 - 1) = 0 .$$

Both sides multiplied by α^2,

$$\frac{\alpha^2}{Q^2}\left(rM^2-1\right)+\alpha^4\left(r-1\right)-2\alpha^2\left(rM^2-1\right)+\left(rM^4-1\right)=0$$

$$\alpha^4\left(r-1\right)+\alpha^2\left(rM^2-1\right)\cdot\left(\frac{1}{Q^2}-2\right)+rM^4-1=0\,. \tag{3B.3}$$

(ii) *Phase condition:*

For two modes has phase difference of $\pm 90^\circ$,

$$\arg(V_b)-\arg(V_a)=\arg(V_b/V_a)=\pm 90^\circ\,. \tag{3B.4}$$

Multiply both numerator and denominator of equation (3B.1) by the complex conjugate of denominator gives

$$\frac{V_b}{V_a}=\frac{N_b}{N_a}\cdot\frac{\left[\frac{f_bM}{Q}+j\left(f_0-\frac{f_b^2M^2}{f_0}\right)\right]}{\left[\frac{f_b}{Q}+j\left(f_0-\frac{f_b^2}{f_0}\right)\right]}\cdot\frac{\left[\frac{f_b}{Q}-j\left(f_0-\frac{f_b^2}{f_0}\right)\right]}{\left[\frac{f_b}{Q}-j\left(f_0-\frac{f_b^2}{f_0}\right)\right]}$$

$$\frac{V_b}{V_a}=\frac{N_b}{N_a}\cdot\frac{\frac{f_b^2M}{Q^2}+\left(f_0-\frac{f_b^2M^2}{f_0}\right)\left(f_0-\frac{f_b^2}{f_0}\right)+j\left[\frac{f_b}{Q}\left(f_0-\frac{f_b^2M^2}{f_0}\right)-\frac{f_bM}{Q}\left(f_0-\frac{f_b^2}{f_0}\right)\right]}{\frac{f_b^2}{Q^2}+\left(f_0-\frac{f_b^2}{f_0}\right)^2}. \tag{3B.5}$$

The $\arg(V_b/V_a)$ is then given by

$$\arg(V_b/V_a)=\tan^{-1}\left\{\frac{\frac{f_b}{Q}\left(f_0-\frac{f_b^2M^2}{f_0}\right)-\frac{f_bM}{Q}\left(f_0-\frac{f_b^2}{f_0}\right)}{\frac{f_b^2M}{Q^2}+\left(f_0-\frac{f_b^2M^2}{f_0}\right)\left(f_0-\frac{f_b^2}{f_0}\right)}\right\}=\pm 90^\circ$$

$$\frac{\frac{f_b}{Q}\left(f_0-\frac{f_b^2M^2}{f_0}\right)-\frac{f_bM}{Q}\left(f_0-\frac{f_b^2}{f_0}\right)}{\frac{f_b^2M}{Q^2}+\left(f_0-\frac{f_b^2M^2}{f_0}\right)\left(f_0-\frac{f_b^2}{f_0}\right)}=\tan(\pm 90^\circ)=\pm\infty. \tag{3B.6}$$

This implies that

$$\frac{f_b^2M}{Q^2}+\left(f_0-\frac{f_b^2M^2}{f_0}\right)\left(f_0-\frac{f_b^2}{f_0}\right)=0$$

$$\frac{f_b^2M}{Q^2}+f_0^2-f_b^2-f_b^2M^2+\frac{f_b^4M^2}{f_0^2}=0. \tag{3B.7}$$

Both sides divided by f_b^2,

$$\frac{M}{Q^2}+\alpha^2-1-M^2+\frac{M^2}{\alpha^2}=0.$$

Both sides multiplied by α^2,

$$\frac{\alpha^2M}{Q^2}+\alpha^4-\alpha^2-\alpha^2M^2+M^2=0$$

$$\alpha^4+\alpha^2\left(\frac{M}{Q^2}-M^2-1\right)+M^2=0. \tag{3B.8}$$

APPENDIX 4A Coupling Impedance Formulas for a Rectangle and the Triangle

4A.1 Closed form summation formulas

The following series closed forms from Gradshteyn [77] have been used in this thesis.

1. $$\sum_{m=1}^{\infty}\frac{1}{m^2+A^2}=\frac{\pi\cosh A\pi}{2A\sinh A\pi}-\frac{1}{2A^2} \quad ; A \text{ is not an integer.} \tag{4A.1.1}$$

2. $$\sum_{m=1}^{\infty}\frac{1}{m^2-A^2}=\frac{1}{2A^2}-\frac{\pi\cos A\pi}{2A\sin A\pi} \tag{4A.1.2}$$

3. $$\sum_{m=1}^{\infty}\frac{(-1)^m}{m^2+A^2}=\frac{\pi}{2A\sinh A\pi}-\frac{1}{2A^2} \tag{4A.1.3}$$

4. $$\sum_{m=1}^{\infty}\frac{(-1)^m}{m^2-A^2}=\frac{1}{2A^2}-\frac{\pi}{2A\sin A\pi} \tag{4A.1.4}$$

5. $$\sum_{m=1}^{\infty}\frac{\cos m\theta}{m^2+A^2}=\frac{\pi\cosh A(\pi-\theta)}{2A\sinh A\pi}-\frac{1}{2A^2} \quad \text{when } 0\le\theta\le 2\pi \tag{4A.1.5}$$

6. $$\sum_{m=1}^{\infty}\frac{\cos m\theta}{m^2-A^2}=\frac{1}{2A^2}-\frac{\pi\cos A(\pi-\theta)}{2A\sin A\pi} \quad \text{when } 0\le\theta\le 2\pi \tag{4A.1.6}$$

7. $$\sum_{m=1}^{\infty}\frac{(-1)^m\cos m\theta}{m^2+A^2}=\frac{\pi\cosh A\theta}{2A\sinh A\pi}-\frac{1}{2A^2} \quad \text{when } -\pi\le\theta\le\pi \tag{4A.1.7}$$

8. $$\sum_{m=1}^{\infty}\frac{(-1)^m\cos m\theta}{m^2-A^2}=\frac{1}{2A^2}-\frac{\pi\cos A\theta}{2A\sin A\pi} \quad \text{when } -\pi\le\theta\le\pi \tag{4A.1.8}$$

9. $$\sum_{m=1}^{\infty}\frac{\sin m\theta}{m(m^2+A^2)}=\frac{\pi-\theta}{2A^2}-\frac{\pi\sinh A(\pi-\theta)}{2A^2\sinh A\pi} \quad \text{when } 0\le\theta\le 2\pi \tag{4A.1.9}$$

10. $$\sum_{m=1}^{\infty}\frac{\sin m\theta}{m(m^2-A^2)}=\frac{\theta-\pi}{2A^2}+\frac{\pi\sin A(\pi-\theta)}{2A^2\sin A\pi} \quad \text{when } 0\le\theta\le 2\pi \tag{4A.1.10}$$

11. $$\sum_{m=1}^{\infty}\frac{(-1)^m\sin m\theta}{m(m^2+A^2)}=\frac{\pi\sinh A\theta}{2A^2\sinh A\pi}-\frac{\theta}{2A^2} \quad \text{when } -\pi\le\theta\le\pi \tag{4A.1.11}$$

12. $$\sum_{m=1}^{\infty}\frac{(-1)^m\sin m\theta}{m(m^2-A^2)}=\frac{\theta}{2A^2}-\frac{\pi\sin A\theta}{2A^2\sin A\pi} \quad \text{when } -\pi\le\theta\le\pi \tag{4A.1.12}$$

13. $$\sum_{m=1}^{\infty}\frac{1}{m^2(m^2-A^2)}=\frac{1}{2A^4}-\frac{\pi\cos A\pi}{2A^3\sin A\pi}-\frac{\pi^2}{6A^2} \qquad (4A.1.13)$$

14. $$\sum_{m=1}^{\infty}\frac{(-1)^m}{m^2(m^2-A^2)}=\frac{1}{2A^4}-\frac{\pi}{2A^3\sin A\pi}+\frac{\pi^2}{12A^2} \qquad (4A.1.14)$$

15. $$\sum_{m=1}^{\infty}\frac{\cos m\theta}{m^2(m^2-A^2)}=\frac{1}{2A^4}-\frac{\pi\cos A(\pi-\theta)}{2A^3\sin A\pi}-\frac{\theta^2}{4A^2}+\frac{\pi\theta}{2A^2}-\frac{\pi^2}{6A^2} \quad \text{when } 0\le\theta\le 2\pi$$

(4A.1.15)

16. $$\sum_{m=1}^{\infty}\frac{(-1)^m\cos m\theta}{m^2(m^2-A^2)}=\frac{1}{2A^4}-\frac{\pi\cos A\theta}{2A^3\sin A\pi}-\frac{\theta^2}{4A^2}+\frac{\pi^2}{12A^2} \quad \text{when } -\pi\le\theta\le\pi \qquad (4A.1.16)$$

In particular, formulas (4A.1.9)-(4A.1.16) are not in [77]. Formulas (4A.1.9)-(4A.1.12) have been obtained, by integration from the formulas (4A.1.5)-(4A.1.8), respectively, in [77]. The formulas (4A.1.15) and (4A.1.16) obtained by double integration from formulas (4A.1.6) and (4A.1.8) respectively.

The formulas (4A.1.13) and (4A.1.14) are obtained from the formulas (4A.1.15) and (4A.1.16), respectively, with taking $\theta=0$.

4A.2 Probe feed input impedance on a rectangle

The coupling impedance between two probe ports, p and q, is given by

$$Z_{pq} = \frac{1}{W_p W_q} \int_{W_p} \int_{W_q} G(x_p, y_p \mid x_q, y_q)\, dy_q\, dy_p \tag{4A.2.1}$$

$$= \frac{j\omega\mu h}{abW_pW_q} \int_{y_p-W_p/2}^{y_p+W_p/2} \int_{y_q-W_q/2}^{y_q+W_q/2} \left\{ -\frac{1}{k^2} + \frac{2a^2}{\pi^2} \sum_{m=1}^{\infty} \frac{\cos\frac{m\pi}{a}x_p \cos\frac{m\pi}{a}x_q}{m^2 - A^2} \right.$$

$$+ \frac{2b^2}{\pi^2} \sum_{n=1}^{\infty} \frac{\cos\frac{n\pi}{b}y_p \cos\frac{n\pi}{b}y_q}{n^2 - B^2}$$

$$\left. + \frac{4}{\pi^2} \sum_{m=1}^{\infty} \sum_{n=1}^{\infty} \frac{\cos\frac{m\pi}{a}x_p \cos\frac{m\pi}{a}x_q \cos\frac{n\pi}{b}y_p \cos\frac{n\pi}{b}y_q}{\frac{m^2}{a^2} + \frac{n^2}{b^2} - \frac{k^2}{\pi^2}} \right\} dy_q\, dy_p. \tag{4A.2.2}$$

Integration of first term

$$-\frac{1}{k^2} \int_{y_p-W_p/2}^{y_p+W_p/2} \int_{y_q-W_q/2}^{y_q+W_q/2} 1\, dy_q\, dy_p = -\frac{W_pW_q}{k^2}. \tag{4A.2.3}$$

Integration of second term

$$\frac{2a^2}{\pi^2} \sum_{m=1}^{\infty} \frac{\cos\frac{m\pi}{a}x_p \cos\frac{m\pi}{a}x_q}{m^2 - A^2} \int_{y_p-W_p/2}^{y_p+W_p/2} \int_{y_q-W_q/2}^{y_q+W_q/2} 1\, dy_q\, dy_p = \frac{2a^2W_pW_q}{\pi^2} \sum_{m=1}^{\infty} \frac{\cos\frac{m\pi}{a}x_p \cos\frac{m\pi}{a}x_q}{m^2 - A^2}. \tag{4A.2.4}$$

Integration of third term

$$\frac{2b^2}{\pi^2} \sum_{n=1}^{\infty} \frac{1}{n^2 - B^2} \int_{y_p-W_p/2}^{y_p+W_p/2} \int_{y_q-W_q/2}^{y_q+W_q/2} \cos\frac{n\pi}{b}y_p \cos\frac{n\pi}{b}y_q\, dy_q\, dy_p \tag{4A.2.5}$$

$$= \frac{2b^4}{\pi^4} \sum_{n=1}^{\infty} \frac{(\sin n\theta_1 - \sin n\theta_2)(\sin n\theta_3 - \sin n\theta_4)}{n^2(n^2 - B^2)} \tag{4A.2.6}$$

where,

$$\int_{y_p-W_p/2}^{y_p+W_p/2}\int_{y_q-W_q/2}^{y_q+W_q/2}\cos\frac{n\pi}{b}y_p\cos\frac{n\pi}{b}y_q\,dy_q\,dy_p$$

$$=\frac{b}{n\pi}\left[\sin\frac{n\pi}{b}\left(y_p+\frac{W_p}{2}\right)-\sin\frac{n\pi}{b}\left(y_p-\frac{W_p}{2}\right)\right]\cdot\frac{b}{n\pi}\left[\sin\frac{n\pi}{b}\left(y_q+\frac{W_q}{2}\right)-\sin\frac{n\pi}{b}\left(y_q-\frac{W_q}{2}\right)\right]$$

$$=\frac{b^2}{n^2\pi^2}(\sin n\theta_1-\sin n\theta_2)(\sin n\theta_3-\sin n\theta_4) \qquad (4A.2.7)$$

and, $\theta_1=\frac{\pi}{b}\left(y_p+\frac{W_p}{2}\right)$; $\theta_2=\frac{\pi}{b}\left(y_p-\frac{W_p}{2}\right)$; $\theta_3=\frac{\pi}{b}\left(y_q+\frac{W_q}{2}\right)$; $\theta_4=\frac{\pi}{b}\left(y_q-\frac{W_q}{2}\right)$.

Integration of fourth term

$$\frac{4}{\pi^2}\sum_{m=1}^{\infty}\sum_{n=1}^{\infty}\frac{\cos\frac{m\pi}{a}x_p\cos\frac{m\pi}{a}x_q}{\frac{m^2}{a^2}+\frac{n^2}{b^2}-\frac{k^2}{\pi^2}}\int_{y_p-W_p/2}^{y_p+W_p/2}\int_{y_q-W_q/2}^{y_q+W_q/2}\cos\frac{n\pi}{b}y_p\cos\frac{n\pi}{b}y_q\,dy_q\,dy_p$$

$$=\frac{4b^2}{\pi^4}\sum_{m=1}^{\infty}\sum_{n=1}^{\infty}\frac{\cos\frac{m\pi}{a}x_p\cos\frac{m\pi}{a}x_q(\sin n\theta_1-\sin n\theta_2)(\sin n\theta_3-\sin n\theta_4)}{n^2\left(\frac{m^2}{a^2}+\frac{n^2}{b^2}-\frac{k^2}{\pi^2}\right)}. \qquad (4A.2.8)$$

Substituting equations (4A.2.3), (4A.2.4), (4A.2.6), (4A.2.8) into equation (4A.2.2), for Z_{pq}, gives the initial non economised coupling impedance formula

$$Z_{pq}=\frac{j\omega\mu h}{abW_pW_q}\left\{-\frac{W_pW_q}{k^2}+\frac{2a^2W_pW_q}{\pi^2}\sum_{m=1}^{\infty}\frac{\cos\frac{m\pi}{a}x_p\cos\frac{m\pi}{a}x_q}{m^2-A^2}\right.$$

$$+\frac{2b^4}{\pi^4}\sum_{n=1}^{\infty}\frac{(\sin n\theta_1-\sin n\theta_2)(\sin n\theta_3-\sin n\theta_4)}{n^2(n^2-B^2)}$$

$$\left.+\frac{4b^2}{\pi^4}\sum_{m=1}^{\infty}\sum_{n=1}^{\infty}\frac{\cos\frac{m\pi}{a}x_p\cos\frac{m\pi}{a}x_q(\sin n\theta_1-\sin n\theta_2)(\sin n\theta_3-\sin n\theta_4)}{n^2\left(\frac{m^2}{a^2}+\frac{n^2}{b^2}-\frac{k^2}{\pi^2}\right)}\right\}. \qquad (4A.2.9)$$

When $q=p$, for a single probe,

$$Z_{pp}=\frac{j\omega\mu h}{abW_p^2}\left\{-\frac{W_p^2}{k^2}+\frac{2a^2W_p^2}{\pi^2}\sum_{m=1}^{\infty}\frac{\cos^2\dfrac{m\pi}{a}x_p}{m^2-A^2}+\frac{2b^4}{\pi^4}\sum_{n=1}^{\infty}\frac{(\sin n\theta_1-\sin n\theta_2)^2}{n^2(n^2-B^2)}\right.$$

$$\left.+\frac{4a^2b^2}{\pi^4}\sum_{m=1}^{\infty}\sum_{n=1}^{\infty}\frac{\cos^2\dfrac{m\pi}{a}x_p(\sin n\theta_1-\sin n\theta_2)^2}{n^2(m^2+D^2)}\right\}, \qquad \text{(4A.2.10)}$$

or,

$$Z_{pp}=\frac{j\omega\mu h}{abW_p^2}\left\{-\frac{W_p^2}{k^2}+\frac{2a^2W_p^2}{\pi^2}S_1(m)+\frac{2b^4}{\pi^4}S_2(n)+\frac{4a^2b^2}{\pi^4}S_3(m,n)\right\} \qquad \text{(4A.2.11)}$$

where, $D^2=\dfrac{a^2n^2}{b^2}-\dfrac{a^2k^2}{\pi^2}=\dfrac{a^2}{b^2}\left(n^2-\dfrac{b^2k^2}{\pi^2}\right)=\dfrac{a^2}{b^2}(n^2-B^2)$.

The infinite series, $S_1(m), S_2(n), S_3(m,n)$, together with their closed forms are given below:

$$S_1(m)=\sum_{m=1}^{\infty}\frac{\cos^2\dfrac{m\pi}{a}x_p}{m^2-A^2}=\frac{1}{2}\sum_{m=1}^{\infty}\frac{1+\cos m\dfrac{2\pi}{a}x_p}{m^2-A^2}$$

$$=\frac{1}{2}\left[\frac{1}{2A^2}-\frac{\pi\cos A\pi}{2A\sin A\pi}+\frac{1}{2A^2}-\frac{\pi\cos A(\pi-2\pi x_p/a)}{2A\sin A\pi}\right]$$

$$=\frac{1}{2}\left[\frac{1}{A^2}-\frac{\pi\left[\cos A\pi+\cos A\pi(1-2x_p/a)\right]}{2A\sin A\pi}\right]$$

$$=\frac{\pi^2}{2a^2k^2}-\frac{\pi^2[\cos ak+\cos k(a-2x_p)]}{4ak\sin ak}, \qquad \text{(4A.2.12)}$$

$$S_2(n)=\sum_{n=1}^{\infty}\frac{(\sin n\theta_1-\sin n\theta_2)^2}{n^2(n^2-B^2)}, \qquad \text{(4A.2.13)}$$

$$S_3(m,n)=\sum_{m=1}^{\infty}\sum_{n=1}^{\infty}\frac{\cos^2\dfrac{m\pi}{a}x_p(\sin n\theta_1-\sin n\theta_2)^2}{n^2(m^2+D^2)}$$

$$= \sum_{n=1}^{\infty} \frac{(\sin n\theta_1 - \sin n\theta_2)^2}{n^2} \cdot \frac{1}{2} \sum_{m=1}^{\infty} \frac{1 + \cos m \dfrac{2\pi x_p}{a}}{m^2 + D^2}$$

$$= \sum_{n=1}^{\infty} \frac{(\sin n\theta_1 - \sin n\theta_2)^2}{n^2} \cdot \frac{1}{2} \left[\frac{\pi \cosh D\pi}{2D \sinh D\pi} - \frac{1}{2D^2} + \frac{\pi \cosh D(\pi - 2\pi x_p / a)}{2D \sinh D\pi} - \frac{1}{2D^2} \right]$$

$$= \sum_{n=1}^{\infty} \frac{(\sin n\theta_1 - \sin n\theta_2)^2}{n^2} \left[\frac{\pi \left[\cosh D\pi + \cosh D\pi (1 - 2x_p / a) \right]}{4D \sinh D\pi} - \frac{1}{2D^2} \right]$$

$$= \frac{b\pi}{4a} \sum_{n=1}^{\infty} \frac{(\sin n\theta_1 - \sin n\theta_2)^2 \left[\cosh \dfrac{a\pi}{b} \sqrt{n^2 - B^2} + \cosh \dfrac{(a - 2x_p)\pi}{b} \sqrt{n^2 - B^2} \right]}{n^2 \sqrt{n^2 - B^2} \sinh \dfrac{a\pi}{b} \sqrt{n^2 - B^2}} - \frac{b^2}{2a^2} S_2(n).$$

(4A.2.14)

The series for $S_1(m)$ is summed to closed form. Substituting $S_1(m)$, and $S_3(m,n)$ from equations (4A.2.12), and (4A.2.14) respectively into equation (4A.2.11) eliminates the terms $-W_p^2 / k^2$, and the infinite series $S_2(n)$. Also the double infinite series $S_3(m,n)$ has been reduced to single series form.

The economised formula for Z_{pp} is then given by

$$Z_{pp} = Z_{in} = j\omega\mu h \left\{ - \frac{\cos ak + \cos k(a - 2x_p)}{2bk \sin ak} \right.$$

$$\left. + \frac{b^2}{W_p^2 \pi^3} \sum_{n=1}^{\infty} \frac{(\sin n\theta_1 - \sin n\theta_2)^2 \left[\cosh \dfrac{a\pi}{b} \sqrt{n^2 - B^2} + \cosh \dfrac{(a - 2x_p)\pi}{b} \sqrt{n^2 - B^2} \right]}{n^2 \sqrt{n^2 - B^2} \sinh \dfrac{a\pi}{b} \sqrt{n^2 - B^2}} \right\}. \quad \text{(4A.2.15)}$$

The single probe port Z_{pp} is obtained in terms of a closed form and a single infinite series.

4A.3 Coupling impedance between probe feed and a perimeter port on a rectangle

The probe to microstrip port coupling impedance formula (Z_{pq}) in terms of the Green's function is given by

$$Z_{pq} = \frac{1}{W_p W_q} \int_{W_p} \int_{W_q} G(x_p, y_p \mid 0, y_q)\, dy_q\, dy_p \,. \tag{4A.3.1}$$

From equation (4A.2.9), with $x_q = 0$,

$$\begin{aligned} Z_{pq} = \frac{j\omega\mu h}{abW_pW_q}\Bigg\{ & -\frac{W_pW_q}{k^2} + \frac{2a^2W_pW_q}{\pi^2}\sum_{m=1}^{\infty}\frac{\cos\dfrac{m\pi}{a}x_p}{m^2 - A^2} \\ & + \frac{2b^4}{\pi^4}\sum_{n=1}^{\infty}\frac{(\sin n\theta_1 - \sin n\theta_2)(\sin n\theta_3 - \sin n\theta_4)}{n^2(n^2 - B^2)} \\ & + \frac{4a^2b^2}{\pi^4}\sum_{m=1}^{\infty}\sum_{n=1}^{\infty}\frac{\cos\dfrac{m\pi}{a}x_p(\sin n\theta_1 - \sin n\theta_2)(\sin n\theta_3 - \sin n\theta_4)}{n^2(m^2 + D^2)}\Bigg\} \end{aligned} \tag{4A.3.2}$$

where, $\theta_1 = \frac{\pi}{b}\left(y_p + \frac{W_p}{2}\right)$; $\theta_2 = \frac{\pi}{b}\left(y_p - \frac{W_p}{2}\right)$; $\theta_3 = \frac{\pi}{b}\left(y_q + \frac{W_q}{2}\right)$; $\theta_4 = \frac{\pi}{b}\left(y_q - \frac{W_q}{2}\right)$,

$D^2 = \frac{a^2n^2}{b^2} - \frac{a^2k^2}{\pi^2} = \frac{a^2}{b^2}\left(n^2 - \frac{b^2k^2}{\pi^2}\right) = \frac{a^2}{b^2}(n^2 - B^2)$, or,

$$Z_{pq} = \frac{j\omega\mu h}{abW_pW_q}\left\{-\frac{W_pW_q}{k^2} + \frac{2a^2W_pW_q}{\pi^2}S_1(m) + \frac{2b^4}{\pi^4}S_2(n) + \frac{4a^2b^2}{\pi^4}S_3(m,n)\right\} \tag{4A.3.3}$$

where, the series, $S_1(m)$, $S_2(n)$, $S_3(m,n)$, together with their closed forms are given below:

$$\begin{aligned} S_1(m) &= \sum_{m=1}^{\infty}\frac{\cos\dfrac{m\pi}{a}x_p}{m^2 - A^2} \\ &= \frac{1}{2A^2} - \frac{\pi\cos A\pi(1 - x_p/a)}{2A\sin A\pi} \\ &= \frac{\pi^2}{2a^2k^2} - \frac{\pi^2\cos k(a - x_p)}{2ak\sin ak}, \end{aligned} \tag{4A.3.4}$$

$$S_2(n)=\sum_{n=1}^{\infty}\frac{(\sin n\theta_1-\sin n\theta_2)(\sin n\theta_3-\sin n\theta_4)}{n^2(n^2-B^2)}, \tag{4A.3.5}$$

$$S_3(m,n)=\sum_{m=1}^{\infty}\sum_{n=1}^{\infty}\frac{\cos\frac{m\pi}{a}x_p(\sin n\theta_1-\sin n\theta_2)(\sin n\theta_3-\sin n\theta_4)}{n^2(m^2+D^2)}$$

$$=\sum_{n=1}^{\infty}\frac{(\sin n\theta_1-\sin n\theta_2)(\sin n\theta_3-\sin n\theta_4)}{n^2}\sum_{m=1}^{\infty}\frac{\cos m\frac{\pi x_p}{a}}{m^2+D^2}$$

$$=\sum_{n=1}^{\infty}\frac{(\sin n\theta_1-\sin n\theta_2)(\sin n\theta_3-\sin n\theta_4)}{n^2}\left[\frac{\pi\cosh D\pi(1-x_p/a)}{2D\sinh D\pi}-\frac{1}{2D^2}\right]$$

$$=\frac{b\pi}{2a}\sum_{n=1}^{\infty}\frac{(\sin n\theta_1-\sin n\theta_2)(\sin n\theta_3-\sin n\theta_4)\cosh\frac{(a-x_p)\pi}{b}\sqrt{n^2-B^2}}{n^2\sqrt{n^2-B^2}\sinh\frac{a\pi}{b}\sqrt{n^2-B^2}}-\frac{b^2}{2a^2}S_2(n).$$

(4A.3.6)

The series for $S_1(m)$ is summed to closed form. Substituting $S_1(m)$, and $S_3(m,n)$ from equations (4A.3.4), and (4A.3.6) respectively into equation (4A.3.3) eliminates the terms $-W_pW_q/k^2$, and the infinite series $S_2(n)$. Also the double infinite series $S_3(m,n)$ has been reduced to a single series.

The economised formula for Z_{pq} is then given by

$$Z_{pq}=j\omega\mu h\left\{-\frac{\cos k(a-x_p)}{bk\sin ak}\right.$$

$$\left.+\frac{2b^2}{W_pW_q\pi^3}\sum_{n=1}^{\infty}\frac{(\sin n\theta_1-\sin n\theta_2)(\sin n\theta_3-\sin n\theta_4)\cosh\frac{(a-x_p)\pi}{b}\sqrt{n^2-B^2}}{n^2\sqrt{n^2-B^2}\sinh\frac{a\pi}{b}\sqrt{n^2-B^2}}\right\}. \tag{4A.3.7}$$

The coupling impedance Z_{pq} is obtained in terms of a closed form and a single infinite series.

4A.4 Probe feed input impedance on the triangle

The two probe ports coupling impedance formula (Z_{pq}) in terms of the Green's function is given by

$$Z_{pq} = \frac{1}{W_p W_q} \int_{W_p} \int_{W_q} G(x_p, y_p \mid x_q, y_q)\, dy_q\, dy_p \tag{4A.4.1}$$

$$= \frac{j2\omega\mu h}{W_p W_q \pi^2} \int_{y_p - W_p/2}^{y_p + W_p/2} \int_{y_q - W_q/2}^{y_q + W_q/2} \left\{ -\frac{\pi^2}{a^2 k^2} \right.$$

$$+ \sum_{m=1}^{\infty} \frac{\left(\cos\frac{m\pi}{a} x_p + (-1)^m \cos\frac{m\pi}{a} y_p \right)\left(\cos\frac{m\pi}{a} x_q + (-1)^m \cos\frac{m\pi}{a} y_q \right)}{m^2 - A^2}$$

$$+ \sum_{m=1}^{\infty} \sum_{n=1}^{\infty} \frac{\left[\cos\frac{m\pi}{a} x_p \cos\frac{n\pi}{a} y_p + (-1)^{m+n} \cos\frac{n\pi}{a} x_p \cos\frac{m\pi}{a} y_p \right]}{m^2 + n^2 - A^2}$$

$$\left. \cdot \left[\cos\frac{m\pi}{a} x_q \cos\frac{n\pi}{a} y_q + (-1)^{m+n} \cos\frac{n\pi}{a} x_q \cos\frac{m\pi}{a} y_q \right] \right\} dy_q\, dy_p . \tag{4A.4.2}$$

Integration of first term

$$-\frac{\pi^2}{a^2 k^2} \int_{y_p - W_p/2}^{y_p + W_p/2} \int_{y_q - W_q/2}^{y_q + W_q/2} 1\, dy_q\, dy_p = -\frac{W_p W_q \pi^2}{a^2 k^2} . \tag{4A.4.3}$$

Integration of second term

$$\int_{y_p - W_p/2}^{y_p + W_p/2} \int_{y_q - W_q/2}^{y_q + W_q/2} \sum_{m=1}^{\infty} \frac{\left[\cos\frac{m\pi}{a} x_p + (-1)^m \cos\frac{m\pi}{a} y_p \right]\left[\cos\frac{m\pi}{a} x_q + (-1)^m \cos\frac{m\pi}{a} y_q \right]}{m^2 - A^2} dy_q\, dy_p \tag{4A.4.4}$$

$$= \sum_{m=1}^{\infty} \left[W_p W_q \cos\frac{m\pi}{a} x_p \cos\frac{m\pi}{a} x_q + (-1)^m \frac{a W_p}{m\pi} (\sin m\theta_3 - \sin m\theta_4) \cos\frac{m\pi}{a} x_p \right.$$

$$\left. + (-1)^m \frac{a W_q}{m\pi} (\sin m\theta_1 - \sin m\theta_2) \cos\frac{m\pi}{a} x_q + \frac{a^2}{m^2 \pi^2} (\sin m\theta_1 - \sin m\theta_2)(\sin m\theta_3 - \sin m\theta_4) \right]$$

$$\cdot 1/(m^2 - A^2) \tag{4A.4.5}$$

where,

$$\int_{y_p-W_p/2}^{y_p+W_p/2}\int_{y_q-W_q/2}^{y_q+W_q/2}\left[\cos\frac{m\pi}{a}x_p+(-1)^m\cos\frac{m\pi}{a}y_p\right]\left[\cos\frac{m\pi}{a}x_q+(-1)^m\cos\frac{m\pi}{a}y_q\right]dy_q\,dy_p$$

$$=\int_{y_p-W_p/2}^{y_p+W_p/2}\int_{y_q-W_q/2}^{y_q+W_q/2}\left[\cos\frac{m\pi}{a}x_p\cos\frac{m\pi}{a}x_q+(-1)^m\cos\frac{m\pi}{a}x_p\cos\frac{m\pi}{a}y_q\right.$$

$$\left.+(-1)^m\cos\frac{m\pi}{a}x_q\cos\frac{m\pi}{a}y_p+\cos\frac{m\pi}{a}y_p\cos\frac{m\pi}{a}y_q\right]dy_q\,dy_p$$

$$=W_pW_q\cos\frac{m\pi}{a}x_p\cos\frac{m\pi}{a}x_q+(-1)^m\frac{aW_p}{m\pi}(\sin m\theta_3-\sin m\theta_4)\cos\frac{m\pi}{a}x_p$$

$$+(-1)^m\frac{aW_q}{m\pi}(\sin m\theta_1-\sin m\theta_2)\cos\frac{m\pi}{a}x_q+\frac{a^2}{m^2\pi^2}(\sin m\theta_1-\sin m\theta_2)(\sin m\theta_3-\sin m\theta_4)$$

(4A.4.6)

and, $\theta_1=\frac{\pi}{a}\left(y_p+\frac{W_p}{2}\right)$; $\theta_2=\frac{\pi}{a}\left(y_p-\frac{W_p}{2}\right)$; $\theta_3=\frac{\pi}{a}\left(y_q+\frac{W_q}{2}\right)$; $\theta_4=\frac{\pi}{a}\left(y_q-\frac{W_q}{2}\right)$.

Integration of third term

$$\int_{y_p-W_p/2}^{y_p+W_p/2}\int_{y_q-W_q/2}^{y_q+W_q/2}\sum_{m=1}^{\infty}\sum_{n=1}^{\infty}\frac{\left[\cos\frac{m\pi}{a}x_p\cos\frac{n\pi}{a}y_p+(-1)^{m+n}\cos\frac{n\pi}{a}x_p\cos\frac{m\pi}{a}y_p\right]}{m^2+n^2-A^2}$$

$$\cdot\left[\cos\frac{m\pi}{a}x_q\cos\frac{n\pi}{a}y_q+(-1)^{m+n}\cos\frac{n\pi}{a}x_q\cos\frac{m\pi}{a}y_q\right]dy_q\,dy_p \tag{4A.4.7}$$

$$=\sum_{m=1}^{\infty}\sum_{n=1}^{\infty}\left[\frac{a^2}{n^2\pi^2}(\sin n\theta_1-\sin n\theta_2)(\sin n\theta_3-\sin n\theta_4)\cos\frac{m\pi}{a}x_p\cos\frac{m\pi}{a}x_q\right.$$

$$+(-1)^{m+n}\frac{a^2}{mn\pi^2}(\sin n\theta_1-\sin n\theta_2)(\sin m\theta_3-\sin m\theta_4)\cos\frac{m\pi}{a}x_p\cos\frac{n\pi}{a}x_q$$

$$\left.+(-1)^{m+n}\frac{a^2}{mn\pi^2}(\sin m\theta_1-\sin m\theta_2)(\sin n\theta_3-\sin n\theta_4)\cos\frac{n\pi}{a}x_p\cos\frac{m\pi}{a}x_q\right.$$

$$+\frac{a^2}{m^2\pi^2}(\sin m\theta_1-\sin m\theta_2)(\sin m\theta_3-\sin m\theta_4)\cos\frac{n\pi}{a}x_p\cos\frac{n\pi}{a}x_q\Bigg]/(m^2+n^2-A^2) \quad (4A.4.8)$$

$$=\sum_{m=1}^{\infty}\sum_{n=1}^{\infty}\Bigg[\frac{2a^2}{m^2\pi^2}(\sin m\theta_1-\sin m\theta_2)(\sin m\theta_3-\sin m\theta_4)\cos\frac{n\pi}{a}x_p\cos\frac{n\pi}{a}x_q$$

$$+(-1)^{m+n}\frac{2a^2}{mn\pi^2}(\sin n\theta_1-\sin n\theta_2)(\sin m\theta_3-\sin m\theta_4)\cos\frac{m\pi}{a}x_p\cos\frac{n\pi}{a}x_q\Bigg]/(m^2+n^2-A^2)$$

$$=\frac{2a^2}{\pi^2}\sum_{m=1}^{\infty}\sum_{n=1}^{\infty}\Bigg[\frac{(\sin m\theta_1-\sin m\theta_2)(\sin m\theta_3-\sin m\theta_4)}{m^2}\cos\frac{n\pi}{a}x_p\cos\frac{n\pi}{a}x_q$$

$$+\frac{(-1)^{m+n}(\sin n\theta_1-\sin n\theta_2)(\sin m\theta_3-\sin m\theta_4)}{mn}\cos\frac{m\pi}{a}x_p\cos\frac{n\pi}{a}x_q\Bigg]/(m^2+n^2-A^2).$$

(4A.4.9)

Due to symmetry that duplicated occurs in equation (4A.4.8), therefore, only the two terms are required in equation (4A.4.9).

Solving the integration of equation (4A.4.7) as below,

$$\int_{y_p-W_p/2}^{y_p+W_p/2}\int_{y_q-W_q/2}^{y_q+W_q/2}\Bigg[\cos\frac{m\pi}{a}x_p\cos\frac{n\pi}{a}y_p+(-1)^{m+n}\cos\frac{n\pi}{a}x_p\cos\frac{m\pi}{a}y_p\Bigg]$$

$$\cdot\Bigg[\cos\frac{m\pi}{a}x_q\cos\frac{n\pi}{a}y_q+(-1)^{m+n}\cos\frac{n\pi}{a}x_q\cos\frac{m\pi}{a}y_q\Bigg]dy_q\,dy_p$$

$$=\int_{y_p-W_p/2}^{y_p+W_p/2}\int_{y_q-W_q/2}^{y_q+W_q/2}\Bigg[\cos\frac{m\pi}{a}x_p\cos\frac{m\pi}{a}x_q\cos\frac{n\pi}{a}y_p\cos\frac{n\pi}{a}y_q$$

$$+(-1)^{m+n}\cos\frac{m\pi}{a}x_p\cos\frac{n\pi}{a}x_q\cos\frac{n\pi}{a}y_p\cos\frac{m\pi}{a}y_q$$

$$+(-1)^{m+n}\cos\frac{n\pi}{a}x_p\cos\frac{m\pi}{a}x_q\cos\frac{m\pi}{a}y_p\cos\frac{n\pi}{a}y_q$$

$$+\cos\frac{n\pi}{a}x_p\cos\frac{n\pi}{a}x_q\cos\frac{m\pi}{a}y_p\cos\frac{m\pi}{a}y_q\Bigg]dy_q\,dy_p$$

$$=\frac{a^2}{n^2\pi^2}(\sin n\theta_1-\sin n\theta_2)(\sin n\theta_3-\sin n\theta_4)\cos\frac{m\pi}{a}x_p\cos\frac{m\pi}{a}x_q$$

$$+(-1)^{m+n}\frac{a^2}{mn\pi^2}(\sin n\theta_1-\sin n\theta_2)(\sin m\theta_3-\sin m\theta_4)\cos\frac{m\pi}{a}x_p\cos\frac{n\pi}{a}x_q$$

$$+(-1)^{m+n}\frac{a^2}{mn\pi^2}(\sin m\theta_1-\sin m\theta_2)(\sin n\theta_3-\sin n\theta_4)\cos\frac{n\pi}{a}x_p\cos\frac{m\pi}{a}x_q$$

$$+\frac{a^2}{m^2\pi^2}(\sin m\theta_1-\sin m\theta_2)(\sin m\theta_3-\sin m\theta_4)\cos\frac{n\pi}{a}x_p\cos\frac{n\pi}{a}x_q. \qquad (4A.4.10)$$

Substitutes equations (4A.4.3), (4A.4.5), (4A.4.9) into (4A.4.2) for Z_{pq}, and the initial non economised coupling impedance formula is given by

$$Z_{pq}=\frac{j2\omega\mu h}{W_pW_q\pi^2}\left\{-\frac{W_pW_q\pi^2}{a^2k^2}+\sum_{m=1}^{\infty}\left[W_pW_q\cos\frac{m\pi}{a}x_p\cos\frac{m\pi}{a}x_q\right.\right.$$

$$+(-1)^m\frac{aW_p}{m\pi}(\sin m\theta_3-\sin m\theta_4)\cos\frac{m\pi}{a}x_p+(-1)^m\frac{aW_q}{m\pi}(\sin m\theta_1-\sin m\theta_2)\cos\frac{m\pi}{a}x_q$$

$$\left.+\frac{a^2}{m^2\pi^2}(\sin m\theta_1-\sin m\theta_2)(\sin m\theta_3-\sin m\theta_4)\right]/(m^2-A^2)$$

$$+\frac{2a^2}{\pi^2}\sum_{m=1}^{\infty}\sum_{n=1}^{\infty}\left[\frac{(\sin m\theta_1-\sin m\theta_2)(\sin m\theta_3-\sin m\theta_4)}{m^2}\cos\frac{n\pi}{a}x_p\cos\frac{n\pi}{a}x_q\right.$$

$$\left.\left.+\frac{(-1)^{m+n}(\sin n\theta_1-\sin n\theta_2)(\sin m\theta_3-\sin m\theta_4)}{mn}\cos\frac{m\pi}{a}x_p\cos\frac{n\pi}{a}x_q\right]/(m^2+n^2-A^2)\right\}.$$

(4A.4.11)

When $q=p$ for a single probe,

$$Z_{pp}=\frac{j2\omega\mu h}{W_p^2\pi^2}\left\{-\frac{W_p^2\pi^2}{a^2k^2}+\sum_{m=1}^{\infty}\left[W_p^2\cos^2\frac{m\pi}{a}x_p\right.\right.$$

$$\left.+(-1)^m\frac{2aW_p}{m\pi}(\sin m\theta_1-\sin m\theta_2)\cos\frac{m\pi}{a}x_p+\frac{a^2}{m^2\pi^2}(\sin m\theta_1-\sin m\theta_2)^2\right]/(m^2-A^2)$$

$$+\frac{2a^2}{\pi^2}\sum_{m=1}^{\infty}\sum_{n=1}^{\infty}\left[\frac{(\sin m\theta_1-\sin m\theta_2)^2}{m^2}\cos^2\frac{n\pi}{a}x_p\right.$$

$$\left.\left.+\frac{(-1)^{m+n}(\sin m\theta_1-\sin m\theta_2)(\sin n\theta_1-\sin n\theta_2)}{mn}\cos\frac{m\pi}{a}x_p\cos\frac{n\pi}{a}x_p\right]/(m^2+n^2-A^2)\right\}$$

$$= \frac{j2\omega\mu h}{W_p^2\pi^2}\left\{-\frac{W_p^2\pi^2}{a^2k^2} + W_p^2\sum_{m=1}^{\infty}\frac{\cos^2(m\pi x_p/a)}{m^2-A^2}\right.$$

$$+\frac{2aW_p}{\pi}\sum_{m=1}^{\infty}\frac{(-1)^m(\sin m\theta_1-\sin m\theta_2)\cos(m\pi x_p/a)}{m(m^2-A^2)} + \frac{a^2}{\pi^2}\sum_{m=1}^{\infty}\frac{(\sin m\theta_1-\sin m\theta_2)^2}{m^2(m^2-A^2)}$$

$$+\frac{2a^2}{\pi^2}\sum_{m=1}^{\infty}\sum_{n=1}^{\infty}\frac{(\sin m\theta_1-\sin m\theta_2)^2\cos^2(n\pi x_p/a)}{m^2(m^2+n^2-A^2)}$$

$$\left.+\frac{2a^2}{\pi^2}\sum_{m=1}^{\infty}\sum_{n=1}^{\infty}\frac{(-1)^{m+n}(\sin m\theta_1-\sin m\theta_2)(\sin n\theta_1-\sin n\theta_2)\cos(m\pi x_p/a)\cos(n\pi x_p/a)}{mn(m^2+n^2-A^2)}\right\},$$

(4A.4.12)

or,

$$Z_{pp} = \frac{j2\omega\mu h}{W_p^2\pi^2}\left\{-\frac{W_p^2\pi^2}{a^2k^2} + W_pS_1(m) + \frac{2aW_p}{\pi}S_2(m) + \frac{a^2}{\pi^2}S_3(m)\right.$$

$$\left.+\frac{2a^2}{\pi^2}S_4(m,n) + \frac{2a^2}{\pi^2}S_5(m,n)\right\}, \qquad (4A.4.13)$$

where, the series, $S_1(m), S_2(m), S_3(m), S_4(m,n), S_5(m,n)$ together with their closed forms are given below:

$$S_1(m) = \sum_{m=1}^{\infty}\frac{\cos^2(m\pi x_p/a)}{m^2-A^2} = \frac{1}{2}\sum_{m=1}^{\infty}\frac{1+\cos m(2\pi x_p/a)}{m^2-A^2}$$

$$= \frac{1}{2}\sum_{m=1}^{\infty}\frac{1}{m^2-A^2} + \frac{1}{2}\sum_{m=1}^{\infty}\frac{\cos m(2\pi x_p/a)}{m^2-A^2}$$

$$= \frac{1}{4A^2} - \frac{\pi\cos A\pi}{4A\sin A\pi} + \frac{1}{4A^2} - \frac{\pi\cos A(\pi-2\pi x_p/a)}{4A\sin A\pi}$$

$$= \frac{\pi^2}{2a^2k^2} - \frac{\pi^2\left[\cos ak + \cos k(a-2x_p)\right]}{4ak\sin ak}, \qquad (4A.4.14)$$

$$S_2(m) = \sum_{m=1}^{\infty}\frac{(-1)^m(\sin m\theta_1-\sin m\theta_2)\cos(m\pi x_p/a)}{m(m^2-A^2)}$$

$$= \frac{1}{2}\sum_{m=1}^{\infty} \frac{(-1)^m \left[\sin m\left(\theta_1 + \frac{\pi x_p}{a}\right) + \sin m\left(\theta_1 - \frac{\pi x_p}{a}\right) - \sin m\left(\theta_2 + \frac{\pi x_p}{a}\right) - \sin m\left(\theta_2 - \frac{\pi x_p}{a}\right)\right]}{m(m^2 - A^2)}$$

where $2\sin A\cos B = \sin(A+B) + \sin(A-B)$.

Let $\theta_5 = \theta_1 + \pi x_p / a$; $\theta_6 = \theta_1 - \pi x_p / a$; $\theta_7 = \theta_2 + \pi x_p / a$; $\theta_8 = \theta_2 - \pi x_p / a$,

$$S_2(m) = \frac{1}{2}\sum_{m=1}^{\infty} \frac{(-1)^m \left[\sin m\theta_5 + \sin m\theta_6 - \sin m\theta_7 - \sin m\theta_8\right]}{m(m^2 - A^2)}$$

$$= \frac{1}{4A^2}(\theta_5 + \theta_6 - \theta_7 - \theta_8) - \frac{\pi}{4A^2 \sin A\pi}(\sin A\theta_5 + \sin A\theta_6 - \sin A\theta_7 - \sin A\theta_8)$$

$$= \frac{W_p \pi}{2aA^2} - \frac{\pi}{4A^2 \sin A\pi}\left[\sin(A\theta_1 + kx_p) + \sin(A\theta_1 - kx_p) - \sin(A\theta_2 + kx_p) - \sin(A\theta_2 - kx_p)\right]$$

$$= \frac{W_p \pi^3}{2a^3k^2} - \frac{\pi^3}{4a^2k^2 \sin ak}\left[2\sin A\theta_1 \cos kx_p - 2\sin A\theta_2 \cos kx_p\right]$$

$$= \frac{W_p \pi^3}{2a^3k^2} - \frac{\pi^3(\sin A\theta_1 - \sin A\theta_2)\cos kx_p}{2a^2k^2 \sin ak}, \qquad \text{(4A.4.15)}$$

$$S_3(m) = \sum_{m=1}^{\infty} \frac{(\sin m\theta_1 - \sin m\theta_2)^2}{m^2(m^2 - A^2)}, \qquad \text{(4A.4.16)}$$

$$S_4(m,n) = \sum_{m=1}^{\infty}\sum_{n=1}^{\infty} \frac{(\sin m\theta_1 - \sin m\theta_2)^2 \cos^2(n\pi x_p / a)}{m^2(m^2 + n^2 - A^2)}$$

$$= \sum_{m=1}^{\infty} \frac{(\sin m\theta_1 - \sin m\theta_2)^2}{m^2} \frac{1}{2}\sum_{n=1}^{\infty} \frac{1 + \cos n(2\pi x_p / a)}{n^2 + E^2}$$

$$= \sum_{m=1}^{\infty} \frac{(\sin m\theta_1 - \sin m\theta_2)^2}{m^2} \frac{1}{2}\left[\frac{\pi \cosh E\pi}{2E \sinh E\pi} - \frac{1}{2E^2} + \frac{\pi \cosh E(\pi - 2\pi x_p / a)}{2E \sinh E\pi} - \frac{1}{2E^2}\right]$$

$$= \sum_{m=1}^{\infty} \frac{(\sin m\theta_1 - \sin m\theta_2)^2}{m^2}\left[\frac{\pi\left[\cosh E\pi + \cosh E\pi(1 - 2x_p / a)\right]}{4E \sinh E\pi} - \frac{1}{2(m^2 - A^2)}\right]$$

$$= \frac{\pi}{4}\sum_{m=1}^{\infty} \frac{(\sin m\theta_1 - \sin m\theta_2)^2\left[\cosh E\pi + \cosh E\pi(1 - 2x_p / a)\right]}{m^2 E \sinh E\pi} - \frac{1}{2}\sum_{m=1}^{\infty} \frac{(\sin m\theta_1 - \sin m\theta_2)^2}{m^2(m^2 - A^2)}$$

$$= \frac{\pi}{4}\sum_{m=1}^{\infty}\frac{(\sin m\theta_1 - \sin m\theta_2)^2\left[\cosh E\pi + \cosh E\pi(1-2x_p/a)\right]}{m^2 E\sinh E\pi} - \frac{1}{2}S_3(m)$$

$$= \frac{\pi}{4}\sum_{m=1}^{\infty}\frac{(\sin m\theta_1 - \sin m\theta_2)^2\left[\cosh \pi\sqrt{m^2-A^2} + \cosh \pi(1-2x_p/a)\sqrt{m^2-A^2}\right]}{m^2\sqrt{m^2-A^2}\sinh \pi\sqrt{m^2-A^2}} - \frac{1}{2}S_3(m)$$

(4A.4.17)

where $E^2 = m^2 - A^2$.

$$S_5(m,n) = \sum_{m=1}^{\infty}\sum_{n=1}^{\infty}\frac{(-1)^{m+n}(\sin m\theta_1 - \sin m\theta_2)(\sin n\theta_1 - \sin n\theta_2)\cos(m\pi x_p/a)\cos(n\pi x_p/a)}{mn(m^2+n^2-A^2)}$$

$$= \sum_{m=1}^{\infty}\frac{(-1)^m(\sin m\theta_1 - \sin m\theta_2)\cos(m\pi x_p/a)}{m}\sum_{n=1}^{\infty}\frac{(-1)^n(\sin n\theta_1 - \sin n\theta_2)\cos(n\pi x_p/a)}{n(m^2+n^2-A^2)}.$$

For n term,

$$\sum_{n=1}^{\infty}\frac{(-1)^n(\sin n\theta_1 - \sin n\theta_2)\cos(n\pi x_p/a)}{n(m^2+n^2-A^2)}$$

$$= \sum_{n=1}^{\infty}\frac{(-1)^n\left[\sin n\theta_1\cos(n\pi x_p/a) - \sin n\theta_2\cos(n\pi x_p/a)\right]}{n(n^2+E^2)}$$

$$= \frac{1}{2}\sum_{n=1}^{\infty}\frac{(-1)^n\left[\sin n(\theta_1+\pi x_p/a) + \sin n(\theta_1-\pi x_p/a) - \sin n(\theta_2+\pi x_p/a) - \sin n(\theta_2-\pi x_p/a)\right]}{n(n^2+E^2)}$$

$$= \frac{1}{2}\sum_{n=1}^{\infty}\frac{(-1)^n\left[\sin n\theta_5 + \sin n\theta_6 - \sin n\theta_7 - \sin n\theta_8\right]}{n(n^2+E^2)}$$

$$= -\frac{1}{4E^2}(\theta_5+\theta_6-\theta_7-\theta_8) + \frac{\pi(\sinh E\theta_5 + \sinh E\theta_6 - \sinh E\theta_7 - \sinh E\theta_8)}{4E^2\sinh E\pi}$$

$$= -\frac{W_p\pi}{2a(m^2-A^2)} + \frac{\pi(\sinh E\theta_5 + \sinh E\theta_6 - \sinh E\theta_7 - \sinh E\theta_8)}{4(m^2-A^2)\sinh E\pi}.$$

So,

$$S_5(m,n) = \sum_{m=1}^{\infty}\frac{(-1)^m(\sin m\theta_1 - \sin m\theta_2)\cos(m\pi x_p/a)}{m}$$

$$\cdot\left[-\frac{W_p\pi}{2a(m^2-A^2)} + \frac{\pi(\sinh E\theta_5 + \sinh E\theta_6 - \sinh E\theta_7 - \sinh E\theta_8)}{4(m^2-A^2)\sinh E\pi}\right]$$

$$= -\frac{W_p \pi}{2a} \sum_{m=1}^{\infty} \frac{(-1)^m (\sin m\theta_1 - \sin m\theta_2) \cos(m\pi x_p / a)}{m(m^2 - A^2)}$$

$$+ \frac{\pi}{4} \sum_{m=1}^{\infty} \frac{(-1)^m (\sin m\theta_1 - \sin m\theta_2)(\sinh E\theta_5 + \sinh E\theta_6 - \sinh E\theta_7 - \sinh E\theta_8) \cos(m\pi x_p / a)}{m(m^2 - A^2) \sinh E\pi}$$

$$= -\frac{W_p \pi}{2a} S_2(m)$$

$$+ \frac{\pi}{4} \sum_{m=1}^{\infty} \frac{(-1)^m (\sin m\theta_1 - \sin m\theta_2)(\sinh E\theta_5 + \sinh E\theta_6 - \sinh E\theta_7 - \sinh E\theta_8) \cos(m\pi x_p / a)}{m(m^2 - A^2) \sinh E\pi}$$

$$= -\frac{W_p \pi}{2a} S_2(m) + \frac{\pi}{2} \sum_{m=1}^{\infty} \frac{(-1)^m (\sin m\theta_1 - \sin m\theta_2)(\sinh \theta_1 \sqrt{m^2 - A^2} - \sinh \theta_2 \sqrt{m^2 - A^2})}{m(m^2 - A^2) \sinh \pi \sqrt{m^2 - A^2}}$$

$$\cdot \cos(m\pi x_p / a) \cosh(\pi x_p \sqrt{m^2 - A^2} / a) \qquad \text{(4A.4.18)}$$

where $\sinh E\theta_5 + \sinh E\theta_6 - \sinh E\theta_7 - \sinh E\theta_8 = 2(\sinh E\theta_1 - \sinh E\theta_2) \cosh(E\pi x_p / a)$.

The series for $S_1(m)$, and $S_2(m)$ are summed to closed form. Substituting $S_1(m)$, $S_2(m)$, $S_4(m,n)$ and $S_5(m,n)$ from equations (4A.4.14), (4A.4.15), (4A.4.17), and (4A.4.18) respectively into equation (4A.4.13) eliminates the terms $-W_p^2 \pi^2 / a^2 k^2$, and the infinite series $S_3(m)$. Also the double infinite series $S_4(m,n)$, and $S_5(m,n)$ have been reduced to single series form.

The economised formula for Z_{pp} is then given by

$$Z_{pp} = j\omega\mu h \left\{ -\frac{\cos ak + \cos k(a - 2x_p)}{2ak \sin ak} - \frac{(\sin A\theta_1 - \sin A\theta_2) \cos kx_p}{ak^2 W_p \sin ak} \right.$$

$$+ \frac{a^2}{W_p^2 \pi^3} \sum_{m=1}^{\infty} \frac{(\sin m\theta_1 - \sin m\theta_2)^2 \left[\cosh \pi \sqrt{m^2 - A^2} + \cosh \pi (1 - 2x_p / a) \sqrt{m^2 - A^2} \right]}{m^2 \sqrt{m^2 - A^2} \sinh \pi \sqrt{m^2 - A^2}}$$

$$+ \frac{2a^2}{W_p^2 \pi^3} \sum_{m=1}^{\infty} \frac{(-1)^m (\sin m\theta_1 - \sin m\theta_2)(\sinh \theta_1 \sqrt{m^2 - A^2} - \sinh \theta_2 \sqrt{m^2 - A^2})}{m(m^2 - A^2) \sinh \pi \sqrt{m^2 - A^2}}$$

$$\left. \cdot \cos(m\pi x_p / a) \cosh(\pi x_p \sqrt{m^2 - A^2} / a) \right\} \qquad \text{(4A.4.19)}$$

The single probe port Z_{pp} is obtained in terms of closed forms and single infinite series.

4A.5 Coupling impedance between probe feed and a port on a perpendicular side on a triangle

The probe to microstrip port of on a perpendicular side coupling impedance formula (Z_{pq}) in terms of the Green's function is given by

$$Z_{pq} = \frac{1}{W_p W_q} \int_{W_p} \int_{W_q} G(x_p, y_p \mid 0, y_q)\, dy_q\, dy_p \,. \tag{4A.5.1}$$

From equation (4A.4.11), with $x_q = 0$,

$$Z_{pq} = \frac{j2\omega\mu h}{W_p W_q \pi^2} \left\{ -\frac{W_p W_q \pi^2}{a^2 k^2} + \sum_{m=1}^{\infty} \left[W_p W_q \cos\frac{m\pi}{a} x_p \right.\right.$$

$$+(-1)^m \frac{aW_p}{m\pi}(\sin m\theta_3 - \sin m\theta_4)\cos\frac{m\pi}{a}x_p + (-1)^m \frac{aW_q}{m\pi}(\sin m\theta_1 - \sin m\theta_2)$$

$$\left. + \frac{a^2}{m^2\pi^2}(\sin m\theta_1 - \sin m\theta_2)(\sin m\theta_3 - \sin m\theta_4) \right] / (m^2 - A^2)$$

$$+ \frac{2a^2}{\pi^2} \sum_{m=1}^{\infty} \sum_{n=1}^{\infty} \left[\frac{(\sin m\theta_1 - \sin m\theta_2)(\sin m\theta_3 - \sin m\theta_4)}{m^2} \cos\frac{n\pi}{a} x_p \right.$$

$$\left. \left. + \frac{(-1)^{m+n}(\sin n\theta_1 - \sin n\theta_2)(\sin m\theta_3 - \sin m\theta_4)}{mn} \cos\frac{m\pi}{a} x_p \right] / (m^2 + n^2 - A^2) \right\}$$

$$= \frac{j2\omega\mu h}{W_p W_q \pi^2} \left\{ -\frac{W_p W_q \pi^2}{a^2 k^2} + W_p W_q \sum_{m=1}^{\infty} \frac{\cos(m\pi x_p / a)}{m^2 - A^2} \right.$$

$$\left. + \frac{aW_q}{\pi} \sum_{m=1}^{\infty} \frac{(-1)^m (\sin m\theta_1 - \sin m\theta_2)}{m(m^2 - A^2)} + \frac{aW_p}{\pi} \sum_{m=1}^{\infty} \frac{(-1)^m (\sin m\theta_3 - \sin m\theta_4)\cos(m\pi x_p / a)}{m(m^2 - A^2)} \right.$$

$$+\frac{a^2}{\pi^2}\sum_{m=1}^{\infty}\frac{(\sin m\theta_1-\sin m\theta_2)(\sin m\theta_3-\sin m\theta_4)}{m^2(m^2-A^2)}$$

$$+\frac{2a^2}{\pi^2}\sum_{m=1}^{\infty}\sum_{n=1}^{\infty}\frac{(\sin m\theta_1-\sin m\theta_2)(\sin m\theta_3-\sin m\theta_4)\cos(n\pi x_p/a)}{m^2(m^2+n^2-A^2)}$$

$$+\frac{2a^2}{\pi^2}\sum_{m=1}^{\infty}\sum_{n=1}^{\infty}\frac{(-1)^{m+n}(\sin n\theta_1-\sin n\theta_2)(\sin m\theta_3-\sin m\theta_4)\cos(m\pi x_p/a)}{mn(m^2+n^2-A^2)}\Bigg\}, \qquad (4A.5.2)$$

where, $\theta_1=\frac{\pi}{a}\left(y_p+\frac{W_p}{2}\right)$; $\theta_2=\frac{\pi}{a}\left(y_p-\frac{W_p}{2}\right)$; $\theta_3=\frac{\pi}{a}\left(y_q+\frac{W_q}{2}\right)$; $\theta_4=\frac{\pi}{a}\left(y_q-\frac{W_q}{2}\right)$, or,

$$Z_{pq}=\frac{j2\omega\mu h}{W_pW_q\pi^2}\Bigg\{-\frac{W_pW_q\pi^2}{a^2k^2}+W_pW_qS_1(m)+\frac{aW_q}{\pi}S_2(m)+\frac{aW_p}{\pi}S_3(m)+\frac{a^2}{\pi^2}S_4(m)$$

$$+\frac{2a^2}{\pi^2}S_5(m,n)+\frac{2a^2}{\pi^2}S_6(m,n)\Bigg\}, \qquad (4A.5.3)$$

where, the series, $S_1(m), S_2(m), S_3(m), S_4(m), S_5(m,n), S_6(m,n)$ together with their closed forms are given below:

$$S_1(m)=\sum_{m=1}^{\infty}\frac{\cos(m\pi x_p/a)}{m^2-A^2}=\frac{1}{2A^2}-\frac{\pi\cos A(\pi-\pi x_p/a)}{2A\sin A\pi}$$

$$=\frac{\pi^2}{2a^2k^2}-\frac{\pi^2\cos k(a-x_p)}{2ak\sin ak}, \qquad (4A.5.4)$$

$$S_2(m)=\sum_{m=1}^{\infty}\frac{(-1)^m(\sin m\theta_1-\sin m\theta_2)}{m(m^2-A^2)}=\frac{\theta_1-\theta_2}{2A^2}-\frac{\pi(\sin A\theta_1-\sin A\theta_2)}{2A^2\sin A\pi}$$

$$=\frac{\pi W_p}{2aA^2}-\frac{\pi(\sin A\theta_1-\sin A\theta_2)}{2A^2\sin A\pi}$$

$$=\frac{W_p\pi^3}{2a^3k^2}-\frac{\pi^3(\sin A\theta_1-\sin A\theta_2)}{2a^2k^2\sin ak}, \qquad (4A.5.5)$$

$$S_3(m)=\sum_{m=1}^{\infty}\frac{(-1)^m(\sin m\theta_3-\sin m\theta_4)\cos(m\pi x_p/a)}{m(m^2-A^2)}, \qquad (4A.5.6)$$

$$S_4(m)=\sum_{m=1}^{\infty}\frac{(\sin m\theta_1-\sin m\theta_2)(\sin m\theta_3-\sin m\theta_4)}{m^2(m^2-A^2)}, \qquad (4A.5.7)$$

$$S_5(m,n)=\sum_{m=1}^{\infty}\sum_{n=1}^{\infty}\frac{(\sin m\theta_1-\sin m\theta_2)(\sin m\theta_3-\sin m\theta_4)\cos(n\pi x_p/a)}{m^2(m^2+n^2-A^2)}$$

$$=\sum_{m=1}^{\infty}\frac{(\sin m\theta_1-\sin m\theta_2)(\sin m\theta_3-\sin m\theta_4)}{m^2}\sum_{n=1}^{\infty}\frac{\cos(n\pi x_p/a)}{n^2+E^2}$$

$$=\sum_{m=1}^{\infty}\frac{(\sin m\theta_1-\sin m\theta_2)(\sin m\theta_3-\sin m\theta_4)}{m^2}\left[\frac{\pi\cosh E(\pi-\pi x_p/a)}{2E\sinh E\pi}-\frac{1}{2E^2}\right]$$

$$=\frac{\pi}{2}\sum_{m=1}^{\infty}\frac{(\sin m\theta_1-\sin m\theta_2)(\sin m\theta_3-\sin m\theta_4)\cosh E\pi(1-x_p/a)}{m^2E\sinh E\pi}$$

$$-\frac{1}{2}\sum_{m=1}^{\infty}\frac{(\sin m\theta_1-\sin m\theta_2)(\sin m\theta_3-\sin m\theta_4)}{m^2(m^2-A^2)}$$

$$=\frac{\pi}{2}\sum_{m=1}^{\infty}\frac{(\sin m\theta_1-\sin m\theta_2)(\sin m\theta_3-\sin m\theta_4)\cosh E\pi(1-x_p/a)}{m^2E\sinh E\pi}-\frac{1}{2}S_4(m) \qquad (4A.5.8)$$

where $E^2=m^2-A^2$.

$$S_6(m,n)=\sum_{m=1}^{\infty}\sum_{n=1}^{\infty}\frac{(-1)^{m+n}(\sin n\theta_1-\sin n\theta_2)(\sin m\theta_3-\sin m\theta_4)\cos(m\pi x_p/a)}{mn(m^2+n^2-A^2)}$$

$$=\sum_{m=1}^{\infty}\frac{(-1)^m(\sin m\theta_3-\sin m\theta_4)\cos(m\pi x_p/a)}{m}\sum_{n=1}^{\infty}\frac{(-1)^n(\sin n\theta_1-\sin n\theta_2)}{n(n^2+E^2)}$$

$$=\sum_{m=1}^{\infty}\frac{(-1)^m(\sin m\theta_3-\sin m\theta_4)\cos(m\pi x_p/a)}{m}\left[\frac{\pi(\sinh E\theta_1-\sinh E\theta_2)}{2E^2\sinh E\pi}-\frac{\theta_1-\theta_2}{2E^2}\right]$$

$$=\frac{\pi}{2}\sum_{m=1}^{\infty}\frac{(-1)^m(\sin m\theta_3-\sin m\theta_4)(\sinh E\theta_1-\sinh E\theta_2)\cos(m\pi x_p/a)}{m(m^2-A^2)\sinh E\pi}$$

$$-\frac{W_p\pi}{2a}\sum_{m=1}^{\infty}\frac{(-1)^m(\sin m\theta_3-\sin m\theta_4)\cos(m\pi x_p/a)}{m(m^2-A^2)}$$

$$=\frac{\pi}{2}\sum_{m=1}^{\infty}\frac{(-1)^m(\sin m\theta_3-\sin m\theta_4)(\sinh E\theta_1-\sinh E\theta_2)\cos(m\pi x_p/a)}{m(m^2-A^2)\sinh E\pi}-\frac{W_p\pi}{2a}S_3(m).$$

(4A.5.9)

The series for $S_1(m)$ and $S_2(m)$ are summed to closed form. Substituting $S_1(m)$, $S_2(m)$, $S_5(m,n)$ and $S_6(m,n)$ from equations (4A.5.4), (4A.5.5), (4A.5.8), and (4A.5.9)

respectively into equation (4A.5.3) eliminates the terms $-W_p W_q \pi^2 / a^2 k^2$, and the infinite series $S_3(m)$, $S_4(m)$. Also the double infinite series $S_5(m,n)$, and $S_6(m,n)$ have been reduced to single series form.

The economised formula for Z_{pq} is then given by

$$Z_{pq} = j\omega\mu h\left\{-\frac{\cos k(a-x_p)}{ak\sin ak}-\frac{\sin A\theta_1-\sin A\theta_2}{ak^2W_p\sin ak}\right.$$

$$+\frac{2a^2}{W_pW_q\pi^3}\sum_{m=1}^{\infty}\frac{(\sin m\theta_1-\sin m\theta_2)(\sin m\theta_3-\sin m\theta_4)\cosh\pi(1-x_p/a)\sqrt{m^2-A^2}}{m^2\sqrt{m^2-A^2}\sinh\pi\sqrt{m^2-A^2}}$$

$$\left.+\frac{2a^2}{W_pW_q\pi^3}\sum_{m=1}^{\infty}\frac{(-1)^m(\sin m\theta_3-\sin m\theta_4)(\sinh\theta_1\sqrt{m^2-A^2}-\sinh\theta_2\sqrt{m^2-A^2})\cos(m\pi x_p/a)}{m(m^2-A^2)\sinh\pi\sqrt{m^2-A^2}}\right\}.$$

(4A.5.10)

The single probe port Z_{pq} is obtained in terms of closed forms and single infinite series.

APPENDIX 5A The Mathcad Program Listing for the Impedance of a Truncated Corners Square Patch

A truncated corners square patch with an offset feed and the segmental structure of the patch are shown in Figure 5A.1.

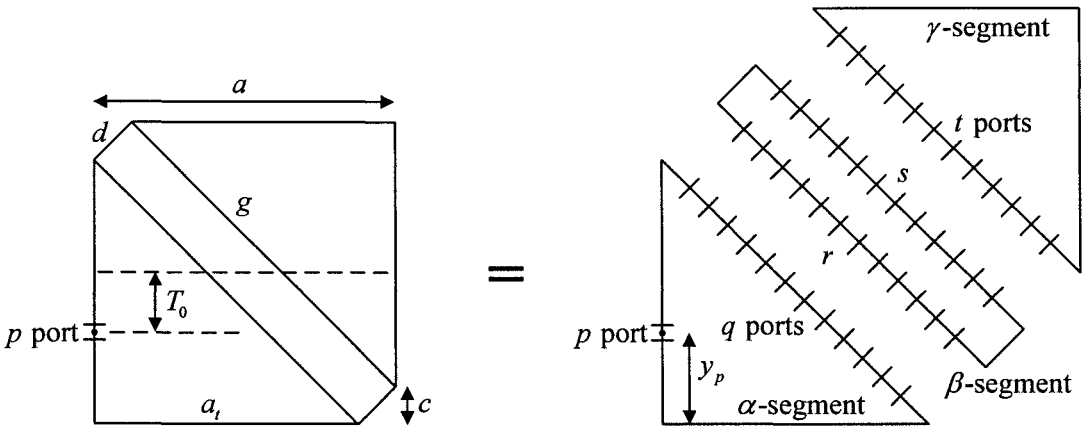

Figure 5A.1. Segmental structure for a truncated corners square patch with an offset feed.

Define : $f, \omega, Q, c_0, \varepsilon_0, \varepsilon_r, \varepsilon_{reff}, \mu_0, \mu_r, \mu, k$(effective wavenumber)

: the dimensions, $h, a, a_t, c, d, g, T_0, y_p, W_p, W_q, W_r, W_s$

: M_t, M_r (the upper limit of summation terms for the triangular (α) segment and the rectangular (β) segment respectively)

: N (port number)

For Z_{pp} :

Let,

$$A := \frac{a_t \cdot k}{\pi} \qquad \theta_1 := \frac{\pi}{a_t} \cdot \left(y_p + \frac{W_p}{2} \right) \qquad \theta_2 := \frac{\pi}{a_t} \cdot \left(y_p - \frac{W_p}{2} \right)$$

$$D := \frac{(-1)^m \cdot \left(\sin(m \cdot \theta_1) - \sin(m \cdot \theta_2) \right) \cdot \left(\sinh\left(\theta_1 \cdot \sqrt{m^2 - A^2} \right) - \sinh\left(\theta_2 \cdot \sqrt{m^2 - A^2} \right) \right)}{m \cdot \left(m^2 - A^2 \right) \cdot \sinh\left(\pi \cdot \sqrt{m^2 - A^2} \right)}$$

$$Z_{pp} := 1i \cdot \omega \cdot \mu \cdot h \cdot \left[\begin{array}{l} \dfrac{\cot(a_t \cdot k)}{a_t \cdot k} + \dfrac{\sin(A \cdot \theta_2) - \sin(A \cdot \theta_1)}{a_t \cdot k^2 \cdot W_p \cdot \sin(a_t \cdot k)} \ldots \\ + \dfrac{2 \cdot a_t^{\,2}}{W_p^{\,2} \cdot \pi^3} \cdot \sum_{m=1}^{M_t} \dfrac{\left(\sin(m \cdot \theta_1) - \sin(m \cdot \theta_2) \right)^2 \cdot \coth\left(\pi \cdot \sqrt{m^2 - A^2} \right)}{m^2 \cdot \sqrt{m^2 - A^2}} \ldots \\ + \dfrac{2 \cdot a_t^{\,2}}{W_p^{\,2} \cdot \pi^3} \cdot \sum_{m=1}^{M_t} D \end{array} \right]$$

For Z_{pq} :

Let,

$$E := \frac{(-1)^m \cdot \left(\sin(m \cdot \theta_1) - \sin(m \cdot \theta_2) \right) \cdot \left(\sin(m \cdot \theta_3) - \sin(m \cdot \theta_4) \right)}{m^2 \cdot \left(m^2 - A^2 \right)}$$

$$F := \frac{(-1)^m \cdot \left(\sin(m \cdot \theta_1) - \sin(m \cdot \theta_2) \right) \cdot \left(\sin(m \cdot 2 \cdot \theta_3) - \sin(m \cdot 2 \cdot \theta_4) \right)}{m^2 \cdot \left(m^2 - \frac{A^2}{2} \right)}$$

$$G := \frac{\dfrac{(-1)^n \cdot \left(\sin(n \cdot \theta_1) - \sin(n \cdot \theta_2) \right)}{n} + \dfrac{(-1)^m \cdot \left(\sin(m \cdot \theta_1) - \sin(m \cdot \theta_2) \right)}{m}}{m^2 + n^2 - A^2}$$

$$H := \frac{\sin\left[(m+n) \cdot \theta_3 \right] - \sin\left[(m+n) \cdot \theta_4 \right]}{m+n} + \frac{\sin\left[(m-n) \cdot \theta_3 \right] - \sin\left[(m-n) \cdot \theta_4 \right]}{m-n}$$

$$
\begin{aligned}
Z_{pq} := \;& \text{for } u \in 0..N-1 \\
& \quad x_q \leftarrow \frac{a_t}{2\cdot N}\cdot(2\cdot u+1) \\
& \quad \theta_3 \leftarrow \frac{\pi}{a_t}\cdot\left(x_q+\frac{W_q}{2\cdot\sqrt{2}}\right) \\
& \quad \theta_4 \leftarrow \frac{\pi}{a_t}\cdot\left(x_q-\frac{W_q}{2\cdot\sqrt{2}}\right) \\
& \quad Z_{0,u} \leftarrow 1i\cdot\omega\cdot\mu\cdot h\cdot\left[\frac{2}{a_t^{\,2}\cdot k^2}+\frac{2\cdot\sqrt{2}\cdot\left[\sin\left[A\cdot(\pi-\theta_3)\right]-\sin\left[A\cdot(\pi-\theta_4)\right]\right]}{a_t\cdot k^2\cdot W_q\cdot\sin(a_t\cdot k)}\ldots\right. \\
& \qquad +\frac{-2\cdot\left(\sin\left(\frac{A}{\sqrt{2}}\cdot\theta_1\right)-\sin\left(\frac{A}{\sqrt{2}}\cdot\theta_2\right)\right)}{a_t\cdot k^2\cdot W_p\cdot\sin\left(\frac{a_t\cdot k}{\sqrt{2}}\right)}\ldots \\
& \qquad +\frac{4\cdot\sqrt{2}\cdot a_t^{\,2}}{W_p\cdot W_q\cdot\pi^4}\cdot\sum_{m=1}^{M_t}E\ldots \\
& \qquad +\frac{\sqrt{2}\cdot a_t^{\,2}}{W_p\cdot W_q\cdot\pi^4}\cdot\sum_{m=1}^{M_t}F\ldots \\
& \qquad \left.+\frac{4\cdot\sqrt{2}\cdot a_t^{\,2}}{W_p\cdot W_q\cdot\pi^4}\cdot\sum_{n=1}^{M_t-1}\sum_{m=n+1}^{M_t}G\cdot H\right] \\
& Z
\end{aligned}
$$

For Z_{qq} :

Let,

$$L := \sin\left[\frac{A}{\sqrt{2}}\cdot(\pi-2\cdot\theta_1)\right]-\sin\left[\frac{A}{\sqrt{2}}\cdot(\pi-2\cdot\theta_2)\right]+\sin\left[\frac{A}{\sqrt{2}}\cdot(\pi-2\cdot\theta_3)\right]-\sin\left[\frac{A}{\sqrt{2}}\cdot(\pi-2\cdot\theta_4)\right]$$

$$M := \frac{\left(\sin(m\cdot\theta_1)-\sin(m\cdot\theta_2)\right)\cdot\left(\sin(m\cdot\theta_3)-\sin(m\cdot\theta_4)\right)}{m^2\cdot\left(m^2-A^2\right)}$$

$$P := \frac{\left(\sin(m\cdot 2\cdot\theta_1)-\sin(m\cdot 2\cdot\theta_2)\right)\cdot\left(\sin(m\cdot 2\cdot\theta_3)-\sin(m\cdot 2\cdot\theta_4)\right)}{m^2\cdot\left(m^2-\frac{A^2}{2}\right)}$$

$$R := \frac{\frac{\sin\left[(m+n)\cdot\theta_1\right] - \sin\left[(m+n)\cdot\theta_2\right]}{m+n} + \frac{\sin\left[(m-n)\cdot\theta_1\right] - \sin\left[(m-n)\cdot\theta_2\right]}{m-n}}{m^2 + n^2 - A^2}$$

$Z_{qq} :=$ for $u \in 0..N-1$

$x_q \leftarrow \frac{a_t}{2\cdot N}\cdot(2\cdot u + 1)$

$\theta_1 \leftarrow \frac{\pi}{a_t}\cdot\left(x_q + \frac{W_q}{2\cdot\sqrt{2}}\right)$

$\theta_2 \leftarrow \frac{\pi}{a_t}\cdot\left(x_q - \frac{W_q}{2\cdot\sqrt{2}}\right)$

for $t \in u..N-1$

$x_q \leftarrow \frac{a_t}{2\cdot N}\cdot(2\cdot t + 1)$

$\theta_3 \leftarrow \frac{\pi}{a_t}\cdot\left(x_q + \frac{W_q}{2\cdot\sqrt{2}}\right)$

$\theta_4 \leftarrow \frac{\pi}{a_t}\cdot\left(x_q - \frac{W_q}{2\cdot\sqrt{2}}\right)$

$$Z_{u,t} \leftarrow 1i\cdot\omega\cdot\mu\cdot h\cdot\left(\begin{array}{l} \frac{1}{a_t^2\cdot k^2} - \frac{\cot\left(\frac{a_t\cdot k}{\sqrt{2}}\right)}{\sqrt{2}\cdot a_t\cdot k} \ldots \\ + \frac{L}{\sqrt{2}\cdot a_t\cdot k^2\cdot W_q\cdot\sin\left(\frac{a_t\cdot k}{\sqrt{2}}\right)} \ldots \\ + \frac{16\cdot a_t^2}{W_q^2\cdot\pi^4}\cdot\sum_{m=1}^{M_t} M + \frac{a_t^2}{2\cdot W_q^2\cdot\pi^4}\cdot\sum_{m=1}^{M_t} P \ldots \\ + \frac{8\cdot a_t^2}{W_q^2\cdot\pi^4}\cdot\sum_{n=1}^{M_t-1}\sum_{m=n+1}^{M_t} R\cdot H \end{array}\right)$$

$Z_{t,u} \leftarrow Z_{u,t}$

Z

For Z_{rr} :

Let,

$$B := \frac{g \cdot k}{\pi}$$

$$S := \frac{\left(\sin\left(n \cdot \theta_1\right) - \sin\left(n \cdot \theta_2\right)\right) \cdot \left(\sin\left(n \cdot \theta_3\right) - \sin\left(n \cdot \theta_4\right)\right) \cdot \coth\left[\frac{d \cdot \pi}{g} \cdot \sqrt{\left(n^2 - B^2\right)}\right]}{n^2 \cdot \sqrt{n^2 - B^2}}$$

$Z_{rr} :=$ for $u \in 0 .. N - 1$

$y_r \leftarrow g - \frac{g \cdot (2 \cdot u + 1)}{2 \cdot N}$

$\theta_1 \leftarrow \frac{\pi}{g} \cdot \left(y_r + \frac{W_r}{2}\right)$

$\theta_2 \leftarrow \frac{\pi}{g} \cdot \left(y_r - \frac{W_r}{2}\right)$

for $t \in u .. N - 1$

$y_r \leftarrow g - \frac{g \cdot (2 \cdot t + 1)}{2 \cdot N}$

$\theta_3 \leftarrow \frac{\pi}{g} \cdot \left(y_r + \frac{W_r}{2}\right)$

$\theta_4 \leftarrow \frac{\pi}{g} \cdot \left(y_r - \frac{W_r}{2}\right)$

$Z_{u,t} \leftarrow 1i \cdot \omega \cdot \mu \cdot h \cdot \left(-\frac{\cot(d \cdot k)}{g \cdot k} \ldots + \frac{2 \cdot g^2}{W_r^2 \cdot \pi^3} \cdot \sum_{n=1}^{M_r} S \right)$

$Z_{t,u} \leftarrow Z_{u,t}$

Z

For Z_{rs}:

Let,

$$V := \frac{\left(\sin\left(n\cdot\theta_1\right) - \sin\left(n\cdot\theta_2\right)\right)\cdot\left(\sin\left(n\cdot\theta_3\right) - \sin\left(n\cdot\theta_4\right)\right)}{n^2\cdot\sqrt{n^2 - B^2}\cdot\sinh\left(\frac{d\cdot\pi}{g}\cdot\sqrt{n^2 - B^2}\right)}$$

$$Z_{rs} := \left|\begin{array}{l} \text{for } u \in 0..N-1 \\ \quad y_r \leftarrow g - \frac{g\cdot(2\cdot u + 1)}{2\cdot N} \\ \quad \theta_1 \leftarrow \frac{\pi}{g}\cdot\left(y_r + \frac{W_r}{2}\right) \\ \quad \theta_2 \leftarrow \frac{\pi}{g}\cdot\left(y_r - \frac{W_r}{2}\right) \\ \quad \text{for } t \in u..N-1 \\ \quad\quad y_s \leftarrow g - \frac{g\cdot(2\cdot t + 1)}{2\cdot N} \\ \quad\quad \theta_3 \leftarrow \frac{\pi}{g}\cdot\left(y_s + \frac{W_s}{2}\right) \\ \quad\quad \theta_4 \leftarrow \frac{\pi}{g}\cdot\left(y_s - \frac{W_s}{2}\right) \\ \quad\quad Z_{u,t} \leftarrow 1i\cdot\omega\cdot\mu\cdot h\cdot\left(\frac{1}{g\cdot k\cdot\sin(d\cdot k)} - \frac{2\cdot g^2}{W_r\cdot W_s\cdot\pi^3}\cdot\sum_{n=1}^{M_r} V\right) \\ \quad\quad Z_{t,u} \leftarrow Z_{u,t} \\ Z \end{array}\right.$$

For Z_{in}:

$$Z_{in} := Z_{pp} - Z_{pq}\cdot\left[Z_{qq} + Z_{rr} - Z_{rs}\cdot\left(Z_{qq} + Z_{rr}\right)^{-1}\cdot Z_{rs}\right]^{-1}\cdot Z_{pq}^{T}$$

The effective dimensions of the patch were used in the above equations. A run time for sweep on 151 points of the input impedance over the frequency vary (2.3 to 2.6 GHz) was less than two minutes.

APPENDIX 6A The Mathcad Program Listing for the Impedance of a U-Slot Rectangular Patch

A U-slot rectangular patch with a probe feed and the segmental structure of the patch are shown in Figure 6A.1.

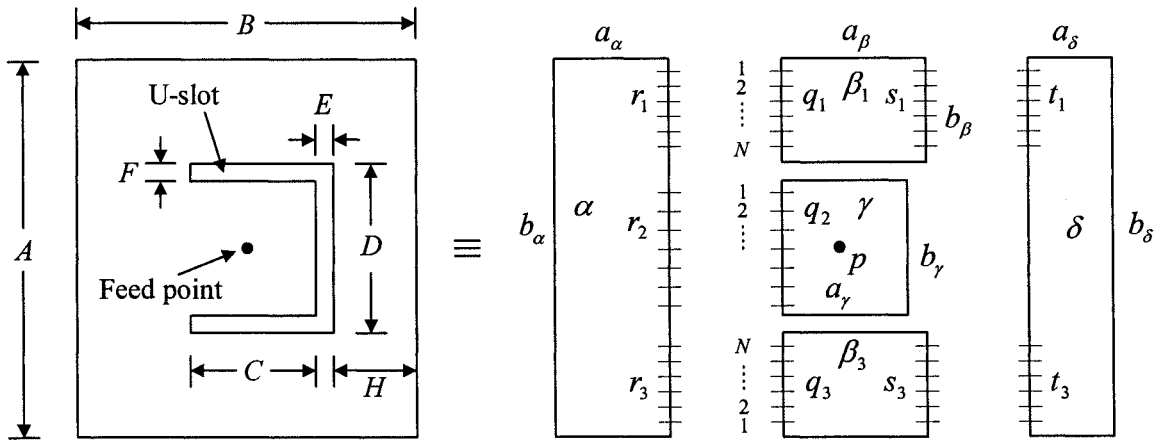

Figure 6A.1. Segmental structure for a U-slot rectangular patch.

Define : $f, \omega, Q, c_0, \varepsilon_0, \varepsilon_r, \varepsilon_{reff}, \mu_0, \mu_r, \mu, k$ (effective wavenumber)

: the dimensions, $h, A, B, C, D, E, F, H, a_\alpha, b_\alpha, a_\beta, b_\beta, a_\gamma, b_\gamma, a_\delta, b_\delta, x_p, y_p,$

$W_{r_1}, W_{r_2}, W_{r_3}, W_{q_1}, W_{q_2}, W_{s_1}, W_{s_2}, W_{t_1}, W_{t_3}, W_p$

: M (the upper limit of summation terms)

: N (port number)

Note : The U-slot rectangular patch antenna is symmetric, so size $\beta_1 = \beta_3$.

For Z_{pp} :

Let,

$$B_1 := \frac{b_\gamma \cdot k}{\pi} \qquad \theta_1 := \frac{\pi}{b_\gamma}\left(y_p + \frac{W_p}{2}\right) \qquad \theta_2 := \frac{\pi}{b_\gamma}\left(y_p - \frac{W_p}{2}\right)$$

$$L := \cosh\left(\frac{a_\gamma \cdot \pi}{b_\gamma} \cdot \sqrt{n^2 - B_1^{\,2}}\right) + \cosh\left[\frac{\left(a_\gamma - 2 \cdot x_p\right) \cdot \pi}{b_\gamma} \cdot \sqrt{n^2 - B_1^{\,2}}\right]$$

$$Z_{pp} := 1i \cdot \omega \cdot \mu \cdot h \cdot \left[-\frac{\cos\left(a_\gamma \cdot k\right) + \cos\left[k \cdot \left(a_\gamma - 2 \cdot x_p\right)\right]}{2 \cdot b_\gamma \cdot k \cdot \sin\left(a_\gamma \cdot k\right)} \ldots + \frac{b_\gamma^{\,2}}{W_p^{\,2} \cdot \pi^3} \cdot \left[\sum_{n=1}^{M} \frac{\left(\sin\left(n \cdot \theta_1\right) - \sin\left(n \cdot \theta_2\right)\right)^2 \cdot L}{n^2 \cdot \sqrt{n^2 - B_1^{\,2}} \cdot \sinh\left(\frac{a_\gamma \cdot \pi}{b_\gamma} \cdot \sqrt{n^2 - B_1^{\,2}}\right)} \right] \right]$$

For Z_{pq_2} :

Let,

$$P := \frac{\left(\sin\left(n \cdot \theta_1\right) - \sin\left(n \cdot \theta_2\right)\right) \cdot \left(\sin\left(n \cdot \theta_3\right) - \sin\left(n \cdot \theta_4\right)\right) \cdot \left[\cosh\left[\frac{\left(a_\gamma - x_p\right) \cdot \pi}{b_\gamma} \cdot \sqrt{n^2 - B_1^{\,2}}\right]\right]}{n^2 \cdot \sqrt{n^2 - B_1^{\,2}} \cdot \sinh\left(\frac{a_\gamma \cdot \pi}{b_\gamma} \cdot \sqrt{n^2 - B_1^{\,2}}\right)}$$

$Z_{pq2} :=$ for $u \in 0 .. N - 1$

$y_{q2} \leftarrow b_\gamma - \frac{b_\gamma \cdot (2 \cdot u + 1)}{2 \cdot N}$

$\theta_3 \leftarrow \frac{\pi}{b_\gamma} \cdot \left(y_{q2} + \frac{W_{q2}}{2}\right)$

$\theta_4 \leftarrow \frac{\pi}{b_\gamma} \cdot \left(y_{q2} - \frac{W_{q2}}{2}\right)$

$Z_{0,u} \leftarrow 1i \cdot \omega \cdot \mu \cdot h \cdot \left[\frac{\cos\left[k \cdot \left(a_\gamma - x_p\right)\right]}{b_\gamma \cdot k \cdot \sin\left(a_\gamma \cdot k\right)} + \frac{2 \cdot b_\gamma^{\,2}}{W_p \cdot W_{q2} \cdot \pi^3} \cdot \sum_{n=1}^{M} P \right]$

Z

For $Z_{q_2q_2}$:

Let,

$$R := \frac{\left(\sin\left(n\cdot\theta_1\right) - \sin\left(n\cdot\theta_2\right)\right)\cdot\left(\sin\left(n\cdot\theta_3\right) - \sin\left(n\cdot\theta_4\right)\right)\cdot\coth\left(\frac{a_\gamma\cdot\pi}{b_\gamma}\cdot\sqrt{n^2 - B_1{}^2}\right)}{n^2\cdot\sqrt{n^2 - B_1{}^2}}$$

$Z_{q2q2} :=$ for $u \in 0..N-1$

$y_{q2} \leftarrow b_\gamma - \frac{b_\gamma\cdot(2\cdot u+1)}{2\cdot N}$

$\theta_1 \leftarrow \frac{\pi}{b_\gamma}\cdot\left(y_{q2} + \frac{W_{q2}}{2}\right)$

$\theta_2 \leftarrow \frac{\pi}{b_\gamma}\cdot\left(y_{q2} - \frac{W_{q2}}{2}\right)$

for $t \in u..N-1$

$y_{q2} \leftarrow b_\gamma - \frac{b_\gamma\cdot(2\cdot t+1)}{2\cdot N}$

$\theta_3 \leftarrow \frac{\pi}{b_\gamma}\cdot\left(y_{q2} + \frac{W_{q2}}{2}\right)$

$\theta_4 \leftarrow \frac{\pi}{b_\gamma}\cdot\left(y_{q2} - \frac{W_{q2}}{2}\right)$

$Z_{u,t} \leftarrow 1i\cdot\omega\cdot\mu\cdot h\cdot\left(-\frac{\cot\left(a_\gamma\cdot k\right)}{b_\gamma\cdot k} + \frac{2\cdot b_\gamma{}^2}{W_{q2}{}^2\cdot\pi^3}\cdot\sum_{n=1}^{M} R\right)$

$Z_{t,u} \leftarrow Z_{u,t}$

Z

For $Z_{q_1q_1}$:

Let,

$$B_2 := \frac{b_\beta \cdot k}{\pi}$$

$$S := \frac{\left(\sin\left(n\cdot\theta_1\right) - \sin\left(n\cdot\theta_2\right)\right)\cdot\left(\sin\left(n\cdot\theta_3\right) - \sin\left(n\cdot\theta_4\right)\right)\cdot\coth\left(\frac{a_\beta\cdot\pi}{b_\beta}\cdot\sqrt{n^2 - B_2{}^2}\right)}{n^2\cdot\sqrt{n^2 - B_2{}^2}}$$

$Z_{q1q1} :=$ for $u \in 0..N-1$

$y_{q1} \leftarrow b_\beta - \frac{b_\beta\cdot(2\cdot u+1)}{2\cdot N}$

$\theta_1 \leftarrow \frac{\pi}{b_\beta}\cdot\left(y_{q1} + \frac{W_{q1}}{2}\right)$

$\theta_2 \leftarrow \frac{\pi}{b_\beta}\cdot\left(y_{q1} - \frac{W_{q1}}{2}\right)$

for $t \in u..N-1$

$y_{q1} \leftarrow b_\beta - \frac{b_\beta\cdot(2\cdot t+1)}{2\cdot N}$

$\theta_3 \leftarrow \frac{\pi}{b_\beta}\cdot\left(y_{q1} + \frac{W_{q1}}{2}\right)$

$\theta_4 \leftarrow \frac{\pi}{b_\beta}\cdot\left(y_{q1} - \frac{W_{q1}}{2}\right)$

$Z_{u,t} \leftarrow 1i\cdot\omega\cdot\mu\cdot h\cdot\left(-\frac{\cot\left(a_\beta\cdot k\right)}{b_\beta\cdot k} + \frac{2\cdot b_\beta{}^2}{W_{q1}{}^2\cdot\pi^3}\cdot\sum_{n=1}^{M} S\right)$

$Z_{t,u} \leftarrow Z_{u,t}$

Z

For $Z_{q_1 s_1}$:

Let,

$$U := \frac{\left(\sin\left(n\cdot\theta_1\right) - \sin\left(n\cdot\theta_2\right)\right)\cdot\left(\sin\left(n\cdot\theta_3\right) - \sin\left(n\cdot\theta_4\right)\right)}{n^2\cdot\sqrt{n^2 - B_2{}^2}\cdot\sinh\left(\frac{a_\beta\cdot\pi}{b_\beta}\cdot\sqrt{n^2 - B_2{}^2}\right)}$$

$Z_{q1s1} :=$ for $u \in 0..N-1$

$y_{q1} \leftarrow b_\beta - \frac{b_\beta\cdot(2\cdot u + 1)}{2\cdot N}$

$\theta_1 \leftarrow \frac{\pi}{b_\beta}\cdot\left(y_{q1} + \frac{W_{q1}}{2}\right)$

$\theta_2 \leftarrow \frac{\pi}{b_\beta}\cdot\left(y_{q1} - \frac{W_{q1}}{2}\right)$

for $t \in u..N-1$

$y_{s1} \leftarrow b_\beta - \frac{b_\beta\cdot(2\cdot t + 1)}{2\cdot N}$

$\theta_3 \leftarrow \frac{\pi}{b_\beta}\cdot\left(y_{s1} + \frac{W_{s1}}{2}\right)$

$\theta_4 \leftarrow \frac{\pi}{b_\beta}\cdot\left(y_{s1} - \frac{W_{s1}}{2}\right)$

$Z_{u,t} \leftarrow 1i\cdot\omega\cdot\mu\cdot h\cdot\left(\frac{1}{b_\beta\cdot k\cdot\sin\left(a_\beta\cdot k\right)} - \frac{2\cdot b_\beta{}^2}{W_{q1}\cdot W_{s1}\cdot\pi^3}\cdot\sum_{n=1}^{M} U\right)$

$Z_{t,u} \leftarrow Z_{u,t}$

Z

For $Z_{n_1 n_1}$:

Let,

$$B_3 := \frac{b_\alpha \cdot k}{\pi}$$

$$V := \frac{\left(\sin\left(n\cdot\theta_1\right) - \sin\left(n\cdot\theta_2\right)\right)\cdot\left(\sin\left(n\cdot\theta_3\right) - \sin\left(n\cdot\theta_4\right)\right)\cdot\coth\left(\frac{a_\alpha\cdot\pi}{b_\alpha}\cdot\sqrt{n^2 - B_3{}^2}\right)}{n^2\cdot\sqrt{n^2 - B_3{}^2}}$$

$Z_{r1r1} :=$ for $u \in 0..N-1$

$y_{r1} \leftarrow b_\alpha - \frac{b_\beta\cdot(2\cdot u+1)}{2\cdot N}$

$\theta_1 \leftarrow \frac{\pi}{b_\alpha}\cdot\left(y_{r1} + \frac{W_{r1}}{2}\right)$

$\theta_2 \leftarrow \frac{\pi}{b_\alpha}\cdot\left(y_{r1} - \frac{W_{r1}}{2}\right)$

for $t \in u..N-1$

$y_{r1} \leftarrow b_\alpha - \frac{b_\beta\cdot(2\cdot t+1)}{2\cdot N}$

$\theta_3 \leftarrow \frac{\pi}{b_\alpha}\cdot\left(y_{r1} + \frac{W_{r1}}{2}\right)$

$\theta_4 \leftarrow \frac{\pi}{b_\alpha}\cdot\left(y_{r1} - \frac{W_{r1}}{2}\right)$

$Z_{u,t} \leftarrow 1i\cdot\omega\cdot\mu\cdot h\cdot\left(\frac{\cot\left(a_\alpha\cdot k\right)}{b_\alpha\cdot k} + \frac{2\cdot b_\alpha{}^2}{W_{r1}{}^2\cdot\pi^3}\cdot\sum_{n=1}^{M} V\right)$

$Z_{t,u} \leftarrow Z_{u,t}$

Z

For $Z_{r_1 r_3}$:

$$
\begin{aligned}
&Z_{r1r3} := \left|\begin{array}{l}
\text{for } u \in 0..N-1 \\
\quad \left|\begin{array}{l}
y_{r1} \leftarrow b_\alpha - \dfrac{b_\beta \cdot (2\cdot u + 1)}{2\cdot N} \\
\theta_1 \leftarrow \dfrac{\pi}{b_\alpha}\cdot\left(y_{r1} + \dfrac{W_{r1}}{2}\right) \\
\theta_2 \leftarrow \dfrac{\pi}{b_\alpha}\cdot\left(y_{r1} - \dfrac{W_{r1}}{2}\right) \\
\text{for } t \in u..N-1 \\
\quad \left|\begin{array}{l}
y_{r3} \leftarrow \dfrac{b_\beta \cdot (2\cdot t + 1)}{2\cdot N} \\
\theta_3 \leftarrow \dfrac{\pi}{b_\alpha}\cdot\left(y_{r3} + \dfrac{W_{r3}}{2}\right) \\
\theta_4 \leftarrow \dfrac{\pi}{b_\alpha}\cdot\left(y_{r3} - \dfrac{W_{r3}}{2}\right) \\
Z_{u,t} \leftarrow 1i\cdot\omega\cdot\mu\cdot h\cdot\left(-\dfrac{\cot\left(a_\alpha\cdot k\right)}{b_\alpha\cdot k} + \dfrac{2\cdot {b_\alpha}^2}{W_{r1}\cdot W_{r3}\cdot \pi^3}\cdot\sum_{n=1}^{M} V\right) \\
Z_{t,u} \leftarrow Z_{u,t}
\end{array}\right.
\end{array}\right. \\
&Z
\end{aligned}
$$

For $Z_{r_2 r_1}$:

$$
\begin{aligned}
Z_{r2r1} := \;& \text{for } u \in 0..N-1 \\
& \quad y_{r2} \leftarrow b_\alpha - b_\beta - F - \frac{b_\gamma \cdot (2 \cdot u + 1)}{2N} \\
& \quad \theta_1 \leftarrow \frac{\pi}{b_\alpha} \cdot \left(y_{r2} + \frac{W_{r2}}{2} \right) \\
& \quad \theta_2 \leftarrow \frac{\pi}{b_\alpha} \cdot \left(y_{r2} - \frac{W_{r2}}{2} \right) \\
& \quad \text{for } t \in 0..N-1 \\
& \quad\quad y_{r1} \leftarrow b_\alpha - \frac{b_\beta \cdot (2 \cdot t + 1)}{2 \cdot N} \\
& \quad\quad \theta_3 \leftarrow \frac{\pi}{b_\alpha} \cdot \left(y_{r1} + \frac{W_{r1}}{2} \right) \\
& \quad\quad \theta_4 \leftarrow \frac{\pi}{b_\alpha} \cdot \left(y_{r1} - \frac{W_{r1}}{2} \right) \\
& \quad\quad Z_{u,t} \leftarrow 1i \cdot \omega \cdot \mu \cdot h \cdot \left(-\frac{\cot(a_\alpha \cdot k)}{b_\alpha \cdot k} + \frac{2 \cdot b_\alpha^{\,2}}{W_{r1} \cdot W_{r2} \cdot \pi^3} \cdot \sum_{n=1}^{M} V \right) \\
& Z
\end{aligned}
$$

For $Z_{r_2r_2}$:

$$
\begin{aligned}
&Z_{r2r2} := \left| \begin{array}{l}
\text{for } u \in 0..N-1 \\
\quad \left| \begin{array}{l}
y_{r2} \leftarrow b_\alpha - b_\beta - F - \dfrac{b_\gamma \cdot (2 \cdot u + 1)}{2N} \\
\theta_1 \leftarrow \dfrac{\pi}{b_\alpha} \cdot \left(y_{r2} + \dfrac{W_{r2}}{2} \right) \\
\theta_2 \leftarrow \dfrac{\pi}{b_\alpha} \cdot \left(y_{r2} - \dfrac{W_{r2}}{2} \right) \\
\text{for } t \in u..N-1 \\
\quad \left| \begin{array}{l}
y_{r2} \leftarrow b_\alpha - b_\beta - F - \dfrac{b_\gamma \cdot (2 \cdot t + 1)}{2N} \\
\theta_3 \leftarrow \dfrac{\pi}{b_\alpha} \cdot \left(y_{r2} + \dfrac{W_{r2}}{2} \right) \\
\theta_4 \leftarrow \dfrac{\pi}{b_\alpha} \cdot \left(y_{r2} - \dfrac{W_{r2}}{2} \right) \\
Z_{u,t} \leftarrow 1i \cdot \omega \cdot \mu \cdot h \cdot \left(-\dfrac{\cot(a_\alpha \cdot k)}{b_\alpha \cdot k} + \dfrac{2 \cdot b_\alpha^{\,2}}{W_{r2}^{\,2} \cdot \pi^3} \cdot \sum_{n=1}^{M} V \right) \\
Z_{t,u} \leftarrow Z_{u,t}
\end{array} \right. \\
Z
\end{array} \right.
\end{aligned}
$$

For $Z_{r_2r_3}$:

$$Z_{r2r3} := \text{submatrix}\left(Z_{r2r1}, N-1, 0, 0, N-1\right)$$

The row elements in $Z_{r_2r_3}$ and $Z_{r_2r_1}$ are the same but in reverse order.

For $Z_{t_1t_1}$:

Let,

$$B_4 := \frac{b_\delta \cdot k}{\pi}$$

$$W := \frac{\left(\sin\left(n\cdot\theta_1\right) - \sin\left(n\cdot\theta_2\right)\right)\cdot\left(\sin\left(n\cdot\theta_3\right) - \sin\left(n\cdot\theta_4\right)\right)\cdot\coth\left(\frac{a_\delta\cdot\pi}{b_\delta}\cdot\sqrt{n^2 - B_4{}^2}\right)}{n^2\cdot\sqrt{n^2 - B_4{}^2}}$$

$Z_{t1t1} :=$ for $u \in 0..N-1$

$y_{t1} \leftarrow b_\delta - \frac{b_\beta\cdot(2\cdot u+1)}{2\cdot N}$

$\theta_1 \leftarrow \frac{\pi}{b_\delta}\cdot\left(y_{t1} + \frac{W_{t1}}{2}\right)$

$\theta_2 \leftarrow \frac{\pi}{b_\delta}\cdot\left(y_{t1} - \frac{W_{t1}}{2}\right)$

for $t \in u..N-1$

$y_{t1} \leftarrow b_\delta - \frac{b_\beta\cdot(2\cdot t+1)}{2\cdot N}$

$\theta_3 \leftarrow \frac{\pi}{b_\delta}\cdot\left(y_{t1} + \frac{W_{t1}}{2}\right)$

$\theta_4 \leftarrow \frac{\pi}{b_\delta}\cdot\left(y_{t1} - \frac{W_{t1}}{2}\right)$

$Z_{u,t} \leftarrow 1i\cdot\omega\cdot\mu\cdot h\cdot\left(-\frac{\cot\left(a_\delta\cdot k\right)}{b_\delta\cdot k} + \frac{2\cdot b_\delta{}^2}{W_{t1}{}^2\cdot\pi^3}\cdot\sum_{n=1}^{M} W\right)$

$Z_{t,u} \leftarrow Z_{u,t}$

Z

For $Z_{t_1 t_3}$:

$$
\begin{aligned}
&Z_{t1t3} := \left|\begin{array}{l}
\text{for } u \in 0..N-1 \\
\quad \left|\begin{array}{l}
y_{t1} \leftarrow b_\delta - \dfrac{b_\beta \cdot (2\cdot u + 1)}{2\cdot N} \\
\theta_1 \leftarrow \dfrac{\pi}{b_\delta}\cdot\left(y_{t1} + \dfrac{W_{t1}}{2}\right) \\
\theta_2 \leftarrow \dfrac{\pi}{b_\delta}\cdot\left(y_{t1} - \dfrac{W_{t1}}{2}\right) \\
\text{for } t \in u..N-1 \\
\quad \left|\begin{array}{l}
y_{t3} \leftarrow \dfrac{b_\beta \cdot (2\cdot t + 1)}{2\cdot N} \\
\theta_3 \leftarrow \dfrac{\pi}{b_\delta}\cdot\left(y_{t3} + \dfrac{W_{t3}}{2}\right) \\
\theta_4 \leftarrow \dfrac{\pi}{b_\delta}\cdot\left(y_{t3} - \dfrac{W_{t3}}{2}\right) \\
Z_{u,t} \leftarrow 1i\cdot\omega\cdot\mu\cdot h\cdot\left(-\dfrac{\cot(a_\delta\cdot k)}{b_\delta\cdot k} + \dfrac{2\cdot b_\delta{}^2}{W_{t1}\cdot W_{t3}\cdot\pi^3}\cdot\sum_{n=1}^{M} W\right) \\
Z_{t,u} \leftarrow Z_{u,t}
\end{array}\right.
\end{array}\right. \\
&Z
\end{aligned}
$$

For Z_M :

$$Z_{zero} := \left| \begin{array}{l} \text{for } u \in 0..N-1 \\ \quad \text{for } t \in 0..N-1 \\ \quad\quad Z_{u,t} \leftarrow 0 \\ Z \end{array} \right.$$

$$Z_A := \text{augment}(Z_{r2r1}, Z_{r2r3})$$

$$Z_B := \text{stack}(\text{augment}(Z_{q1s1}, Z_{zero}), \text{augment}(Z_{zero}, Z_{q1s1}))$$

$$Z_C := \text{stack}(\text{augment}(Z_{q1q1} + Z_{t1t1}, Z_{t1t3}), \text{augment}(Z_{t1t3}, Z_{q1q1} + Z_{t1t1}))$$

$$Z_D := \text{stack}(\text{augment}(Z_{r1r1} + Z_{q1q1}, Z_{r1r3}), \text{augment}(Z_{r1r3}, Z_{r1r1} + Z_{q1q1}))$$

$$Z_M := Z_{q2q2} + Z_{r2r2} + Z_A \cdot \left(Z_B \cdot Z_C^{-1} \cdot Z_B - Z_D\right)^{-1} \cdot Z_A^{T}$$

For Z_{in} :

$$Z_{in} := Z_{pp} - Z_{pq2} \cdot Z_M^{-1} \cdot Z_{pq2}^{T}$$

The effective dimensions of the patch were used in the above equations. A run time for sweep on 251 points of the input impedance over the frequency vary (2.2 to 2.7 GHz) was less than one minute.